第 46 回
フラーレン・ナノチューブ・グラフェン総合シンポジウム
The 46th Fullerenes-Nanotubes-Graphene General Symposium

講演要旨集
Abstracts

2014 年 3 月 3 日（月）～ 5 日（水）
東京大学 伊藤国際学術研究センター 伊藤謝恩ホール
The University of Tokyo, Ito International Research Center

主催 フラーレン・ナノチューブ・グラフェン学会
The Fullerenes, Nanotubes and Graphene Research Society

共催	日本化学会	The Chemical Society of Japan
	JST 戦略的国際共同研究プロジェクト IRENA	IRENA Project by JST-EC DG RTD, Strategic International Collaborative Research Program, SICORP
	東京大学 GMSI	The University of Tokyo Graduate Program for Mechanical Systems Innovation
協賛	日本物理学会	The Physical Society of Japan
	応用物理学会	The Japan Society of Applied Physics
	高分子学会	The Society of Polymer Science, Japan
	電気化学会	The Electrochemical Society of Japan

インテル® シミュレーションを高速化

Parallel Studio XE 2013

高速化のための Fortran、C/C++ コンパイラー、性能解析ツール、パフォーマンス・ライブラリーなどが同梱された総合開発ツールです。 最新のプロセッサーや、インテル® Xeon Phi™ コプロセッサーに対応した高速なアプリケーションを開発することができます。

［ 主なバンドル製品 ］

⊙ インテル® Composer XE 2013

- マルチコア / メニーコア・プロセッサーの性能を最大限に引き出せるように、最適化されたバイナリーを生成する Fortran、C/C++ コンパイラー
- BLAS、LAPACK、高速フーリエ変換などを含む、最適化、並列化済みの数値演算ライブラリー

⊙ インテル® VTune™ Amplifier XE 2013

数クリックのみでパフォーマンス問題の原因を特定できるマルチスレッド対応分析ツール

⊙ インテル® Inspector XE 2013

メモリーリーク、メモリー破壊、データ競合、デッドロックなどの問題を素早く検出する、マルチスレッド・エラー / メモリーエラー検出ツール

⊙ インテル® Advisor XE 2013

マルチスレッド化の候補を見つけ出し、効果予測や問題の診断を行える並列化と高速化のアドバイスツール

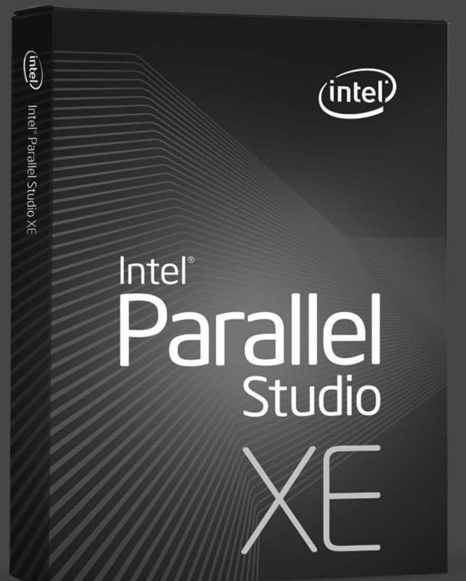

インテル® コンパイラーによる最先端のパフォーマンス（数値が大きいほど高性能）

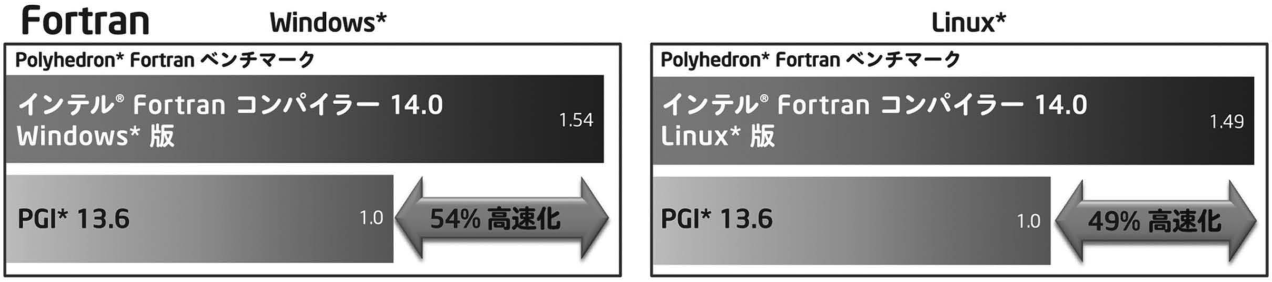

構成システム - コンパイラー: インテル® Fortran 14.0, PGI* 13.6; H/W: Blue Hills ATX Media IVB Desktop DZ77BH-55K-IDD; インテル® Core™ i7-3770K CPU @ 3.50GHz, TurboBoost 有効, HyperThreading 無効, 16GB RAM; Windows* OS: Windows* 7 Enterprise, SP 1; Linux* OS: Red Hat* Enterprise Linux Server release 6.3 (Santiago); Kernel 2.6.32-279.el6.x86_64; コンパイラー・オプション (Windows* および Linux*): インテル® Fortran コンパイラー 14.0: ifort -O3 -fast -parallel -ipo -no-prec-div, PGI 13.6: pgf95 -fastsse -Munroll=n:4 -Mipa=fast,inline -Mconcur=bind . Polyhedron* ベンチマーク (www.polyhedron.com) はインテル コーポレーションによって 2013 年 8 月 20 日に実施されました。

性能に関するテストに使用されるソフトウェアとワークロードは、性能がインテル® マイクロプロセッサー用に最適化されていることがあります。SYSmark* や MobileMark* などの性能テストは、特定のコンピューター・システム、コンポーネント、ソフトウェア、操作、機能に基づいて行ったものです。結果はこれらの要因によって異なります。製品の購入を検討される場合は、他の製品と組み合わせた場合の本製品の性能など、ほかの情報や性能テストも参考にして、パフォーマンスを総合的に評価することをお勧めします。
Intel、インテル、Intel ロゴ、Cilk、Intel Core、VTune は、アメリカ合衆国および / またはその他の国における Intel Corporation の商標です。Windows、Visual Studio は、米国 Microsoft Corporation および / またはその関連会社の商標です。
* その他の社名、製品名などは、一般に各社の表示、商標または登録商標です。
最適化に関する注意事項 : インテル® コンパイラーは、互換マイクロプロセッサー向けには、インテル製マイクロプロセッサー向けと同等レベルの最適化が行われない可能性があります。 これには、インテル® ストリーミング SIMD 拡張命令 2 (インテル® SSE2)、インテル® ストリーミング SIMD 拡張命令 3 (インテル® SSE3)、ストリーミング SIMD 拡張命令 3 補足命令 (SSSE3) 命令セットに関連する最適化およびその他の最適化が含まれます。インテルでは、インテル製ではないマイクロプロセッサーに対して、最適化の提供、機能、効果を保証していません。本製品のマイクロプロセッサー固有の最適化は、インテル製マイクロプロセッサーでの使用を目的としています。インテル® マイクロアーキテクチャーに非固有の特定の最適化は、インテル製マイクロプロセッサー向けに予約されています。この注意事項の適用対象である特定の命令セットの詳細は、該当する製品のユーザー・リファレンス・ガイドを参照してください。

改訂 #20110804

無料評価版はこちら ⊙

http://www.xlsoft.com/intel

製品の詳細に関するお問い合わせ先 :

XLSOFT エクセルソフト株式会社
〒 108-0073 東京都港区三田 3-9-9 森伝ビル 6F
Tel: 03-5440-7875 Fax: 03-5440-7876 E-mail: intel@xlsoft.com

インテル® ソフトウェア製品のパフォーマンス / 最適化に関する詳細は、http://software.intel.com/en-us/articles/optimization-notice/#opt-jp を参照してください。
Intel、インテル、Intel ロゴ、Intel Xeon Phi、VTune は、アメリカ合衆国および / またはその他の国における Intel Corporation の商標です。* その他の社名、製品名などは、一般に各社の表示、商標または登録商標です。© 2014 Intel Corporation. 無断での引用、転載を禁じます。
XLsoft のロゴ、XLsoft は XLsoft Corporation の商標です。Copyright © 2014 XLsoft Corporation.

Contents

Time Table ・・・・・・・・・・・・・・・・・・・・ i
Chairperson ・・・・・・・・・・・・・・・・・・・iii
Program Japanese ・・・・・・・・・・・・・ iv
English ・・・・・・・・・・・・・・ xix
Abstracts Plenary Lecture, Special Lecture ・・・ 1
General Lecture ・・・・・・・・・・・ 9
Poster Preview ・・・・・・・・・・・・43
Author Index ・・・・・・・・・・・・・・・・・・193

目次

早見表 ・・・・・・・・・・・・・・・・・・・・ i
座長一覧・・・・・・・・・・・・・・・・・・・・iii
プログラム 和文・・・・・・・・・・・・・・・・・・iv
英文・・・・・・・・・・・・・・・・・ xix
講演予稿 基調講演・特別講演・・・・・・・・・ 1
一般講演・・・・・・・・・・・・・・・・ 9
ポスター発表・・・・・・・・・・・・・43
発表索引・・・・・・・・・・・・・・・・・・・ 193

プログラム早見表

	3月3日（月）
	受付開始 8:30〜 講演開始 9:30〜
9:30	基調講演（佐々木幹夫） 9:30-10:00
10:00	一般講演 3件 （フラーレン・金属内包フラーレン・フラーレンの応用） 10:00-10:45
10:45	休憩 10:45-11:00
11:00	特別講演（豊國伸哉） 11:00-11:30
11:30	一般講演 2件 （ナノ炭素粒子・その他）11:30-12:00
12:00	昼食 （幹事会） 12:00-13:15
13:15	特別講演（上野啓司） 13:15-13:45
13:45	一般講演 4件 （グラフェンの応用・グラフェンの物性） 13:45-14:45
14:45	ポスタープレビュー （ 1P-1 〜 1P-50 ） 14:45-15:45
15:45	ポスターセッション （多目的スペース） 15:45-17:30
17:30	休憩 17:30-18:00
18:00	チュートリアル 講師: 大野雄高 名古屋大学 准教授 （伊藤謝恩ホール） 18:00-19:30
19:30	

	3月4日（火）
	受付開始 8:30〜 講演開始 9:00〜
9:00	特別講演（Yan Li） 9:00-9:30
9:30	一般講演 4件 （ナノチューブの生成と精製） 9:30-10:30
10:30	休憩 10:30-10:45
10:45	特別講演（本間芳和） 10:45-11:15
11:15	一般講演 4件 （ナノチューブの生成と精製・ナノチューブの物性・ナノチューブの応用） 11:15-12:15
12:15	昼食 12:15-13:30
13:30	授賞式 13:30-14:15
14:15	ポスタープレビュー （ 2P-1 〜 2P-50 ） 14:15-15:15
15:15	ポスターセッション （多目的スペース） 15:15-17:00
17:00	特別講演（田島右副） 17:00-17:30
17:30	一般講演 4件 （フラーレンの化学・フラーレンの応用・金属内包フラーレン） 17:30-18:30
18:30	懇親会 （多目的スペース） 18:30-20:30
20:30	

	3月5日（水）
	受付開始 8:30〜 講演開始 9:00〜
9:00	基調講演（Esko I. Kauppinen） 9:00-9:45
9:45	一般講演 3件 （ナノチューブの応用） 9:45-10:30
10:30	休憩 10:30-10:45
10:45	一般講演 4件 （グラフェンの応用） 10:45-11:45
11:45	昼食 11:45-13:00
13:00	ポスタープレビュー （ 3P-1 〜 3P-50 ） 13:00-14:00
14:00	ポスターセッション （多目的スペース） 14:00-15:45
15:45	特別講演（小林俊之） 15:45-16:15
16:15	一般講演 5件 （グラフェンの物性・グラフェンの応用・グラフェン生成） 16:15-17:30
17:30	

基調講演　発表40分・質疑5分
特別講演　発表25分・質疑5分
一般講演　発表10分・質疑5分
ﾎﾟｽﾀｰﾌﾟﾚﾋﾞｭｰ　発表1分・質疑なし

Time table

	March 3 (Mon.)
	Registration begins at 8:30 Lectures begin at 9:30
9:30	Plenary Lecture (Mikio Sasaki) 9:30–10:00
10:00	General Lectures [3] (Fullerenes・Endohedral metallofullerenes・ Applications of fullerenes) 10:00–10:45
10:45	Coffee Break 10:45–11:00
11:00	Special Lecture (Shinya Toyokuni)11:00–11:30
11:30	General Lectures [2] (Carbon nanoparticles・ Other topics) 11:30–12:00
12:00	Lunch (Administrative meeting) 12:00–13:15
13:15	Special Lecture (Keiji Ueno) 13:15–13:45
13:45	General Lectures [4] (Applications of graphene・ Properties of graphene) 13:45–14:45
14:45	Poster Preview (1P–1 through 1P–50) 14:45–15:45
15:45	Poster Session (Event Space) 15:45–17:30
17:30	Coffee Break 17:30–18:00
18:00	Tutorial Lecturer: Yutaka Ohno Nagoya University (Ito Hall) 18:00–19:30
19:30	

	March 4 (Tue.)
	Registration begins at 8:30 Lectures begin at 9:00
9:00	Special Lecture (Yan Li) 9:00–9:30
9:30	General Lectures [4] (Formation and purification of nanotubes) 9:30–10:30
10:30	Coffee Break 10:30–10:45
10:45	Special Lecture (Yoshikazu Homma)10:45–11:15
11:15	General Lectures [4] (Formation and purification of nanotubes ・Properties of nanotubes・ Applications of nanotubes) 11:15–12:15
12:15	Lunch 12:15–13:30
13:30	Award Ceremony 13:30–14:15
14:15	Poster Preview (2P–1 through 2P–50) 14:15–15:15
15:15	Poster Session (Event Space) 15:15–17:00
17:00	Special Lecture (Yusuke Tajima) 17:00–17:30
17:30	General Lectures [4] (Chemistry of fullerenes・ Applications of fullerenes・ Endohedral metallofullerenes) 17:30–18:30
18:30	Banquet (Event Space) 18:30–20:30
20:30	

	March 5 (Wed.)
	Registration begins at 8:30 Lectures begin at 9:00
9:00	Plenary Lecture (Esko I. Kauppinen) 9:00–9:45
9:45	General Lectures [3] (Applications of nanotubes) 9:45–10:30
10:30	Coffee Break 10:30–10:45
10:45	General Lectures [4] (Applications of graphene) 10:45–11:45
11:45	Lunch 11:45–13:00
13:00	Poster Preview (3P–1 through 3P–50) 13:00–14:00
14:00	Poster Session (Event Space) 14:00–15:45
15:45	Special Lecture (Toshiyuki Kobayashi) 15:45–16:15
16:15	General Lectures [5] (Properties of graphene・ Applications of graphene・ Graphene synthesis) 16:15–17:30
17:30	

Plenary Lecture: 40min (Presentation) + 5min (Discussion)
Special Lecture: 25min (Presentation) + 5min (Discussion)
General Lecture: 10min (Presentation) + 5min (Discussion)
Poster Preview: 1min (Presentation)

座長一覧

3月3日(月)　　　　（敬称略）

	時　　間	座　　長
基調講演（佐々木幹夫）	9:30 ～ 10:00	篠原　久典
一般講演	10:00 ～ 10:45	小久保　研
特別講演（豊國伸哉）	11:00～ 11:30	湯田坂　雅子
一般講演	11:30 ～ 12:00	湯田坂　雅子
特別講演（上野啓司）	13:15 ～ 13:45	齋藤　理一郎
一般講演	13:45 ～ 14:45	町田　友樹
ポスタープレビュー	14:45 ～ 15:45	佐藤　健太郎 野内　亮
チュートリアル（大野雄高）	18:00 ～ 19:30	丸山　茂夫

3月4日（火）

	時　　間	座　　長
特別講演(Yan Li)	9:00 ～ 9:30	丸山　茂夫
一般講演	9:30 ～ 10:30	千足　昇平
特別講演(本間芳和)	10:45 ～ 11:15	山本　貴博
一般講演	11:15 ～ 12:15	片浦　弘道
ポスタープレビュー	14:15 ～ 15:15	宮内　雄平 平野　篤
特別講演(田島右副)	17:00 ～ 17:30	松尾　豊
一般講演	17:30 ～ 18:30	松尾　豊

3月5日（水）

	時　　間	座　　長
基調講演(Esko I. Kauppinen)	9:00 ～ 9:45	大野　雄高
一般講演	9:45 ～ 10:30	吾郷　浩樹
一般講演	10:45 ～ 11:45	竹延　大志
ポスタープレビュー	13:00 ～ 14:00	宮田　耕充 長谷川　馨
特別講演(小林俊之)	15:45 ～ 16:15	高井　和之
一般講演	16:15 ～ 17:30	岡田　晋

3月3日（月）

基調講演　発表25分 ・ 質疑応答5分
特別講演　発表25分 ・ 質疑応答5分
一般講演　発表10分 ・ 質疑応答5分
ポスタープレビュー　発表1分 ・ 質疑応答なし

基調講演（9:30-10:00）

1S-1　企業の眼から見たナノカーボンの現状と将来展望　1
佐々木　幹夫

一般講演（10:00-10:45）
フラーレン ・ 金属内包フラーレン ・ フラーレンの応用

1-1　FIB-SEMによるC_{60}マイクロチューブとAAO膜接合界面の構造解析　9
＊宮澤 薫一, 下村 周一, 若原 孝次, 橘 勝

1-2　単原子内包フラーレンの光電子スペクトル　10
＊宮崎 隆文, 清野 友真, 野田 祥子, 八木 創, 篠原 久典, 日野 照純

1-3　チオフェン含有フラーレン誘導体を用いた有機薄膜太陽電池素子特性　11
＊林　達也, Lee Heaseong, Im Inseob, Lee Seungjoo, Jang Jin, Pac Chyongjin,　森山　広思

＞＞＞＞＞＞＞ 休憩（10:45-11:00）＜＜＜＜＜＜＜

特別講演（11:00-11:30）

1S-2　多層カーボンナノチューブにおいて中皮腫発がんに関わる重要因子について　2
豊國　伸哉

一般講演（11:30-12:00）
ナノ炭素粒子 ・ その他

1-4　爆轟法ナノダイヤモンドの分散：最近の成果　12
＊佐々木 修一, 山野井 亮子, 大澤 映二

1-5　複数段トラップ気相移動度測定装置の開発　13
＊菅井 俊樹, 廣芝 泰祐, 見上 仁奈子, 陣内 涼太

＞＞＞＞＞＞＞ 昼食（12:00-13:15）＜＜＜＜＜＜＜

特別講演（13:15-13:45）

1S-3　カルコゲナイド系層状物質の原子膜エレクトロニクス応用　3
上野　啓司

一般講演（13:45-14:45）
グラフェンの応用 ・ グラフェンの物性

1-6　Vertical transport in meal/2D crystal/graphene layered heterostructures　14
＊Yoshihisa Inoue, Takehiro Yamaguchi, Sei Morikawa, Satoru Masubuchi, Kenji Watanabe, Takashi Taniguchi, Rai Moriya, Tomoki Machida

1-7　Stabilities and Electronic Structures of Hexagonal Boron-Nitride Bilayers　15
＊Yoshitaka Fujimoto, Takashi Koretsune, Susumu Saito

3月3日（月）

1-8	Effect of Band Nesting on Optical Properties in Two-dimensional Transition Metal Dichalcogenides ＊小澤 大知, Rajeev Sharma Kumar, Alexandra Carvalho, Amara Kiran Kumar, Weijie Zhao, Minglin Toh, Ricardo Mendes Ribeiro, Antonio H. Castro Neto, 松田 一成, 江田 剛輝	16
1-9	ゲート電圧によるグラフェン端の光化学エッチングの制御 ＊野内 亮, 三苫 伸彦, 松本 守広	17

ポスタープレビュー（14:45-15:45）
ポスターセッション（15:45-17:30）　（☆）若手奨励賞候補
フラーレンの化学

1P-1	硫酸化フラーレンの分子軌道計算と理論的評価 ＊野地 直樹, 佐野 喜章, 井上 和美, 片岡 洋右, 緒方 啓典	43
1P-2	Excited State Electronic Interactions in Push–Pull-Chromophore–[60]Fullerene Conjugates * Michio Yamada, Francesca Tancini, Michael Sekita, Dirk M. Guldi, Mariza N. Alberti, W. Bernd Schweizer, François Diederich	44

フラーレンの応用

1P-3	C_{60}–C_{70}2成分ナノウィスカーの合成 ＊今野 俊生, 若原 孝次, 宮澤 薫一	45
1P-4	Transport Characteristics of Fullerene Nano-Whisker Field Effect Transistor using Ionic Liquid Gate * Naoto Toriumi, Yoshiaki Ito, Daiki Momiyama, Wataru Akiyama, Naoto Nakamura, Taishi Takenobu, Jonathan Bird, Yuichi Ochiai, Nobuyuki Aoki	46

金属内包フラーレン

1P-5 ☆	Photoinduced Charge Separation in Supramolecules between Lithium-ion-encapsulated PCBM Fullerene and Anionic Porphyrins ＊川島 雄樹, 大久保 敬, 岡田 洋史, 松尾 豊, 福住 俊一	47
1P-6	空フラーレンの分布からみた金属内包フラーレン生成メカニズムの研究 ＊小林 樹来, 兒玉 健, 藤田 渉, 菊地 耕一, 阿知波 洋次	48

フラーレン

1P-7	水分子を内包したC_{60}ダイマーのエネルギー論 ＊野村 和哉, 岡田 晋	49
1P-8 ☆	High-Resolution Transmission Electron Microscopic Study of Electron-Beam-Irradiated C_{60} Single Crystal Films * Hideki Masuda, Hidehiro Yasuda, Jun Onoe	50

ナノチューブの物性

1P-9	単層カーボンナノチューブ膜の電気伝導性におけるX線照射の影響 ＊荒木 拓馬, 村上 俊也, 木曽田 賢治, 伊東 千尋	51
1P-10 ☆	内部熱交換式反応器を用いたサブミリメータ長カーボンナノチューブの 流動層合成 ＊陳 忠明, 長谷川 馨, 金 東榮, 大沢 利男, 野田 優	52
1P-11	Coherent G-band phonons in single wall carbon nanotubes ＊アフマド ヌグラハ, エッドウィ ハスデオ, 齋藤 理一郎	53

3月3日（月）

1P-12 プロピルアミン存在下におけるSWNTsの光化学的挙動 54
＊前田　優, 蓮池 悠平, 山田 道夫, 長谷川 正, 赤阪 健

1P-13 ☆ 酸素ドープ単層カーボンナノチューブに対するその場フォトルミネッセンス分光電気化学 55
＊白石 智也, 秋月 直人, 宮内 雄平, 松田 一成, 中嶋 直敏

1P-14 Far-Infrared and THz Spectroscopy of Multi-Walled Carbon Nanotubes 56
Keijiro Sakai, Takahiro Morimoto, Toshiya Okazaki

1P-15 Prediction of Redox Potentials of Semiconducting Single-Walled Carbon Nanotubes 57
Gergely Juhasz, Yasuhiko Hirana, Naotoshi Nakashima

1P-16 ☆ Photoluminescence Spectroelectrochemistry of a Single SWNT Molecule 58
＊洪 流, 毛利 真一郎, 宮内 雄平, 松田 一成, 中嶋 直敏

1P-17 Electric Characterization of Chirality Controlled Single-Walled Carbon Nanotubes 59
＊津田 悠作, 相良 拓実, 吉田 圭佑, 石井 宏治, 山川 健一, 矢島 博文, 岩田 展幸, 山本 寛

ナノチューブの応用

1P-18 ☆ Hydrogen evolution from benzene with single-walled carbon nanotubes as a photocatalyst 60
＊高野 直樹, 大久保 敬, 福住 俊一

1P-19 フレキソ印刷プロセスによるカーボンナノチューブ薄膜トランジスタの高速製造技術−微細トップゲート素子の作製− 61
＊前田 迪彦, 樋口 健太郎, 岸本 茂, 中嶋 勇太, 外村 卓也, 武居 正史, 畑 克彦, 大野 雄高

1P-20 ☆ CNTトランジスタ動特性評価 62
＊殿内 規之, 遠藤 浩幸, 二瓶 史行, 沼田 秀昭, 横田 知之, 関谷 毅, 染谷 隆夫, 眞子 隆志

1P-21 遊星ボールミル・SPSを用いたAl-CNT複合体の作製及び特性評価 63
＊後藤 匠, 寺嶋 慶起, 関戸 大

1P-22 ☆ Multi-walled carbon nanotubes and carbon black supported platinum nanoparticles for catalyst of polymer electrolyte membrane fuel cells 64
Zehui Yang, Berber Mohamed, Tsuyohiko Fujigaya, Naotoshi Nakashima

1P-23 電界増強効果によるCNT薄膜電極から半導体薄膜への低電圧キャリア注入 65
＊山田 竜也, 岸本 茂, 大野 雄高

1P-24 Highly durable membrane electrode assembly consists of poly(vinylphosphonic acid)-polybenzimidazole electrolyte and carbon nanotubes based-electrocatalyst 66
Mohamed Berber, Tsuyohiko Fujigaya, Naotoshi Nakashima

1P-25 ☆ 単層カーボンナノチューブ／イオン液体ポリマーナノコンポジットの増強ゼーベック効果 67
＊中野 元博, 野々口 斐之, 中嶋 琢也, 河合 壯

1P-26 eDIPSの大量半金分離とTFTへの応用 68
藤井 俊治郎, 田中 丈士, 杉田 知子, 浅野 敏, 清宮 維春, 斎藤 毅, ＊片浦 弘道

ナノチューブの生成と精製

1P-27 2液相分離した単層カーボンナノチューブのラマン分光法による金属/半導体比評価 69
金澤 尚宜, ＊鈴木 信三, 田中 優, 山崎 昴, 宮崎 大輝, 小野 晶

1P-28 ☆ 小径SWCNTの単一カイラリティ分離と光物性 70
＊魏 小均, 伊藤 靖浩, 平川 琢也, 平野 篤, 藤井 俊治郎, 宮内 雄平, 松田 一成, 田中 丈士, 片浦 弘道

3月3日（月）

1P-29 短尺化カーボンナノチューブ作製に向けた金属ナノロッドの作製 71
＊佐田 貴生, 藤ヶ谷 剛彦, 中嶋 直敏

1P-30 Growth of single-walled carbon nanotube from fullerene seeds by chemical vapor deposition and in situ scanning electron microscopy observation 72
＊汪 華鋒, 山田 千悟, 加藤 大樹, 本間 芳和

1P-31 ☆ Rapid separation of high-purity and micrometer-long semiconducting carbon nanotubes by gel filtration 73
** Boanerges Thendie, Yasumitsu Miyata, Haruka Omachi, Ryo Kitaura, Yuhei Miyauchi, Kazunari Matsuda, Hisanori Shinohara*

1P-32 高温パルスアーク放電の圧力制御による二層カーボンナノチューブの効率的生成 74
＊菊地 隼斗, 寺田 勝英, 菅井 俊樹

1P-33 金属触媒Ni-Y－Moを用いた単層カーボンナノチューブ（SWNTs）の作製と評価 75
＊孫 博, 井上 栄, 鈴木 智子, 山本 隆之, 柳 智大, 安藤 義則

1P-34 FT-ICR質量分析器を用いた水および酸素とコバルトクラスターの化学反応の研究 76
＊戸張 雄太, 小笠原 一樹, 千足 昇平, 丸山 茂夫, 菅井 俊樹

内包ナノチューブ

1P-35 高配向・高密度カーボンナノチューブ膜へのカルボラン内包 77
＊藤田 隼, 乗松 航, 楠 美智子

1P-36 ☆ 固液界面接触アーク放電法による固相分離ステンレス合金内包カーボンナノチューブの生成 78
＊相良 拓也, 胡桃 聡, 松田 健一, 鈴木 薫

1P-37 透過電子顕微鏡法の為の高真空下におけるカーボンナノチューブ内部空間へのガス分子の封入法 79
＊小林 慶太, 斎藤 毅, 清宮 維春, 保田 英洋

ナノホーン

1P-38 Light-assisted in-situ polymer formation on carbon nanohorns 80
*Mei Yang, * Minfang Zhang, Masao Kunioka, Sumio Iijima, Masako Yudasaka*

1P-39 カーボンナノホーンに含まれるグラファイト様シート端部の選択的カルボキシル化 81
＊中村 真紀, 入江 路子, 弓削 亮太, 市橋 鋭也, 飯島 澄男, 湯田坂 雅子

グラフェン生成

1P-40 グラフェンのトポロジー制御された合成法 82
＊井上 長三

1P-41 ☆ エッチング析出法によるグラフェンの誘電体基板上直接合成 83
＊小坂 昌輝, 長谷川 馨, 野田 優

1P-42 固体原料としてテトラフェニルポルフィリンを用いた窒素ドープグラフェンのCVD成長 84
＊杉崎 祐真, 北浦 良, 大町 遼, 篠原 久典

1P-43 In situ doping of Electrochemical foliation- Mechanism 85
** Shang-Lin Tsai, Mario Hofmann, Ya-Ping Hsieh*

1P-44 ヘテロエピタキシャルCu上でのmmサイズのグラフェングレインのCVD成長 86
河原 憲治, 祝迫 佑, 辻 正治, ＊吾郷 浩樹

3月3日（月）

グラフェンの物性

1P-45 Quantum interference in a ballistic graphene *n-p-n* junction: from Fabry-Perot to edge channel interference 87
☆ *＊森川 生, 増渕 覚, 守谷 頼, 渡邊 賢司, 谷口 尚, 町田 友樹*

1P-46 単層遷移金属ダイカルコゲナイドにおける励起子消滅 88
＊小鍋 哲, 岡田 晋

1P-47 半導体グラフェンナノリボンの電子輸送におけるエッジラフネス効果 89
☆ *＊高島 健悟, 藤井 宏武, 山本 貴博*

その他

1P-48 単層WSe_2における偏光フォトルミネッセンスの温度依存性 90
☆ *＊周 利中, 宮内 雄平, 毛利 真一郎, トー ミンリン, 江田 剛輝, 松田 一成*

1P-49 単原子層遷移金属ダイカルコゲナイドにおける非線形発光 91
＊毛利 真一郎, 周 利中, 壷井 佑夏, 宮内 雄平, トー ミンリン, 小鍋 哲, 江田 剛輝, 岡田 晋, 松田 一成

1P-50 CVD法を用いて合成した単層MoS_2の発光測定 92
☆ *＊壷井 佑夏, 小澤 大知, 宮内 雄平, 毛利 真一郎, 松田 一成*

＞＞＞＞＞＞＞ 休憩（17:30-18:00）＜＜＜＜＜＜＜

チュートリアル（18:00-19:30）

カーボンナノチューブ薄膜のエレクトロニクス応用
大野 雄高

3月4日（火）

特別講演　　発表25分　・　質疑応答5分
一般講演　　発表10分　・　質疑応答5分
ポスタープレビュー　　発表1分　・　質疑応答なし

特別講演（9:00-9:30）

2S-4　Structure and Property Controlled Growth of Single-Walled Carbon Nanotubes on Substrates　4
** Yan Li, Feng Yang, Xiaojun Qin, Fei Peng, Juan Yang*

一般講演（9:30-10:30）
ナノチューブの生成と精製

2-1　単層カーボンナノチューブ成長と触媒反応の分子シミュレーション　18
＊久間 馨, 川鈴木 智哉, 野口 拓哉, 千足 昇平, 多田 朋史, 丸山 茂夫

2-2　半導体CNTの選択的成長とトランジスタ特性　19
＊桜井 俊介, 山田 真保, 中村 紘子, フタバドン, 畠 賢治

2-3　Low-temperature catalyst activator: Mechanism study of CNT forest densification by “STEP” growth method using synchrotron radiation　20
*Akito Takashima, Yudai Izumi, Eiji Ikenaga, Takuo Ohkochi, Masato Kotsugi, Tomohiro Matsushita, * Takayuki Muro, Akio Kawabata, Tomo Murakami, Mizuhisa Nihei, Naoki Yokoyama*

2-4　(5,5)および(6,5)カーボンナノチューブの成長機構　21
＊阿知波 洋次, 兒玉 健, 橋本 健朗, 城丸 春夫

＞＞＞＞＞＞＞ 休憩（10:30-10:45）＜＜＜＜＜＜＜

特別講演（10:45-11:15）

2S-5　カーボンナノチューブの水との相互作用　5
＊本間 芳和, 千足 昇平, 山本 貴博

一般講演（11:15-12:15）
ナノチューブの生成と精製 ・ナノチューブの物性 ・ナノチューブの応用

2-5　脱着可能な超分子型可溶化剤による半導体性カーボンナノチューブの高純度精製　22
＊利光 史行, 中嶋 直敏

2-6　The effect of DNA adsorption on optical transitions in single-walled carbon nanotube　23
＊伊藤 雅浩, 伊藤 悠介, 二井 大輔, 梅村 和夫, 加藤 大樹, 本間 芳和

2-7　ゲルを用いた単層カーボンナノチューブの半金分離のメカニズム　24
＊平野 篤, 田中 丈士, 片浦 弘道

2-8　半導体単層カーボンナノチューブアレイ作製に向けた有機薄膜中の全長ブレイクダウン　25
＊大塚 慶吾, 井ノ上 泰輝, 千足 昇平, 丸山 茂夫

＞＞＞＞＞＞＞ 昼食（12:15-13:30）＜＜＜＜＜＜＜

3月4日（火）

大澤賞･飯島賞･若手奨励賞の授賞式（13:30-14:15）

ポスタープレビュー（14:15-15:15）
ポスターセッション（15:15-17:00）　（☆）若手奨励賞候補

フラーレンの化学

2P-1　^{2}H NMR分光法による水酸化フラーレン固体の分子ダイナミクスの評価　93
＊佐野 喜章, 馬場 啓輔, 緒方 啓典

2P-2　ケトラクタム構造をもつ新しい開口C_{60}誘導体の合成　94
☆　*＊橋川 祥史, 村田 理尚, 若宮 淳志, 村田 靖次郎*

フラーレンの応用

2P-3　A Novel Ligand-free ZnO Particle for Fullerene:Polymer Inverted Organic Solar Cell　95
＊IL Jeon, James Ryan, Kee Sheng Yeo, Tafu Nakazaki, Yuichi Negishi, Yutaka Matsuo

2P-4　有機薄膜太陽電池への応用に向けたコバルトジチオレンフラーレン錯体の合成　96
＊小汲 佳祐, 中川 貴文, 松尾 豊

2P-5　C_{60}薄膜への光渦照射による光重合体の表面特性　97
＊穐山 航, 籾山 大輝, 鳥海 直人, 仲村 直人, 宮本 克彦, 尾松 孝茂, Jonathan P Bird , 落合 勇一, 青木 伸之

金属内包フラーレン

2P-6　Extraction and Isolation of Missing Small-Bandgap Metallofullerenes through Exterior Functionalization　98
☆　*＊王 志永, 中西 勇介, 野田 祥子, 丹羽 宏之, 张 锦英, 北浦 良, 篠原 久典*

2P-7　Supercapacitor using Lithium-Ion Endohedral Metallofullerene　99
＊Eunsang Kwon, Ken-ichirou Komatsu, Yoichi Yamada, Yuri Hasegawa, Sho Sato, Seiji Sakai, Kazuhiko Kawachi, Kuniyoshi Yokoo, Shoichi Ono, Yasuhiko Kasama, Shinobu Aoyagi, Tomoaki Endo, Tomoyuki Ogawa, Migaku Takahashi

フラーレン

2P-8　電界による十重付加体C_{60}のスピン制御　100
＊成田 康平, 岡田 晋

2P-9　C_{32}ポリマーの安定構造と電子状態　101
☆　*＊丸山 実那, 岡田 晋*

ナノチューブの物性

2P-10　X線照射による単層カーボンナノチューブの電子構造変化　102
＊村上 俊也, 山本 勇樹, 松田 充晃, 木曽田 賢治, 西垣 宏, 蓮池 紀幸, 播磨 弘, 伊東 千尋

2P-11　単層カーボンナノチューブにおけるフォノンの非調和効果　103
＊水野 将志, 齋藤 理一郎

2P-12　SWNT表面上でのコール酸ナトリウムとDNAの置換反応の解析　104
☆　*＊續 明子, 中嶋 直敏*

3月4日（火）

2P-13 Chirality Dependence of Quantum Thermal Transport in Carbon Nanotubes at Low Temperatures: A First-Principles Study 105
＊畑 智行, 河合 宏樹, 大戸 達彦, 山下 晃一

2P-14 単層カーボンナノチューブに内包させたアントラキノンのリチウムイオン電池電極特性 106
＊川崎 晋司, 松浦 智拓, 田代 広祐, Song Hayong

2P-15 ☆ 水蒸気雰囲気下SWNTのRBM振動数の直径依存性 107
＊本間 直樹, 千足 昇平, 本間 芳和, 山本 貴博

2P-16 PL分光法を用いたカーボンナノチューブ上におけるDNA構造変化のセンシング 108
＊伊藤 悠介, 伊藤 雅浩, 二井 大輔, 加藤 大樹, 梅村 和夫, 本間 芳和

2P-17 Observation of a gate-induced photoluminescence peak in individual carbon nanotubes 109
＊Yuto Ueda, Masahiro Yoshida, Akihiro Ishii, Takushi Uda, Yuichiro K. Kato

2P-18 体積率を変えた垂直配向SWNT膜の伝熱特性 110
＊車 振赫, 長谷川 馨, 千足 昇平, 三浦 飛鳥, イ ジョンユン, ワードル ブライアン, 野田 優, 塩見 淳一郎, 丸山 茂夫

ナノチューブの応用

2P-19 ☆ 半絶縁性シリコンカーバイド上の高密度カーボンナノチューブフォレストの面内電導 111
＊稲葉 優文, 李 智宇, 鈴木 和真, 渋谷 恵, 平岩 篤, 増田 佳穂, 乗松 航, 楠 美智子, 川原田 洋

2P-20 n型単層カーボンナノチューブの作製と熱電発電シートへの展開 112
＊野々口 斐之, 大橋 賢次, 河合 壯

2P-21 ☆ カーボンナノチューブ/シリコンカーバイド界面の接触抵抗及びSchottky障壁高さの評価 113
＊鈴木 和真, 稲葉 優文, 渋谷 恵, 李 智宇, 明道 三穂, 平岩 篤, 増田 佳穂, 乗松 航, 楠 美智子, 川原田 洋

2P-22 高純度半導体型単層カーボンナノチューブネットワークを用いた赤外線センサー 114
＊工藤 光, 加治 聖也, 河合 英輝, 竹延 大志, 柳 和宏

2P-23 ☆ プラスチック基板上に作製したカーボンナノチューブ集積回路の動作速度向上 115
＊三善 利忠, カスケラ アンティ, ライホ パトリック, ナシブリン アルバート, 岸本 茂, カウピネン エスコ, 大野 雄高

2P-24 空間選択Cs内包SWNTs薄膜によるpnホモ接合の光起電力特性 116
＊安彦 嘉浩, 加藤 俊顕, 赤間 俊紀, 畠山 力三, 金子 俊郎

2P-25 ☆ 金属性、半導体性単層カーボンナノチューブへの分子認識 117
＊黄 文シン, 藤ヶ谷 剛彦, 中嶋 直敏

2P-26 High Photovoltaic Performance of MoO_3-doped Single-walled Carbon Nanotube/Si Solar Cells 118
＊Feijiu Wang, Daichi Kozawa, Yuhei Miyauchi, Shinichiro Mouri, Yutaka Ohno, Kazunari Matsuda

2P-27 Solubility control of SWCNTs by using photofunctional dispersants 119
＊松澤 洋子, 高田 裕子, 木原 秀元, 吉田 勝

3月4日（火）

ナノチューブの生成と精製

2P-28 触媒担持方法としてディップコート法を用いたCNTの生成 120
＊藤井 恵介, 安藤 義則, 大河内 正人

2P-29 フラビン誘導体およびイソアロキサジン誘導体による単層カーボンナノチューブのカイラリティ選択的可溶化 121
☆ *＊福澤 将史, 利光 史行, 加藤 雄一, 中嶋 直敏*

2P-30 結晶鋳型法による金属型/半導体型SWCNTs高配向集合体の自己組織形成 122
＊河合 英輝, 長谷川 凱, 内藤 泰久, 高木 勇樹, 和田 義史, 竹延 大志, 柳 和宏

2P-31 混合界面活性剤を用いたゲルカラムクロマトグラフィーにおける単層カーボンナノチューブの構造選択的脱着 123
☆ *＊蓬田 陽平, 都築 真由美, 平野 篤, 藤井 俊治郎, 田中 丈士, 片浦 弘道*

2P-32 FT-ICRによるCoクラスターへのアセトニトリル吸着反応分析 124
＊小笠原 一樹, 戸張 雄太, 千足 昇平, 菅井 俊樹, 丸山 茂夫

内包ナノチューブ

2P-33 Synthesis and TEM-based Structural Characterization of C_{60}-Flattened CNT Nanopeapods 125
☆ ** Qing Wang, Ryo Kitaura, Yuta Yamamoto, Shigeo Arai, Hisanori Shinohara*

2P-34 カーボンナノチューブ内部での複数チオフェンオリゴマーの配向に関する密度汎関数法計算 126
＊湯村 尚史, 山下 裕生

2P-35 多環芳香族炭化水素分子を内包したカーボンナノチューブのエネルギー論と電子状態 127
☆ *＊木暮 聖太, 岡田 晋*

ナノホーン

2P-36 標的光温熱がん治療を目指したカーボンナノホーンの機能化 128
＊張 民芳, 楊 梅, 丁 武孝, 飯島 澄男, 湯田坂 雅子

2P-37 炭素被覆したグラファイト/気相成長炭素繊維/カーボンナノホーン複合体を使ったリチウムイオン電池の急速充放電特性 129
＊弓削 亮太, 田村 宜之, 眞子 隆志, 中野 嘉一郎, 中原 謙太郎

ナノワイヤー

2P-38 カーボンナノスペースを用いたヨウ化銀ナノワイヤの合成と構造解析 130
＊成瀬 しほの, 北浦 良, 野田 優, 篠原 久典

グラフェン生成

2P-39 High-yielding synthesis of graphene by supuercritical fluid 131
＊岡 伸人, 笘居 高明, 本間 格

2P-40 Fabrication of wide terraces on SiC (0001) for pit-free graphene growth in Ar atmosphere 132
☆ ** Wang Chenxing , Hitoshi Nakahara, Koji Asaka, Yahachi Saito*

2P-41 *In situ* observation of graphene formation on polycrystalline Cu 133
** Huafeng Wang, Pei Zhao, Shohei Chiashi, Shigeo Maruyama, Yoshikazu Homma*

2P-42 窒素雰囲気下で形成されるグラフェン/SiCの界面構造 134
☆ *＊増田 佳穂, 乗松 航, 楠 美智子*

3月4日（火）

2P-43 アンジップ2層カーボンナノチューブを成長核とした多層グラフェンナノリボンの形成 135
＊北川 治樹, 根岸 良太, 田中 啓文, 福森 稔, 小川 琢治, 小林 慶裕

グラフェンの応用

2P-44 WSe_2薄膜を用いたフレキシブルトランジスタとインバータ 136
☆ *＊Kazuma Funahashi, Jiang Pu, Lain-Jong Li, Yoshihiro Iwasa, Taishi Takenobu*

2P-45 高密度・高配向グラフェンナノリボンの化学修飾によるドーピング制御 137
＊Solís-Fernández Pablo, Bissett Mark , 辻 正治, 吾郷 浩樹

グラフェンの物性

2P-46 酸化グラフェンの発光機構 138
＊横井 裕之, 谷口 貴章, 鯉沼 陸央, 松本 泰道

2P-47 酸化グラフェンにおける近赤外発光機構 139
☆ *＊小澤 大知, 宮内 雄平, 毛利 真一郎, 市田 正夫, 松田 一成*

2P-48 2層グラフェンの層間の水分子の分子動力学シミュレーション 140
＊齋藤 理一郎, 水野 将志

その他

2P-49 ガス中グラファイトレーザーアブレーションによるフラーレンとポリインの生成 141
＊阿部 百合香, 遠藤 瞳, 阿知波 洋次, 城丸 春夫

2P-50 ポリイン分子の禁制遷移における振電相互作用の研究 142
＊若林 知成

特別講演（17:00-17:30）

2S-6 フラーレン酸化物の合成、構造および求核置換反応 6
田島 右副

一般講演（17:30-18:30）
フラーレンの化学 ・ フラーレンの応用 ・ 金属内包フラーレン

2-9 スピロアセタール化フラーレンの環立体配座におけるアノマー効果 26
＊小久保 研, 山﨑 優, 増田 寛之, 伊熊 直彦

2-10 バルクヘテロジャンクション型有機薄膜太陽電池における優れたN型半導体材料を志向したスピロアセタールおよびチオアセタールフラーレンの太陽電池特性評価 27
＊三木江 翼, 佐伯 昭紀, 増田 寛之, 伊熊 直彦, 小久保 研, 関 修平

2-11 $[Li@C_{60}](PF_6)$の誘電的相転移 28
＊青柳 忍, 杉本 邦久, 岡田 洋史, 星野 哲久, 芥川 智行

2-12 リチウムイオン内包フラーレンとポルフィリノイドの超分子錯体の光電子移動反応と光電変換特性 29
＊大久保 敬, 川島 雄樹, 酒井 隼人, 羽曾部 卓, Sastre-Santos Angela , 福住 俊一

３月５日（水）

基調講演　　発表４０分 ・ 質疑応答５分
特別講演　　発表２５分 ・ 質疑応答５分
一般講演　　発表１０分 ・ 質疑応答５分
ポスタープレビュー　　発表１分 ・ 質疑応答なし

基調講演（9:00-9:45）

3S-7 Floating catalyst CVD synthesis of SWNTs for thin film electronics applications 7
Esko I. Kauppinen

一般講演（9:45-10:30）
ナノチューブの応用

3-1 湿式紡糸法により作製した高い導電率を有するポリマーフリーカーボンナノチューブ線 30
＊向 健, 安積 欣志, 村上 俊也, 伊東 千尋, 斎藤 毅, 湯村 守雄

3-2 軽量･高性能･低コストな電気化学キャパシタ電極を目指した カーボンナノチューブ3次元集電体の開発 31
＊キンテーロ リカルド, 金 東榮, 長谷川 馨, 山田 裕貴, 山田 淳夫, 野田 優

3-3 Green, scalable, binderless fabrication of a single-wall carbon nanotube nonwoven fabric based on an ancient Japanese paper process 32
＊小橋 和文, 平林 達也, 阿多 誠介, 山田 健郎, フタバドン, 畠 賢治

＞＞＞＞＞＞＞ 休憩（10:30-10:45）＜＜＜＜＜＜＜

一般講演（10:45-11:45）
グラフェンの応用

3-4 SiO_2/Si上グラフェンナノリボンの電子伝導特性についての大規模第一原理計算 33
＊實宝 秀幸, 尾崎 泰助, 大淵 真理

3-5 インターカレーションしたCVD合成多層グラフェンの分析 34
＊近藤 大雄, 中野 美尚, 周 波, 井 亜希子, 林 賢二郎, 山口 淳一, 高橋 慎, 佐藤 信太郎, 横山 直樹

3-6 Graphene as a Material for Next Generation Fuel Cells 35
** Stephen Lyth, Jianfeng Liu, Thomas Bayer, Sean Bishop, Kazunari Sasaki*

3-7 Graphene enabled micromechanical switches 36
** Shao-Wei Ma, Ya-Ping Hsieh*

＞＞＞＞＞＞＞ 昼食（11:45-13:00）＜＜＜＜＜＜＜

ポスタープレビュー（13:00-14:00）
ポスターセッション（14:00-15:45）　　（☆） 若手奨励賞候補
フラーレンの化学

3P-1 Thermal Bis-silylation, Carbosilylation, and Bis-germylation of Fullerenes 143
＊稲葉 大樹, 南 和也, 宮部 恭輔, 飯田 亮介, 加固 昌寛, 前田 優, 山田 道夫, 長谷川 正, 赤阪 健

3P-2 新規バルクヘテロ接合型有機薄膜太陽電池への応用を視野に入れたフラーレン誘導体の開発 144
＊徳冨 尚志, 関戸 大

3月5日（水）

金属内包フラーレン

3P-3 超原子型リチウム内包フラーレンの電解合成 145
☆ *＊上野 裕, 伊熊 直彦, 大久保 敬, 森山 広, 福住 俊一, 小久保 研*

3P-4 反応系中でのトリフルオロメチル化による小さなバンドギャップを有する金属内包フラーレン$Gd@C_{60}$の分離 146
＊丹羽 宏之, 中西 勇介, 王 志永, 北浦 良, 大町 遼, 篠原 久典

ナノチューブの物性

3P-5 Spontaneous exciton dissociation in carbon nanotubes 147
*Yusuke Kumamoto, Masahiro Yoshida, Akihiro Ishii, Akio Yokoyama, * Takashi Shimada, Yuichiro K. Kato*

3P-6 Quantum interference effect in Raman spectra of metallic nanotubes and graphene 148
＊ハスデオ エッドウイ, ヌグラハ アフマド, 齋藤 理一郎

3P-7 単層カーボンナノチューブにおけるアップコンバージョン発光の観測 149
☆ *＊秋月 直人, 宮内 雄平, 毛利 真一郎, 松田 一成*

3P-8 電荷蓄積された欠陥を有するCNTの電子状態 150
＊石山 佑, 岡田 晋

3P-9 単層カーボンナノチューブの蛍光およびラマンスペクトルにおける金属蒸着効果 151
＊小竿 明彦, 千足 昇平, 山口 元太, 本間 芳和

3P-10 ^{13}Cを濃縮した単層カーボンナノチューブにおけるNMR測定 152
☆ *＊芦田 昇, 中井 祐介, 宮田 耕充, 真庭 豊, 斉藤 毅*

3P-11 Numerical study of electronic states in double-walled carbon nanotubes ---Formation of metallic bands by covalent bridge between tubes--- 153
** Yuhei Natsume*

3P-12 Electronic Structure of Carbon and BN Nanotubes: A Comparative First Principles Study 154
** Yuya Uchida, Takashi Koretsune, Susumu Saito*

3P-13 Photoconductivity spectroscopy of individual suspended carbon nanotubes 155
** Takushi Uda, Yusuke Kumamoto, Masahiro Yoshida, Akihiro Ishii, Yuichiro K. Kato*

ナノチューブの応用

3P-14 環境負荷の小さい水溶性ナノチューブ合成法 156
ラーマン モハマド ジェルール, ＊三重野 哲

3P-15 ACCVD法を用いた多孔質ガラス(PG)板材への単層カーボンナノチューブ作成の試み 157
長尾 杏平, ＊鈴木 信三, 大上 真司, 伊藤 洋介, 長澤 浩, 阿知波 洋次

3P-16 単層カーボンナノチューブバンドルの溝を認識する分子 158
＊藤ヶ谷 剛彦, ユ ジョンテ, 中嶋 直敏

3P-17 化学修飾したMWNT/PA6ナノコンポジットの開発と特性評価 159
＊村岡 慶美, 佐藤 宏紀, 関戸 大

3P-18 Printed SWCNT thin film CMOS inverters based on chemically doped ion gels 160
☆ *＊和田 義史, 狗飼 良太, 藤本 太陽, 濱畑 裕紀, 松崎 怜樹, 柳 和宏, 竹延 大志*

3月5日（水）

3P-19 光照射により生じるベンジルラジカル誘導体による多層カーボンナノチューブの表面修飾 161
＊高田 知哉, バトブヤン ムンフォド, 阿部 薫明

3P-20 ☆ ”Laminated” ion-gel film as high capacitance insulator for carbon-nanotube transistor 162
＊Taiyo Fujimoto, Ryo Shimizu, Yuki Takagi, Yoshifumi Wada, Kazuhiro Yanagi, Taishi Takenobu

3P-21 Polyglycerol-functionalized single-walled carbon nanotubes for drug loading and delivery 163
＊Qin Hongmei, Li Zhao, Keisuke Nakamura, Takahide Kimura, Naoki Komatsu

3P-22 ☆ フレキシブルエレクトロニクスを目指したカーボンナノチューブの簡易なロスフリー印刷技術 164
＊白江 宏之, 金 東榮, 長谷川 馨, 野田 優

3P-23 Chemical Vapor Deposition of MoS_2 on Carbon Nanotube for Organic Thin Film Solar Cells 165
＊IL JEON, Dai Kutsuzawa, Yu Hashimoto, Takashi Yanase, Taro Nagahama, Toshihiro Shimada, Yutaka Matsuo

3P-24 ベルト型共役高分子のSWCNTのラッピングによる高度可溶化 166
＊佐川 弥, 高橋 正洋, 岸川 圭希, 幸本 重男

ナノチューブの生成と精製

3P-25 薄膜トランジスタ応用に向けたDNA修飾カーボンナノチューブのカイラリティ分離 167
＊桑原 有紀, 二瓶 史行, 大森 滋和, 斎藤 毅

3P-26 ☆ パルスプラズマCVDによる高純度(6,5)単層カーボンナノチューブ合成におけるパルス効果 168
＊許 斌, 加藤 俊顕, 村越 幸史, 金子 俊郎

3P-27 モノアルキル鎖含有ポリフルオレンによる太い半導体性単層カーボンナノチューブの選択的抽出 169
＊福丸 貴弘, 利光 史行, 藤ヶ谷 剛彦, 中嶋 直敏

3P-28 チューブ端からの単層CNTのクローニング成長 170
＊海野 貴徳, 井ノ上 泰輝, 千足 昇平, 丸山 茂夫

3P-29 ☆ 熱伝導材料応用に向けた高密度カーボンナノチューブ垂直配向膜の合成 171
＊羅 ヌリ, 長谷川 馨, 野田 優

3P-30 Selective Growth of Single-Walled Carbon Nanotubes with Specific Diameter and Chirality by Irradiating Free Electron Laser during Growth 172
＊吉田 圭佑, 相良 拓実, 津田 悠作, 石井 宏治, 山川 健一, 矢島 博文, 岩田 展幸, 山本 寛

内包ナノチューブ

3P-31 ☆ 単層カーボンナノチューブにおける物質内包によるゼーベック係数の制御 173
＊上田 智大, 中井 祐介, 宮田 耕充, 真庭 豊

3P-32 分子動力学計算によるチオフェンオリゴマー内包単層カーボンナノチューブの分子配向 174
＊田畑 裕夢, 関根 亮紀, 井上 和美, 片岡 洋佑, 緒方 啓典

グラフェン生成

3P-33 ☆ グラフェンの化学反応性における成長基板の影響 175
＊井上 凌介, 宮田 耕充, 真庭 豊

3P-34 Synthesis and Characterization of Metal Intercalated bilayers Graphene 176
＊今井 健太郎, 松木 国治, 佐藤 祥吾, 岩田 展幸, 山本 寛

3P-35 Cu(100)表面上でのグラフェンナノリボンのCVD成長 177
☆ * Mohamad Yunus Rozan , 宮下 雅大, 辻 正治, 日比野 浩樹, 吾郷 浩樹

3P-36 トリフェニレン誘導体によるグラファイトからグラフェンの液相剥離 178
＊船橋 竜介, 劉 剛, 青沼 秀児, 木村 隆英, 小松 直樹

3P-37 急速加熱プラズマCVDによるNiナノバーからのグラフェンナノリボン合成におけるプラズマ効果 179
☆ ＊鈴木 弘朗, 加藤 俊顕, 金子 俊郎

3P-38 Influence of electrolyte concentration for electrochemical exfoliation of graphene 180
＊沖本 治哉, 黒沼 寛紀, 佐野 正人

グラフェンの応用

3P-39 遷移金属ダイカルコゲナイドを用いた高ゲインCMOSインバータ 181
☆ ＊蒲 江, Huang Jing-Kai, 岩佐 義宏, Li Lain-Jong , 竹延 大志

3P-40 High efficiency graphene doping 182
* Kai-Wen Cheng, Po-shin Lin, Ya-Ping Hsieh

グラフェンの物性

3P-41 サイズ分離されたグラフェン量子ドットにおける劇的な発光特性の変化 183
＊冬野 直人, 小澤 大知, 宮内 雄平, 毛利 真一郎, 北浦 良, 篠原 久典, 保田 德, 小松 直樹, 松田 一成

3P-42 グラフェン端のエネルギー論と電子状態 184
☆ ＊山中 綾香, 岡田 晋

3P-43 グラファイト状カーボンの酸化度の精密制御 185
仁科 勇太, ＊森本 直樹

ナノ炭素粒子

3P-44 Structural and magnetic changes of nanodiamond-copper composites during HPHT Sintering Process 186
Fedor Shakhov, Vladimir Osipov, Sergei Kidalov, * Kazuyuki Takai, Toshiaki Enoki, Alexander Vul’

3P-45 カーボンナノマテリアル上に担持されたPt, Pt-Ru粒子の合成と特性評価 187
＊早瀬 勝平, 吉竹 晴彦, 王 志朋, 緒方 啓典

3P-46 Hydration of Nanodiamond Surface Revisited : Intercalation Hypothesis 188
＊山野井 亮子, Amanda Barnard, 佐々木 修一, 大澤 映二

その他

3P-47 自己組織化した界面活性剤表面での金属硝酸塩水和物の縮合を利用した酸化鉄ナノチューブへの亜鉛ドープ 189
＊小杉 優太, 坂東 俊治

3P-48 鉄微粉末を使用したカーボンナノコイルのシート状合成物表面への高純度合成および不純物の低減 190
☆ ＊清水 慶明, 丸山 皓司, 飯田 哲生, 須田 善行, 田上 英人, 滝川 浩史, 植 仁志, 清水 一樹, 梅田 良人

3月5日（水）

3P-49 遷移金属ダイカルコゲナイドにおける二次元半導体ヘテロ接合の合成と評価 191
☆ *＊森 勝平, 宮田 耕充, 真庭 豊*

3P-50 MoS_2—単層カーボンナノチューブ複合薄膜の電気化学特性 192
遠藤 秀晃, ＊河合 英輝, 長谷川 凱, 加治 聖也, 柳 和宏

特別講演（15:45-16:15）

3S-8 ソニーにおけるグラフェン研究開発　－溶液プロセスによるTFTとCVDによる透明導電膜－ 8
小林 俊之

一般講演（16:15-17:30）
グラフェンの物性　・ グラフェンの応用　・ グラフェン生成

3-8 積層構造がねじれた2層グラフェンにおけるGバンド強度増大の角度依存性 37
＊佐藤 健太郎, 齋藤 理一郎

3-9 含窒素グラフェンのX線光電子分光分析 38
＊山田 泰弘, キム ジョンピル, 松尾 晋太郎, 佐藤 智司

3-10 液相成長法により石英基板上の微細穴内に形成されたグラフェン膜の光学・ラマン分光による解析 39
＊日浦 英文

3-11 Novel transfer method for clean and high mobility CVD graphene 40
*Ya-Ping Hsieh, Mario Hofmann, * Bo-Suei Chiang*

3-12 Mechanism and impact of ad-layer formation on CPCVD graphene 41
** Yi-Wen Wang, Ya-Ping Hsieh, Mario Hofmann*

March 3rd, Mon.

Plenary Lecture: 25min (Presentation) + 5min (Discussion)
Special Lecture: 25min (Presentation) + 5min (Discussion)
General Lecture: 10min (Presentation) + 5min (Discussion)
Poster Preview: 1min (Presentation)

Plenary Lecture（9:30–10:00）

1S–1 Current Status and Vision of Fullerene Business in Mitsubishi Corporation 1
Mikio Sasaki

General Lecture（10:00–10:45）
Fullerenes ・ Endohedral metallofullerenes ・ Applications of fullerenes

1–1 Structural analysis of C_{60} microtube-AAO membrane joint interfaces by FIB-SEM 9
** Kun'ichi Miyazawa, Shuichi Shimomura, Takatsugu Wakahara, Masaru Tachibana*

1–2 Photoelectron Spectra of Encapsulated Mono-metal fullerenes 10
** Takafumi Miyazaki, Yuuma Seino, Shoko Noda, Hajime Yagi, Hisanori Shinohara, Shojun Hino*

1–3 Organic Photovoltaic Device Characteristics using Fullerene Derivatives with a Thiophene Moiety 11
** Tatsuya Hayashi, Heaseong Lee, Inseob Im, Seungjoo Lee, Jin Jang, Chyongjin Pac, Hiroshi Moriyama*

＞＞＞＞＞＞＞ Coffee Break（10:45–11:00）＜＜＜＜＜＜＜

Special Lecture（11:00–11:30）

1S–2 Critical factors in multi-walled carbon nanotubes in mesothelial carcinogenesis 2
Shinya Toyokuni

General Lecture（11:30–12:00）
Carbon nanoparticles ・ Other topics

1–4 Dispersion of detonation nanodiamond: A progress report 12
** Shuichi Sasaki, Ryoko Yamanoi, Eiji Osawa*

1–5 Development of Ion Mobility System with Multi-stage Ion Trap 13
** Toshiki Sugai, Yasuhiro Hiroshiba, Ninako Mikami, Ryota Jinnouchi*

＞＞＞＞＞＞＞ Lunch Time（12:00–13:15）＜＜＜＜＜＜＜

Special Lecture（13:15–13:45）

1S–3 Application of layered chalcogenide materials to the aomic-layer electronics 3
Keiji Ueno

General Lecture（13:45–14:45）
Applications of graphene ・ Properties of graphene

1–6 Vertical transport in meal/2D crystal/graphene layered heterostructures 14
** Yoshihisa Inoue, Takehiro Yamaguchi, Sei Morikawa, Satoru Masubuchi, Kenji Watanabe, Takashi Taniguchi, Rai Moriya, Tomoki Machida*

March 3rd, Mon.

1-7 Stabilities and Electronic Structures of Hexagonal Boron-Nitride Bilayers 15
** Yoshitaka Fujimoto, Takashi Koretsune, Susumu Saito*

1-8 Effect of Band Nesting on Optical Properties in Two-dimensional Transition Metal Dichalcogenides 16
** Daichi Kozawa, Rajeev Sharma Kumar, Alexandra Carvalho, Amara Kiran Kumar, Weijie Zhao, Minglin Toh, Ricardo Mendes Ribeiro, Antonio H. Castro Neto, Kazunari Matsuda, Goki Eda*

1-9 Gate-controlled ultraviolet photo-etching of graphene edges 17
** Ryo Nouchi, Nobuhiko Mitoma, Morihiro Matsumoto*

Poster Preview (14:45–15:45)
Poster Session (15:45–17:30) (☆)Candidates for the Young Scientist Poster Award
Chemistry of fullerenes

1P-1 Semiempirical molecular orbital estimation of the relative stability of sulfated fullerene 43
** Naoki Noji, Yosiaki Sano, Kazumi Inoue, Yosuke Kataoka, Hironori Ogata*

1P-2 Excited State Electronic Interactions in Push–Pull-Chromophore–[60]Fullerene Conjugates 44
** Michio Yamada, Francesca Tancini, Michael Sekita, Dirk M. Guldi, Mariza N. Alberti, W. Bernd Schweizer, François Diederich*

Applications of fullerenes

1P-3 Synthesis of C_{60}-C_{70} Two-Component Fullerene Nanowhiskers 45
** Toshio Konno, Takatsugu Wakahara, Kun'ichi Miyazawa*

1P-4 Transport Characteristics of Fullerene Nano-Whisker Field Effect Transistor using Ionic Liquid Gate 46
** Naoto Toriumi, Yoshiaki Ito, Daiki Momiyama, Wataru Akiyama, Naoto Nakamura, Taishi Takenobu, Jonathan Bird, Yuichi Ochiai, Nobuyuki Aoki*

Endohedral metallofullerenes

1P-5 Photoinduced Charge Separation in Supramolecules between Lithium-ion-encapsulated PCBM Fullerene and Anionic Porphyrins 47
☆ ** Yuki Kawashima, Kei Ohkubo, Hiroshi Okada, Yutaka Matsuo, Shunichi Fukuzumi*

1P-6 Formation mechanism of metallofullerenes suggested by the distribution of empty fullerenes 48
** Tatsuki Kobayashi, Takeshi Kodama, Wataru Fujita, Koichi Kikuchi, Yohji Achiba*

Fullerenes

1P-7 Energetics of water molecules encapsulated into C_{60} dimer 49
** Kazuya Nomura, Susumu Okada*

1P-8 High-Resolution Transmission Electron Microscopic Study of Electron-Beam-Irradiated C_{60} Single Crystal Films 50
☆ ** Hideki Masuda, Hidehiro Yasuda, Jun Onoe*

Properties of nanotubes

1P-9 X-ray irradiation effect on the electric conductivity of single-walled carbon nanotube films 51
** Takuma Araki, Toshiya Murakami, Kenji Kisoda, Chihiro Itoh*

March 3rd, Mon.

1P-10 Fluidized Bed CVD of Submillimeter-Long Carbon Nanotubes Using an Internal Heat-Exchange Reactor 52
☆ _* Zhongming CHEN, Kei HASEGAWA, Dong Young KIM, Toshio OSAWA, Suguru NODA_

1P-11 Coherent G-band phonons in single wall carbon nanotubes 53
* Ahmad Nugraha, Eddwi Hasdeo, Riichiro Saito

1P-12 Photochemical Behavior of Single-walled Carbon Nanotubes in the Presence of Propylamine 54
* Yutaka Maeda, Yuhei Hasuike, Michio Yamada, Tadashi Hasegawa, Takeshi Akasaka

1P-13 In-situ Photoluminescence-spectroelectrochemistry of Oxygen-doped Single-walled Carbon Nanotubes 55
☆ _* Tomonari Shiraishi, Naoto Akizuki, Yuhei Miyauchi, Kazunari Matsuda, Naotoshi Nakashima_

1P-14 Far-Infrared and THz Spectroscopy of Multi-Walled Carbon Nanotubes 56
* Keijiro Sakai, Takahiro Morimoto, Toshiya Okazaki

1P-15 Prediction of Redox Potentials of Semiconducting Single-Walled Carbon Nanotubes 57
* Gergely Juhasz, Yasuhiko Hirana, Naotoshi Nakashima

1P-16 Photoluminescence Spectroelectrochemistry of a Single SWNT Molecule 58
☆ _* Liu Hong, Shinichiro Mouri, Yuhei Miyauchi, Kazunari Matsuda, Naotoshi Nakashima_

1P-17 Electric Characterization of Chirality Controlled Single-Walled Carbon Nanotubes 59
* Yusaku Tsuda, Takumi Sagara, Keisuke Yoshida, Koji Ishii, Kenichi Yamakawa, Hirofumi Yajima, Nobuyuki Iwata, Hiroshi Yamamoto

Applications of nanotubes

1P-18 Hydrogen evolution from benzene with single-walled carbon nanotubes as a photocatalyst 60
☆ _* Naoki Kohno, Kei Ohkubo, Shunichi Fukuzumi_

1P-19 High-throughput fabrication of carbon nanotube thin-film transistors with flexographic printing process: Fabrication of short channel top-gate devices 61
* Michihiko Maeda, Kentaro Higuchi, Shigeru Kishimoto, Yuta Nakajima, Takuya Tomura, Masafumi Takesue, Katsuhiko Hata, Yutaka Ohno

1P-20 Evaluation of Dynamic Performance of CNT Random Network Transistors 62
☆ _* Noriyuki Tonouchi, Hiroyuki Endoh, Fumiyuki Nihey, Hideaki Numata, Tomoyuki Yokota, Tsuyoshi Sekitani, Takao Someya, Manako Takashi_

1P-21 Preparation of Al-CNT Nanocomposites using Mechanical Alloying 63
* Takumi Goto, Yoshiki Terashima, Masaru Sekido

1P-22 Multi-walled carbon nanotubes and carbon black supported platinum nanoparticles for catalyst of polymer electrolyte membrane fuel cells 64
☆ _* Zehui Yang, Berber Mohamed, Tsuyohiko Fujigaya, Naotoshi Nakashima_

1P-23 Low-voltage carrier injection into semiconductor thin film from CNT thin film utilizing field enhancement effect 65
* Tatsuya Yamada, Shigeru Kishimoto, Yutaka Ohno

1P-24 Highly durable membrane electrode assembly consists of poly(vinylphosphonic acid)-polybenzimidazole electrolyte and carbon nanotubes based-electrocatalyst 66
* Mohamed Berber, Tsuyohiko Fujigaya, Naotoshi Nakashima

March 3rd, Mon.

1P-25 Single-Walled Carbon Nanotubes/Poly(Ionic Liquids) Nanocomposites for Extremely High Thermovoltage 67
☆ ** Motohiro Nakano, Yoshiyuki Nonoguchi, Takuya Nakashima, Tsuyoshi Kawai*

1P-26 Large-scale separation of eDIPS for application to TFTs 68
*Shunjiro Fujii, Takeshi Tanaka, Tomoko Sugita, Satoshi Asano, Masaharu Kiyomiya, Takeshi Saito, * Hiromichi Kataura*

Formation and purification of nanotubes

1P-27 Evaluation of the ratio of metal/semiconductive single-wall carbon nanotubes separated in two immiscible aqueous solution phases by utilizing Raman spectroscopy technique 69
*Naoki Kanazawa, * Shinzo Suzuki, Yu Tanaka, Akira Yamasaki, Daiki Miyazaki, Akira Ono*

1P-28 Single Chirality Separation and Optical Properties of Small-diameter Single-Wall Carbon Nanotubes 70
☆ ** Xiaojun Wei, Yasuhiro Ito, Takuya Hirakawa, Atsushi Hirano, Shunjiro Fujii, Yuhei Miyauchi, Kazunari Matsuda, Takeshi Tanaka, Hiromichi Kataura*

1P-29 Fabrication of metal nanorods for the synthesis of short-carbon nanotubes 71
** Takao Sada, Tsuyohiko Fujigaya, Naotoshi Nakashima*

1P-30 Growth of single-walled carbon nanotube from fullerene seeds by chemical vapor deposition and in situ scanning electron microscopy observation 72
** Huafeng Wang, Chisato Yamada, Hiroki Kato, Yoshikazu Homma*

1P-31 Rapid separation of high-purity and micrometer-long semiconducting carbon nanotubes by gel filtration 73
☆ ** Boanerges Thendie, Yasumitsu Miyata, Haruka Omachi, Ryo Kitaura, Yuhei Miyauchi, Kazunari Matsuda, Hisanori Shinohara*

1P-32 Efficiency Synthesis of Double Wall Carbon Nanotubes by Pressure Control of High-temperature Pulsed-arc Discharge 74
** Hayato Kikuchi, Katsuhide Terada, Toshiki Sugai*

1P-33 Synthesis and Evaluation of Single-Walled Carbon Nanotubes Using Metal Catalyst Ni-Y-Mo 75
** Bo Sun, Sakae Inoue, Tomoko Suzuki, Takayuki Yamamoto, Chihiro Yanagi, Yoshinori Ando*

1P-34 Studies on Chemical Reactions of Cobalt Clusters with Water and Oxygen by FT-ICR Mass Spectrometer 76
** Yuta Tobari, Kazuki Ogasawara, Shohei Chiashi, Shigeo Maruyama, Toshiki Sugai*

Endohedral nanotubes

1P-35 Encapsulating Carborane within Aligned and Dense Carbon Nanotubes on SiC Substrate 77
** Hayato Fujita, Wataru Norimatsu, Michiko Kusunoki*

1P-36 Synthesis of a carbon nanotube filled with solid-phase separating stainless alloy by liquid and solid interfacial arc discharge method 78
☆ ** Takuya Sagara, Satoshi Kurumi, Ken-ichi Matsuda, Kaoru Suzuki*

1P-37 Containment method for transmission electron microscopy of gas molecules within the inner space of carbon nanotubes under high vacuum 79
** Keita Kobayashi, Takeshi Saito, Masaharu Kiyomiya, Hidehiro Yasuda*

March 3rd, Mon.

Nanohorns

1P-38 Light-assisted in-situ polymer formation on carbon nanohorns 80
*Mei Yang, * Minfang Zhang, Masao Kunioka, Sumio Iijima, Masako Yudasaka*

1P-39 Selective carboxylation of graphite-like thin sheet edges in carbon nanohorn aggregates 81
** Maki Nakamura, Michiko Irie, Ryota Yuge, Toshinari Ichihashi, Sumio Iijima, Masako Yudasaka*

Graphene synthesis

1P-40 Topological Controlled Synthesis of Graphene Sheet 82
** Chozo Inoue*

1P-41 ☆ Direct growth of graphene on dielectric substrates by etching-precipitation method 83
** Masaki Kosaka, Kei Hasegawa, Suguru Noda*

1P-42 CVD-growth of nitrogen-doped graphene using tetraphenyl porphyrin as a solid precursor 84
** Yuma Sugisaki, Ryo Kitaura, Haruka Omachi, Hisanori Shinohara*

1P-43 In situ doping of Electrochemical foliation- Mechanism 85
** Shang-Lin Tsai, Mario Hofmann, Ya-Ping Hsieh*

1P-44 CVD Growth of Millimeter-Sized Graphene Grains on Heteroepitaxial Cu 86
*Kenji Kawahara, T Iwaizako, Masaharu Tsuji, * Hiroki Ago*

Properties of graphene

1P-45 ☆ Quantum interference in a ballistic graphene *n-p-n* junction: from Fabry-Perot to edge channel interference 87
** Sei Morikawa, Satoru Masubuchi, Rai Moriya, Kenji Watanabe, Takashi Taniguchi, Tomoki Machida*

1P-46 Exciton-Exciton Annihilation in Monolayer Transition-Metal Dichalcogenides 88
** Satoru Konabe, Susumu Okada*

1P-47 ☆ Edge-Roughness Effect on Electronic Transport in Semiconductor Graphene Nanoribbons 89
** Kengo Takashima, Hiromu Fujii, Takahiro Yamamoto*

Other topics

1P-48 ☆ Temperature dependence of polarization-resolved photoluminescence in monolayer WSe_2 90
** Lizhong Zhou, Yuhei Miyauchi, Shinichiro Mouri, Minglin Toh, Goki Eda, Kazunari Matsuda*

1P-49 Nonlinear Photoluminescence Properties in Monolayer Transition Metal Dichalcogenides 91
** Shinichiro Mouri, Lizhong Zhou, Yuka Tsuboi, Yuhei Miyauchi, Minglin Toh, Satoru Konabe, Goki Eda, Susumu Okada, Kazunari Matsuda*

1P-50 ☆ Photoluminescence Imaging of Monolayer MoS_2 Synthesized by Chemical Vapor Deposition Method 92
** Yuka Tsuboi, Daichi Kozawa, Yuhei Miyauchi, Shinichiro Mouri, Kazunari Matsuda*

＞＞＞＞＞＞＞ Coffee Break（17:30–18:00）＜＜＜＜＜＜＜

Tutorial（18:00–19:30）

Electronics applications of carbon nanotube thin films
Yutaka Ohno

March 4th, Tue.

Special Lecture: 25min (Presentation) + 5min (Discussion)
General Lecture: 10min (Presentation) + 5min (Discussion)
Poster Preview: 1min (Presentation)

Special Lecture（9:00–9:30）

2S–4 Structure and Property Controlled Growth of Single-Walled Carbon Nanotubes on Substrates 4
** Yan Li, Feng Yang, Xiaojun Qin, Fei Peng, Juan Yang*

General Lecture（9:30–10:30）
Formation and purification of nanotubes

2–1 Molecular Simulations of Single-Walled Carbon Nanotube Growth and Chemical Reaction of Catalyst Cluster 18
** Kaoru Hisama, Tomoya Kawasuzuki, Takuya Noguchi, Shohei Chiashi, Tomofumi Tada, Shigeo Maruyama*

2–2 Synthesis and transfer properties of single-walled carbon nanotubes array with semiconductor-type selectivity 19
** Shunsuke Sakurai, Maho Yamada, Hiroko Nakamura, Don Futaba, Kenji Hata*

2–3 Low-temperature catalyst activator: Mechanism study of CNT forest densification by “STEP” growth method using synchrotron radiation 20
*Akito Takashima, Yudai Izumi, Eiji Ikenaga, Takuo Ohkochi, Masato Kotsugi, Tomohiro Matsushita, * Takayuki Muro, Akio Kawabata, Tomo Murakami, Mizuhisa Nihei, Naoki Yokoyama*

2–4 What causes a different behavior in the tube growth between (5,5) and (6,5) caps? 21
** Yohji Achiba, Takeshi Kodama, Kenro Hashimoto, Haruo Shiromaru*

＞＞＞＞＞＞＞ Coffee Break（10:30–10:45）＜＜＜＜＜＜＜

Special Lecture（10:45–11:15）

2S–5 Interaction of carbon nanotube with water 5
** Yoshikazu Homma, Shohei Chiashi, Takahiro Yamamoto*

General Lecture（11:15–12:15）
Formation and purification of nanotubes・Properties of nanotubes・Applications of nanotubes

2–5 Highly efficient purification of semiconducting single-walled carbon nanotubes using detachable supramolecular solubilizer 22
** Fumiyuki Toshimitsu, Nakashima Naotoshi*

2–6 The effect of DNA adsorption on optical transitions in single-walled carbon nanotube 23
** Masahiro Ito, Yuusuke Ito, Daisuke Nii, Kazuo Umemura, Hiroki Kato, Yoshikazu Homma*

2–7 Mechanistic insight into the metal/semiconductor separation of single-wall carbon nanotubes using hydrogels 24
** Atsushi Hirano, Takeshi Tanaka, Hiromichi Kataura*

2–8 Organic Film-Assisted Full-Length Electrical Breakdown for Arrays of Semiconducting Single-Walled Carbon Nanotubes 25
** Keigo Otsuka, Taiki Inoue, Shohei Chiashi, Shigeo Maruyama*

March 4th, Tue.

＞＞＞＞＞＞＞ Lunch Time （12:15−13:30） ＜＜＜＜＜＜＜

Awards Ceremony （13:30−14:15）

Poster Preview （14:15−15:15）

Poster Session （15:15−17:00） （☆）Candidates for the Young Scientist Poster Award

Chemistry of fullerenes

2P−1 Investigation of molecular dynamics of fullernol solids by ²H NMR spectroscopy 93
** Yoshiaki Sano, Keisuke Baba, Hironori Ogata*

2P−2 ☆ Synthesis of a Novel Open-cage C_{60} Derivative with a Ketolactam Moiety 94
** Yoshifumi Hashikawa, Michihisa Murata, Atsushi Wakamiya, Yasujiro Murata*

Applications of fullerenes

2P−3 A Novel Ligand-free ZnO Particle for Fullerene:Polymer Inverted Organic Solar Cell 95
** IL Jeon, James Ryan, Kee Sheng Yeo, Tafu Nakazaki, Yuichi Negishi, Yutaka Matsuo*

2P−4 Synthesis of Penta(aryl)[60]fullerene Cobalt Dithiolene Complexes for Organic Solar Cells 96
** Keisuke Ogumi, Takafumi Nakagawa, Yutaka Matsuo*

2P−5 Characterization of surface layer of C_{60} thin-film polymerized by optical vortex 97
** Wataru Akiyama, Daiki Momiyama, Naoto Toriumi, Naoto Nakamura, Katsuhiko Miyamoto, Takashige Omatsu, Jonathan P Bird, Yuichi Ochiai, Nobuyuki Aoki*

Endohedral metallofullerenes

2P−6 ☆ Extraction and Isolation of Missing Small-Bandgap Metallofullerenes through Exterior Functionalization 98
** Zhiyong Wang, Yusuke Nakanishi, Shoko Noda, Hiroyuki Niwa, Jinying Zhang, Ryo Kitaura, Hisanori Shinohara*

2P−7 Supercapacitor using Lithium-Ion Endohedral Metallofullerene 99
** Eunsang Kwon, Ken-ichirou Komatsu, Yoichi Yamada, Yuri Hasegawa, Sho Sato, Seiji Sakai, Kazuhiko Kawachi, Kuniyoshi Yokoo, Shoichi Ono, Yasuhiko Kasama, Shinobu Aoyagi, Tomoaki Endo, Tomoyuki Ogawa, Migaku Takahashi*

Fullerenes

2P−8 Spin-state Tuning of Deca-Methyl C_{60} by an Electric Field 100
** Kouhei Narita, Susumu Okada*

2P−9 ☆ Geometric and electronic structures of two-dimensionally polymerized C_{32} 101
** Mina Maruyama, Susumu Okada*

Properties of nanotubes

2P−10 Electronic structure change of single-walled carbon nanotube by X-ray irradiation 102
** Toshiya Murakami, Yuki Yamamoto, Mitsuaki Matsuda, Kenji Kisoda, Hiroshi Nishigaki, Noriyuki Hasuike, Hiroshi Harima, Chihiro Itoh*

2P−11 Anharmonic effects on phonons in single-walled carbon nanotubes 103
** Masashi Mizuno, Riichiro Saito*

2P−12 ☆ The Analysis of Exchange Reactions of Sodium Cholate and Double-Stranded DNA on Single-Walled CNTs 104
** Akiko Tsuzuki, Naotoshi Nakashima*

2P-13 Chirality Dependence of Quantum Thermal Transport in Carbon Nanotubes at Low Temperatures: A First-Principles Study 105
** Tomoyuki Hata, Hiroki Kawai, Tatsuhiko Ohto, Koichi Yamashita*

2P-14 Li-ion battery electrode property of anthraquinone molecules encapsulated in single-walled carbon nanotubes 106
** Shinji Kawasaki, Tomohiro Matsuura, Kosuke Tashiro, Hayong Song*

2P-15 ☆ Diameter dependence of RBM frequency of SWNTs in water vapor 107
** Naoki Homma, Shohei Chiashi, Yoshikazu Homma, Takahiro Yamamoto*

2P-16 Optical Detection of DNA Hybridization and Denaturation on Single-Walled Carbon Nanotube Surface 108
** Yusuke Ito, Masahiro Ito, Daisuke Nii, Hiroki Kato, Kazuo Umemura, Yoshikazu Homma*

2P-17 Observation of a gate-induced photoluminescence peak in individual carbon nanotubes 109
** Yuto Ueda, Masahiro Yoshida, Akihiro Ishii, Takushi Uda, Yuichiro K. Kato*

2P-18 Thermal Properties of SWNT Forest with Various Volume Fraction 110
** JinHyeok Cha, Kei Hasegawa, Shohei Chiashi, Asuka Miura, Jeonyoon Lee, Brian L Wardle, Suguru Noda, Junichiro Shiomi, Shigeo Maruyama*

Applications of nanotubes

2P-19 ☆ In-plane conductivity of dense carbon nanotube forest on semi-insulating silicon carbide 111
** Masafumi Inaba, Chih-Yu Lee, Kazuma Suzuki, Megumi Shibuya, Atsushi Hiraiwa, Yoshiho Masuda, Wataru Norimatsu, Michiko Kusunoki, Hiroshi Kawarada*

2P-20 Systematic Conversion of Single Walled Carbon Nanotubes into n-type Thermoelectric Materials by Molecular Dopants 112
** Yoshiyuki Nonoguchi, Kenji Ohashi, Tsuyoshi Kawai*

2P-21 ☆ Evaluation of the contact resistivity and Schottky barrier height at carbon nanotubes/silicon carbide interface 113
** Kazuma Suzuki, Masafumi Inaba, Megumi Shibuya, Chih-Yu Lee, Miho Myodo, Atsushi Hiraiwa, Yoshiho Masuda, Wataru Norimatsu, Michiko Kusunoki, Hiroshi Kawarada*

2P-22 Infra-Red Light Sensor using High-Purity Semiconducting Single-Wall Carbon Nanotube Networks 114
** Hikaru Kudo, Seiya Kaji, Hideki Kawai, Taishi Takenobu, Kazuhiro Yanagi*

2P-23 ☆ Operation Speed Improvement of Carbon Nanotube Integrated Circuits on Plastic Substrate 115
** Toshitada Sanzen, Antti Kaskela, Patrik Laiho, Albert Nasibulin, Shigeru Kishimoto, Esko Kauppinen, Yutaka Ohno*

2P-24 Photovoltaic features of p-n homo-junction with position selective Cs encapsulated single-walled carbon nanotubes thin films 116
** Yoshihiro Abiko, Toshiaki Kato, Toshiki Akama, Rikizo Hatakeyama, Toshiro Kaneko*

2P-25 ☆ Molecular recognition on surfaces of metallic and semiconducting single-walled carbon nanotubes 117
** Wenxin Huang, Tsuyohiko Fujigaya, Naotoshi Nakashima*

March 4th, Tue.

2P-26 High Photovoltaic Performance of MoO_3-doped Single-walled Carbon Nanotube/Si Solar Cells 118
** Feijiu Wang, Daichi Kozawa, Yuhei Miyauchi, Shinichiro Mouri, Yutaka Ohno, Kazunari Matsuda*

2P-27 Solubility control of SWCNTs by using photofunctional dispersants 119
** Yoko Matsuzawa, Yuko Takada, Hideyuki Kihara, Masaru Yoshida*

Formation and purification of nanotubes

2P-28 Growth of CNT using the dip coat method as the catalyst support 120
** Keisuke Fujii, Yoshinori Ando, Masato Ohkohchi*

2P-29 ☆ Chirality selective solubilization of single-walled carbon nanotubes using flavin and isoalloxazine derivatives 121
** Masashi Fukuzawa, Fumiyuki Toshimitsu, Yuichi Kato, Naotoshi Nakashima*

2P-30 Self-assembly of Highly Aligned Metallic/Semiconducting SWCNTs using Crystal Templates 122
** Hideki Kawai, Kai Hasegawa, Yasuhisa Naitoh, Yuki Takagi, Yoshifumi Wada, Taishi Takenobu, Kazuhiro Yanagi*

2P-31 ☆ Chirality selective desorption of SWCNTs using mixed surfactant gel column chromatography 123
** Yohei Yomogida, Mayumi Tsuzuki, Atsushi Hirano, Shunjiro Fujii, Takeshi Tanaka, Hiromichi Kataura*

2P-32 FT-ICR Study of Chemical Reaction of Cobalt Clusters with Acetonitrile 124
** Kazuki Ogasawara, Yuta Tobari, Shohei Chiashi, Toshiki Sugai, Shigeo Maruyama*

Endohedral nanotubes

2P-33 ☆ Synthesis and TEM-based Structural Characterization of C_{60}-Flattened CNT Nanopeapods 125
** Qing Wang, Ryo Kitaura, Yuta Yamamoto, Shigeo Arai, Hisanori Shinohara*

2P-34 Modulating the Electronic Properties of Multimeric Thiophene Oligomers by Utilizing Carbon Nanotube Confinement 126
** Takashi Yumura, Hiroki Yamashita*

2P-35 ☆ Energetics and Electronic Structures of Carbon Nanotubes Encapsulating Polycyclic Aromatic Hydrocarbon Molecules 127
** Shota Kigure, Susumu Okada*

Nanohorns

2P-36 Functionalization of Carbon Nanohorns for Targeted Photo-Thermal Cancer Therapy 128
** Minfang Zhang, Mei Yang, Wuxiao Ding, Sumio Iijima, Masako Yudasaka*

2P-37 Quick charge/discharge properties of Li-ion battery using carbon-coated composites of graphites, vapor grown carbon fibers, and carbon nanohorns 129
** Ryota Yuge, Noriyuki Tamura, Takashi Manako, Kaichiro Nakano, Kentaro Nakahara*

Nanowires

2P-38 Synthesis and TEM structural characterizations of AgI nanowires formed inside carbon nanospace 130
** Shihono Naruse, Ryo Kitaura, Suguru Noda, Hisanori Shinohara*

March 4th, Tue.

Graphene synthesis

2P-39 High-yielding synthesis of graphene by supuercritical fluid 131
** Nobuto Oka, Takaaki Tomai, Itaru Honma*

2P-40 ☆ Fabrication of wide terraces on SiC (0001) for pit-free graphene growth in Ar atmosphere 132
** Wang Chenxing , Hitoshi Nakahara, Koji Asaka, Yahachi Saito*

2P-41 *In situ* observation of graphene formation on polycrystalline Cu 133
** Huafeng Wang, Pei Zhao, Shohei Chiashi, Shigeo Maruyama, Yoshikazu Homma*

2P-42 ☆ Interface structures between graphene and SiC formed in the nitrogen atmosphere 134
** Yoshiho Masuda, Wataru Norimatsu, Michiko Kusunoki*

2P-43 Preparation of multilayer graphene nanoribbons on very narrow graphene templates of unzipped DWCNT 135
** Haruki Kitakawa, Ryota Negishi, Hirofumi Tanaka, Minoru Fukumori, Takuji Ogawa, Yoshihiro Kobayashi*

Applications of graphene

2P-44 ☆ Flexible transistor and inverter of large-area WSe_2 thin film 136
** Kazuma Funahashi, Jiang Pu, Lain-Jong Li, Yoshihiro Iwasa, Taishi Takenobu*

2P-45 Controlled doping in densely aligned graphene nanoribbons by covalent functionalization 137
** Pablo Solís-Fernández, Mark Bissett, Masaharu Tsuji, Hiroki Ago*

Properties of graphene

2P-46 Mechanism of photoluminescence in graphene oxide 138
** Hiroyuki Yokoi, Takaaki Taniguchi, Michio Koinuma, Yasumichi Matsumoto*

2P-47 ☆ Mechanisms of Near-Infrared Photoluminescence from Graphene Oxides 139
** Daichi Kozawa, Yuhei Miyauchi, Shinichiro Mouri, Masao Ichida, Kazunari Matsuda*

2P-48 Molecular dynamics simulation for water molecules between two graphene layers 140
** Riichiro Saito, Masashi Mizuno*

Other topics

2P-49 Formation of fullerenes and polyynes by graphite laser ablation in ambient gases 141
** Yurika Abe, Hitomi Endo, Yohji Achiba, Haruo Shiromaru*

2P-50 Vibronic Interaction in the Forbidden Transition of Polyyne Molecules 142
** Tomonari Wakabayashi*

Special Lecture（17:00–17:30）

2S-6 Chemistry of Fullerene Epoxides: Structure and Nucleophilic Substitution-Addition Reactivity 6
Yusuke Tajima

General Lecture（17:30–18:30）

Chemistry of fullerenes ・ Applications of fullerenes ・ Endohedral metallofullerenes

2-9 Anomeric effect on the ring conformation of spiro-acetalyzed [60]fullerenes 26
** Ken Kokubo, Yu Yamazaki, Hiroyuki Masuda, Naohiko Ikuma*

March 4th, Tue.

2-10 Spiro-acetalized and -thioacetalized [60]fullerene as efficient acceptor materials for bulk heterojunction solar cells 27

** Tsubasa Mikie, Akinori Saeki, Hiroyuki Masuda, Naohiko Ikuma, Ken Kokubo, Shu Seki*

2-11 Dielectric Phase Transition of [Li@C_{60}](PF_6) at Low Temperature 28

** Shinobu Aoyagi, Kunihisa Sugimoto, Hiroshi Okada, Norihisa Hoshino, Tomoyuki Akutagawa*

2-12 Photoinduced Electron Transfer and Photoelectrochemical Properties of Supramolecular Complexes Composed of Lithium Ion-Encapsulated Fullerene and Porphyrinoids 29

** Kei Ohkubo, Yuki Kawashima, Hayato Sakai, Taku Hasobe, Angela Sastre-Santos, Shunichi Fukuzumi*

March 5th, Wed.

Plenary Lecture: 40min (Presentation) + 5min (Discussion)
Special Lecture: 25min (Presentation) + 5min (Discussion)
General Lecture: 10min (Presentation) + 5min (Discussion)
Poster Preview: 1min (Presentation)

Plenary Lecture (9:00–9:45)

3S-7 Floating catalyst CVD synthesis of SWNTs for thin film electronics applications 7
Esko I. Kauppinen

General Lecture (9:45–10:30)
Applications of nanotubes

3-1 A wet spinning method of a continuous polymer-free carbon nanotube fiber with the high electrical conductivity 30
** Ken Mukai, Kinji Asaka, Toshiya Murakami, Chihiro Itoh, Takeshi Saito, Motoo Yumura*

3-2 Carbon nanotube 3D current collectors for lightweight, high performance and low cost electrochemical capacitor electrodes 31
** Ricardo Quintero, Dong Young Kim, Kei Hasegawa, Yuki Yamada, Atsuo Yamada, Suguru Noda*

3-3 Green, scalable, binderless fabrication of a single-wall carbon nanotube nonwoven fabric based on an ancient Japanese paper process 32
** Kazufumi Kobashi, Tatsuya Hirabayashi, Seisuke Ata, Takeo Yamada, Don Futaba, Kenji Hata*

>>>>>>> Coffee Break (10:30–10:45) <<<<<<<

General Lecture (10:45–11:45)
Applications of graphene

3-4 Large-scale first-principles study of the electronic transport properties of graphene nanoribbons on SiO_2/Si 33
** Hideyuki Jippo, Taisuke Ozaki, Mari Ohfuchi*

3-5 Analysis of intercalated multi-layer graphene synthesized by CVD 34
** Daiyu Kondo, Haruhisa Nakano, Bo Zhou, Akiko I, Kenjiro Hayashi, Junichi Yamaguchi, Makoto Takahashi, Shintaro Sato, Naoki Yokoyama*

3-6 Graphene as a Material for Next Generation Fuel Cells 35
** Stephen Lyth, Jianfeng Liu, Thomas Bayer, Sean Bishop, Kazunari Sasaki*

3-7 Graphene enabled micromechanical switches 36
** Shao-Wei Ma, Ya-Ping Hsieh*

>>>>>>> Lunch Time (11:45–13:00) <<<<<<<

Poster Preview (13:00–14:00)
Poster Session (14:00–15:45) (☆)Candidates for the Young Scientist Poster Award
Chemistry of fullerenes

3P-1 Thermal Bis-silylation, Carbosilylation, and Bis-germylation of Fullerenes 143
** Daiki Inaba, Kazuya Minami, Kyosuke Miyabe, Ryosuke Iida, Masahiro Kako, Yutaka Maeda, Michio Yamada, Tadashi Hasegawa, Takeshi Akasaka*

March 5th, Wed.

3P-2 Synthesis of [60]Fullerene Derivative with 1,3-Dipolar Cycloaddition as a Novel Structure for Bulk-Heterojunction Photovoltaic Cells 144
** Hisashi Tokutomi, Masaru Sekido*

Endohedral metallofullerenes

3P-3 ☆ Electrochemical synthesis of Li@C_{60} supraatom 145
** Hiroshi Ueno, Naohiko Ikuma, Kei Ohkubo, Hiroshi Moriyama, Shunichi Fukuzumi, Ken Kokubo*

3P-4 Separation of a missing small-bandgaped metallofullerene Gd@C_{60} by *in situ* trifluoromethylation 146
** Hiroyuki Niwa, Yusuke Nakanishi, Zhiyong Wang, Ryo Kitaura, Haruka Omachi, Hisanori Shinohara*

Properties of nanotubes

3P-5 Spontaneous exciton dissociation in carbon nanotubes 147
*Yusuke Kumamoto, Masahiro Yoshida, Akihiro Ishii, Akio Yokoyama, * Takashi Shimada, Yuichiro K. Kato*

3P-6 Quantum interference effect in Raman spectra of metallic nanotubes and graphene 148
** Eddwi H. Hasdeo, Ahmad R. T. Nugraha, Riichiro Saito*

3P-7 ☆ Observation of Upconversion Photoluminescence from Single-walled Carbon Nanotubes 149
** Naoto Akizuki, Yuhei Miyauchi, Shinichiro Mouri, Kazunari Matsuda*

3P-8 Electronic structures of CNT with a defect under carrier accumulations 150
** U Ishiyama, Susumu Okda*

3P-9 Metal Deposition Effects on Photoluminescence and Raman Scattering Spectra of Suspended Single-walled Carbon Nanotubes 151
** Akihiko Ozao, Shohei Chiashi, Genta Yamaguchi, Yoshikazu Homma*

3P-10 ☆ NMR study of ^{13}C enriched single-wall carbon nanotubes 152
** Noboru Serita, Yusuke Nakai, Yasumitsu Miyata, Yutaka Maniwa, Takeshi Saito*

3P-11 Numerical study of electronic states in double-walled carbon nanotubes ---Formation of metallic bands by covalent bridge between tubes--- 153
** Yuhei Natsume*

3P-12 Electronic Structure of Carbon and BN Nanotubes: A Comparative First Principles Study 154
** Yuya Uchida, Takashi Koretsune, Susumu Saito*

3P-13 Photoconductivity spectroscopy of individual suspended carbon nanotubes 155
** Takushi Uda, Yusuke Kumamoto, Masahiro Yoshida, Akihiro Ishii, Yuichiro K. Kato*

Applications of nanotubes

3P-14 Environment-friendly functionalization method to obtain water-dispersible carbon nanotubes 156
*Mohammad Jellur Rahman, * Tetsu Mieno*

3P-15 A test for the growth of single-wall carbon nanotubes on the porous glass (PG) sheet by ACCVD technique 157
*Kyohei Nagao, * Shinzo Suzuki, Shinji Ogami, Yosuke Ito, Hiroshi Nagasawa, Yohji Achiba*

3P-16 Molecular recognition on external grooves of bundled surfaces of single-walled carbon nanotubes 158
** Tsuyohiko Fujigaya, JongTae Yoo, Naotoshi Nakashima*

3P-17 Fabrication and Properties of Functionalized Multiwall Carbonnanotube/PA-6 Composite 159
** Yoshimi Muraoka, Hiroki Sato, Masaru Sekido*

3P-18 ☆ Printed SWCNT thin film CMOS inverters based on chemically doped ion gels 160
** Yoshifumi Wada, Ryota Inukai, Taiyo Fujimoto, Hiroki Hamahata, Satoki Matsuzaki, Kazuhiro Yanagi, Taishi Takenobu*

3P-19 Surface modification of multi-walled carbon nanotubes with benzyl radical derivatives generated by photo-irradiation 161
** Tomoya Takada, Batbuyan Munkh-od, Shigeaki Abe*

3P-20 ☆ ”Laminated” ion-gel film as high capacitance insulator for carbon-nanotube transistor 162
** Taiyo Fujimoto, Ryo Shimizu, Yuki Takagi, Yoshifumi Wada, Kazuhiro Yanagi, Taishi Takenobu*

3P-21 Polyglycerol-functionalized single-walled carbon nanotubes for drug loading and delivery 163
** Qin Hongmei, Li Zhao, Keisuke Nakamura, Takahide Kimura, Naoki Komatsu*

3P-22 ☆ Simple and loss-free printing of carbon nanotubes for flexible electronics 164
** Hiroyuki Shirae, Dong Yong Kim, Kei Hasegawa, Suguru Noda*

3P-23 Chemical Vapor Deposition of MoS_2 on Carbon Nanotube for Organic Thin Film Solar Cells 165
** IL JEON, Dai Kutsuzawa, Yu Hashimoto, Takashi Yanase, Taro Nagahama, Toshihiro Shimada, Yutaka Matsuo*

3P-24 Dispersion of SWCNTs in Wrapping of Belt-Type pi-Conjugated Polymer 166
** Wataru Sagawa, Masahiro Takahashi, Keiki Kishikawa, Shigeo Kohmoto*

Formation and purification of nanotubes

3P-25 Chirality purification of DNA-wrapped single-walled carbon nanotubes toward thin film transistors 167
** Yuki Kuwahara, Fumiyuki Nihey, Shigekazu Ohmori, Takeshi Saito*

3P-26 ☆ Effects of pulse conditions on growth of (6,5) enriched single-walled carbon nanotubes under pulse plasma CVD 168
** Bin Xu, Toshiaki Kato, Koshi Murakoshi, Toshiro Kaneko*

3P-27 Selective recognition of semiconducting single-walled carbon nanotubes with large diameters by using polyfluorenes carrying mono-alkyl chain 169
** Takahiro Fukumaru, Fumiyuki Toshimitsu, Tsuyohiko Fujigaya, Naotoshi Nakashima*

3P-28 Cloning Growth of Single-Walled Carbon Nanotubes from Activated Nanotube Edges 170
** Takanori Umino, Taiki Inoue, Shohei Chiashi, Shigeo Maruyama*

3P-29 ☆ Growth of high-density carbon nanotube arrays toward thermal interface materials 171
** Nuri Na, Kei Hasegawa, Suguru Noda*

3P-30 Selective Growth of Single-Walled Carbon Nanotubes with Specific Diameter and Chirality by Irradiating Free Electron Laser during Growth 172
** Keisuke Yoshida, Takumi Sagara, Yusaku Tsuda, Koji Ishii, Kenichi Yamakawa, Hirofumi Yajima, Nobuyuki Iwata, Hiroshi Yamamoto*

March 5th, Wed.

Endohedral nanotubes

3P-31 Tuning the Seebeck coefficient of single-wall carbon nanotubes by encapsulation of guest materials 173
☆ ** Tomohiro Ueda, Yusuke Nakai, Yasumitsu Miyata, Yutaka Maniwa*

3P-32 Molecular structure of the thiophene oligomers encapsulated in single-walled carbon nanotubes by molecular dynamics simulations 174
** Hiromu Tabata, Akinori Sekine, Kazumi Inoue, Yousuke Kataoka, Hironori Ogata*

Graphene synthesis

3P-33 Influence of growth substrates on chemical reactivity of CVD graphene 175
☆ ** Ryosuke Inoue, Yasumitsu Miyata, Yutaka Maniwa*

3P-34 Synthesis and Characterization of Metal Intercalated bilayers Graphene 176
** Kentaro Imai, Kuniharu Matsuki, Shogo Sato, Nobuyuki Iwata, Hiroshi Yamamoto*

3P-35 CVD Growth of Graphene Nanoribbons on Cu (100) Film 177
☆ ** Rozan Mohamad Yunus, Masahiro Miyashita, Masaharu Tsuji, Hiroki Hibino, Hiroki Ago*

3P-36 Liquid-phase exfoliation of graphene from graphite with triphenylene derivatives 178
** Ryusuke Funahashi, Gang Liu, Shuji Aonuma, Tkahide Kimura, Naoki Komatsu*

3P-37 Plasma effects on growth of graphene nanoribbon from nickel nanobar under rapid heating plasma CVD 179
☆ ** Hiroo Suzuki, Toshiaki Kato, Toshiro Kaneko*

3P-38 Influence of electrolyte concentration for electrochemical exfoliation of graphene 180
** Haruya Okimoto, Hiroki Kuronuma, Masahito Sano*

Applications of graphene

3P-39 High gain CMOS inverters based on transition metal dichalcogenides 181
☆ ** Jiang Pu, Jing-Kai Huang, Yoshihiro Iwasa, Lain-Jong Li, Taishi Takenobu*

3P-40 High efficiency graphene doping 182
** Kai-Wen Cheng, Po-shin Lin, Ya-Ping Hsieh*

Properties of graphene

3P-41 Drastic Change in Photoluminescence Properties of Size-separated Graphene Quantum Dots 183
** Naoto Fuyuno, Daichi Kozawa, Yuhei Miyauchi, Shinichiro Mouri, Ryo Kitaura, Hisanori Shinohara, Toku Yasuda, Naoki Komatsu, Kazunari Matsuda*

3P-42 Energetics and Electronic Structure of Graphene Edges 184
☆ ** Ayaka Yamanaka, Susumu Okada*

3P-43 Fine Control of Oxidation of Graphitic Carbons by Oxidation of Graphite or Reduction of Highly Oxidized Graphene Oxide 185
*Yuta Nishina, * Naoki Morimoto*

Carbon nanoparticles

3P-44 Structural and magnetic changes of nanodiamond-copper composites during HPHT Sintering Process 186
*Fedor Shakhov, Vladimir Osipov, Sergei Kidalov, * Kazuyuki Takai, Toshiaki Enoki, Alexander Vul'*

March 5th, Wed.

3P-45 Synthesis and characterization of Pt , Pt-Ru nanoparticles on carbon nanomaterials by one-step electrodeposition 187
** Shohei Hayase, Haruhiko Yoshitake, Wang Zhipeng, Hironori Ogata*

3P-46 Hydration of Nanodiamond Surface Revisited : Intercalation Hypothesis 188
** Ryoko Yamanoi, Amanda Barnard, Shuichi Sasaki, Eiji Osawa*

Other topics

3P-47 Doping of zinc to the iron oxide nanotubes by using a poly-condensation of metal nitrate hydrates on the surface of self-assembled surfactant 189
** Yuta Kosugi, Shunji Bandow*

3P-48 Synthesis of high purity carbon nanocoils on the sheet-like carbon deposits and reduction of byproducts using Fe fine particles 190
☆ ** Yoshiaki Shimizu, Koji Maruyama, Tetsuo Iida, Yoshiyuki Suda, Hideto Tanoue, Hirofumi Takikawa, Hitoshi Ue, Kazuki Shimizu, Yoshito Umeda*

3P-49 Synthesis and characterization of two-dimensional semiconductor heterojunction based on transition metal dichalcogenides 191
☆ ** Shohei Mori, Yasumitsu Miyata, Yutaka Maniwa*

3P-50 Electro-Chemical Doping Properties of MoS_2-Single Wall Carbon Nanotube Hybrid Film 192
*Hideaki Endo, * Hideki Kawai, Kai Hasegawa, Seiya Kaji, Kazuhiro Yanagi*

Special Lecture（15:45-16:15）

3S-8 Graphene R&D conducted in Sony
Solution-processed TFTs and CVD-grown transparent conductive films 8
Toshiyuki Kobayashi

General Lecture（16:15-17:30）

Properties of graphene ・ Applications of graphene ・ Graphene synthesis

3-8 Twisting angle dependence of G band Raman intensity enhancement of twisted bilayer graphene 37
** Kentaro Sato, Riichiro Saito*

3-9 Nitrogen-containing graphene analyzed by X-ray photoelectron spectroscopy 38
** Yasuhiro Yamada, Junpil Kim, Shintaro Matsuo, Satoshi Sato*

3-10 Optical and Raman Analysis of Graphene Films Formed within Microholes on Quartz Glass Substrates by Liquid Phase Growth Method 39
** Hidefumi Hiura*

3-11 Novel transfer method for clean and high mobility CVD graphene 40
*Ya-Ping Hsieh, Mario Hofmann, * Bo-Suei Chiang*

3-12 Mechanism and impact of ad-layer formation on CPCVD graphene 41
** Yi-Wen Wang, Ya-Ping Hsieh, Mario Hofmann*

基調講演
Plenary Lecture

特別講演
Special Lecture

1S – 1 ～ 1S – 3
2S – 4 ～ 2S – 6
3S – 7 ～ 3S – 8

1S-1

Current Status and Vision of Fullerene Business in Mitsubishi Corporation

Mikio Sasaki

Former Chairman、Senior Advisor To The Board, Mitsubishi Corporation, Tokyo 100-8086, Japan

Mitsubishi Corporation established Frontier Carbon Corporation in Y2001 as a world's frontrunner, and has been persistently supplying fullerene products for the researchers and developers. Approximately 20 years has passed since my encounter to fullerene which was in Y1993. Our initial vision, our business attempts, and future vision toward nano carbon will be presented from Mitsubishi Corporation's perspective.

1. First Encounter to Fullerene
2. Incubation of Fullerene Business
3. R&D Strategy and Fullerene Business Status of Mitsubishi Corporation
4. Vision of Fullerene Business
5. Expectation toward Researcher, Developer, and Companies

1S-2

Critical factors in multi-walled carbon nanotubes in mesothelial carcinogenesis

○Shinya Toyokuni

Department of Pathology and Biological Responses, Nagoya University Graduate School of Medicine, 65 Tsurumai-cho, Showa-ku, Nagoya 466-8550, Japan

Multi-walled carbon nanotubes (MWCNTs) have potential for widespread applications in engineering and materials science. However, due to their needle-like, nanoscale shape and high durability, concerns have been raised that MWCNTs of certain characteristics may induce asbestos-like pathogenicity. Even though recent studies have demonstrated various types of reactivities induced by MWCNTs, the physicochemical features of MWCNTs that determine or trigger the cytotoxicity and carcinogenicity in mesothelial cells remain unclear. In the present study we show that the deleterious effects of non-functionalised MWCNTs on human mesothelial cells are associated with their diameter-dependent piercing of the cell membrane. Thin MWCNTs with high crystallinity showed mesothelial cell piercing and cytotoxicity *in vitro* and subsequent mesotheliomagenicity *in vivo*. In contrast, thick or tangled MWCNTs were much less toxic and carcinogenic, whereas all MWCNTs affected macrophages similarly. Furthermore, we show that the target genes for MWCNT-induced mesothelial carcinogenesis were the same as those by asbestos. Our results suggest that control of the diameter of MWCNTs may contribute to reduce the risks to human health. The final results of carcinogenesis study along with those of asbestos study will also be shown.

[1] S. Toyokuni. Nagoya J. Med. Sci. **71**, 1 (2009).
[2] H. Nagai *et al.* Proc. Natl. Acad. Sci. U.S.A. **108**, E1330 (2011).
[3] L. Jiang *et al.* J. Pathol. **228**, 366 (2012).
[4] S. Toyokuni. Adv. Drug Deliv. Rev. [Epub ahead of print] (2013).
[5] H. Nagai *et al.* Pathol. Int. **63**, 457 (2013).

Corresponding Author: S. Toyokuni
Tel: +81-52-744-2086, Fax: +81-52-744-2091,
E-mail: toyokuni@med.nagoya-u.ac.jp

1S-3

Application of layered chalcogenide materials to the aomic-layer electronics

○Keiji Ueno[1]

[1] *Graduate School of Science and Engineering, Saitama University, Saitama 338-8570, Japan*

Graphene, a unit layer of graphite, is now widely and progressively studied due to its novel physical properties. Meanwhile, other layered materials having similar stacking structures to graphene are also attracting much attention. Like graphene, new properties of their single- or few-layer flakes are actively investigated. Device fabrication is also studied using single-crystalline films of semiconducting layered materials, which have finite band gaps unlike graphene [1,2]. In the presentation, I will introduce kinds, properties, and thin film preparation methods of layered chalcogenide materials. My recent studies on the fabrication of field-effect transistors (FETs) of layered chalcogenides will be also presented.

Figure 1 shows the crystal structure of $2H_b$-MoS_2. Its single unit-layer consists of S-Mo-S three atomic layers connected by strong covalent bonds, and unit-layers are bound together by weak van der Waals forces [3]. It can be easily cleaved by an adhesive tape like graphite, and single- or few-layer flakes can be transferred onto SiO_2/Si gate substrates. Figure 2 is an optical image of MoS_2 FET prepared from the transferred MoS_2 flake. Source and drain electrodes were fabricated by painting gold paste onto the flake. On the SiO_2 gate dielectric surface, a self-assembled monolayer of hexamethyldisilazane (HMDS) was deposited to reduce carrier traps. Figure 3 shows a cross-sectional view of FET. By inserting the HMDS layer, the field-effect carrier mobility was drastically improved to 39 cm^2/Vs.

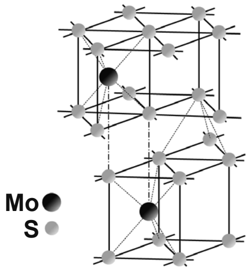

Fig.1 Crystal structure of $2H_b$-MoS_2.

Until now, only n-type FETs have been obtained from MoS_2 flakes. In the case of WSe_2, however, both n- and p-type FETs have been realized by using artificial single-crystals grown by the vapor transport method. N-type crystals were obtained when I_2 was added as a transport agent, and p-type ones could be grown when no halogen agent was used. The carrier type and density of crystals were determined by Hall effect measurements, and their FETs were fabricated like MoS_2 FETs. Figure 4 shows output characteristics of n- and p-type WSe_2 FETs prepared from n- and p-type single crystals, respectively. Other FETs prepared from various layered chalcogenide materials will be introduced in the presentation.

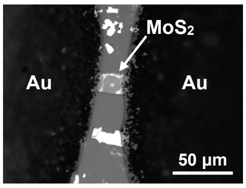

Fig.2 Optical image of MoS_2 FET.

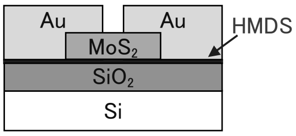

Fig.3 Cross section of MoS_2 FET.

[1] M. Xu *et al.*, Chem. Rev. **113**, 3766 (2013).
[2] S. Z. Butler *et al.*, ACS Nano **7**, 2898 (2013).
[3] J. A. Wilson and A. D. Yoffe, Adv. Phys. 18, 193 (1969).

Corresponding Author: K. Ueno
Tel: +81-48-858-3388, Fax: +81-48-858-3388,
E-mail: kei@chem.saitama-u.ac.jp

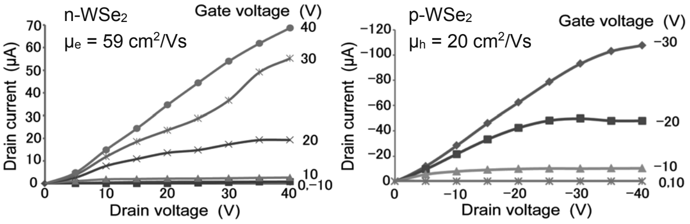

Fig.4 Output characteristics of n- and p-type WSe_2 FETs.

2S-4

Structure and Property Controlled Growth of Single-Walled Carbon Nanotubes on Substrates

○Yan Li, Feng Yang, Xiaojun Qin, Fei Peng, Juan Yang

Beijing National Laboratory for Molecular Science, Key Laboratory for the Physics and Chemistry of Nanodevices, State Key Laboratory of Rare Earth Materials Chemistry and Applications, College of Chemistry and Molecular Engineering, Peking University, Beijing 100871, China

Controlled growth of single-walled carbon nanotubes (SWNTs) chemical vapor deposition (CVD) on insulating substrates is a crucial issue for the application of SWNTs in nanoelectronics. In the growth process, catalysts play an essential role in controlling the structure of SWNTs. Over the years, we have systematically studied the controlled synthesis of catalyst nanoparticles and also developed some new catalysts. By careful design of catalysts, high quality SWNTs and the structure/property controlled growth of SWNTs were achieved. Figure 1 shows that by using ceria as catalyst supports, we were able to grow semiconducting SWNTs at the content of >95%.

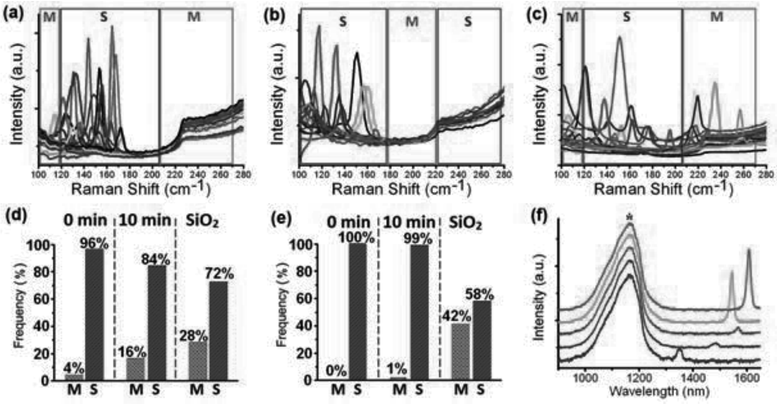

Figure 1. (a-c) Raman spectra of SWNTs synthesized with unreduced Fe/CeO_2 measured with 532 nm laser (a) and 633 nm laser (b) and Fe/SiO_2 measured by 532 nm laser (c), respectively. (d,e) Statistics of m-SWNTs (denoted as M) and s-SWNTs (denoted as S) by using Fe/CeO_2 reduced with H_2 for 0 min and 10 minutes and Fe/SiO_2 measured with 532 nm laser (d) and 633 nm laser (e), respectively. (f) Photoluminescence (PL) spectra of SWNTs synthesized by using unreduced Fe/CeO_2 excited with 532 nm laser. The broad peaks marked with star (*) correspond to the PL spectra of silicon.

[1] Y. Li *et al.*, Adv. Mater. 22, 1508(2010)
[2] W. Zhou *et al.*, Nano Lett. 6, 987(2006).
[3] Z. Jin *et al.*, Nano Lett. 7, 2073(2007).
[4] Y. Liu *et al.*, Adv. Funct. Mater. 21, 986(2011).
[5] X. Qin *et al.*, Nano Lett., DOI 10.1021/nl403515c

Corresponding Author: Yan Li
Tel& Fax: +86-10-6275-6773
E-mail: yanli@pku.edu.cn

Interaction of carbon nanotube with water

○Yoshikazu Homma[1], Shohei Chiashi[2], Takahiro Yamamoto[3]

[1]*Dept. of Physics, Tokyo University of Science, Shinjuku, Tokyo 162-8601, Japan*
[2]*Dept. of Mechanical Engineering, The University of Tokyo, Bunkyo, Tokyo 113-8656, Japan*
[3]*Dept. of Liberal Arts, Tokyo University of Science, Katsushika, Tokyo 125-8585, Japan*

The interaction between water molecules and a non-polar surface is of great interest. Hydrophobicity of graphene surface is under intense debate [1]. Although the interaction of a non-polar surface with water molecules is weaker than that between water molecules, it does exist. Single-walled carbon nanotubes (SWNTs) are ideal for the study of the interaction. The van der Waals potential originates only from carbon atoms in a single atomic layer, and the surface is inert and smooth owing to sp^2 carbon-carbon bonds. The effect of water molecule adsorption on an SWNT can be probed by optical measurements resonant to the one-dimensional singular density of states of electrons, because the optical transitions in the monolayer material are strongly influenced by the surrounding environment. Furthermore, the phenomena occurring on SWNTs can be simulated with molecular dynamics (MD).

We have performed photoluminescence (PL) and Raman scattering spectroscopic measurements using individual SWNTs suspended between micropillars and MD simulations of the SWNT-water system to investigate the behavior of water molecules on/in SWNTs [2,3]. We found that water molecules form a stable adsorption layer of 1–2 monolayer thickness on the outer surface of nanotube and they show rapid adsorption and desorption transition at a critical pressure (10^{-2} of saturation vapor pressure). This adsorption layer is created by lateral hydrogen bonding of water molecules trapped in the weak van der Waals potential of the surface. It is thermodynamically in equilibrium with the external vapor phase at room temperature. MD simulation showed that the layer persists even in liquid water. These features indicate that the condensed water layer is not a part of bulk water or a simple adsorption layer. It is a few-layer liquid phase of water, which differs from bulk solid, liquid and vapor phases. In spite of hydration, carbon nanotubes exhibit hydrophobicity macroscopically.

Water molecules confined in SWNTs take different configurations from that on the SWNT surface because of the steric hindrance due to a small tube diameter. Thus, the transition pressure and temperature of encapsulation are different from those of adsorption. Water encapsulation can also be probed by PL and Raman scattering spectroscopic measurements.

[1] Editorial, Nat. Mater. 12, 865 (2013).
[2] Y. Homma *et al*. Phys. Rev. Lett. **110**, 157402 (2013).
[3] S. Chiashi *et al*. J. Phys. Chem. Lett. 5, 408 (2014).

Corresponding Author: Y. Homma
Tel: +81-3-5228-8244, Fax: +81-3-5261-1023,
E-mail: homma@rs.tus.ac.jp

2S-6

Chemistry of Fullerene Epoxides: Structure and Nucleophilic Substitution-Addition Reactivity

○Yusuke Tajima[1,2]
[1] *Organic Optoelectronics Laboratory, RIKEN, Wako, Saitama 351-0198, Japan*
[2] *FLOX Corporation, Kawasaki, Kanagawa 210-0858, Japan*

Fullerene epoxides, $C_{60}O_n$, having epoxide groups directly attached to the fullerene cage, constitute an interesting class of fullerene derivatives. In particular, the chemical transformations of fullerene epoxides are expected to play an important role in the development of functionalized fullerenes. This is because such transformations can readily afford a variety of mono- or polyfunctionalized fullerene derivatives while conserving the epoxy ring arrangement on the fullerene surface, as seen in representative regioisomeric fullerene polyepoxides. The first part of this lecture addresses the synthesis and structural characterization of fullerene epoxides. The formation of fullerene epoxides through different oxidation reactions is then explored. Adequate characterization of the isolated fullerene epoxides was achieved by concerted use of NMR and LC-MS techniques [1]. The second part of this lecture describes the substitution of fullerene epoxides in the presence of a Lewis acid catalyst. Most major substitution products have been isolated as pure compounds and their structures established through spectroscopic methods [2]. The correlation between the structure of the substitution product and the oxygenation pattern of the starting materials allows elucidation of the mechanistic features of this transformation. This approach promises to lead to rigorous regioselective production of various fullerene derivatives for a wide range of applications.

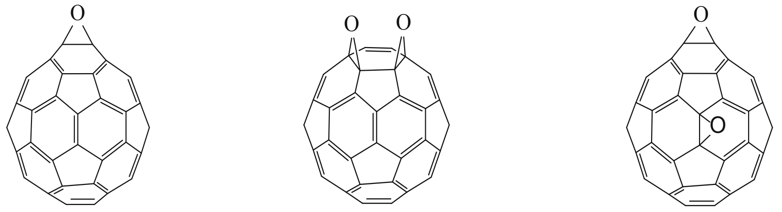

1a **1b** (*cis*-1 isomer) **1c** (*equatorial* isomer)

Figure. Fullerene mono-epoxide and regioisomeric di-epoxides.

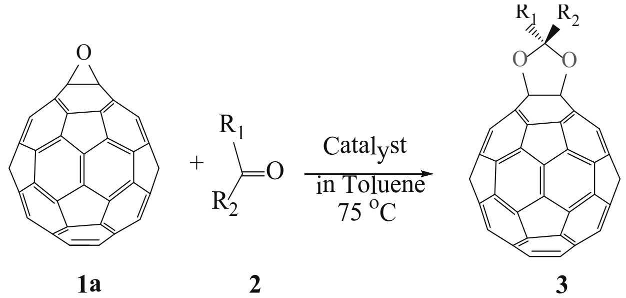

1a **2** **3**

Scheme. Acetalization of fullerene epoxide **1a** with carbonyl compound.

[1] Y. Tajima and K. Takeuchi, J. Org. Chem. **67**, 1696 (2002).

[2] Y. Tajima, *et al.* Molecules, **17**, 6395 (2012).

Corresponding Author: Y. Tajima
Tel: +81-48-467-5499, Fax: +81-48-467-5689,
E-mail: tajima@riken.jp

3S-7

FLOATING CATALYST CVD SYNTHESIS OF SWNTs FOR THIN FILM ELECTRONICS APPLICATIONS

Esko I. Kauppinen
Department of Applied Physics, Aalto University School of Science
Puumiehenkuja 2, P.O. Box 16100, FI-00076 Aalto, FINLAND

esko.kauppinen@aalto.fi

We discuss (n,m) distributions of our floating catalyst chemical vapor deposition (FFCVD) synthesis of SWCNTs from CO using Fe catalyst clusters made via direct evaporation using hot wire generator as well as via thermal decomposition of ferrocene, and with the addition of trace amounts for CO_2 and water vapor. Here both the tube diameter as well as length can be tailored by changing the reactor temperature profile as well as CO_2 concentration. Chiral i.e. (n,m) distribution as determined with ED/TEM is biased towards large chiral angles with the maximum population at about 23 degrees. Then we proceed to explore the effect of carbon source gas, by adding C_2H_4 together with CO and looking at the effect of temperature when producing catalysts via ferrocene decomposition.

To study the effect of Fe catalyst cluster size and concentration in the floating catalyst synthesis, we have developed a novel catalyst particle production method via physical vapor deposition, based on arc discharge between two electrodes i.e. the spark generator. This methods allows to control separately both the catalyst particle size and concentration when fed into the floating catalyst SWCNT synthesis reactor. Preliminary results show that when reducing catalyst particle gas phase number concentration, the bundle size of the produced tubes also is reduced, and we reduce the tube diameter below 1 nm and narrow the chiral angle distribution towards armchair when reducing synthesis temperature and CO concentration. Interestingly, the SWNT mean diameter does not significantly change when controlling catalyst number mean diameter from 4 nm to 10 nm.

We present current status of transparent conducting films and field effect thin film transistors manufactured by direct, dry deposition of SWNTs for

3S-8

Graphene R&D conducted in Sony
Solution-processed TFTs and CVD-grown transparent conductive films

○Toshiyuki Kobayashi[1]

[1] *Advanced Materials Laboratories, Sony Corporation, Kanagawa 243-0014, Japan*

Sony has been engaged in nanocarbon research since early 1990s. It started with fullerene and extended to carbon nanotube (CNT) in 2000. At that time, target applications were proton conductors and hydrogen storage for fuel cells, solar cells, field emitters, transistors, and transparent conductive films (TCF).

The graphene research started separately from the fullerene-CNT line. Sony has also been working on organic thin-film transistors (TFT) and in late 2000s, we were in search for a high-mobility and solution-processable alternative. The chemically-derived graphene nanoribbon and graphene oxide were promising candidates at that time due to their reported high mobility exceeding 100 cm^2/Vs [1]. To test the possibility of using graphene for TFTs of flat panel displays (FPD), we developed a solution process which enables uniform fabrication of semiconductive graphene oxide thin film over a large area; in particular, wafer size. Although, the fabricated TFTs showed excellent process yield that all devices show clear transistor characteristics [2,3], the field-effect mobility (< 1 cm^2/Vs) and on/off ratio (< 3) were both insufficient for FPD. The on/off ratio was improved up to 10^3 by controlling the reduction of graphene oxide [4]; however, degrading mobility by increasing on/off ratio suggested that graphene oxide is not suitable for FPD application.

In 2009, CNT team working on TCFs joined graphene research. Stimulated by a report of 30-inch roll-based production of high-quality CVD graphene [5], we started working on CVD synthesis of high-quality graphene film from early 2010. First, we followed the CVD synthesis of graphene on copper foil in quartz tube furnace and then tried to extend it to rol-to-roll process without degrading the quality of the graphene film. We also examined several different possibilities, including plasma CVD and thermal CVD with local heating of the copper foil, and found that thermal CVD by directly Joule heating the copper foil is the most promising. After verifying graphene growth in a small glass reactor, we calculated thermal, mechanical, and electrical specifications necessary to design a novel roll-to-roll CVD reactor. The reactor was fabricated in the summer of 2011 and soon we succeeded in growing a graphene film longer than 50 m. After optimizing the process conditions to grow high-quality graphene, in early 2012, we grew graphene film longer than 100 m and transferred it to a PET film by roll-to-roll film bonding and copper etching processes. The obtained graphene TCF exhibited a sheet resistance as low as 150 Ω/sq [6], which is sufficiently low for touch screens.

[1] C. Gomez-Navarro *et al*. Nano Lett. **7**, 3499 (2007). X. Li *et al*. Science **319**, 1229 (2008).

[2] T. Kobayashi *et al*. International Symposium on Graphene Devices. (2008).

[3] T. Kobayashi *et al*. small. **6**, 1210 (2010).

[4] T. Kobayashi *et al*., MRS Fall meeting (2010).

[5] S. Bae *et al*., arXiv:0912.5485 (2009).

[6] T. Kobayashi *et al*. Appl. Phys. Lett. **102**, 023112 (2013).

Corresponding Author: T. Kobayashi

Tel: +81-46-226-3708, Fax: +81-50-3809-2000, E-mail: Toshiyuki.Kobayashi@jp.sony.com

一般講演
General Lecture

1 – 1 ～ 1 – 9
2 – 1 ～ 2 – 12
3 – 1 ～ 3 – 12

1-1

Structural analysis of C_{60} microtube-AAO membrane joint interfaces by FIB-SEM

○Kun'ichi Miyazawa[1], Shuichi Shimomura[2], Takatsugu Wakahara[1], Masaru Tachibana[3]

[1] Fullerene Engineering Group, [2]Carbon Composite Materials Group, Materials Processing Unit, National Institute for Materials Science, Tsukuba, Ibaraki 305-0044, Japan
[3] Department of Materials System Science, Yokohama City University, 22-2 Seto, Kanazawa-ku, Yokohama 236-0027, Japan

In 2007, it was found that C_{60} microtubes (C_{60}MTs) can grow vertically on a porous anodic aluminum oxide (AAO) membrane by slowly injecting isopropyl alcohol (IPA) into a C_{60}-saturated toluene solution through holes of the alumina membrane, using an electric piston - syringe system. This method is called the diaphragm liquid-liquid interfacial precipitation method (DLLIP). The length of C_{60} microtubes grown by DLLIP reaches more than 100 μm and their outer diameter is typically about 30 μm (Fig.1).

The formation mechanism of V-C_{60}MTs should be known in order to control the morphology and size of the vertically grown C_{60} whiskers, since the DLLIP method has a high potential to synthesize fullerene nanowhiskers that are vertically grown on the other various conductive substrates which will be useful for electronic applications such as solar cells.

In order to know the growth mechanism of V-C_{60}MTs, longitudinal cross-sectional images of the V-C_{60}MT - AAO membrane interfaces were investigated by transmission electron microscopy (TEM). The V-C_{60}MTs were machined by a SEM-focused ion beam system (FIB-SEM, Hitachi NB5000) at an accelerating voltage of 40 kV using a Ga liquid metal ion source [2]. Fig.2 shows a FIB-SEM image for a C_{60} microtube - AAO membrane joint interface of a thin foil fabricated by FIB. No cracks are observed along the joint interface, showing the good wetting and stress reduction mechanism between the C_{60} crystal and the AAO membrane.

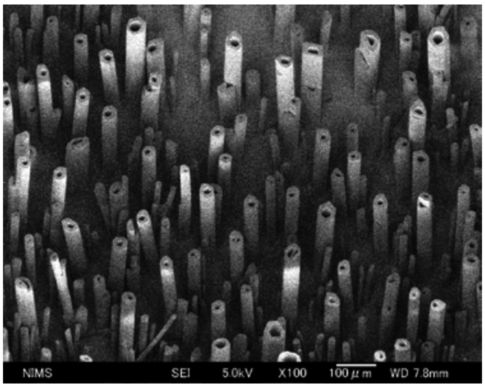

Fig.1 SEM image of C_{60} microtubes vertically grown on an AAO membrane.

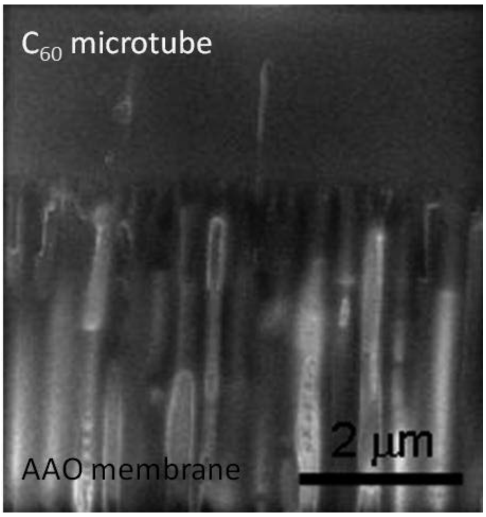

Fig.2 FIB-SEM image of a C_{60} microtube – AAO membrane joint interface.

[1]S. I. Cha, K. Miyazawa and J.-D. Kim, Chem.Mater. **20**(2008)1667.
[2]K. Miyazawa, R. Kuriyama, S. Shimomura, T. Wakahara and M. Tachibana, J. Cryst. Growth, **388**(2014)5.

Corresponding Author: K. Miyazawa
Tel: +81-29-860-4528, Fax: +81-29-860-4667
E-mail: miyazawa.kunichi@nims.go.jp

1-2

Photoelectron Spectra of Encapsulated Mono-metal fullerenes

○Takafumi Miyazaki[1], Yuuma Seino[1], Noda Shoko[3], Hajime Yagi[1],
Hisanori Shinohara[3] and Shojun Hino[1]
[1]*Graduate School of Science and Engineering, Ehime University, Matsuyama 790-8577, Japan*
[2]*Institute for Molecular Science, Okazaki, 444-8585, Japan*
[3]*Graduate School of Science, Nagoya University, Nagoya 464-8602, Japan*

We have been measuring ultraviolet photoelectron spectra (UPS) of endohedral fullerenes and revealed their electronic structure. Here, we present UPS and X-ray photoelectron spectra (XPS) of Eu@C_{82} (I), (III) and Pr@C_{82} (I), (II) and discuss their electronic structures in conjunction with M@C_{82} (M= Y, Lu, Er, Tm, etc.).

The UPS were measured at UVSOR BL8B of Institute for Molecular Science with incident photon energy hv= 20～60 eV and the XPS were measured by a SCIENTA SES-100 electron analyzer using the Mg-Kα (*hv* =1253.6eV) line.

The UPS onset energy of Eu@C_{82} (I) and (III) is the same 0.9 eV and that of Pr@C_{82} (I) and (II) is 0.3 eV, which are smaller than that of empty C_{82} (1.2 eV). These of deeper valence band UPS (BE >5 eV) shows good correspondence with those of other endohedral fullerenes. The upper valence band UPS of Eu@C_{82} (I) are analogous to those of Tm@C_{82} (I) of which electronic configuration is Tm^{2+}@C_{82}^{2-}. The XPS Eu4d peaks of Eu@C_{82} appear at higher binding energy side than those of Eu metal. The amounts of the transferred electrons from the encapsulated Er to the C_{82} cage are estimated to be two electrons as was in Tm@C_{82}.

The UPS of Pr@C_{82} (I) resemble those of Y@C_{82}, Lu@C_{82} and Er@C_{82} in which encapsulated metal atom donates three electrons to the cage. This finding suggests Pr^{3+}@C_{82}^{3-} electronic configuration. The XPS Pr4d of Pr@C_{82} appears at higher binding energy side than those of Pr metal, which also supports above elucidation.

Present results are another example to support the empirical rule that the electronic structure of the endohedral fullerenes is principally governed by the cage structure and the number of transferred electrons.

Corresponding Authors: T. Miyazaki, E-mail: miyazaki@eng.ehime-u.ac.jp, phone: 089-927-9930; S. Hino, E-mail: hino@eng.ehime-u.ac.jp, phone: 089-927-9924.

1-3

Organic Photovoltaic Device Characteristics using Fullerene Derivatives with a Thiophene Moiety†

○Tatsuya Hayashi[1], Haeseong Lee[2,3], Inseob Im[3], Seung Joo Lee[4], Jin Jang[4],
Chyongjin Pac[1,5], and Hiroshi Moriyama[1]

[1]*Department of Chemistry, Toho University, Miyama2-2-1, Funabashi, Japan*
[2]*TAKOMA Technology Co., Ltd., Nosung-myeon, Nonsan-city, Chungnam, Korea*
[3]*Department of Advanced Materials Jeonju University, Wansangu Jeonju, Korea*
[4]*Department of Information Display, Kyung Hee University, Seoul, Korea*
[5]*Department of Materials Chemistry, Korea University, Sejong Jochiwon, Chung-Nam, Korea*

Bulk heterojunction (BHJ)-type organic photovoltaic (OPV) cells have attracted significant attention for next-generation solar cells because of their light weight, solution process construction and flexibility. One of the most representative OPVs is based on a blend of poly(3-hexyl thiophene) (P3HT) as an electron donor and a C_{60} derivative, [6,6]phenyl-C_{61}-butyric acid methyl ester (PCBM), as an electron acceptor. In this study, we synthesized a new series of fullerene derivatives (5-HThCEB, 5-EThCEB, 3-MeOThCEB) with a thienyl group that has potential affinity with the P3HT donor. The synthetic scheme for these fullerene derivatives is based on that of PCBM [1]. The two fullerene derivatives (5-HThCEB and 5-EThCEB) have different alkyl chains (R_1 = C_2H_5 and C_6H_{13}) 3-MeOThCEB has a methoxy group that is expected to raise the LUMO level.

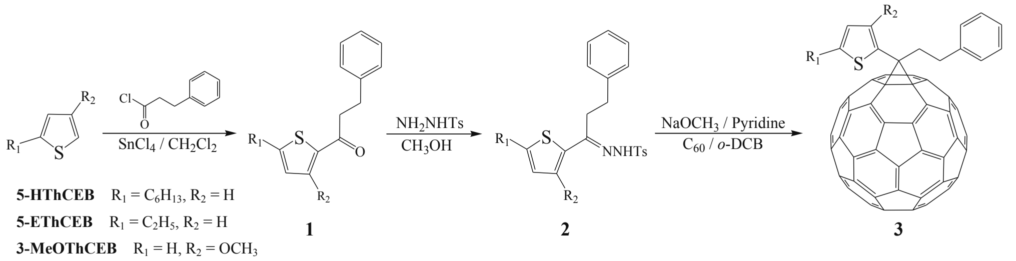

We fabricated OPV cells using P3HT as a donor and the newly designed fullerene derivatives as an acceptor. The performance of the novel fullerene derivatives was found to be lower than that of PCBM, although the V_{OC} of 5-EThCEB and 3-MeOThCEB is higher than that of PCBM.

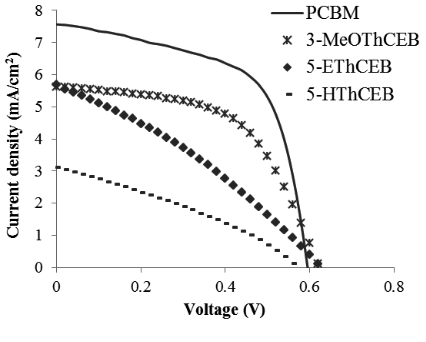

Table 1. Photovoltaic parameters using new C_{60} derivatives.

	J_{SC} (mA/cm^2)	V_{OC} (V)	FF (%)	PCE (%)
PCBM	7.61	0.587	60.3	**2.69**
5-HThCEB	3.04	0.566	32	**0.550**
5-EThCEB	5.63	0.628	32.3	**1.14**
3-MeOThCEB	5.58	0.624	53.9	**1.87**

Figure 1. *J–V* characteristics of the devices fabricated with P3HT and the new C_{60} derivatives.

[1] J. C. Hummelen, B. W. Knight, F. LePeq, F. Wudl, J. Yao, C. L. Wilkins, *J. Org. Chem.* **1995**, *60,* 532–538.

† This work is supported by Bilateral International Collaborative R&D Program (Project number: GT-2009-CL-OT-0058, Ministry of Knowledge Economy, Republic of Korea and a MEXT-Supported Program for the Strategic Research Foundation at Private Universities, Japan.

Corresponding Author : Hiroshi Moriyama TEL : +81-47-472-1211, FAX : +81-47-476-9449, E-mail : moriyama@chem.sci.toho-u.ac.jp

1-4

Dispersion of Detonation Nanodiamond: A Progress Report

○Shuichi Sasaki*, Ryoko Yamanoi and Eiji Ōsawa*

NanoCarbon Research Institute, AREC, Faculty of Textile Science and Engineering,
Shinshu University, 3-15-1 Tokida, Ueda, Nagano 386-8567, Japan

Even though the primary particles of detonation nanodiamond have been observed to be of single-nano size under TEM, dispersion of their agglutinates has been difficult and the true picture of its primary particles still remains unknown. We succeeded in 2002 to disintegrate the agglutinates by attrition milling into aqueous colloid with about 5 nm in diameter. Continued improvements in the disintegration conditions eventually led to further decrease in the diameter to 2.8 nm, which could be the final value (**Fig. 1**). Taguchi method of experimental design [1] played a key role in optimizing conditions. The most important factor is the concentration of initial agglutinates. Mechanism of disintegration involves not only the attrition with zirconia beads but also self-ablation among nanodiamond particles. Stable dispersion seems to have been achieved by hydration of the surface graphitic layer [2].

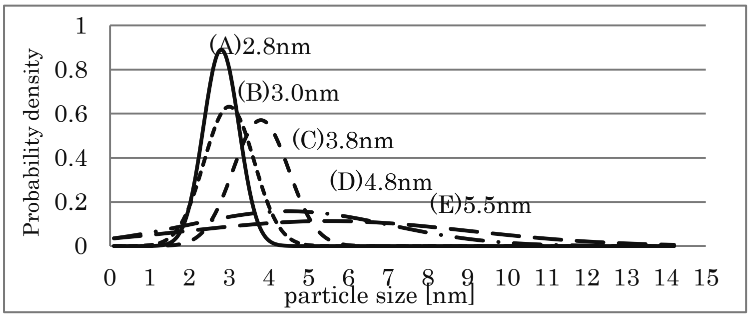

Fig. 1. Normalized DLS particle-size distributions of disintegrated detonation nanodiamond: A Taguchi method III, 2013. B Taguchi method II, 2012. C Taguchi method I, 2011. D Sonication included, 2004. E Unoptimized attrition milling, 2002.

A couple of enigmatic phenomena have been noted in the course of disintegration under the optimized conditions. First, a transient peak appeared in the DLS particle-size distribution graphs in the initial stage of disintegration (**Fig. 2**, left, A), which shifts to larger size with milling time and merges into 2.8 nm range at the end. We believe 1.7 nm corresponds to the true core size of the primary nanodiamond particle. Second, centrifugal treatment of our final colloid at 12,000 rpm produced two additional colloidal layers above and below the layer of 2.8 nm particles. Surprisingly, the uppermost layer (**Fig. 2**, right, C) consists of 4.8 nm particles! The nature of these larger particles is under study.

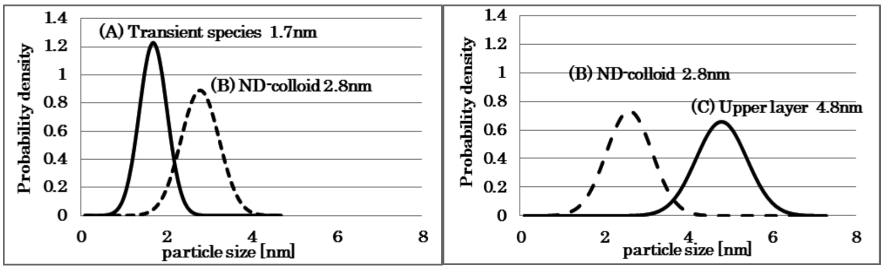

Fig. 2. Transition of size distribution in detonation nanodiamond during attrition milling. *Left*: Initial stage, DLS of aliquot from milling. Peak A dominates. *Right*: After the milling, the final colloidal solution was subjected centrifugation to give three fractions. Size-distribution of upper and middle layers shown. See text.

[1] Taguchi, G. e*t al*. Taguchi's Quality Engineering Handbook, Wiley-Interscience, 2004.

[2] Yamanoi, R. *et al*., presented in the poster session of this Symposium.

Particle-size distribution was determined on a DLS equipment FPAR-1000 (Otsuka Electronic Co.). Diameters are based on volume concentration. Corresponding Authors: sasaki@bruvas.com. osawa@nano-carbon.jp, Tel: +81-268-75-8381, Fax: +81-268-75-8551.

1-5

Development of Ion Mobility System with Multi-stage Ion Trap

○Toshiki Sugai, Yasuhiro Hiroshiba, Ninako Mikami, and Ryota Jinnouchi

Department of Chemistry, Toho University, Miyama 2-2-1 Funabashi, 274-8510, Japan

Ion mobility measurements have been a powerful tool for analysis on structures of nanocarbon materials. Structures of Metal-fullerenes show significant dependence on the number of metal atoms and the cage size and their novel structures have been also clarified[1]. To study further, we have been developing an ion trap mobility system and structural changes of polystyrene particles were monitored for more than 2 hours[2]. The measurements have revealed the stability and the sensitivity of the system. Despite of these advantages, the trap system has low mobility resolution because of the small size of the trap. To improve the resolution and to research nano materials, several groups have been also developing trap assisted IMS systems[3]. Here we present the development of an ion mobility measurement system with multi-stage ion trap.

The system consists of a laser ionization source for polystyrene particles, an ion funnel, and a linear ion trap for long movement and ion separation (Fig. 1). Those functions are realized by a newly developed power supply for the system. The power supply manipulates the particles for long distant and long-time movement with controlled RF and DC voltage to realize efficient measurement (Fig. 2). Without this power supply the particles cannot be hold on the center axis of the trap and eventually are lost by hitting the electrodes. With this system, we have achieved long and stable particle movements which contribute to particle size separation by mobility. The details of the system will be presented.

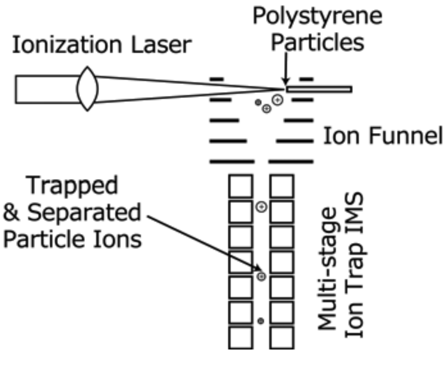

Fig. 1 Multi-stage Ion Trap IMS.

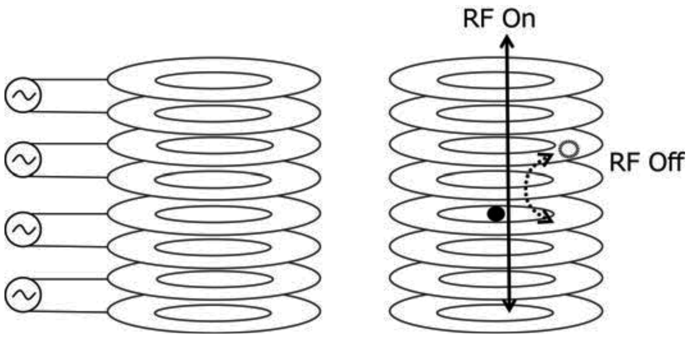

Fig. 2 RF effect on particle movements.

[1] T. Sugai *et al.*, *J. Am. Chem. Soc.* ***123***, 6427 (2001).

[2] T. Sugai *et al.*, The 38,44,45th symposium.

[3] F. Fernandez-Lima *et al.*, Int. J. Ion Mobil. Spec. ***14***, 93 (2011).

TEL: +81-47-472-4406, E-mail: sugai@chem.sci.toho-u.ac.jp

1-6

Vertical transport in meal/2D crystal/graphene layered heterostructures

○Yoshihisa Inoue [1], Takehiro Yamaguchi [1], Sei Morikawa [1], Satoru Masubuchi [1,2]
Kenji Watanabe [3], Takashi Taniguchi [3], Rai Moriya [1], and Tomoki Machida [1,2]

[1] *Institute of Industrial Science, University of Tokyo, Tokyo 153-8505, Japan*
[2] *INQIE, University of Tokyo, Tokyo 153-8505, Japan*
[3] *National Institute for Materials Science, Tsukuba 305-0044, Japan*

Recently, two-dimentional crystals (2DCs) such as graphene (Gr), h-BN, MoS_2, WS_2 and heterostructures of these materials have been revealed various extraordinal electrical and optical properties and received lots of attention for fundamental and application point of view. We fabricate various types of metal/2DC/Gr vertical heterostructures by using mechanical exfoliation and dry transfer technique. This technique enables us layer-by-layer control of 2DC heterostructure fabrication at the same time realizing high quality interface. By tuning the layer number and material of 2DC, the vertical transport of the metal/2DC/Gr structure can be controlled between tunneling and thermionic emission.

Among then, h-BN reveals highest potential barrier height with respect to graphene and as a result, we observed tunneling-type transport for the layer number from 1 to 4 monolayers (MLs). By fabricating $Ni_{81}Fe_{19}$/1ML h-BN/bilayer-graphene structure, we demonstrate electrical spin injection from ferromagnetic $Ni_{81}Fe_{19}$ to graphene at room temperature [1] as shown in Fig. 1(a).

The MoS_2 and WS_2 exhibit lower barrier height than h-BN. In this case, we observe the tunneling-dominated transport through the 2DC layer when its thickness is 3 MLs or less. In this regime, tunnel conductance is determined by the available density of states in the graphene electrode. When the layer number is more than 3MLs, the tunneling conductance is suppressed and instead of this, the thermionic emission through the Schottky barrier between Gr and 2DC becomes dominant in the vertical transport. Such a thermionic emission current can be strongly modulated with the gate voltage V_G. With utilizing this, we demonstrated large current modulation as well as large current density in Ti/MoS_2/Gr vertical FET structure as shown in Fig. 1(b).

These results show the potential high performance of the 2DC heterostrucuture for electronics and spintronics applications.

[1] T. Yamaguchi, Y. Inoue *et al.*, Appl. Phys. Express **6**, 073001 (2013).

Corresponding Author: Y. Inoue
Tel: +81-3-5452-6158,
E-mail: y-inoue@iis.u-tokyo.ac.jp

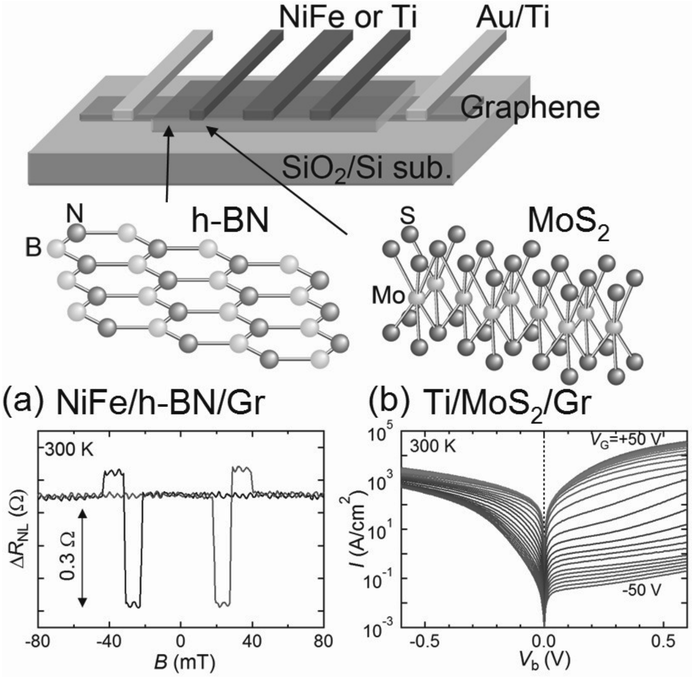

Fig.1 (a) Non-local magnetoresistance in NiFe/1ML h-BN/Gr spin valve. (b) Gate voltage V_G dependence of *I-V* characteristics in Ti/37 ML MoS_2/Gr vertical FET.

Stabilities and Electronic Structures of Hexagonal Boron-Nitride Bilayers

○Yoshitaka Fujimoto, Takashi Koretsune, and Susumu Saito

Department of Physics, Tokyo Institute of Technology, Tokyo 152-8551, Japan

Two-dimensional monolayer sheet of hexagonal boron nitride (h-BN) has attracted much attention from the viewpoint of basic nanoscience and applicable nanotechnology since it possesses several similar properties as in a graphene sheet. On the other hand, the electronic structure of the h-BN monolayer is quite different from that of graphene; graphene is a zero-gap semiconductor, whereas the h-BN monolayer is a wide-gap semiconductor [1]. The h-BN monolayer with the semiconducting properties is therefore the promising candidate for next-generation nanoelectronics materials.

Strain engineering is one of the promising ways to tune the electronic properties of two-dimensional nanomaterials such as band gap and electron transport [2-4]. For example, the Fermi velocity of graphene can be changed by applying uniaxial strains, and it depends on the directions of the strains [2]. It is found that the band gap of h-BN monolayer sheet can be also changed under strains [4].

We here investigate stabilities and electronic structures of bilayer h-BN sheets using a first-principles density-functional calculation. The energetics of the stacking patterns of h-BN bilayers and their electronic structures are examined and carbon-impurity doping effects into them are also studied. We show that the donor and acceptor-type states appear when boron and nitrogen atoms are replaced by C atoms, respectively, as in the case of the h-BN monolayer sheet. In this talk, we present strain effects on the electronic properties of h-BN bilayers. We discuss similarities and differences between C-doped and undoped h-BN bilayer sheets.

[1] K.Watanabe, T. Taniguchi, and H. Kanda, Nat. Mater. **3** (2004) 404.

[2] S. M. Choi, S. H. Jhi, and Y. W. Son, Phys. Rev. B **81** (2010) 081407.

[3] Y. Fujimoto, T. Koretsune, and S. Saito, JPS Conf. Proc., in press.

[4] Y. Fujimoto, T. Koretsune, and S. Saito, Submitted.

Corresponding Author: Yoshitaka Fujimoto
TEL: +81-3-5734-2368, FAX: +81-3-5734-2368, E-mail: fujimoto@stat.phys.titech.ac.jp

1-8

Effect of Band Nesting on Optical Properties in Two-dimensional Transition Metal Dichalcogenides

○Daichi Kozawa[1], Rajeev Sharma Kumar[2], Alexandra Carvalho[2],
Amara Kiran Kumar[2], Weijie Zhao[2], Minglin Toh[2], Ricardo M. Ribeiro[2],
A. H. Castro Neto[2], Kazunari Matsuda[1], and Goki Eda[2]

[1] *Institute of Advanced Energy, Kyoto University, Uji, Kyoto 611-0011, Japan*
[2] *National University of Singapore, 2 Science Drive 3, 117542, Singapore*

Two-dimensional (2D) crystals of semiconducting transition metal dichalcogenides (TMD) absorb as much as 10% of incident photons in the visible frequencies despite being atomically thin. It has been suggested that the strong absorption is due to the parallel band or "band nesting" effect resulting in diverging joint density of states. Here, we show using photoluminescence excitation (PLE) spectroscopy and *ab initio* density functional theory (DFT) calculation that the band nesting in mono- and bilayer MX_2 (M = Mo, W and X = S, Se) results in excitation-energy-dependent characteristic relaxation pathways of the photoexcited carriers.

Since group 6 MX_2 is isoelectronic, the general features of electronic structure are similar for these compounds. For monolayer MX_2, the conduction band minimum and the valence band maximum are both at the K point of the Brillouin zone [1] as shown in Figure 1a. The PL intensity is enhanced when the excitation energy is in resonance with the B exciton absorption [2]. In contrast, the PLE spectrum for monolayer MoS_2 shows suppressed PL intensity at the C absorption peak (Figure 1b). In the DFT calculation, we have estimated the relaxation pathway of photoexcited carriers generated in the band nesting. Our experimental and simulation results reveal that photoexcited electrons and holes in the nesting region of the phase space relax towards immediate local minima with opposite momentum. These effects, which were found to be prominent in monolayer and bilayer TMD, imply that the loss of photocarriers due to direct exciton recombination is delayed for certain resonance conditions. Our findings highlight the potential for efficient hot carrier collection using these materials as the absorbers in optoelectronic devices.

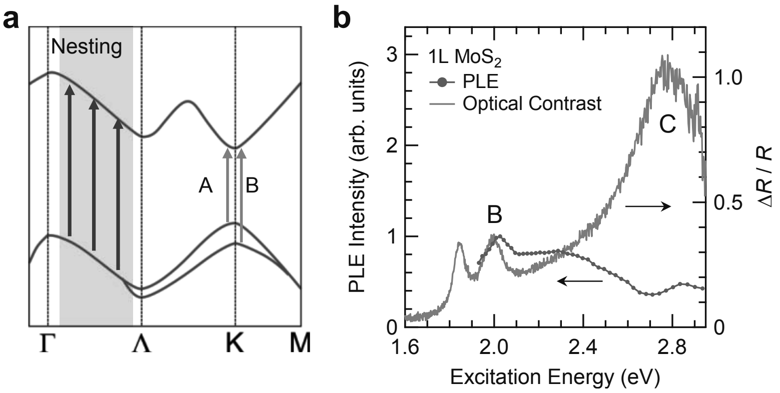

Figure 1 a, Simplified band structure of monolayer of MX_2. The arrows indicate the transition in A, B and the band nesting. **b,** PLE spectrum for band gap emission for monolayer MoS_2. The optical contrast spectrum is also shown for comparison

References

[1] Weijie Zhao and Goki Eda. *et al., Nano Lett.* **13**, 5627 (2013).

[2] Shinichiro Mouri, Yuhei Miyauchi and Kazunari Matsuda, *Nano Lett.* **13**, 5944 (2013).

Corresponding Author: D. Kozawa
Tel: +81-774-38-3465
Fax: +81-774-38-3467,
E-mail:
d-kozawa@iae.kyoto-u.ac.jp

1-9

Gate-controlled ultraviolet photo-etching of graphene edges

○Ryo Nouchi[1], Nobuhiko Mitoma[1,2], Morihiro Matsumoto[1]

[1] Nanoscience and Nanotechnology Research Center, Osaka Prefecture University, 1-2 Gakuen-cho, Naka-ku, Sakai, Osaka 599-8570, Japan
[2] International Center for Materials Nanoarchitectonics, National Institute for Materials Science, 1-1 Namiki, Tsukuba, Ibaraki 305-0044, Japan

Graphene is a one-atom thick material where carbon atoms are arranged into a honeycomb lattice structure. All carbon atoms belong to its surface, and thus electronic properties of graphene are sensitive to surface conditions such as adsorption of foreign atoms/molecules. Especially, adsorption of air molecules such as oxygen is of great importance due to their ubiquitousness. Oxygen adsorption onto bilayer graphene has been found to be controllable by applying gate voltages with a field-effect-transistor (FET) structure [1]. In this presentation, we connect the gate-voltage controllability of oxygen adsorption and post-adsorption UV treatment to perform gate-voltage controlled photo-oxidation of graphene. The oxidation reaction is found to occur selectively at edges [2], which might offer a novel methodology to fabricate graphene nanoribbons.

Graphene layers were fabricated by mechanical exfoliation onto a Si substrate with a thermal oxide layer on top of it. Cr/Au electrodes were fabricated onto the graphene layers by electron beam lithography, vacuum deposition, and liftoff processes. UV light was irradiated to the fabricated graphene FETs in operation in air at room temperature. Edge-selective photochemical etching is clearly shown in Figure 1. The etching was not observed under conditions with positive gate voltages and/or low drain voltages, indicating possible fine-tunability of the reaction by adjusting gate and drain voltages.

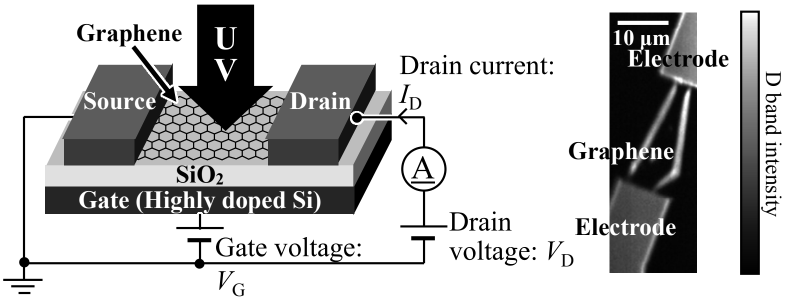

Fig.1 Schematic of the experimental setup (left) and Raman *D* band mapping after 20-min UV irradiation with V_G of −60 V and V_D of 10 mV (right).

[1] Y. Sato, K. Takai, T. Enoki, Nano Lett. **11**, 3468 (2011).
[2] N. Mitoma and R. Nouchi, Appl. Phys. Lett. **103**, 201605 (2013).

Corresponding Author: R. Nouchi
Tel: +81-72-254-8394, Fax: +81-72-254-8394,
E-mail: r-nouchi@21c.osakafu-u.ac.jp

2-1

Molecular Simulations of Single-Walled Carbon Nanotube Growth and Chemical Reaction of Catalyst Cluster

○Kaoru Hisama[1], Tomoya Kawasuzuki[1], Takuya Noguchi[1], Shohei Chiashi[1],
Tomofumi Tada[2] and Shigeo Maruyama[1]

[1] *Department of Mechanical Engineering, The University of Tokyo, Tokyo 113-8656, Japan*
[2] *Materials Research Center for Element Strategy, Tokyo Institute of Technology*
Yokohama 226-8503, Japan

It is highly important to understand the growth mechanism of single-walled carbon nanotubes (SWNTs) in order to develop structure-controlled growth techniques. In experiment, the role of metal catalyst is important for SWNT growth. Thus, we performed molecular dynamics (MD) simulation to investigate the catalyst activity. The interactions among carbon and metal atoms (Fe and Co) are expressed by our home-made Tersoff-type potentials [1]. We prepared metal clusters and supplied them with carbon atoms with constant number (n) in the fully periodic cell ($10\times10\times10$ nm^3) in gas phase. We observed cap formation, cap lift-off, and elongation process of SWNTs. Chirality (n, m) of the SWNT structure can be partially assigned. For example, the tube structure of Fig. 1 is close to (11, 6).

We also observed two types of growth modes, 'Octopus' and so-called 'VLS (Vapor-Liquid-Solid)' [2] depending on simulation conditions (temperature, gas carbon density and catalyst metal species). These two modes seem to correspond to the growth modes proposed by Loiseau group [3]. Octopus mode is 'tangential mode' in which SWNTs have the same diameter as the catalyst, and the VLS mode is "perpendicular mode" in which SWNTs have smaller diameter than catalyst. In MD simulation, Octopus mode is typically observed in SWNTs from Co catalyst while VLS mode is shown in SWNTs from Fe catalyst at high temperature. As the temperature is lower, SWNTs from Fe catalyst shows the Octopus mode. These two modes show different carbon structures on the catalyst surface. Graphene sheet structure and carbon chains appear on the metal surface in Octopus mode (Fig. 2) but much less in VLS mode. The mechanism of chirality determination for each mode is discussed. Furthermore, the preliminary result of *ab initio* simulation of chemical reaction of molecules on small metal clusters will be discussed.

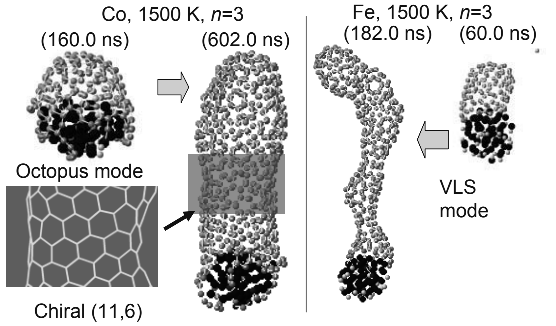

Fig. 1 Octopus growth (with local chirality assignment) and VLS growth

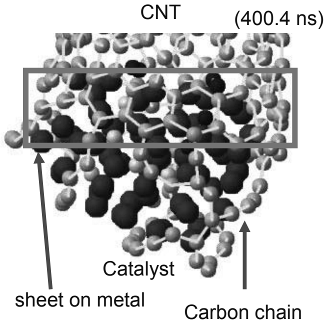

Fig. 2 Sheet and carbon chain structure on the catalyst surface
(Co, 1500 K, n=3)

[1] T. Matsuo, *et al.,* to be submitted. [2] M. Ribas, *et al., J. Chem. Phys.*, **131**, 224501 (2009).
[3] M. F. C. Fiawoo, *et al., PRL,* **108**, 195503 (2012).

Corresponding Author: Shigeo Maruyama
Tel: +81-3-5841-6421, Fax: +81-3-5800-6983,
E-mail: maruyama@photon.t.u-tokyo.ac.jp

2-2

Synthesis and transfer properties of single-walled carbon nanotubes array with semiconductor-type selectivity

○Shunsuke Sakurai[1,2], Maho Yamada[1,2], Hiroko Nakamura[1,2], Don N. Futaba[1,2], Kenji Hata[1,2]

[1]Green Nanoelectronics Center, National Institute of Advanced Industrial Science and Technology (AIST), Tsukuba 305-8565, Japan
[2]Nanotube Research Center, National Institute of Advanced Industrial Science and Technology (AIST), Tsukuba 305-8565, Japan

Coexisting of metallic and semiconducting carbon nanotube (CNT) is one of the major problems on the application of CNT in semiconductor electronics. Although post-synthesis separation approaches such as electrophoresis, gel-chromatography, and selective elimination of metallic CNTs has been reported [1], direct synthesis of semiconductor-CNT is an ideal approach to obtain semiconductor-CNT array without impurity and damage on CNT. However, direct control of the ratio of metal/semiconductor CNT and/or chirality distribution is still one of the biggest challenge in the field of CNT synthesis [2,3]. Here, we present our approach for the preferential growth of semiconducting CNTs, and the properties of field-effect transistor (FET) fabricated from CNT arrays with semiconductor-type selectivity.

Selective growth has been achieved by pre-annealing the catalyst iron nanoparticle with the small amounts of H_2O and H_2 as shown in Figure 1. We found out that precise control of gas ambient is necessary to achieve the preferential growth of semiconductor-CNT, i.e., too much H_2O amount led to no growth of CNT and too little H_2O amount did not invoke the preferential growth. These results suggest that the control of catalyst activity is important.

Importantly, performances of FET devices consisting of the as-grown CNT films as channel layer are quite good, especially at a relatively short channel length. At a a relatively short channel length (5 μm), high on/off ratio (c.a. 10^4), and high on-current density (> 1 μS/μm) has been obtained. We note that these performances are almost comparative to those fabricated from the inks of the separated semiconductor CNT [3]. The relationship of FET performances and selectivity is also presented.

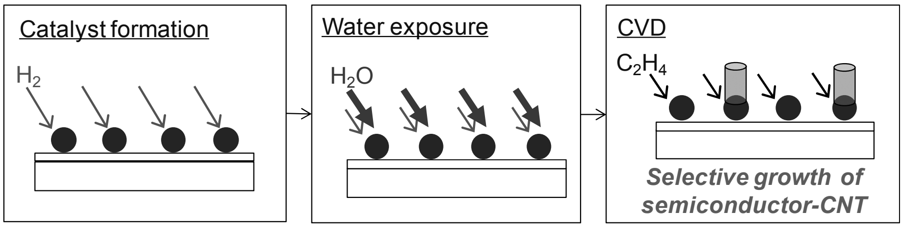

Figure 1. Schematic representation of the preferential growth of semiconductor-CNT

This research is granted by JSPS through “Funding Program for World-Leading Innovative R&D on Science and Technology (FIRST Program)”, initiated by CSTP.

[1] H. Liu, D. Nishide, T. Tanaka, H. Kataura, Nature Commun. **2** (2011) 309.
[2] W. H. Chiang, R. M. Sankaran, Nature Mater. **8** (2009) 882.
[3] C. Wanget al., Nano Lett., **12** (2012) 1527.

Corresponding Author: Kenji Hata
TEL: +81-29-861-6205, FAX: +81-29-861485-1169, E-mail: kenji-hata@aist.go.jp

2-3

Low-temperature catalyst activator: Mechanism study of CNT forest densification by “STEP” growth method using synchrotron radiation

Akito Takashima[1], Yudai Izumi[1], Eiji Ikenaga[1], Takuo Ohkochi[1], Masato Kotsugi[1],
Tomohiro Matsushita[1], ○Takayuki Muro[1],
Akio Kawabata[2], Tomo Murakami[2], Mizuhisa Nihei[2], Naoki Yokoyama[2]

[1] Japan Synchrotron Radiation Research Institute (JASRI), Hyogo 679-5198, Japan
[2] Collaborative Research Team Green Nanoelectronics Center (GNC), National Institute of Advanced Industrial Science and Technology (AIST), Ibaraki 305-8569, Japan

We recently developed a thermal chemical vapor deposition method named “STEP” for the growth of dense carbon nanotube (CNT) forests [1]. A Ti film is used as the underlayer for an Fe catalyst film. A characteristic point is that C_2H_2 feeding is begun at a low temperature of 450 °C in the course of a temperature elevation from room temperature (RT) to 800 °C. Any pretreatments are not used for the ex-situ deposited catalyst. A growth result showed that the CNT packing density obtained by the STEP process was 20 times higher than that obtained by a process in which C_2H_2 was supplied at 800 °C [1]. This suggests that the Fe layer, oxidized due to air exposure, was reduced and transformed into nanoparticles at or near 450 °C. This temperature is, however, unusually low to reduce Fe oxides. It is still unknown how the STEP process densified the CNTs. To address the mechanism, we studied the chemical and morphological states of the Fe/Ti catalyst system (denoted by Fe/Ti) under vacuum annealing.

Fe/Ti has 2- and 1-nm-thick Fe and Ti layers, respectively, on a Si substrate. We also prepared a comparative sample (Fe/Si) without the Ti layer. All the analyses were performed at SPring-8. The Fe layers were analyzed at BL27SU using soft x-ray photoemission spectroscopy (SXPES) with a probing depth of ~1.4 nm. For the buried Ti layer, hard x-ray photoemission spectroscopy (HAXPES) with a probing depth of ~8 nm was used at BL47XU. Surface images were observed at BL17SU using photoemission electron microscopy (PEEM). Finally, a CNT growth experiment at 450 °C was performed at BL27SU, where the catalyst chemical states were observed by soft x-ray absorption spectroscopy (XAS).

The result of Fe 2*p* SXPES showed that the Fe chemical states of Fe/Ti at 450 °C were dominated by metallic Fe, whereas those of Fe/Si were still dominated by Fe oxides. In the Ti 2*p* HAXPES spectrum of Fe/Ti at 450 °C, the TiO peak, which was dominantly seen at RT, disappeared and the TiO_2 peak was solely observed. These results indicate that the Ti layer reduced the initially oxidized Fe layer at 450 °C. An SXPES analysis also suggests that the Fe layer of Fe/Ti transformed into nanoparticles on TiO_2 at 450 °C. The PEEM image on Fe/Ti at 800 °C showed large Fe islands with sizes of a few 100 nm, causing sparse CNTs. We consider that the Ti layer activated the Fe catalyst at 450 °C in the STEP process and densified the CNTs. We will present the CNT growth results for Fe/Ti and Fe/Si at 450 °C, which strongly support our conclusion.

This research is granted by JSPS through FIRST Program initiated by CSTP.

[1] A. Kawabata, T. Murakami, M. Nihei, and N. Yokoyama, Jpn. J. Appl. Phys. **52**, 110117 (2013).

Corresponding Author: T. Muro
Tel: +81-791-58-0802 (ext. 3869), Fax: +81-791-58-0830,
E-mail: muro@spring8.or.jp

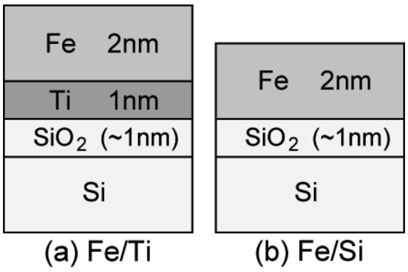

Fig. 1 (a) Fe/Ti catalyst system used for STEP.
(b) Comparative sample without the Ti layer.

2-4

What causes a different behavior in the tube growth between (5,5) and (6,5) caps? -Competition between tube and fullerene growth-

○Yohji Achiba, Takeshi Kodama, Kenro Hashimoto and Haruo Shiromaru

Department of Chemistry, Tokyo Metropolitan University, Hachioji, 192-0397, Japan

A semispherical cap structure consisting of 6 pentagons and infinite numbers of hexagons has generally been believed to play an essential role on the formation of nano-structured carbons. Actually, the chirality of a carbon nanotube is totally dependent on the cap structures formed at a very early stage in the tube growth. It has also been generally accepted that in the tube growth process, the tube structure so called “near armchair” is the one of being the most abundant among many other structural candidates. Particularly, the chiral tube characterized by a (6,5) chiral index is of possessing the high selectivity, and thus, is definitely one of the most plausible potential candidate as a future carbon nanotube electronic device with a single chirality. On the other hand, the production yield of (5,5) tube whose diameter as well as chirality are quite similar to those of the (6,5) tube is quite low or sometimes is almost zero. Therefore, a simple question like what causes such a significant difference between the (6,5) and (5,5) chiral structures may occur. In the present work, we will discuss the stability and reactivity of these two caps on the basis of theoretical considerations.

Although the experimental evidence whether the cap is really present or not as a growth-reaction intermediate is still unclear, we intended to clarify the properties of these hypothetical structures by means of a theoretical calculation. For the purpose of the reaction selectivity of specific cap structures, we performed density functional calculations on many kinds of isomeric cap structures with different sizes. For example, since the difference in the structures between (5,5) and (6,5) cap first appears upon replacing one pentagon of the (5,5) cap by a hexagon at C_{30}, we started to investigate the stability and reactivity of cap structures at the size of C_{30} and C_{31} for the (5,5) and (6,5) cap structures, respectively. In order to find out the major reaction channels for the further growth, we extended the calculations to every sizes up to C_{60} including many isomeric forms characerized by more than 200 different structures. As a result, it was found that the highly selective reaction channels leading to the formation of I_hC_{60} fullerene as well as (6,5) chiral tube were able to be specified.

Corresponding Author: Yohji Achiba

E-mail: achiba-yohji@tmu.ac.jp、Tel:+81-42-677-2534, Fax:+81-42-677-2525

2-5

Highly efficient purification of semiconducting single-walled carbon nanotubes using detachable supramolecular solubilizer

○Fumiyuki Toshimitsu[1], Naotoshi Nakashima[1, 2, 3]

[1] *Department of Applied Chemistry, Kyushu University, Fukuoka 819-0395, Japan*
[2] *WPI-I^{2}CNER, Kyushu University, Fukuoka 819-0395, Japan*
[3] *JST-CREST, Chiyoda-ku, Tokyo 102-0075, Japan*

Highly purified single-walled carbon nanotubes (SWNTs) are essential for fundamental studies and applications toward next-generation nanotechnology [1]. Especially, unique optical and electrical properties of semiconducting-SWNTs (s-SWNTs) would be fully utilized only when they are separated from poisoning metallic-tubes [2]. Despite several technical methods have been reported for the separation, the development of a new powerful separation method is still a great challenge. We have previously reported polymer wrapping techniques which efficiently solubilize/extract semiconducting SWNTs with high chiral-selectivity by developing polyfluorene derivatives (PFOs) [3,4]. However, there are serious problems when using these solubilizing methods; that is, difficulty in the removal of the wrapping surfactants or polymers as well as their low extraction yields.

In order to solve these problems simultaneously, here we developed a newly designed, detachable solubilizer **1** (Fig. 1) based on a supramolecular approach. Thanks to the metal coordination bonds into PFO, the new polymers not only recognize semiconducting chirality but also breakable so as to remove from s-SWNT surfaces. The resulted coordination polymer of **1** and four metal ions (Co, Ni, Cu or Zn) successfully extracted s-SWNTs (Fig. 2). Furthermore, the extraction yield of solubilized SWNTs are greater by ~10 times compared to conventional PFOs The solubilized SWNT could be further purified by removing the wrapping polymers, simply by treating in an acidic condition. The quantitative elimination of solubilizer **1** and metal ions were confirmed by UV-vis-Near IR, raman and two-dimensional PL mapping spectroscopies. The details of this study will be presented at the meeting.

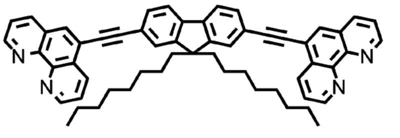

Figure 1. Chemical structures of ligand **1**.

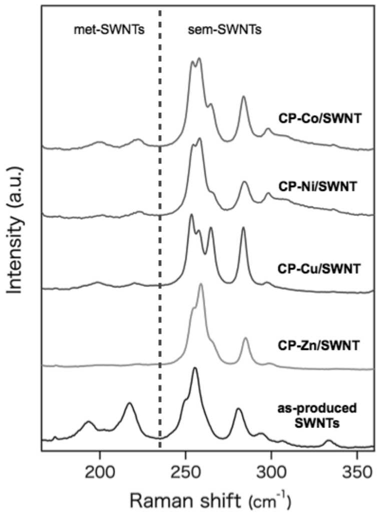

Figure 2. Raman spectra of extracted s-SWNTs using coordination polymer of ligand **1**. Excitation ; 633 nm.

Referneces

[1] H. J. Dai, *Acc. Chem. Res.* **35**, 1035 (2002).

[2] Cao, Q. & Rogers, J. A., *Adv. Mat.* **21**, 29–53 (2009).

[3] H. Ozawa, N. Ide, T. Fujigaya, Y. Niidome, and N. Nakashima, *Chem. Lett.* **40**, 239 (2011).

[4] K. Akazaki, F. Toshimitsu, H. Ozawa, T. Fujigaya, and N. Nakashima, *J. Am. Chem. Soc.*, **134**, 12700 (2012).

Corresponding Author: N. Nakashima
Tel: +81-92-802-2845, Fax: +81-92-802-2845
E-mail: nakashima-tcm@mail.cstm.kyushu-u.ac.jp

2-6

The effect of DNA adsorption on optical transitions in single-walled carbon nanotube

○Masahiro Ito, Yusuke Ito, Daisuke Nii, Hiroki Kato, Kazuo Umemura, Yoshikazu Homma.

Department of Physics, Tokyo University of Science, Tokyo 162-8601, Japan

DNA adsorption on single-walled carbon nanotubes (SWNTs) makes SWNTs solubilize and functionalize [1,2]. The hybridization of DNA and SWNT (DNA-SWNT) is of great interest in chemical and biochemical fields. As a result of DNA adsorption, SWNTs are isolated individually and photoluminescence (PL) from DNA-SWNTs can be obtained. Because PL from an SWNT is sensitive to its environment, PL spectra should reflect the information of adsorbed DNA. However, PL from DNA-SWNT ensemble makes spectrum analysis difficult.

Recently, we revealed that PL could be observed even from DNA-SWNTs lying on the substrate i.e. under dry condition [3]. In this study, we investigated the intrinsic effect of single stranded DNA (ssDNA) and double stranded DNA (dsDNA) adsorption on the optical transition in isolated DNA-SWNTs under the dry condition.

We diluted DNA-SWNT solution low enough and obtained mono-dispersed DNA-SWNTs on the substrate as shown in Fig. 1. PL spectra from SWNT suspended between micro structures (solid line), ssDNA-SWNT (dash line) and dsDNA-SWNT (dot line) are shown in Fig. 2. Three spectra were obtained from the same chirality (8,6). The difference in emission wavelength is attributed to the difference in the thickness of ssDNA and dsDNA. Figure 3 shows emission spectra under the wet and dry conditions. The emission wavelength of ssDNA-SWNT depends on the environment. On the other hand, the emission wavelength of dsDNA-SWNT is retained. This means that ssDNA-SWNT is more sensitive to environmental change. The quantum yield in an isolated DNA-SWNT will also be discussed in comparison with that of a suspended SWNT.

[1] N. Nakashima, *et al.*: Chem. Lett. **32** (2003) 456. [2] M. Zheng, *et al.*: Nature Mater. **2** (2003) 338.
[3] M. Ito, *et al.*: Appl. Phys. Lett. in press.

Corresponding Author: Yoshikazu Homma
Tel: +81-3-3260-4271 (ext. 2298), Fax: +81-3-5261-1023,
E-mail: homma@rs.tus.ac.jp

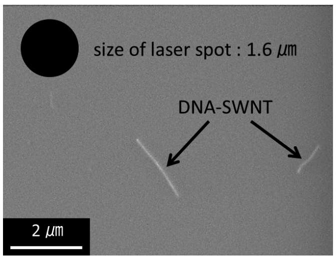

Fig. 1. SEM image of isolated DNA-SWNTs.

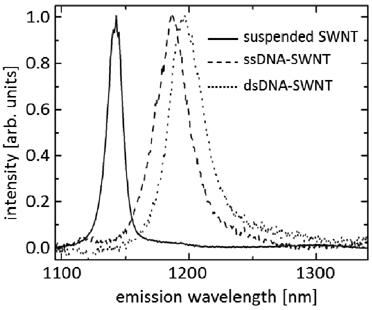

Fig. 2. PL spectra of suspended SWNT, ssDNA-SWNT, and dsDNA-SWNT under the dry condition.

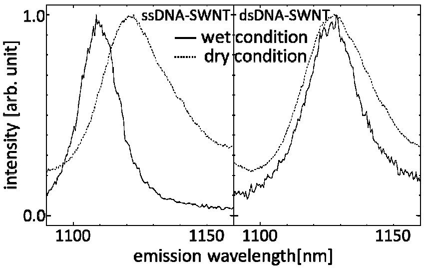

Fig 3. PL spectra under the wet and dry conditions.

2-7

Mechanistic insight into the metal/semiconductor separation of single-wall carbon nanotubes using hydrogels

○Atsushi Hirano, Takeshi Tanaka, Hiromichi Kataura

Nanosystem Research Institute, National Institute of Advanced Industrial Science and Technology, Tsukuba, Ibaraki 305-8562, Japan

Single-wall carbon nanotubes (SWCNTs) suspended in sodium dodecyl sulfate (SDS) are separated into metallic and semiconducting species using hydrogel columns [1]. Understanding the mechanism helps improve the quality and quantity of the separation. In this study, we provide a mechanistic model for the separation, which was derived from pH-dependent adsorption of SWCNTs onto the hydrogels.

The adsorbability of SWCNTs on the hydrogels is reduced under acidic pH conditions. The metallic SWCNTs are more readily desorbed from the hydrogels than the semiconducting SWCNTs (Fig. 1). Because reversible oxidation of SWCNTs in aqueous solution depends on O_2, H^+/H_2O reduction potential [2], the pH dependence of the adsorption is likely ascribed to the oxidation of SWCNTs. Based on the results, a mechanistic model of the metal/semiconductor separation is proposed as follows (Fig. 2):

1. Metallic SWCNTs is more readily oxidized because of the smaller band gaps.
2. Oxidized SWCNTs are positively charged.
3. More SDS molecules are electrostatically bound to more positively charged SWCNTs.
4. Fully coated SWCNTs with SDS result in their desorption from the hydrogel.

The metallic SWCNTs thus tend to desorbed from the hydrogel column compared with semiconducting SWCNTs, leading to the separation [3]. This property of the adsorption is used for improvement of the quality of the separation.

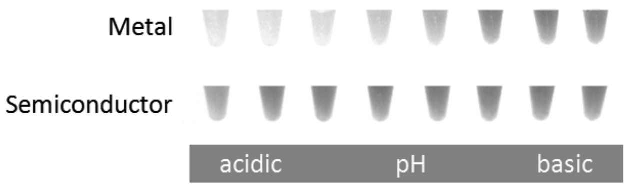

Fig. 1 Photograph of the SWCNTs adsorbed onto the hydrogels at various pH values.

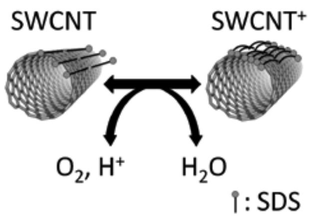

Fig. 2 Schematic representation of the reversible oxidation of the SWCNTs accompanied by the SDS condensation on the SWCNTs.

Acknowledgment. This work was supported in part by KAKENHI of MEXT, Japan.

[1] T. Tanaka *et al.* Appl. Phys. Express 2, 125002 (2009)
[2] A. Nish and R. J. Nicholas. Phys. Chem. Chem. Phys. **8**, 3547 (2006)
[3] A. Hirano *et al.* ACS Nano **7**, 10285 (2013)

Corresponding Author: T. Tanaka
Tel: +81-29-861-2903, Fax: +81-29-861-2786,
E-mail: tanaka-t@aist.go.jp

2-8

Organic Film-Assisted Full-Length Electrical Breakdown for Arrays of Semiconducting Single-Walled Carbon Nanotubes

○Keigo Otsuka, Taiki Inoue, Shohei Chiashi, Shigeo Maruyama
Department of Mechanical Engineering, The University of Tokyo, Tokyo 113-8656, Japan

Semiconducting (s-) single-walled carbon nanotubes (SWNTs) are one of the attractive channel materials for field-effect transistors (FETs), and highly pure s-SWNT arrays are required for monolithic device integration. Since selective growth techniques have not yet attained a required purity of s-SWNTs, post growth removal of metallic (m-) SWNTs is still necessary. Among various techniques, electrical breakdown [1] has sufficient selectivity between s- and m-SWNTs. However, it oxidizes only small regions (~100 nm) of m-SWNTs and most parts of m-SWNTs remain after the process, and therefore it lacks in scalability. In this study, we propose an organic film-assisted full-length electrical breakdown of m-SWNTs toward pure s-SWNT arrays.

Horizontally-aligned SWNTs grown on crystal quartz were transferred onto SiO_2/Si substrates and used as channels of back-gate FETs. Molecular glass, small-molecule organic material, was deposited onto the substrates, covering the SWNTs. It was previously used as thermocapillary resists [2] but here we use it to assist oxidation of m-SWNTs. A drain voltage was increased from 0 to 40 V at a rate of ~0.67 V/min to gradually heat up m-SWNTs, while a positive gate voltage (~10 V) was applied. After the full-length breakdown process, organic film was removed with acetone. Transfer characteristics of an FET after the process (Fig. 1) show improvement in on/off current ratio from ~2 to ~10,000, indicating selective removal of m-SWNTs. Figure 2 shows scanning electron microscopy (SEM) images of the FET before and after the process. The SWNT indicated by the arrows in Fig. 2 was removed over its full length (16.4 μm) and the length is over 100 times larger than the removal length by conventional in-air electrical breakdown. Removal of SWNTs was confirmed also by Raman mapping measurement. Atomic force microscopy observations indicated that molecular glass around m-SWNTs was locally involved in chemical reactions along with the SWNTs and induced the long-length removal of m-SWNTs. Since a rate of increase of drain voltage affected the removal length, we speculate that molecular glass heated up by Joule heating of SWNTs prevented rapid cooling of the SWNTs after the breakdown, thus increasing the removal length.

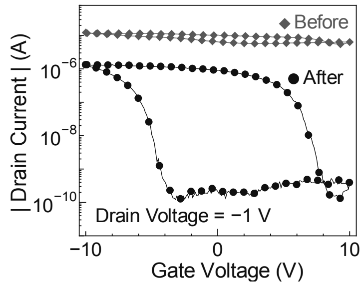

Fig. 1 Transfer characteristics of the FET before and after the process.

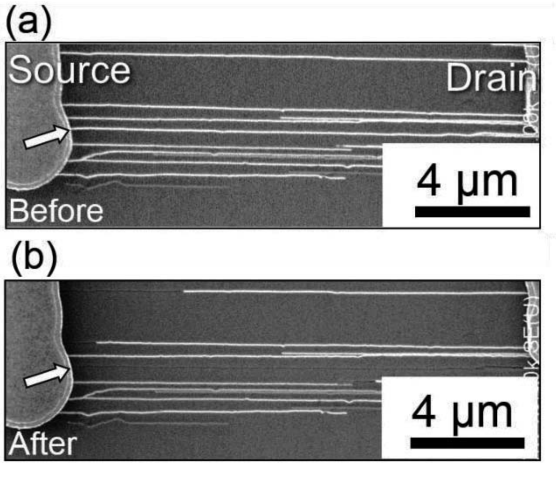

Fig.2 SEM images of an SWNT array (a) before and (b) after the breakdown process.

[1] P. G. Colins *et al*., Science **292**, 706 (2001).
[2] S. H. Jin *et al*., Nat. Nanotechnol. **8**, 347 (2013).

Corresponding Author: S. Maruyama
Tel: +81-3-5841-6421, Fax: +81-3-5841-6983,
E-mail: maruyama@photon.t.u-tokyo.ac.jp

Anomeric effect on the ring conformation of spiro-acetalyzed [60]fullerenes

○Ken Kokubo, Yu Yamazaki, Hiroyuki Masuda, Naohiko Ikuma

Division of Applied Chemistry, Graduate School of Engineering, Osaka University,
2-1 Yamadaoka, Suita, Osaka 565-0871, Japan.

The anomeric effect is a kind of stereoelectronic effect that is originally observed in pyranose rings with heteroatomic substituents adjacent to an oxygen atom within a tetrahydropyran ring. The substituent, generally hydroxyl or alkoxy group, prefers the axial position instead of the sterically less hindered equatorial position. In the present study, we first found such anomeric effect in specially designed fullerene derivatives, such as spiro-acetalyzed [60]fullerenes, on the steric conformation of *exo*- and *endo*-isomers.

Spiro-acetalyzed fullerenes were synthesized by $TiCl_4$-mediated acetalization of cyclohexanone-fused fullerene, which was prepared by Diels-Alder reaction of C_{60} with 2-trimethylsilyloxy-1,3-butadiene followed by hydrolysis, with various diols [1]. While simple diols $HO(CH_2)_nOH$ ($n = 2, 3, 4$) gave the corresponding 5-, 6-, and 7-membered ring spiro-acetalyzed fullerenes as a single product, respectively, 2-substituted-1,3-propanediol $HOCH_2CHRCH_2OH$ (R = Me, Ph) gave the two separable isomers. By ^1H and ^{13}C NMR spectroscopy along with X-ray structural analysis, the structures of major and minor products were determined as *exo*- and *endo*- ring-flipped isomers, respectively. The DFT calculations revealed that *endo*-isomer is more stable than *exo*-isomer, although the former seems to be more sterically hindered. This result can be well explained by the anomeric effect.

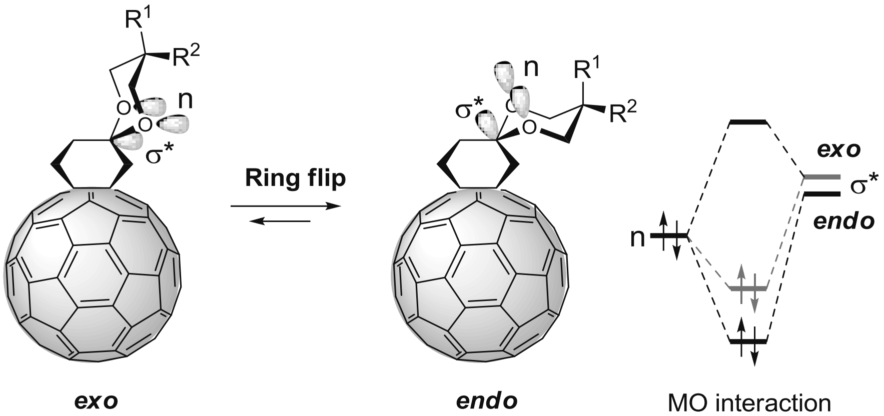

Calcd. by DFT
at B3LYP/6-31G*

		exo	endo
$R^1 = R^2 = H$	$\Delta\Delta H$ =	0 kJ/mol	–0.90 kJ/mol
$R^1 = R^2 = Me$		0 kJ/mol	–0.66 kJ/mol
$R^1 = Me, R^2 = H$		0 kJ/mol	+3.85 kJ/mol
$R^1 = H, R^2 = Me$		0 kJ/mol	–4.32 kJ/mol

[1] Kokubo, K.; Masuda, H.; Ikuma, N.; Mikie, T.; Oshima, T. *Tetrahedron Lett.* **2013**, *54*, 3510.

Corresponding Author: K. Kokubo
Tel: +81-6-6879-4592, Fax: +81-6-6879-4593, E-mail: kokubo@chem.eng.osaka-u.ac.jp

2-10

Spiro-acetalized and –thioacetalized [60]fullerene as efficient acceptor materials for bulk heterojunction solar cells

○Tsubasa Mikie, Akinori Saeki, Hiroyuki Masuda, Naohiko Ikuma, Ken Kokubo, Shu Seki

Department of Applied Chemistry, Graduate School of Engineering, Osaka University,
2-1 Yamadaoka, Suita, Osaka 565-0871, Japan.

Although functionalized fullerene derivatives are the most promising electron acceptor materials in organic photovoltaics (OPV), the successful examples have been limited in [6,6]-phenyl-C_{61}-butylic acid methyl ester ($PC_{61}BM$) and indene C_{60} bis-adducts (ICBAs). This is due to the difficulty in simultaneous achievement of solubility, miscibility with p-type polymer, and electron accepting and transporting ability. Besides, simplified schemes of synthesis and purification are strongly required in the practical applications.

Herein, we report a systematic study on OPV of spiro-acetalized and -thioacetalized [60]fullerene derivatives as a n-type materials and poly(3-hexylthiophene) (P3HT) as a p-type material. The spiro-acetalized [60]fullerene having 7-membered ring synthesized by two-step reactions (**3c** in Fig.1a) demonstrates the power conversion efficiency (PCE) of 4.04%, which is comparable to that of $PC_{61}BM$. Interestingly the PCEs are increased linearly with the solubility of the mono-adduct fullerenes and saturated at > 5 mg/ml (Fig. 1b), indicating the PCE is primarily dominated by the solubility relating to the film morphology. Accordingly we measured hole and electron mobilities (μ_h and μ_e) for the fullerenes showing > 2.5% PCE by space-charge limited current (SCLC) technique. As shown in Fig. 1c, it was found that the balance between μ_h and μ_e scales with the PCE, revealing that μ_e/μ_h is the secondary dominant factor, in accordance with the reported simulation result. To our surprise, **3c** showed perfectly balanced mobilities, which may evolve further advancement in PEC by extra molecular engineering of spiro-acetalized fullerene family.

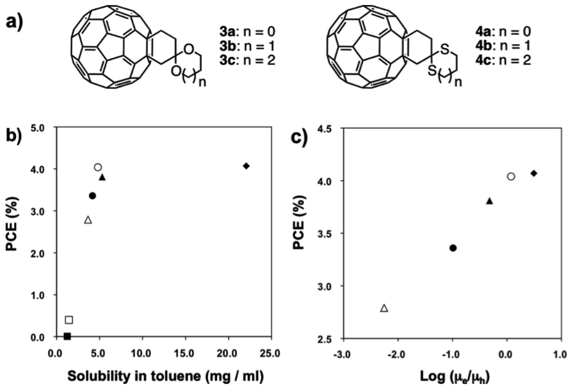

Figure 1. a) Structure of spiro-acetalized and –thioacetalized [60]fullerene derivatives. Correlation of the PCE if P3HT:fullerenes OPV with b) solubility of fullerenes in toluene and with c) log (μ_e/μ_h).

[1] Kokubo, K.; Masuda, H.; Ikuma, N.; Mikie, T.; Oshima, T. *Tetrahedron Lett.*, **2013**, *54*, 3510.

*Corresponding Author: Shu Seki
Tel: +81-6-6879-4586, Fax: +81-6-6879-4586, E-mail: seki@chem.eng.osaka-u.ac.jp

2-11

Dielectric Phase Transition of [Li@C_{60}](PF_6) at Low Temperature

○Shinobu Aoyagi[1], Kunihisa Sugimoto[2], Hiroshi Okada[3],
Norihisa Hoshino[4], Tomoyuki Akutagawa[4]

[1] Department of Info. and Bio. Sciences, Nagoya City University, Nagoya 467-8501, Japan
[2] SPring-8/JASRI, Kouto, Sayo, Hyogo 679-5198, Japan
[3] Department of Chemistry, The University of Tokyo, Tokyo 113-0033, Japan
[4] Institute of Multidisciplinary Research for Advanced Materials and Graduate School of Engineering, Tohoku University, Sendai 980-8577, Japan

Endohedral lithium fullerene Li^+@C_{60} can have a dielectric polarization by the off-centered location of the Li^+ cation inside the C_{60} cage. The x-ray structure analysis of the PF_6^- salt [Li@C_{60}](PF_6) revealed that the Li^+ cation occupies two off-centered equivalent positions at 20 K and hence the crystal is non-polar [1]. The disordered structure at low temperature is explained by a static orientation disorder of polar Li^+@C_{60} cations and/or a dynamic tunneling of the Li^+ cation inside the C_{60} cage. The Li^+ tunneling would be suppressed by an intermolecular interaction at lower temperature and a dielectric phase transition might be induced. We reveal the dielectric property and crystal structure of [Li@C_{60}](PF_6) below 20 K in this study.

The temperature dependence of the dielectric permittivity was measured for the single crystal down to 9 K. The dielectric permittivity increases with decreasing temperature according to the Curie-Weiss law. Such a behavior was also observed in H_2O@C_{60} crystal but not in empty C_{60} crystal [2]. No dielectric phase transition was observed in H_2O@C_{60} down to 8 K. In contrast, a dielectric anomaly suggesting a phase transition was observed in [Li@C_{60}](PF_6) around 18 K. The x-ray diffraction experiment below 20 K was also performed at SPring-8 BL02B1. The crystal has a cubic structure at 20 K [1]. The temperature dependence of the cubic lattice constant shows no anomaly around 18 K. However, diffraction peaks that are forbidden for the given structure appear below 18 K. Thus the crystal symmetry is lowered by the dielectric phase transition. We present the result of the crystal structure analysis of the newly discovered low-temperature phase.

[1] S. Aoyagi *et al*. Angew. Chem. Int. Ed. **51**, 3377 (2012).
[2] S. Aoyagi *et al*. Chem. Commun. **50**, 524 (2014).

Corresponding Author: S. Aoyagi
Tel: +81-52-872-5061,
E-mail: aoyagi@nsc.nagoya-cu.ac.jp

2-12

Photoinduced Electron Transfer and Photoelectrochemical Properties of Supramolecular Complexes Composed of Lithium Ion-Encapsulated Fullerene and Porphyrinoids

○Kei Ohkubo [1], Yuki Kawashima [1], Hayato Sakai [2], Taku Hasobe [2], Ángela Sastre-Santos [3], Shunichi Fukuzumi [1]

[1] Department of Material and Life Science, Graduate School of Engineering, Osaka University, ALCA, Japan Science and Technology Agency, Osaka 565-0871, Japan
[2] Department of Chemistry, Faculty of Science and Technology, Keio University, Yokohama, 223-8522, Japan
[3] División de Química Orgánica Instituto de Bioingeniería, Universidad Miguel Hernández, Elche 03202, Spain

Photoelectrochemical cells (PECs) have been widely investigated as a next-generation solar cell because of their simple structures. The photoinduced charge separation between the excited state of dye and the electrode plays an important role in improvement of PEC performance. Extensive efforts have so far been devoted to design and synthesize electron donor-acceptor linked molecules to achieve efficient photoinduced charge separation for applications to PECs. Porphyrins and the related macrocyclic molecules such as phthalocyanines and chlorins are widely used as the electron donor due to the efficient electron transfer and light harvesting properties. We have recently designed and synthesized simple electron donor-acceptor supramolecular complexes composed of lithium ion encapsulated fullerene ($Li^+@C_{60}$) and sulfonated zinc *meso*-tetraphenylporphyrin ($ZnTPPS^{4-}$). Photoexcitation of the supramolecule exhibited extremely slow charge-recombination of the CS state (τ = 0.3 ms) in benzonitrile (PhCN).[1] The driving force of photoinduced electron transfer from $ZnTPPS^{4-}$ to the triplet excited state of $Li^+@C_{60}$ is highly positive ($-\Delta G_{ET}$ = 0.98 eV) in polar PhCN,[1] which is large enough to afford the CS states even under the non-polar environment in nanoclusters. We report herein photovoltaic cells using $Li^+@C_{60}/ZnTPPS^{4-}$ nanoclusters, which are assembled on optically transparent electrode (OTE) of nanostructured SnO_2 (OTE/SnO_2) as shown in Scheme 1.

The maximum IPCE value attained in these experiments was 77% at 450 nm [2]. When $ZnTPPS^{4-}$ is replaced by anionic zinc phthalocyanine and zinc chlorin derivatives [3], efficient photocurrent generation behaviours were also observed under the similar experimental conditions.

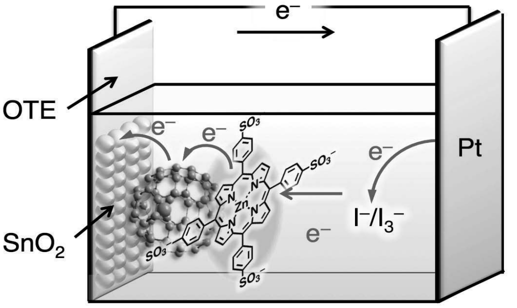

Scheme 1 Schematic image of photoelectrochemical cell of $OTE/SnO_2/ZnTPPS^{4-}/Li^+@C_{60}$

[1] Ohkubo, K.; Kawashima, Y.; Fukuzumi, S. *Chem. Commun.* **2012**, *48*, 4314
[2] Ohkubo, K.; Kawashima, Y.; Sakai, H.; Hasobe, T.; Fukuzumi, S. *Chem. Commun.* **2013**, *49*, 4474.
[2] Kawashima, Y.; Ohkubo, K.; Mase, K.; Fukuzumi, S. *J. Phys. Chem. C* **2013**, *117*, 21166.

Corresponding Author: K. Ohkubo
Tel: +81-6-6879-7369, Fax: +81-6-6879-7370,
E-mail: ookubo@chem.eng.osaka-u.ac.jp

3-1

A wet spinning method of a continuous polymer-free carbon nanotube fiber with the high electrical conductivity

○Ken Mukai [1], Kinji Asaka [1], Toshiya Murakami [2], Chihiro Itoh [2],
Takeshi Saito [3,4], Motoo Yumura [3,4]

[1] *Health Research Institute, National Institute of Advanced Industrial Science and Technology (AIST), Ikeda 563-8577, Japan*
[2] *Department of Materials Science and Chemistry, Wakayama University, Wakayama 640-8510, Japan*
[3] *Nanotube Research Center, National Institute of Advanced Industrial Science and Technology (AIST), Tsukuba 305-8565, Japan*
[4] *Technology Research Association for Single Wall Carbon Nanotubes (TASC), Tsukuba 305-8562, Japan*

Fibers composed of carbon nanotubes (CNTs) have the potential to form high strength, lightweight, thermally and electrical conducting materials.

As one of typical methods to fabricate CNT fiber, wet spinning method is widely known. In an established method of fabricating CNT fiber by wet spinning method, coagulating solution contains a polymer in order to allow easy fabrication and structural stability.[1] On the other hand, the insulating characteristics of polymer in the CNT fiber results in a lowering of the electrical conductivity.

We have successfully developed a novel wet-spinning method of a continuous polymer-free CNT fiber. We here shows remarkably high electrical conductivity, more than 7000 $\mathrm{Scm^{-1}}$ of the polymer-free CNT fiber.

This achievement was possible due to the CNT alignment in CNT fiber by stretching the strong CNT fiber composed of `the enhanced direct injection pyrolytic synthesis method (e-Dips)' CNTs during drying process.

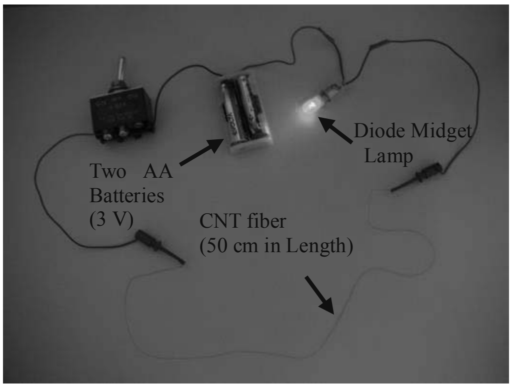

Fig. 1 Lighting up of Midget Lamp.

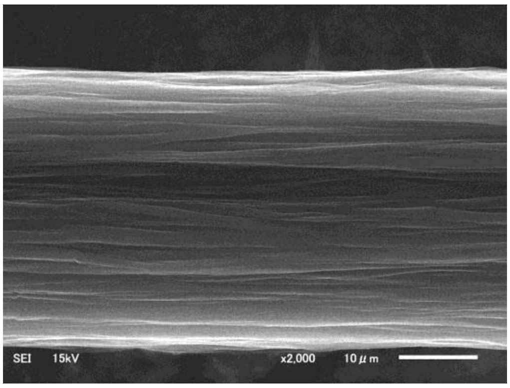

Fig. 2 SEM photograph of CNT fiber after stretching process.

[1] B. Vigolo, *et al.*, Scinece **290**, 1331 (2000).

Corresponding Author: K. Mukai
Tel: +81-72-751-8376, Fax: +81-72-751-8370,
E-mail: mukai-ken@aist.go.jp

3-2

Carbon nanotube 3D current collectors for lightweight, high performance and low cost electrochemical capacitor electrodes

○ Ricardo Quintero[1,2], Dong Young Kim[2], Kei Hasegawa[2], Yuki Yamada[1], Atsuo Yamada[1]
and Suguru Noda[2,*]

[1]Department of Chemical System Engineering, The University of Tokyo, 7-3-1 Hongo, Bunkyo-ku, Tokyo 113-8656, Japan
[2]Department of Applied Chemistry, Waseda University, 3-4-1 Okubo, Shinjuku-ku, Tokyo 169-8555, Japan

In the electrochemical capacitor (EC) field, extensive research has been made to increase the specific capacitance of active materials. These materials often lack enough electrical conductivity and the addition of conductive fillers is necessary in practical application, with the trade-off of reduction of maximum specific capacitance of devices. Metal current collectors account for a significant part of the weight of practical devices, and by replacing them with lightweight materials, the performance of an entire capacitor device can be further improved [1]. We propose here the development of simpler electrode architecture in order to achieve higher performances. By capturing activated carbon (AC), a low cost capacitive material, inside a matrix made using a small amount of FWCNTs, light-weighted hybrid electrodes were fabricated [2].

Self-supporting electrodes were obtained through the systematic combination of AC with sub millimeter long FWCNTs (6–10 nm diameter, 0.4 mm length, 99 wt% purity, 3 walls on average) [3]. To evaluate the performance of the FWCNT 3D collector matrix, different configurations of a Ti mesh connected to the carbon electrodes were prepared (Fig. 1). Long FWCNTs provide mechanical stability and less contact/junction resistances, making possible to produce electrodes featuring no additional binder materials and able to contain capacitive particles at a weight 9 times as much as its own weight. The FWCNT matrix effectively improved the capacitance of the inexpensive, high surface area AC to 169 F/g at a slow scan rate of 5 mV/s, and to 131 F/g at a fast scan rate of 100 mV/s, in fairly thick (~200 mm) electrodes. Connection to a metallic collector at the film edge only, which significantly reduced the use of metal, retained much larger capacitance for the AC-FWCNT hybrid film (107 F/g) than for the conventional AC electrode with binder (PTFE) and conductive filler (AB) (3.9 F/g) at a practical voltage scan rate, 100 mV/s (Fig 2).

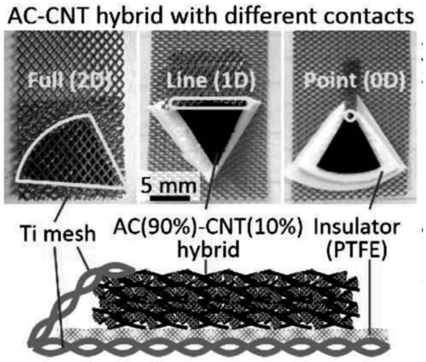

Fig.1 Schematic of proposed electrode architecture and metal collector connections.

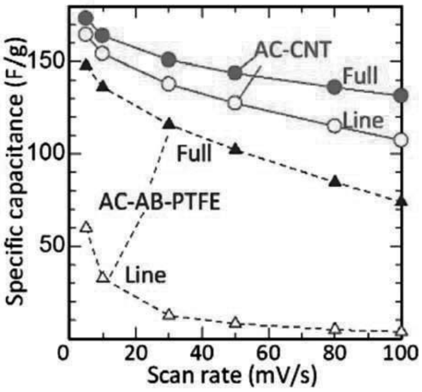

Fig.2 Rate capability of AC-FWCNT and AC-AB-PTFE electrodes in different metal collector configurations.

[1] P. Simon, Y. Gogotsi, Nat Mater 7 (2008) 845.
[2] R. Quintero, et al., RSC Adv., in press.
[3] D.Y. Kim, et al., Carbon 49 (2011) 1972.

Corresponding Author: Suguru Noda
Tel/Fax: +81-3-5286-2769, E-mail: noda@waseda.jp

3-3

Green, scalable, binderless fabrication of a single-wall carbon nanotube nonwoven fabric based on an ancient Japanese paper process

○Kazufumi Kobashi [1,2], Tatsuya Hirabayashi [2], Seisuke Ata [1,2], Takeo Yamada [1,2], Don N. Futaba [1,2], Kenji Hata [1,2]

[1] Technology Research Association for Single Wall Carbon Nanotubes (TASC), Tsukuba, 305-8565, Japan
[2] Nanotube Research Center, National Institute of Advanced Industrial Science and Technology (AIST), Tsukuba, 305-8565, Japan

We propose a fabrication method for carbon nanotube (CNT) nonwoven fabrics based on an ancient Japanese papermaking process where paper is made from natural plant fibers [1]. In our method, CNT nonwoven fabrics are made by a scalable process of filtering binder-free, aqueous suspensions of CNTs. The aqueous suspension of these entangled single-wall carbon nanotube (SWNT) aggregates enabled smooth filtration through a cellulose filter with large pores (8um). The "wet SWNT cakes," which comprised solely of SWNT and water and obtained after filtration, were press dried to fabricate a SWNT nonwoven fabric. This environmentally friendly process employs water and the raw CNT material alone, and demonstrates a great advantage over conventional CNT nonwoven fabric (Buckypaper) manufacturing technology which utilizes large quantities of organic solvent and binders, which must subsequently be disposed and removed, respectively. Moreover, the scalability of this process was demonstrated by manufacturing a large area (A3, 30x42 cm, thickness, 40–150 μm), self-supporting SWNT nonwoven fabric with a density of 0.4 g/cm^3, basis weight of 0.2 g/m^2 , porosity of 63%, and specific surface area of 740 m^2/g. This SWNT nonwoven fabric is anticipated to find application as functional particle-supported sheets, electrode materials, filters.

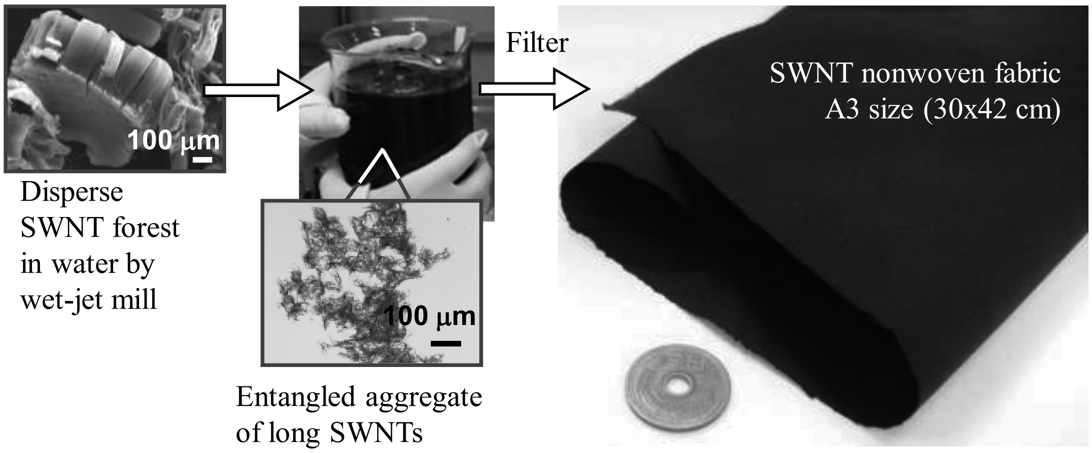

Figure 1 Green, scalable, binderless fabrication of nonwoven fabric (A3 size) from aqueous suspension of entangled SWNT aggregates.

[1] K. Kobashi *et al.* ACS Appl. Mater. Interfaces. **5**, 12602 (2013).

Corresponding Author: Kenji Hata
Tel: +81-29-861-4654, Fax: +81-29-861-4851,
E-mail: kenji-hata@aist.go.jp

3-4

Large-scale first-principles study of the electronic transport properties of graphene nanoribbons on SiO_2/Si

○Hideyuki Jippo[1], Taisuke Ozaki[2], Mari Ohfuchi[1]

[1] Fujitsu Laboratories Ltd., 10-1 Morinosato-wakamiya, Atsugi, Kanagawa 243-0197, Japan
[2] JAIST, 1-1 Asahidai, Nomi, Ishikawa 923-1292, Japan

Graphene is normally supported on insulators such as SiO_2 in electronic devices. The electronic transport properties of graphene on SiO_2 are remarkably different from those of suspended graphene [1,2]. The surface treatment of SiO_2 even changes the electric transport properties [3]. In this article, we investigate the electronic transport properties of armchair graphene nanoribbon (AGNR) transistors on SiO_2/Si with long channel lengths of 9.91 and 15.1 nm. We also show the difference between O- and OH-termination of the SiO_2 surface.

The models of AGNRs on SiO_2/Si with the channel length of 9.91 nm are shown in Fig. 1. The channel of AGNRs is sandwiched between semi-infinite AGNR leads. The numbers of atoms for the models with channel lengths of 9.91 and 15.1 nm amount to 1974 and 3030, respectively. For transport calculations, we employ the nonequilibrium Green's function method implemented in the density functional theory code, OpenMX [4].

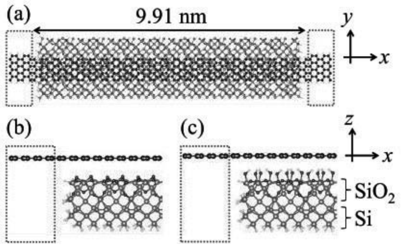

Fig. 1. (a) Top view and (b)(c) side views of the left edge of the model of AGNRs on SiO_2/Si with a channel length of 9.91 nm. The SiO_2 surfaces are terminated by (b) O and (c) OH. The dotted rectangles represent the unit cell of leads.

Figure 2 shows currents evaluated by integrating the transmission at a bias voltage of 0 V over the energy regime of 0.5 eV with respect to the center energy of the integration region. For freestanding AGNRs [(a) and (b)], the on/off current ratio for the longer channel (15.1 nm) is larger by a factor of 10^7 than that for the shorter channel (9.91 nm). On the other hand, for AGNRs on O-terminated SiO_2/Si [(c) and (d)], the ratio does not depend on the channel length. The current gaps are shifted by 0.7 eV, indicating p-type conduction. The current on/off ratio 10^5 is significantly smaller than those for freestanding AGNRs. The value 10^5 is consistent with the experimental data for GNRs on SiO_2 [1]. We also investigated AGNRs on OH-terminated SiO_2/Si [5]. The on/off current ratio for the OH-terminated surface (e) is smaller on the p side than that for the O-terminated surface (c). We found that the OH groups have broad states around the valence band maximum of AGNRs and more holes are injected from OH-terminated SiO_2 to AGNRs than O-terminated SiO_2. This is considered to contribute the smaller on/off current ratio and may relate to the Dirac point shift and the degraded mobility found in the measurements for graphene on OH-terminated SiO_2 [3].

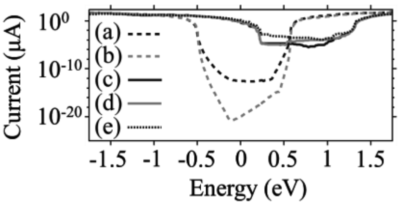

Fig. 2. Currents for (a)(b) freestanding AGNR, (c)(d) AGNR on O-terminated SiO_2/Si, and (e) AGNR on OH-terminated SiO_2/Si. The channel lengths are 9.91 nm for (a)(c)(e) and 15.1 nm for (b)(d).

[1] X. Li *et al.*, Science 319, 1229 (2008). [2] M.-W. Lin *et al.*, Nanotechnology 22, 265201 (2011).
[3] K. Nagashio *et al.*, J. Appl. Phys. 110, 024513 (2011).
[4] http://www.openmx-square.org/ [5] H. Jippo *et al.*, Appl. Phys. Express, to be published.

Corresponding Author: H. Jippo
Tel: +81-46-250-8843, Fax: +81-46-250-8274, E-mail: jippo.hideyuki@jp.fujitsu.com

3-5

Analysis of intercalated multi-layer graphene synthesized by CVD

○Daiyu Kondo, Haruhisa Nakano, Bo Zhou, Akiko I, Kenjiro Hayashi, Junichi Yamaguchi
Makoto Takahashi, Shintaro Sato and Naoki Yokoyama

Collaborative Research Team Green Nanoelectronics Center (GNC), AIST, 16-1 Onogawa,
Tsukuba 305-8569, Japan

Nano-carbon materials including graphene [1] are one of promising electronic materials for future LSIs due to their excellent physical properties. Especially their tolerance to a high current density might make them replace cupper (Cu) as future interconnect materials, since the reliability of Cu interconnects decreases with their line width. However, nano-carbon materials have generally indicated a resistivity higher than that of Cu. For instance, the resistivity of high-quality graphene peeled off from HOPG is an order of magnitude higher than Cu. Recently, we reported that intercalated MLG interconnects synthesized by chemical vapor deposition (CVD) had a resistivity of the same order as that of Cu [2]. On the other hand, the amount of $FeCl_3$ intercalated into MLG grown by CVD was not as large as that intercalated into MLG peeled off from HOPG reported previously, according to Raman spectroscopy [3]. To find the origin of these differences, we analyzed the distribution of $FeCl_3$ molecules in the MLG by using EELS, EDX and PEEM measurements.

MLG was synthesized on a 200-nm cobalt catalyst film sputtered on a sapphire c plane by thermal CVD at around 1000C$^{\circ}$. As process gases, CH_4, H_2 and Ar were utilized. After MLG interconnects were fabricated by the conventional photo lithography, the intercalation of $FeCl_3$ into MLG interconnects was performed at 310C$^{\circ}$.

Figure 1 shows a cross sectional STEM image of the intercalated MLG interconnect and the line profile of EELS spectra. From the line profile, it is clear that Fe and Cl have nonuniform distributions across the MLG interconnect, implying nonuniform intercalation into MLG. The details will be discussed in the presentation.

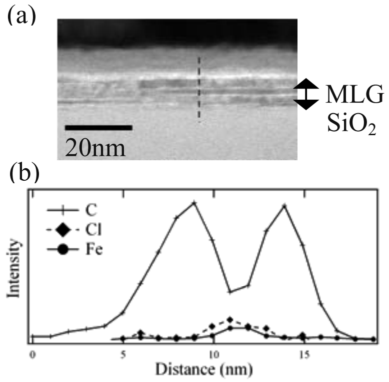

Figure 1 Cross sectional STEM image of the intercalated MLG interconnect and the line profile of EELS spectra measured along blue dot lines.

This work was supported by JSP through the “FIRST Program,” initiated by CSTP. A part of this work was conducted at the Nano-Processing Facility, supported by IBEC Innovation Platform, AIST. The synchrotron radiation experiments were performed at the BL17SU of SPring-8 with the approval of the Japan Synchrotron Radiation Research Institute (JASRI) (Proposal No. 2012B1029 and 2013A1017).

[1] K.S. Novoselov *et al.*, Science **306**, 666 (2004).
[2] D. Kondo *et al.*, IEEE International Interconnect Technology Conference 2013, pp 190.
[3] W.J. Zhao *et al.*, J. Am. Chem. Soc. **133**, 5941 (2011).

Corresponding Author: D. Kondo
Tel: +81-29-849-1074, Fax: +81-29-849-1186,
E-mail: kondo.daiyu@aist.go.jp

3-6

Graphene as a Material for Next Generation Fuel Cells

Stephen Matthew Lyth[1], Jianfeng Liu[2], Thomas Bayer[1], Sean Bishop[1], Kazunari Sasaki[1,2]

[1] *International Institute for Carbon-Neutral Energy Research, Fukuoka 819-0395, Japan*
[1] *Department of Mechanical Engineering, Kyushu University, Fukuoka 819-0395, Japan*

Graphene is an extremely promising material for use in fuel cells, due to its high strength, large surface area, and excellent thermal and electronic conductivities.. Fuel cells are extremely efficient energy conversion devices which react fuel (e.g. hydrogen) and oxygen in an electrochemical process to produce electricity. They have high energy density, are quite, durable, and can be carbon-neutral if renewably sourced hydrogen is used as a fuel.

We are exploring the application of graphene in polymer electrolyte membrane fuel cells (PEMFCs) as high surface area platinum electrocatalyst supports; as metal-free non-precious catalysts; and we are utilizing graphene oxide as a new proton-conducting material.

We synthesize large surface area, defective graphene foam (GF) by combustion of sodium ethoxide, followed by several high-temperature treatment steps to reduce oxygen content, increase crystallinity, and improve electronic conductivity (Figure 1a). This is decorated with platinum nanoparticles and applied as a cathode catalyst for PEMFCs. Our results are promising, with Pt/GF having a higher mass activity (the catalytic activity normalized to the mass of platinum) than the industry standard; Pt-decorated carbon black. (Figure 1b). However, we are still working on improving durability and PEMFC power density.

We also make nitrogen-doped defective graphene foam (GF_N). We apply this as a non-precious catalyst for electrochemical oxygen in PEMFCs. By virtue of the large surface area, we observe very high current density despite absence of metal. We use these results to shed insight on the catalytic mechanism of electrochemistry on nitrogen-doped carbons.

Graphene oxide (GO) is produced by acid treatment of graphite. It is an electronically insulating, water dispersible analogue of graphene. The surface oxygen functionalities and the affinity for water make GO a potential material for ionic membranes in PEMFCs. We have probed the fundamental ionic conductivity of graphene oxide membranes, and successfully made GO membrane fuel cells that operate at elevated temperature (Figure 1c).

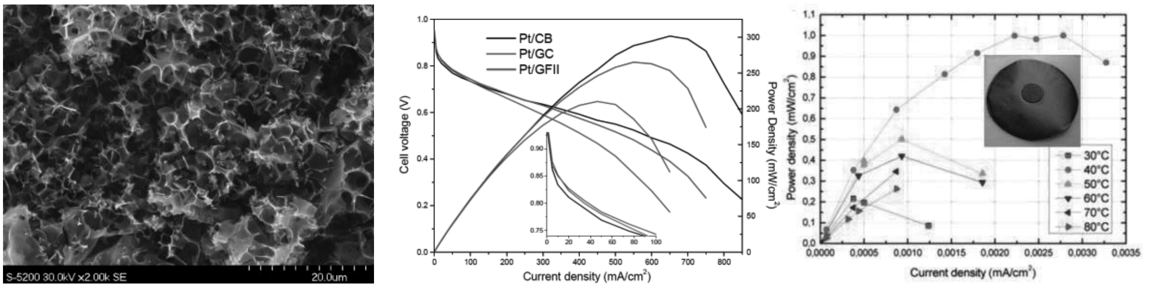

Figure 1. (a) Scanning electron microscopy image of our defective graphene foam. PEMFC voltage and power density using (b) a Pt/GF electrocatalyst layer and (c) a GO proton-conducting membrane.

[1] J. Liu, K. Sasaki, S. M. Lyth, ECS Transactions **58**, 1751 (2013)
[2] J. Liu, K. Sasaki, S. M. Lyth, ECS Transactions **58**, 1529 (2013)
[3] S. M Lyth, et al, International Journal of Hydrogen Energy 39 (1), 376-380

Corresponding Author: S. M. Lyth
Tel: +81-92-802-6742, Fax: +81-92-802-6742. E-mail: lyth@i2cner.kyushu-u.ac.jp

3-7

Graphene enabled micromechanical switches

Shao-Wei Ma[1], Ya-Ping Hsieh *

[1] *Graduate of Institute of Opto-Mechatronics, National Chung Cheng University, ROC*
**corresponding email: yphsieh@ccu.edu.tw*

Power consumption is the major technical problem affecting the development and application of electronic devices. Especially leakage currents in the off-state are a fundamental issue of semiconductor devices. Micro-electromechanical switches have demonstrated significantly lower leakage currents due to their dissimilar underlying operation mechanism. Their high complexity, large scale and low switching speed, however, make them unsuitable for universal integration in electronics.

We here demonstrate the application of graphene, a single-atomic layer of graphite. Graphene's low mass density and high strength make it ideally suited for high switching speed while its chemical and mechanical stability allows the application of high current densities.

We developed a novel three-terminal device layout where suspended graphene-membranes are forced into contact with a bottom electrode by application of a gate bias, resulting in the micromechanical equivalent of a transistor. Using facile self-assembly techniques, large arrays of these switches are produced at low cost and with easy scalability. The use of large scale switch arrays allows the control of high current values.

The presented results highlight the potential of graphene-enabled microswitches and open up new opportunities for mobile and ubiquitous electronic devices.

Twisting angle dependence of G band Raman intensity enhancement of twisted bilayer graphene

○Kentaro Sato [1], Riichiro Saito [2]

[1] *Sendai National College of Technology, Sendai 989-3128, Japan*
[2] *Department of Physics, Tohoku University, Sendai 980-8578, Japan*

Twisted bilayer graphene (TBG) is a kind of bilayer graphene. When the first or second graphene layer of bilayer graphene rotates about an axis perpendicular to the graphene surface, a structure with a much larger unit cell than that of graphene appears at a twisting angle. Since the physical properties of TBG depends on the twisting angle [1], it is important to estimate the angle in order to understand its physical properties.

Several groups have reported that G band Raman intensity of TBG is enhanced more than 30 times as large as that of monolayer graphene at specific excitation laser energy (E_{laser}) and twisting angle because of singularity in density of states [2-5]. Since resonance Raman spectra give us information to characterize not only the number of graphene layers but also the stacking structure, we can estimate the angle of TBG sample from the Raman spectra.

In this presentation, we study the G band Raman intensity of TBG as a function of twisting angle for more than 150 samples with different twisting angles and E_{laser}. The intensity of TBG is enhanced at a specific twisting angle and E_{laser} because the density of states of TBG is divergent and the energy difference between the singular points in the density of states correspond to E_{laser}. We calculate density of states and Raman intensity of TBG as a function of twisting angle in order to compare experimental results with calculation directly and study the relation between Raman intensity and twisting angle [6]. The density of states is calculated based on the tight binding method. The Raman intensity is given by calculating electron-photon and electron-phonon matrix elements.

[1] G. Trambly *et al.*, Nano Lett. 10, 804 (2010).
[2] Z. Ni *et al.*, Phys. Rev. B 80, 125404 (2009).
[3] R. W. Havener *et al.*, Nano Lett. 12, 3162 (2012).
[4] K. Kim *et al.*, Phys. Rev. Lett. 108, 246103 (2012).
[5] K. Sato *et al.* Phys. Rev. B 86, 125414 (2012).
[6] G.S.N. Eliel, H.B. Ribeiro, K. Sato *et al.* unpublished.

Corresponding Author: K. Sato
Tel: +81-22-391-5575
E-mail: kentaro@sendai-nct.ac.jp

3-9

Nitrogen-containing graphene analyzed by X-ray photoelectron spectroscopy

○Yasuhiro Yamada, Jungpil Kim, Shintaro Matsuo, Satoshi Sato

Graduate School of Engineering, Chiba University, 1-33 Yayoi, Inage, Chiba 263-8522, Japan

X-ray photoelectron spectroscopy (XPS) is among the most commonly used analytical methods for N-containing graphene. However, mainly three unclear problems such as C1s shifts, sp^2- or sp^3-hybridized carbon, and quaternary N (Q-Ns) still exist. In this work, XPS spectra of N-containing graphene were simulated using density functional theory (DFT).

Peak shifts and FWHMs of C1s and N1s XPS spectra of N-containing graphene such as pyridinic, sp^{2}C-NH$_2$(Fig. 1a), sp^{3}C-NH$_2$, pyrrolic, sp^{2}C-CN, sp^{3}C-CN, and valley quaternary N (Q-N) on edges and sp^{3}C-NH$_2$, center amine (Fig. 1b), and center Q-N in the basal plane were simulated using DFT calculation (B3LYP/6-31g(d) pop=full gfprint, Gaussian 09), and our recently developed method [1]. Binding energies of these model structures were obtained using an approximation based on the modified Koopmans theory (Fig. 2).

Assignments of N1s shifts were well fitted with reported shifts (Fig. 3), and assignments of C1s and N1s shifts of various unreported functional groups could be obtained. Three major problems could be mostly solved. For example, the shifts of main peaks of C1s spectra of graphene with various N-containing functional groups were revealed. There were clear differences of C1s and N1s shifts between sp^{2}C-NH$_2$ and sp^{3}C-NH$_2$ on edges. Also, assignments of amine groups and Q-Ns at valley and center positions were obtained. N1s shifts revealed that shifts of center Q-Ns were different from valley Q-Ns, valley amine, and center amine. This type of fine XPS analysis of N-containing functional groups using C1s and N1s shifts, and FWHMs has not been conducted elsewhere.

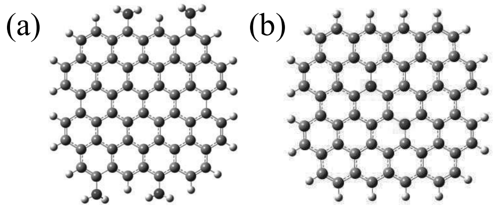

Fig.1 Modeled structures of N- containing graphene

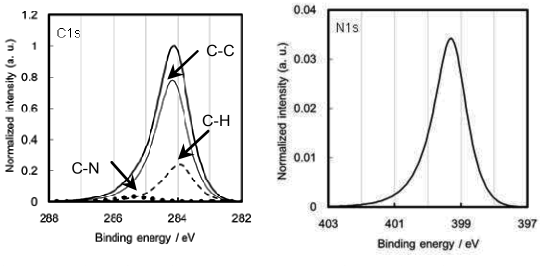

Fig.2 Simulated spectra of graphene in Fig. 1a

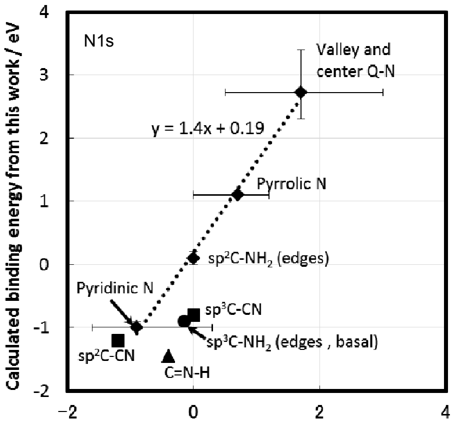

Fig.3 Correlations between calculated binding energies and averaged binding energies from references of N1s spectra

[1] Y. Yamada *et al.* J. Mater. Sci. **48**, 8171 (2013).

Corresponding Author: Y. Yamada
Tel: +81-43-290-3376, Fax: +81-43-290-3376,
E-mail: y-yamada@faculty.chiba-u.jp

3-10

Optical and Raman Analysis of Graphene Films Formed within Microholes on Quartz Glass Substrates by Liquid Phase Growth Method

○Hidefumi Hiura

[1] *Smart Energy Research Laboratories, NEC Corporation, Tsukuba, Ibaraki 305-8501, Japan*

Since graphene has unique and excellent properties, many applications have been proposed so far. In particular, graphene is promising for next-generation electronics as a channel of transistors because it has extremely high field-effect mobility of more than 200,000 $cm^2 V^{-1}s^{-1}$ even at room temperature. In the future when fabricating graphene devices in an industrial scale, it will be necessary to develop graphene-on-insulator substrates. In the past Symposia, we reported a novel production method of graphene using liquid phase growth (LPG), thereby making it possible to synthesize graphene films directly on many kinds of insulating substrates from many kinds of solid carbon materials [1, 2].

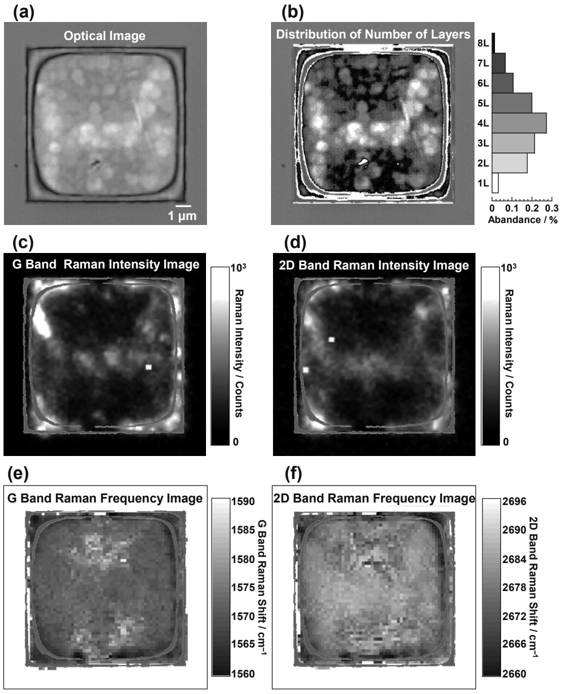

Fig.1 Images of graphene films formed within a 10-μm-side square microholes, (a) optical reflection image, (b) color plot of the number of graphene layers, (c) Raman intensity mapping image of G band, (d) Raman intensity mapping image of 2D band, (e) Raman frequency mapping image of G band, (f) Raman frequency mapping image of 2D band.

As reported in [2], the LPG method enables us to form graphene films selectively within the microholes on the surface of a quartz substrate. An example is shown in Fig. 1. An optical analysis based on the multilayer and multiple reflection model [3, 4] reveals that the number of graphene layers is distributed from 1 *L* up to 8 *L* as depicted in Fig. 1(b). Raman mapping analyses clearly demonstrate that both G band and 2D band tend to increase in intensity as the number of graphene layers increases as shown in Fig. 1 (c) and (d). On the contrast, there is no apparent correlation between the number of graphene layers and Raman frequencies both of G and 2D bands as shown in Fig 1(e) and (f), respectively. As a whole, the closer graphene films lie to the circumference of the microhole, the lower Raman frequencies both of G and 2D bands are: the lowest G band frequency is around 1560 cm^{-1} and can be found in the cutting edge of the microhole. These observations may be explained in part by differences in strain of graphene films. Namely, the graphene films in the central part become strained due to the firm contact with the bottom of the microhole, while the graphene films in the peripheral have no strain because they are suspended in the air.

[1] H. Hiura *et al.* The 40th Commemorative Fullerene-Nanotubes General Symposium, 3-7 (2011).
[2] H. Hiura *et al.* The 42nd Fullerene-Nanotubes-Graphene General Symposium, 3-2 (2012).
[3] P. Blake *et al.* Appl. Phys. Lett. **91**, 06124 (2007).
[4] H. Hiura *et al.* NEW DIAMOND, **27(3)**, 42-46 (2011).

Corresponding Author: H. Hiura

Tel: +81-29-850-1116, Fax: +81-29-856-6139,

E-mail: h-hiura@bq.jp.nec.com

3-11

Novel transfer method for clean and high mobility CVD graphene

○Ya Ping Hsieh[1], Mario Hofmann [2], Bo Suei Chiang [3]

[1] Department of Opto-Mechatronics, National Chung Cheng University, Taiwan
[2] Department of Materials Science and Engineering, National Cheng Kung University, Taiwan
[3.] Department of Opto-Mechatronics, National Chung Cheng University, Taiwan

Using Chemical vapor deposition (CVD) to synthesis graphene is known to produce high quality and large area graphene. The employed conductive catalytic substrate necessitates a transfer process after graphene growth. Surface contamination of graphene with polymer residues has been a significant problem in graphene transfer. Various reports show that the incomplete bond-scission and covalent bonding of Poly(methyl methacrylate)(PMMA) with graphene will deteriorate the quality and thus limit the achievable carrier mobility.

Here we report a new method of transferring graphene using alkane-based polymer supports. XPS, FTIR and Raman analysis show that these polymers produce less defects in the graphene which attributed to the absence of oxygen functional groups. The lower thermal and chemical stability of the alkenes used furthermore assists in the cleaner removal as confirmed by Atomic force microscopy. These advantageous properties result in a higher carrier mobility in graphene after transfer as determined by both Hall-effect and field effect mobility measurements.

Our approach makes transferring graphene cheaper and easier and opens up a route to enhance the mobility of graphene for future electronic applications.

Corresponding Author: Ya Ping Hsieh
Tel: 05-2720411, Fax:
E-mail: yphsieh@ccu.edu.tw

3-12

Mechanism and impact of ad-layer formation on CPCVD graphene

Yi-Wen Wang[1], Ya-Ping Hsieh[1], Mario Hofmann [2]

[1] *Graduate of Institute of Opto-Mechatronics, National Chung Cheng University, ROC.*
[2] *Department of Material Science and Engineering, National Cheng Kung University, ROC.*

Graphene, a two-dimensional carbon allotrope, has the potential to revolutionize transparent optical conductors (TOCs) for use as electrodes in solar cells and novel electronics. controlled chamber Chemical vapor deposition (CPCVD) has emerged as a promising synthesis method of large scale and high quality graphene. The conductance of one layer of graphene, however, is too low for many applications. Therefore, multi-layer graphene formation is being investigated to improve electrical performance of TOCs.

We here present a study on the formation of a second layer during graphene CPCVD. From the dependence of ad-layer growth rate, grain shape, and nucleation density on CPCVD parameters such as pressure and carbon feedstock concentration we extract the formation mechanism and its energetics.

We furthermore demonstrate that depending on the extent and density of this ad-layer, an enhancement or deterioration of the single-layer carrier mobility is observed. These observations are explained by the competition of scattering interactions and parallel conduction pathways.

The presented findings provide both methods and guidelines for further optimization of graphene morphology for TOC applications.

Corresponding Author: Ya-Ping Hsieh
Tel: +886-52720411#23601
E-mail: yapinglab@gmail.com

ポスター発表
Poster Preview

1P – 1 〜 1P – 50
2P – 1 〜 2P – 50
3P – 1 〜 3P – 50

1P-1

Semiempirical molecular orbital estimation of the relative stability of sulfated fullerenes

○Naoki Noji[2], Yosiaki Sano[2], Kazumi Inoue[1,2], Yosuke Kataoka[1], Hironori Ogata[1,2,]

[1] Graduate School of Engineering, Hosei University , Tokyo 113-8656, Japan
[2] Department of Faculty of Biosci Applied Chem., Hosei University ,Tokyo 113-8656, Japan

Polyhydroxylated fullerenes ($C_{60}(OH)_x$:fullerenols) have been thought to have potential applications in a variety of areas, including optoelectronics, medical therapeutics, biochemistry, polymer materials science, and electrochemistry, owing to its high solubility in large variety of solvents (depending on the number of hydroxyl groups x). The structure and solid state properties of fullerenol solids composed of a single fullerenol element are very interesting. However, fullerenols obtained by the normal synthetic procedures are all mixtures of various compositions and structural isomers. Figure 1 shows the typical MALDI TOF mass spectrum of fullerenol($C_{60}(OH)_x$, x=4-9) sample. Fullerenols were synthesized via hydrolysis of polycyclosulfted fullerene precursors1). So, the stable molecular structure of fullerenols can be speculated from the molecular structure of the polycyclosulfted fullerenes.

In this work, the energies and heats of formation of $C_{60}(SO_4)n$ (n=1-6) molecules were calculated by using AM1 semi-empirical Molecular Orbital (MO) calculations. Table 1 shows the results of heats of formation about most stable sulfated fullerene molecules.

In this presentation, the possible stable molecular structures of $C_{60}(OH)_x$ will be discussed.

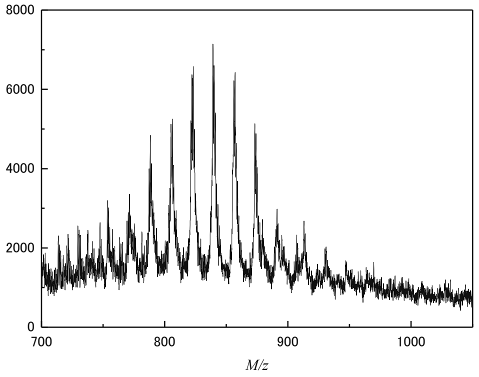

Figure 1. MALDI TOF mass spectrum of the fullerenol $C_{60}(OH)_x$(x=4-9).

Table 1. Heats of formation of $C_{60}(SO_4)_n$ (n=1-6) molecules.

Substance	$C_{60}SO_4$	$C_{60}(SO_4)_2$	$C_{60}(SO_4)_3$	$C_{60}(SO_4)_4$	$C_{60}(SO_4)_5$	$C_{60}(SO_4)_6$
Heats of formation [kcal/mol]	807	640	472	306	136	−28

[1] L. Y. Chiang et al. ,J. Org. Chem.59(1994) 3960.
[2] Zhongfang Chen et al. Journal of Molecular Structure (Theochem) 498 (2000) 227.
[3] Bo-Cheng Wang et al. Journal of Molecular Structure (Theochem) 391 (1997) 179-187

Corresponding Author:Hironori Ogata hogata@hosei.ac.jp, Tel. &Fax: 81-42-387-6229

1P-2

Excited State Electronic Interactions in Push–Pull-Chromophore–[60]Fullerene Conjugates

○Michio Yamada[1], Francesca Tancini[2], Michael Sekita[3], Dirk M. Guldi[3], Mariza N. Alberti[2],
W. Bernd Schweizer[2], François Diederich[2]

[1] Department of Chemistry, Tokyo Gakugei University, Koganei, Tokyo 184-8501, Japan
[2]Laboratorium für Organische Chemie, ETH Zürich, Zürich, Switzerland
[3]Department of Chemistry and Pharmacy and Interdisciplinary Center for Molecular Materials, Friedrich-Alexander-Universität Erlangen-Nürnberg, Erlangen, Germany

A variety of push–pull-chromophore–[60]fullerene conjugates was successfully synthesized by applying "click chemistry" to the corresponding acetylene-appended fullerene precursors (see below). When the C_{60} units and push–pull motifs were linked through pyrrolidine rings, no interactions occurred between the two moieties in the ground states. Instead, an electron transfer proceeded upon light excitation, giving the charge-separated states, which was corroborated by time-resolved transient absorption measurements.[1]

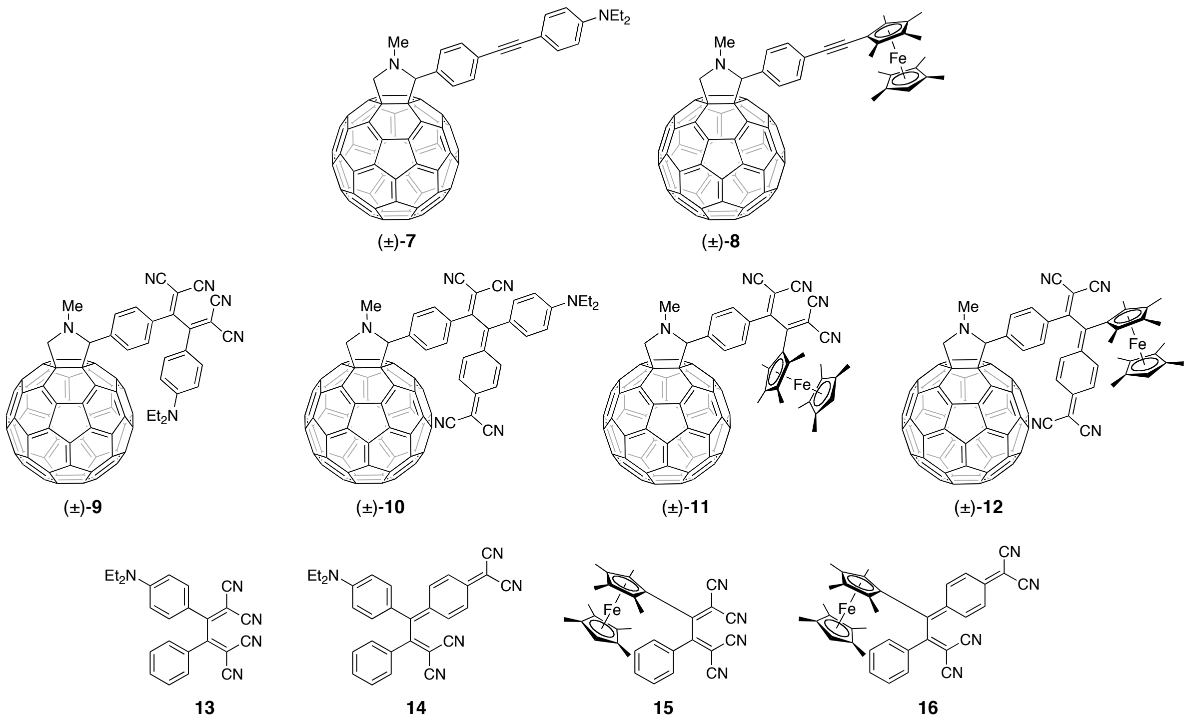

List of compounds for this study.

[1] M. Yamada et al. *Fullerenes, Nanotubes, Carbon Nanostruct.*, in press (2014).

Corresponding Author: M. Yamada
Phone & Fax: +81-(0)42-329-7493
E-mail: myamada@u-gakugei.ac.jp

1P-3

Synthesis of C_{60}-C_{70} Two-Component Fullerene Nanowhiskers

○Toshio Konno, Takatsugu Wakahara, Kun'ichi Miyazawa

Fullerene Engineering Group, Materials Processing Unit, National Institute for Materials Science, Tsukuba, Ibaraki, 305-0044, Japan

Fullerene nanowhiskers (FNWs) are thin single crystal nanofibers composed of fullerene molecules. Since FNWs are dissoluble in organic solvents, fullerene molecules can be reused by redissolving FNWs into organic solvents. For this recyclability of FNWs, FNWs have a variety of material applications.

Various combinations of fullerene molecules are possible in FNWs. In this study, we attempt to synthesize C_{60}-C_{70} two-component FNWs with C_{70} molecules uniformly solid-soluted in mother phase of C_{60}, since these have absorption bands of both C_{60} and C_{70}, and are available as new unique semiconductors with a wide wavelength range of light absorption.

We synthesized C_{60}-C_{70} two-component FNWs by the liquid-liquid interfacial precipitation method[1] at 288 K with toluene as a good solvent for fullerene and isopropyl alcohol as a poor solvent for fullerene, shifting the ratio of C_{70} to C_{60}. We conducted chemical composition analyses on C_{60}-C_{70} FNWs redissolved toluene solution by high-performance liquid chromatography. As the result, from 9 to 14 mass% C_{70} is solid-soluted in C_{60}-C_{70} FNWs. We conducted Raman spectroscopic analyses on C_{60}-C_{70} FNWs and particles. As the result, C_{70} peak area ratios of C_{60}-C_{70} FNWs are from 15 to 27 % and C_{70} peak area ratios of particles are from 58 to 86 %. That is, the excess C_{70} molecules over the solid solubility limit to C_{60} mother phase form particles. We conducted Raman spectroscopic analyses on the surface and the inside of C_{60}-C_{70} FNWs. As the result, C_{70} peak area ratios of the surface of C_{60}-C_{70} FNWs are from 15 to 27 % and C_{70} peak area ratios of the inside of C_{60}-C_{70} FNWs are from 60 to 81 %. That is, there are more C_{70} on the inside of C_{60}-C_{70} FNWs than on the surface of C_{60}-C_{70} FNWs. Using a focused ion beam system (Hitachi NB5000), we cut a C_{60}-C_{70} whisker along the direction normal to the growth axis by gallium ion beams, and obtained a cross-section of C_{60}-C_{70} whisker. We observed the cross-section of C_{60}-C_{70} whisker by scanning electron microscopy. Figure 1 shows the micrograph of the sample. We conducted X-ray diffraction analyses on C_{60}-C_{70} FNWs and C_{60}NWs. As the result, C_{60}-C_{70} FNWs contain a small amount of rhombohedral phase, and have a lattice constant of face-centered cubic phase that is larger by 0.77% than that of C_{60}NWs. We conducted ultraviolet-visible spectroscopic analyses on C_{60}-C_{70} FNWs and C_{60}NWs. As the result, C_{60}-C_{70} FNWs show the stronger visible light absorption than C_{60}NWs, especially at 600 nm.

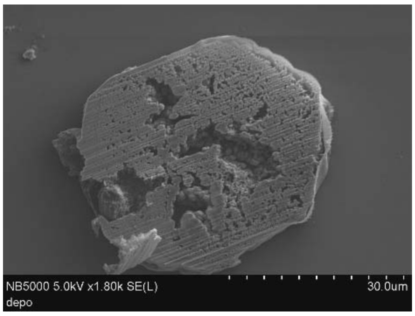

Fig.1 SEM image of the cross-section of C_{60}-C_{70} whisker.

[1] K. Miyazawa, Y. Kuwasaki, A. Obayashi, and M. Kuwabara, *J. Mater. Res.*, **17**, 83-88(2002).

Corresponding Author: K. Miyazawa
Tel: +81-(0)29-860-4528, Fax: +81-(0)29-860-4667
E-mail: miyazawa.kunichi@nims.go.jp

1P-4

Transport Characteristics of Fullerene Nano-Whisker Field Effect Transistor using Ionic Liquid Gate

○Naoto Toriumi[1], Yoshiaki Ito[1], Daiki Momiyama[1], Wataru Akiyama[1], Naoto Nakamura[1],
Taishi Takenobu[2], Jonathan P. Bird[3], Yuichi Ochiai[1], and Nobuyuki Aoki[1]

[1] Graduate School of Advanced Integration Science, Chiba University,
Chiba, 263-8522 Japan
[2] Department of Applied Physics, Waseda University, Shinjuku 169-8555, Japan
[3] Department of Electrical Engineering, University at Buffalo, SUNY, Buffalo, NY 14260-1920, USA

Ionic liquid (IL) shows highly polarized and low melting point at around room temperature. Recently, the application to the electrical device is actively carried out. Using IL as a gate dielectric layer of the field effect transistor (FET), electric double layer can be formed at the interface of the semiconductor and the IL by applying a bias voltage. Since the thickness of the layer is approximately 1 nm, extremely high electric field can be realized even by applying a few voltages. Consequently, a low voltage operation is achieved in organic FETs [1]. In this study, we applied the technique to an FET composed of fullerene nano-whisker (FNW) and observed the transport characteristics.

The FNWs were prepared by liquid-liquid interfacial precipitation (LLIP) [2] and then we used *m*-xylene or toluene as the rich solvent. The FNW-FETs were put on preformed Au electrodes on a SiO_2/n^{++}-Si substrate to form a bottom-contact structure. Observations of the transport characteristics were carried out using a probe station in vacuum (~10^{-6} torr) after thermal annealing at 440 K for 12 hours. IL (EMIM-TFSI) was dropped on FNW using one of the probes in vacuum after cooled down to room temperature and then the probe was used as an electrode for the top-IL gate.

Typical transfer and output characteristics of the FNW-FET using the IL gate is shown in Fig. 1 (a) and (b), respectively. Using the IL, a low threshold voltage (V_{th} = 0.13 V) was achieved. The mobility is estimated as 4.1 × 10^{-2} cm^2/Vs. The detail of the characteristics of the FNW-FET will be discussed in the presentation.

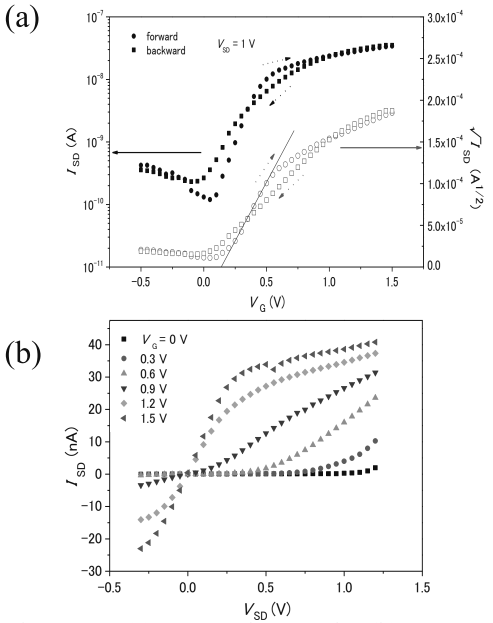

Fig. 1. (a) Transfer and (b) output characteristics of FNW-FET using IL-gate.

[1] S. Ono *et al.*, Appl. Phys. Lett. **92** 103313 (2008)
[2] K. Miyazawa *et al.*, J. Mater. Res. **17** 83 (2002)

Corresponding Author: N. Toriumi
Tel: +81-43-290-3430, Fax: +81-43-290-3427,
E-mail: n.toriumi@chiba-u.jp

1P-5

Photoinduced Charge Separation in Supramolecules between Lithium-ion-encapsulated PCBM Fullerene and Anionic Porphyrins

○Yuki Kawashima[1], Kei Ohkubo[1], Hiroshi Okada[2], Yutaka Matsuo[2], Shunichi Fukuzumi[1]

[1] Department of Material and Life Science, Graduate School of Engineering, Osaka University, ALCA, Japan Science and Technology Agency, Osaka 565-0871, Japan
[2] Department of Chemistry, School of Science, The University of Tokyo, Tokyo, 113-0033, Japan

Various supramolecular donor-acceptor compounds composed of lithium-ion-encapsulated C_{60} ($Li^+@C_{60}$) as an electron acceptor have merited special attention, because $Li^+@C_{60}$ has much more efficient electron acceptability as compared with pristine fullerene.[1] Non-polar solvents have usually been employed to construct supramolecular electron donor-acceptor compounds with strong binding. In contrast, supramolecules composed of $Li^+@C_{60}$ and anionic porphyrinoids can be formed by utilizing ionic interaction in a polar solvent, which stabilizes the charge-separated (CS) state by solvation. When anionic porphyrins ($MTPPS^{4-}$: M = Zn, H_2, Fig. 1) were employed as electron donors, the supramolecules exhibited long lifetimes of the CS state (ca. 300 μs).[2] However, the energy of the CS state is low because the LUMO level of $Li^+@C_{60}$ is significantly lower than that of C_{60}. When an electron acceptor with higher LUMO level is employed to the donor-acceptor supramolecule, the energy of the CS state can be increased. We report herein construction of supramolecule composed of $MTPPS^{4-}$ and lithium-ion-encapsulated [6,6]-phenyl-C61-butyric acid methyl ester ($Li^+@PCBM$, Fig. 1),[3] which has a higher LUMO level than that of $Li^+@C_{60}$.

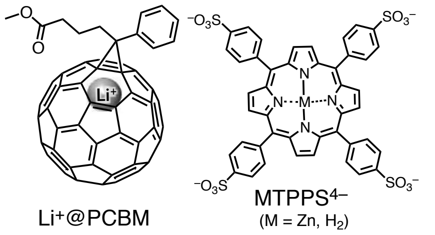

Fig. 1 Chemical structure of $Li^+@PCBM$

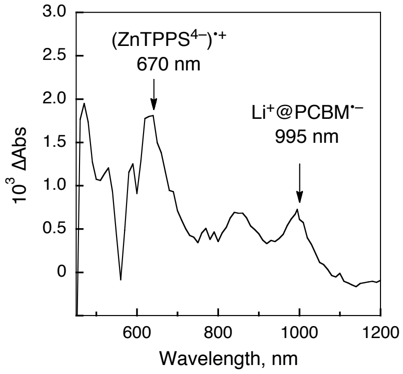

Fig. 2 Transient absorption spectrum of $ZnTPPS^{4-}$ (2.5×10^{-5} M) and $Li^+@PCBM$ (5.0×10^{-5} M) in PhCN measured at 30 μs after laser excitation at 450 nm.

UV-vis absorption spectra of $ZnTPPS^{4-}$ in PhCN at 298 K are changed upon addition of $Li^+@PCBM$, where the Q band at 558 and 599 nm are red-shifted to 562 nm and 602 nm, respectively. The formation constant (K) was determined from the titration to be 9.3×10^4 M^{-1}. This results exhibit that strong supramolecular binding between $ZnTPPS^{4-}$ and $Li^+@PCBM$ occurs by ionic interaction in PhCN. The transient absorption spectrum of the $ZnTPPS^{4-}/Li^+@PCBM$ supramolecular complex was measured by nanosecond laser flash photolysis as shown in Fig. 2. The absorption band at 670 and 995 nm can be assigned to $[ZnTPPS^{4-}]^{\bullet+}$ and $Li^+@PCBM^{\bullet-}$, respectively. This clearly indicates formation of the CS state. The lifetime of the CS state in the supramolecular complex was determined to be 560 μs at 298 K.

[1] Aoyagi, S. *et al. Nature Chem.* **2010**, *2*, 678–683. [2] Ohkubo K. *et al. Chem. Commun.* **2012**, *48*, 4314–4316. [3] Matsuo, Y. *et al. Org. Lett.* **2012**, *14*, 3784–3787.

Corresponding Author: S. Fukuzumi,
Tel: +81-6-6879-7369, Fax: +81-6-6879-7370, E-mail: fukuzumi@chem.eng.osaka-u.ac.jp

1P-6

Formation mechanism of metallofullerenes suggested by the distribution of empty fullerenes

○Tatsuki Kobayashi[1], Takeshi Kodama[2], Wataru Fujita[2], Koichi Kikuchi[2], Yohji Achiba[2]

[1] *School of Science, Kitasato University, Sagamihara, 252-0373, Japan*
[2] *Department of Chemistry, Tokyo Metropolitan University, Hachioji, 192-0397, Japan*

Recently, we have found that some kinds of dimetallofullerenes such as $Y_2@C_{80}$ and $Sc_2@C_{80}$ are extracted as a "*soluble and stable*" fullerene when we choose a mixed solvent of triethylamine (TEA) and acetone for extraction[1,2]. This fact strongly suggested that, in general, the metallofullerenes that have never been extracted by a conventional organic solvent like 1,2,4-trichlorobenzene or CS_2 are generated in growth process, but are insoluble due to the electronic properties induced by the metal atoms inside. Furthermore, it was also found that the mixed solvent works well on the stabilizing even some kinds of empty fullerenes such as C_{74} and C_{80} in solution. These phenomena can be rationalized by a charge transferring effect on the "*insoluble*" fullerenes from TEA. Therefore, the more systematic experiments by varying metal atoms combined with use of the mixed solvent for both empty- and metallo-fullerenes seem to shed a new light on understanding the growth properties of fullerenes in more detail.

Soot containing metallofullerenes was produced by direct-current (typically 60 A) arc discharge of M/C composite rods (atomic ratio M:C=2:98, M=Ba, Gd, Lu, or Sc) under a 500 Torr He atmosphere. As a reference, pure carbon rods were also arc discharged at the same condition. The raw soot was extracted for 8 h with a mixed solvent of TEA and acetone (volume ratio 1:3).

Figure 1 shows the LD-TOF-MS spectra of the extracts. It is clearly shown that the MS intensity of C_{60}-C_{90} region significantly decreases by adding metals, and these intensity changes depend on the sum of 1st and 2nd ionization energies of the metals used. We will discuss in more detail in the symposium.

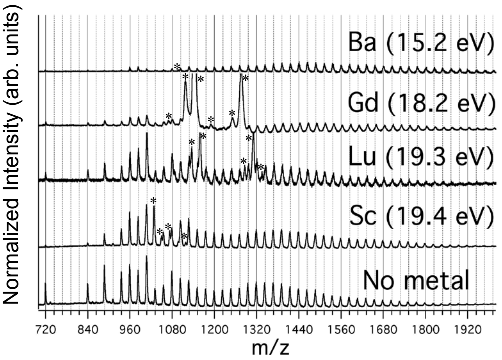

Fig. 1 LD-TOF-MS spectra of extracts by a mixed solvent extraction. Intensity is normalized by setting the peak height of C_{140} (m/z=1680) same for all the spectra. The sum of 1st and 2nd ionization potentials is shown in parenthesis. The peaks with asterisk are assigned to metallofullerenes, MC_n or M_2C_n.

[1] T. Kodama, et al. *The 41st Fullerenes-Nanotubes-Graphene General Symposium* 31 (2011).

[2] A. Togashi, et al. *The 44th Fullerenes-Nanotubes-Graphene General Symposium* 144 (2013).

Corresponding Author: Takeshi Kodama

E-mail: kodama-takeshi@tmu.ac.jp

Tel:+81-42-677-2530, Fax:+81-42-677-2525

Energetics of water molecules encapsulated into C_{60} dimer

○Kazuya Nomura and Susumu Okada

Graduate School of Pure and Applied Sciences, University of Tsukuba
1-1-1 Tennodai, Tsukuba, Ibaraki 305-8571, Japan

Fullerenes are known to accommodate forging molecules and atoms within their spherical inner space with the diameter of about 1 nm. For instance, the metal atoms can be accommodated within several fullerene cages resulting in the metalofullerenes which exhibit interesting diversity in their physical properties. In addition to atoms, recently, molecules such as hydrogen and water are also encapsulated into C_{60} by molecular surgery schemes. Since the interaction between host C_{60} and guest molecule are important to form these complexes, the physical properties of these materials are not the simple sum of those of constituent units. Therefore, detailed energetic stability and electronic structures of these complexes are still unclear. In this work, we study the energetics and electronic structures of C_{60} dimer encapsulating water molecules by first-principles total-energy calculations in the framework of density functional theory. In particular, we elucidate the dipole-dipole interaction between two H_2O molecules encapsulated into C_{60}. In the calculation, C_{60} dimer possesses [2+2] intermolecular covalent bonds and each C_{60} contains H_2O molecule with various mutual dipole directions to the adjacent H_2O molecule.

Figure 1 shows the geometric structure of C_{60} dimer encapsulating H_2O molecules. Calculated encapsulation energy of H_2O is -1.1eV/molecule indicating that the encapsulation reaction is exothermic. We find that the dipole moment of H_2O points to the intermolecular bonds of C_{60} dimer under their ground state dipole arrangement as shown in Fig. 1 in sharp contrast to the ground state configuration for two dipole moments in the classical electrodynamics. The fact indicates that the π electrons in C_{60} dimer decisively affect the energetics of encapsulated H_2O molecules and sufficiently screen the dipole moment of H_2O.

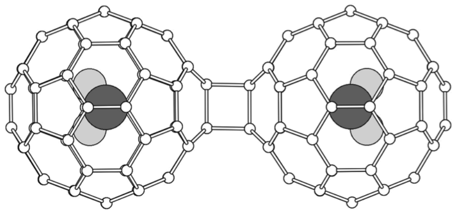

Fig1: An optimized structure of ground state of C_{60} dimer encapsulating H_2O molecules. Large and small gray circles denote O and H atoms, respectively.

Corresponding Author: K. Nomura
Tel: +81-29-853-5600(ext. 8233), Fax: +81-29-853-5924,
E-mail: sokada@comas.frsc.tsukuba.ac.jp

1P-8

High-Resolution Transmission Electron Microscopic Study of Electron-Beam-Irradiated C_{60} Single Crystal Films

○Hideki Masuda[1], Hidehiro Yasuda[2], and Jun Onoe[1*]

[1] Research Laboratory for Nuclear Reactor, Tokyo Institute of Technology, Tokyo 152-8550
[2] Research Center for Ultra-High Voltage Electron Microscopy, Osaka University, Osaka 567-0047

We reported that one-dimensional (1D) uneven peanut-shaped C_{60} polymer is formed by electron-beam (EB) irradiation of a pristine C_{60} film [1], and exhibits novel physical properties such as the geometric curvature effects on the Tomonaga-Luttinger liquid states [2]. Although *in situ* infrared spectra and density-functional calculations suggest that the 1D polymer has a cross-kinked structure close to the waist structure of the P08 C_{120} isomer obtained from the general Stone-Wales transformation, the exact structure is not still understood at this stage. In the present study, we examined the structure of the 1D polymer formed from a C_{60} single crystal film, using HRTEM and electron diffraction (ED).

The 1D C_{60} polymer film was formed on a mica substrate in an UHV chamber. After confirming the formation of the 1D polymer using *in situ* infrared spectroscopy [3], we ripped the film off the mica by putting it into pure water and mounted the film on a Cu micro-grid under the atmospheric condition, and observed the film by HRTEM.

Figure 1 (a) and (b) show a HRTEM image and ED pattern of the pristine C_{60} film (20 nm thick), respectively. This film is oriented along [111] and main spots of ED are spot-A corresponding to (220) series of FCC. Since the film contains some twins as stacking faults on (111), spot-B appears at 1/3 of (422) series (spot-C).

Figure 1 (c) and (d) show the HRTEM and ED pattern of the EB-irradiated C_{60} single crystal film (20 nm thick). Main spots of ED are spot-B. The increase in reflection intensity of spot-B indicates the increase in stacking faults. Namely, a part of the FCC molecular crystalline [111] stacking structure changes into the HCP [001] stacking.

Comparison between (b) and (d) shows some other differences such as doubleness and circular form of spot-A. These can be well explained using an HCP lattice model with a decrease in the closest C_{60}-C_{60} distance, which is the same as for the P08 isomer, along one given direction.

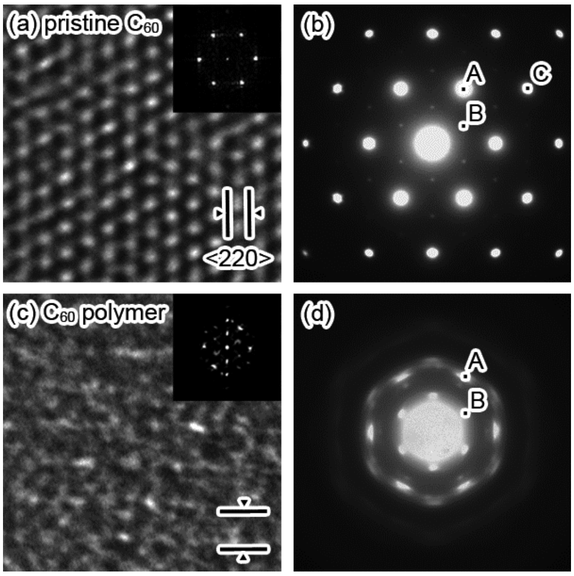

Fig. 1. HRTEM images (insets: FFT patterns) and ED patterns of pristine C_{60} (a, b) and 1D C_{60} polymer (c, d) formed from single crystal films.

[1] J. Onoe *et al.*, *Appl. Phys. Lett.* **82**, 595 (2003).
[2] J. Onoe *et al.*, *Europhys. Lett.* **98**, 27001 (2012), and references therein.
[3] A. Takashima, T. Nishii, and J. Onoe, *J. Phys. D*: *Appl. Phys.* **45**, 485302 (2012).
*Corresponding Author: J. Onoe, E-mail: jonoe@nr.titech.ac.jp

1P-9

X-ray irradiation effect on the electric conductivity of single-walled carbon nanotube films

○Takuma Araki[1], Toshiya Murakami[1], Kenji Kisoda[2], and Chihiro Itoh[1]

[1]Department of Materials Science and Chemistry, Wakayama University, Wakayama 640-8510, Japan
[2]Department of Physics, Wakayama University, Wakayama 640-8510, Japan

Single-walled carbon nanotubes (SWNTs) have many attractive properties because of their quasi-one-dimensional structure. In particular, the strong correlation between the electrical property and the geometric structure, so-called chirality, gives flexibility of controlling the electronic properties of SWNTs. We have shown that the X-ray irradiation generates defects efficiently and that the defect formation eventually leads to the structural change of SWNTs.[1] We concluded that the X-ray-induced defect is a pair of an interstitial and a vacancy (Frenkel pair) based on the results of thermal annealing study.[2] In order to clarify the irradiation effect on the electric conductivity of SWNT, we have measured the temperature dependence of the electric conductivity of SWNT films.

SWNTs grown by chemical vapor deposition were dispersed in 1wt%- aqueous solution of sodium dodecyl sulfate. In order to enrich each of the metallic (m-) or the semiconducting (s-) SWNTs, we processed the solution by gel-column-chromatographic technique.[3] The enriched SWNTs were collected by filtering the processed aqueous dispersion by a membrane filter and shaped into the film on silicon substrates by removing the filter with organic solvent vapor. The SWNT films were irradiated with 277-eV X-ray in vacuum. The electrical conductivities of X-ray irradiated films were measured at 160-300 K in vacuum (4 × 10^{-5} Pa).

Figure 1 shows the semilogarithmic plot of the normalized electrical conductivity vs $T^{-1/4}$ for pristine and the irradiated films. The evident linear relation suggests that the electrical conductivities of the SWNT films are governed by the hopping conduction. We also found that the irradiation made the slope of the temperature dependence of both films steep. On the basis of these results, it is conceivable that the carriers in SWNTs tend to localize by the formation of defects.

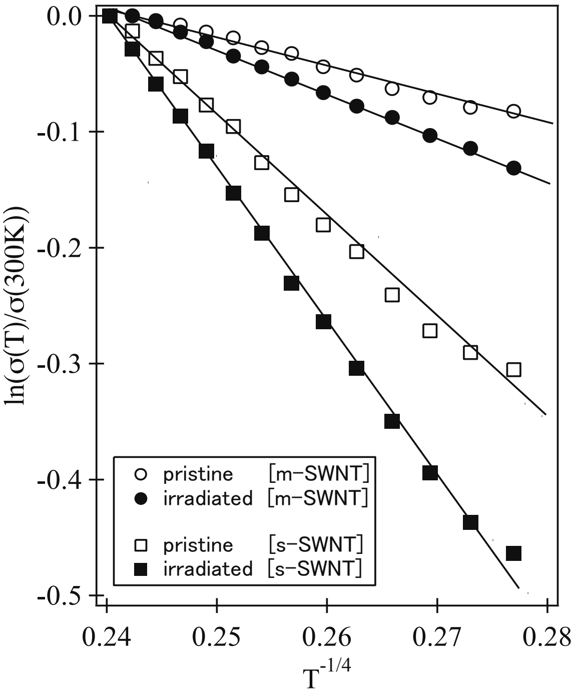

Fig.1 Temperature dependence of the electric conductivity of pristine and the irradiated SWNT films.

[1] C. Itoh *et al.* Nucl. Instr. Meth. B **266** (2008) 2772.
[2] M.Matsuda, *et al.*, 45th FNTG symposium, 2P-16.
[3] T. Tanaka, *et. al.*, App. Phys. Exp.**2** (2009) 125002.

Corresponding Author: T. Araki,
Tel: +81-73-457-8532,
E-mail: s143001@center.wakayama-u.ac.jp

1P-10

Fluidized Bed CVD of Submillimeter-Long Carbon Nanotubes Using an Internal Heat-Exchange Reactor

○Zhongming Chen[1,2], Kei Hasegawa [2], Dong Young Kim [2], Toshio Osawa [2], Suguru Noda [2*]

[1] Department of Chemical System Engineering, The University of Tokyo, Japan
[2] Department of Applied Chemistry, Waseda University, Tokyo 169-8555, Japan

Low cost production of carbon nanotubes (CNTs) will open many opportunities for the practical applications such as batteries/capacitors. Fluidized bed chemical vapor deposition (FBCVD) has realized mass production of multi-wall CNTs (MWCNTs) at several hundred tons annually per plant, but suchCNTs are short, thick, entangled, and thus less conductive. Large-scale, low-cost production of long and thin CNTs are of highly demanded. We previously developed an original FBCVD and realized semi-continuous production of submillimeter-long few-wall CNTs from C_2H_2 at a high yield $\geq$ 70% and short gas residence time ～ 0.3 s [1]. But the high gas feed causes insufficient heating of the bead bed when scaled up (Fig. 1a). This time, we designed and developed a new FBCVD reactor having an internal heat-exchange and preheating zone (Fig. 1b) and examined its performance in producing submillimter- long CNTsusing a reactor with three-times enlarged cross sectional area.

All processes for catalyst (re-)deposition, catalyst reduction, CNT growth, CNT separation, and removal of residual carbons were performed in a single fluidized bed reactor (Fig. 1b). All the gases except for the catalyst vapor were fed to the outer tube, flown down and preheated by the furnace and the hot effluent gas in the inner tube, and then flown into the inner tube through the distributor at the bottom. Catalyst vapors (aluminum-isopropoxide and ferrocene, carried by 4 vol% O_2/Ar at 20 slm) were fed directly to the bed through the catalyst line penetrating the distributor from the bottom. After catalyst deposition for 4 min, the catalyst was reduced by flowing 26 vol% H_2/ 0.06 vol% H_2O/ Ar at 9.48 slm for 10 min. CVD was performed by flowing 1.1 vol% C_2H_2/ 26 vol% H_2/ 600 ppmv H_2O/ Ar at 9.48 slm for 20 min. CNTs were separated from the beads by vigorously fluidizing the bed by Ar for 10 min. The residual carbon on the beads was removed by flowing 20 vol% O_2/Ar for 5 min. These processes were repeated at 745 °C by changing the gas flow.

The bead bed expanded from 3 cm (Fig. 1c) to 12 cm (Fig. 1d) after CVD for 20 min. The CNT yield was increased from 0.25 to 0.81 g/cycle (Fig. 1e) while CNTs retained the submillimter- long array structure (Fig. 1f). From the transmission electron microscopy (TEM) analysis, we found that the average diameter of the CNTs is 11 nm. We reduced the total supply of Ar carrier for ferrocene to one fifth and the concentration of C_2H_2 to 0.73 vol%, and realized the diameter reduction to 6.5 nm in average. The FBCVD reactor with the internal heat exchanger will realize further scale-up for practical mass production.

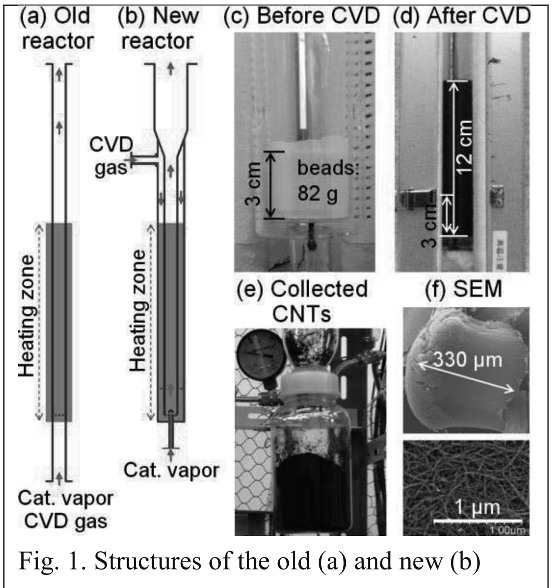

Fig. 1. Structures of the old (a) and new (b) reactors, photos of the bead-bed before (c) and after (d) CVD, photo of CNTs collected in container (e), and SEM images of the CNTs (f).

[1] D Y Kim, et al., Carbon 49, 1972 (2011).

Corresponding Author: S. Noda
Tel: +81-3-5286-2769, Fax: +81-3-5286-2769, E-mail: noda@waseda.jp

1P-11

Coherent G-band phonons in single wall carbon nanotubes

○ Ahmad R.T. Nugraha, Eddwi H. Hasdeo, Riichiro Saito
Department of Physics, Tohoku University, Sendai 980-8578, Japan

In this work, we discuss the probe energy dependence of the coherent G-band phonon intensity. In a single wall carbon nanotube (SWNT) sample, ultrashort laser pulses (~10 fs) are known to induce coherent lattice vibrations. The coherent phonon motions are been observed as oscillations of optical constants (such as reflectivity or transmittance) as a function of time in the pump-probe spectroscopy measurement, which is directly related to the modulations of absorption coefficient [1,2]. Using Fourier transform of the reflectivity or transmittance, we obtain a power spectrum as a function of phonon frequencies. The peaks in the power spectrum correspond to the coherent phonon frequencies. Some important SWNT phonon modes can be observed from this spectrum, such as the radial breathing mode (RBM) with frequency of 100-200 cm^{-1} and the G-band with frequency of about 1580 cm^{-1} [1]. For the RBM, oscillations of optical constants are already understood as a result of a diameter-dependent bandgap [2, 3]. On the other hand, while the G-band phonons can also modify absorption coefficient of SWCNTs, a previous theoretical calculation predicted that the modulations of absorption coefficient due to G-band phonons are about 1000 times smaller than those caused by the RBM [4].

However, a recent experimental measurement showed that the coherent G-band signal is comparable to the RBM signal [5]. Therefore, it indicates that a different mechanism is necessary. We recently notice that the previous theory calculated the change of absorption coefficient due to the G-band phonons by considering the same concept of energy-gap modulations as induced by RBM phonons. Instead of the energy gap modulations, here we expect that the modulations of electron-photon (or exciton-photon) interaction as a function of time should be responsible for the coherent G-band intensity. The coherent G-band vibration could cause larger change in the optical matrix elements than the RBM vibration, in which the time-dependence of optical matrix elements was not necessary.

[1] A. Gambetta et al., Nat. Phys. 2, 515-520 (2006).

[2] Y.-S. Lim et al., Nano Lett. 6, 2696-2700 (2006); J.-H. Kim et al., Phys. Rev. Lett. 102, 037402 (2009).

[3] A. R. T. Nugraha et al., PRB **84**, 174302 (2011).

[4] G. D. Sanders et al., PRB **79**, 205434 (2009).

[5] J.-H. Kim et al, PRB 86, 161415 (2012).

Corresponding Author: A. R. T. Nugraha
TEL: +81-22-795-6442, FAX: +81-22-795-6447, E-mail: nugraha@flex.phys.tohoku.ac.jp

1P-12

Photochemical Behavior of Single-walled Carbon Nanotubes in the Presence of Propylamine

○Yutaka Maeda,[1] Yuhei Hasuike,[1] Michio Yamada,[1] Tadashi Hasegawa,[1]Takeshi Akasaka[1,2]

[1]*Department of Chemistry, Tokyo Gakugei University, Koganei, Tokyo 184-8501, Japan*
[2]*Life Science Center of Tsukuba Advanced Research Alliance, University of Tsukuba, Ibaraki 305-8577, Japan*

Single-walled carbon nanotubes (SWNTs) have excellent mechanical and electrical properties that are desirable in many potential applications. SWNTs are typically grown as bundles of metallic and semiconducting SWNTs, hindering the widespread application of SWNTs. Therefore, practical use of SWNTs requires exfoliation of the bundles and separation of the metallic and semiconducting SWNTs. Various types of interactions of SWNTs with organic compounds have been studied in order to understand not only the properties of SWNTs, but also their dispersion and separation. The dispersion and separation of metallic SWNTs or semiconducting SWNTs have been achieved by sonication with various organic compounds, such as porphyrins, aromatic compounds, flavin, and so on, followed by centrifugation. We have studied the dispersion and separation of SWNTs in organic solvent using amines.[1] Interestingly, metallic SWNTs were extracted selectively from pristine SWNTs into THF containing an aliphatic amine. In recent years, much interest has been directed toward the photochemical properties of SWNTs because of the evolution of their possible applications, e.g., photovoltaic cells. Photochemical reactions of unsaturated hydrocarbons such as benzene, stilbene, and fullerene with amines are well known to afford the corresponding adducts via an electron transfer process. However, the interaction of SWNTs with amines in the excited state has not been clarified. We report here the photochemical behavior of SWNTs in the presence of propylamine. Optical and Raman spectroscopic analyses and ESR experiments reveal that the photoinduced electron transfer from the amine to the excited SWNTs causes the sidewall functionalization of small-diameter SWNTs.

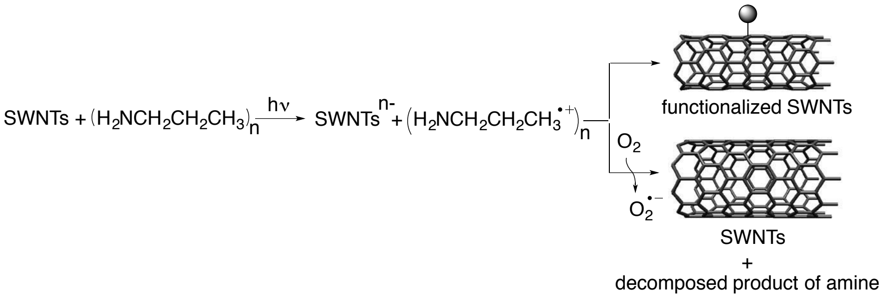

[1] Maeda, Y. et al. *Nano.* **2012**, *7*, 1130001.

Corresponding Author: Y. Maeda
Tel: +81-42-329-7512, Fax: +81-42-329-7512
E-mail: ymaeda@u-gakugei.ac.jp

1P-13

In-situ Photoluminescence-spectroelectrochemistry of Oxygen-doped Single-walled Carbon Nanotubes

Tomonari Shiraishi[1], Naoto Akizuki[2], Yuhei Miyauchi[2,3], Kazunari Matsuda[2],
Naotoshi Nakashima[1,4,5]

[1] Department of Applied Chemistry, Graduate School of Engineering, Kyushu University, 744 Motooka, Fukuoka 819-0395, Japan
[2] Institute of Advanced Energy, Kyoto University, Uji, Kyoto 611-0011, Japan
[3] PRESTO, Japan Science and Technology Agency, 4-1-8 Honcho Kawaguchi, Saitama 332-0012, Japan
[4] WPI-I2CNER, Kyushu University, 744 Motooka, Fukuoka 819-0395, Japan
[5] CREST, Japan Science and Technology Agency, 5 Sanbancho, Chiyoda-ku, Tokyo 102-0075, Japan

Local luminescent states in single-walled carbon nanotubes (SWNTs) have been of great interest due to the bright photoluminescence (PL) from such states promising for their applications in optoelectronics and bioimaging. Recently, Miyauchi *et al.* [1] have reported the extraordinary exciton brightening in such local states generated by oxygen-doping [2] and clarified the mechanism of the PL enhancement induced by dimensionality modification of excitons. However, detailed electronic structure of the oxygen-derived local states has been still unclear. To investigate the origin of the local states, it is important to evaluate the electron potentials in conduction and valence bands of the oxygen-doped SWNTs. We have reported that electronic potentials of (*n*,*m*)SWNTs can be determined based on *in situ* PL spectroelectrochemistry [3]. Here, we used this method to determine the electronic potentials of the oxygen-doped SWNTs dispersed in a carboxymethylcellulose (CMC) film.

Oxygen-doped SWNTs in a sodium dodecyl benzene sulfonate (SDBS) solution were prepared according to the previous paper [1], and the SDBS molecules were replaced with CMC. A CMC film containing the oxygen-doped SWNTs was formed on an ITO plate and used for the PL spectroelectrochmical measurements in an aqueous solution.

Fig. 1 shows a 2D-PL map obtained from the oxygen-doped SWNTs in a CMC film. The clear spot at around 1000 nm is the PL of the (6,5) SWNTs. The broad spot found at around 1150-1270 nm is the new band generated by the oxygen doping [2]. The PL intensities of the new band were found to change by applying the electrochemical potentials to the ITO electrode; thus the oxidation and reduction potentials of the local states in the oxygen-doped (6,5) SWNTs could be determined. In the meeting, we will provide detailed results of the electronic states of the oxygen-doped SWNTs.

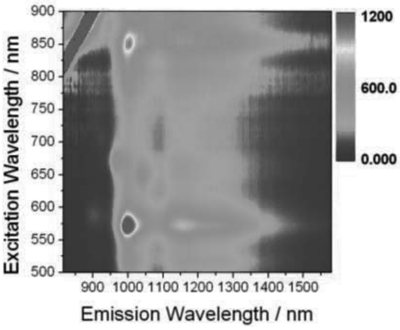

Fig. 1. 2D-PL mapping of a film of the oxygen-doped SWNTs on an ITO electrode.

[1] Y. Miyauchi *et al. Nat. Photonics,* **7**, 715 (2013).
[2] S. Ghosh *et al.*, Science 330, 1656 (2010)
[3] N. Nakashima *et al. Angew. Chem. Int. Ed.* **48**, 7655 (2009); N. Nakashima et al. *Scientific. Rep*orts, **3**, art. no. 2959 (2013).

Corresponding Author: Naotoshi Nakashima
E-mail: nakashima-tcm@mail.cstm.kyushu-u.ac.jp
Tel&Fax: +81-92-802-2840

1P-14

Far-Infrared and THz Spectroscopy of Multi-Walled Carbon Nanotubes

○Keijiro Sakai,[1] Takahiro Morimoto[1] and Toshiya Okazaki,[2,1,*]

[1] Technology Research Association for Single Wall Carbon Nanotubes (TASC), c/o Nanotube Research Center, AIST, Tsukuba 305-8565, Japan

[2]Nanotube Research Center, AIST, Tsukuba 305-8565, Japan,

Carbon nanotubes (CNTs) show very unique optical properties associating with their low-dimensionality over wide spectral ranges. Even in the far infrared (FIR) and terahertz (THz) frequency ranges, there is a broad absorption peak around a few 100 cm^{-1}. Recently, we reported the FIR-THz spectroscopic study of various SWCNT samples of different tube lengths [1]. Each SWCNT was cut via strong sonication with a different duration. Importantly, the sonication processes did not affect the diameter distribution, which was confirmed using resonance Raman and UV-Vis-NIR absorption spectroscopy. The obtained FIR-THz absorption frequencies exhibited a linear correlation with the inverse of the tube length, which agrees well with the one-dimensional (1D) dispersion relation. Moreover, the different effects of doping on the FIR-THz spectra between metallic and semiconducting SWCNTs indicate that the motion of the photo-induced carriers predominantly accounts for the optical response. It was also found that the observed resonance peaks were very sensitive to the presence of defects on the tube wall and correlated with the electric resistance of the samples. These observations suggest that the 1D current path length of the SWCNTs determines the plasmon resonance conditions.

Here we report the FIR-THz study of various multi-walled CNT (MWCNT) samples having different tube diameter and quality. Some MWCNTs show the intense peak in the FIR-THz region whereas the other exhibit no signal. Detailed characterization including the tube length dependence will be discussed in the symposium.

Reference

[1] T. Morimoto, S.-K. Joung, T. Saito, D. N. Futaba, K. Hata, T. Okazaki, submitted.

Corresponding author: Toshiya Okazaki

toshi.okazaki@aist.go.jp

1P-15

Prediction of Redox Potentials of Semiconducting Single-Walled Carbon Nanotubes

○Gergely Juhász[1], Yasuhiko Hirana[1], Naotoshi Nakashima [1]

[1] *Department of Applied Chemistry, Graduate School of Engineering, Kyushu University, Fukuoka 819-0395, Japan*

Semiconducting single-walled carbon nanotubes (SWNTs) are promising candidates for construction of nanoelectronics for their diverse semiconducting properties. Nanotubes with each chirality have well defined electronic properties which uniquely determined by the chirality index (*n,m*). For practical application, the determination of the precise value of these properties are essential.

We have previous reported a spectroelectrochemical method based on photoluminescence (PL) spectroscopy to determine the precise value of redox potentials of (*n,m*)SWNTs embedded in a film of carboxymethylcellulose sodium salt. [1] Such method allowed the accurate determination of a large set of nanotubes (tube diameters (*d*) = 0.75 -1.10 nm). However, the methods is limited by the effectiveness of dispersant can be used and it can be used only with nanotubes with well observable PL peaks. These limitations highlight the importance of empirical and theoretical predictions of electronic properties.

In this study, an empirical formula is derived from the experimentally determined redox properties of semiconducting SWNTs, and compared to a theoretical calculation on the band structure of the nanotubes. The calculations were performed on periodic models using Density Functional based Tight Binding (DFTB) method, without considering the effect of the polymer matrix. This method is capable to handle systems of several hundreds or thousands atoms, therefore it is possible to extend the calculations more complex electrochemical systems.

Experiments showed that chirality family behavior is clearly observable in the reduction potentials (E_{red}), however hardly effects the oxidation potentials (E_{ox}). In agreement with the experiments, the family behavior is more pronounced in the conducting band energies and it has small effect on valence band energies around the band gap. The results suggest that accurate prediction of redox / electronic properties of nanotubes is possible even with moderate computational resources.

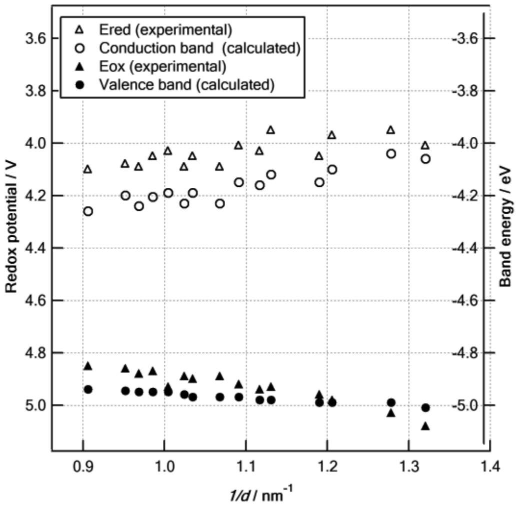

Fig.1 The calculated electronic properties and experimental redox potentials (E_{red}, E_{ox}) plotted as a function of the inverse nanotube diameter (1/*d*).

[1] Y. Tanaka *et al.* Angew. Chem. Int. Ed. **48**, 7655 (2009)

[2] Y. Hirana *et al*. Sci. Reports **3**, 2959 (2013)

[3] M. Elstner *et al.* Phys. Rev. B **58**,7260 (1998)

Corresponding Author: N. Nakashima
Tel: +81-92-802-2840, Fax: +81-92-802-2840,
E-mail: nakashima-tcm@mail.cstm.kyushu-u.ac.jp

1P-16

Photoluminescence Spectroelectrochemistry of a Single SWNT Molecule

○Liu Hong[1], Shinichiro Mouri[2], Yuhei Miyauchi[2],
Kazunari Matsuda[2], Naotoshi Nakashima[1, 3, 4]

[1] *Department of Applied Chemistry, Graduate School of Engineering, Kyushu University, Fukuoka 819-0395, Japan*
[2] *Institute of Advanced Energy, Kyoto University, Uji 611-0011, Japan*
[3] *International Institute for Carbon Neutral Energy Research (WPI-I2CNER), Fukuoka 819-0395, Japan*
[4] *JST-CREST, Tokyo 102-0075, Japan*

Many attempts have been made to investigate the electronic properties of single-walled carbon nanotubes (SWNTs) by means of scanning tunneling spectroscopy, chemical doping and Raman spectroelectrochemistry [1]. We have developed a photoluminescence (PL) spectroelectrochemical method in determining redox potentials of individual SWNTs [2]. Here we report our trial study on the PL spectroelectrochemical measurement of a single SWNT molecule, which is expected to open up a new way in characterizing electronic states of SWNTs.

CoMoCAT-SWNTs were dispersed in a toluene solution of poly[(9,9-dioctylfluorenyl-2,7-diyl)-alt-co-(6,6’-{2,2’-bypyridine})] (PFO-Bpy) by sonication, and a diluted supernatant after centrifugation was spin-cast on an ITO substrate so that the SWNT could be isolated. The fluorescence from single nanotube has been successfully observed by means of fluorescence imaging. PL spectroelectrochemical measurement of single nanotube was carried out with a conventional three-electrode setup (Fig. 1) in aqueous electrolyte. It has been observed that fluorescence of single nanotube was gradually quenched as the applied potential to ITO substrate increased, and this quenching behavior was in agreement with the plots of PL response from macroscopic SWNTs sample against potentials as previously reported. Detail will be reported at the meeting.

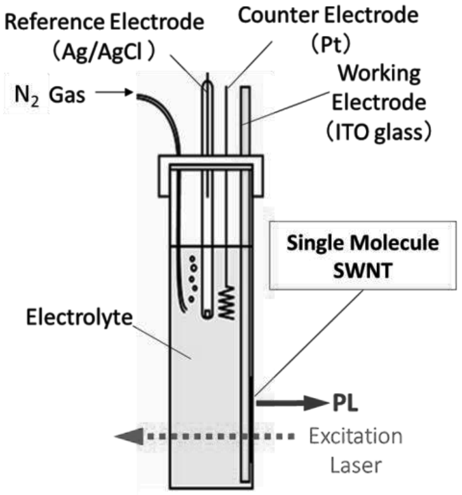

Fig.1 setup of PL spectroelectro-chemical measurement

[1] a) J. W. G. Wildoer *et al*. Nature. **391**, 59 (1998); b) M. J. O’Connell *et al.* Nat. Mater. **4**, 412 (2005); c) K. Okazaki *et al.* Phys. Rev. B. **68**, 035434 (2003).

[2] a) Y. Tanaka *et al.* Angew. Chem. Int. Ed. **48**, 7655 (2009); b) Y. Hirana *et al.* J. Am. Chem. Soc. **132**, 13072 (2010).

Corresponding Author: N. Nakashima
Tel: +81-92-802-2840, Fax: +81-92-802-2840,
E-mail: nakashima-tcm@mail.cstm.kyushu-u.ac.jp

1P-17

Electric Characterization of Chirality Controlled Single-Walled Carbon Nanotubes

○Yusaku Tsuda[1], Takumi Sagara[1], Keisuke Yoshida[1], Koji Ishii[2], Kenichi Yamakawa[1],
Hirofumi Yajima[2], Nobuyuki Iwata[1] and Hiroshi Yamamoto[1]

[1] *Department of Electronics & Computer Science,College of Science & Technology,*
Nihon University, 7-24-1 Narashinodai, Funabashi, Chiba 274-8501 Japan
[2] *Department of Applied Chemistry, Faculty of Science, Tokyo University of Science, 1-3*
Kagurazaka, Shinjyuku-ku, Tokyo 162-0826, Japan

Single-walled carbon nanotubes (SWNTs) have been regarded as one of the best candidates for future applications in nanoelectronic devices due to its high mobility, high current-carrying capacities, and so on. In our previous report, position selective growth of single-walled carbon nanotubes (SWNTs) is carried out on a surface treated SiO_2 (300nm)/Si substrate between electrodes by cold-wall chemical vapor deposition (CC-CVD) method in μm-scale. In addition, chirality controlled growth of the SWNTs is also done by irradiating free electron laser (FEL) with the wavelength of 800 nm during CC-CVD growth [1]. The grown SWNTs are all semiconducting investigated by a multi excited laser Raman analysis. However, the grown SWNTs direction is random on SiO_2 (300nm)/Si substrate. The remained issue for applications of the field effect transistor (FET) using just one SWNTs is the in-plane alignment synthesis process. In addition, chirality controlled and semiconducting SWNTs growth is expected by just Raman spectra. The purpose of this study is not only to align the SWNTs but also to clarify the semiconducting property by electric measurement. The CC-CVD growth was carried out on the SiO_2/Si and annealed *r*-cut sapphire substrate for the purpose of the in-plane alignment [2]. The Co/Mo catalysts were adhered by dipping technique followed by firing. The electrodes will be deposited before and/or after the CVD process with the FEL irradiation. The chirality controlled electric property will be discussed.

[1] K. Sakai, S. Doi, N. Iwata, H. Yajima, and H. Yamamoto, IEICE Trans. Electron. E94-C (**2011**) 1861-1866.
[2]H. Ago, K. Imamoto, N. Ishigami, R. Ohdo, K. Ikeda and M.Tsuji, “Competition and cooperation between lattice-oriented growth and step-templated growth of aligned carbon nanotubes on sapphire”, Applied Physics Letters 90, 123 (**2007**).

1P-18

Hydrogen evolution from benzene with single-walled carbon nanotubes as a photocatalyst

○Naoki Kohno [1], Kei Ohkubo [1], Shunichi Fukuzumi [1]

[1] *Department of Material and Life Science, Graduate School of Engineering, Osaka University, ALCA, Japan Science and Technology Agency, Osaka 565-0871, Japan*

Hydrogen is regarded as a clean fuel for the next generation but most hydrogen supplied for industries is produced from fossil fuels by the steam-reforming reaction at high temperature. To solve this problem, extensive efforts have been devoted to the development of various photocatalytic hydrogen production. So far, noble metals such as Pt or semiconductors have been used as a photocatalyst. However, there is no report on photocatalytic hydrogen evolution using organic compounds as a photocatalyst. Single-walled carbon nanotubes (SWNTs) have merited great interest because of their unique optical property and large hydrogen storage capacity[1]. We report herein the use of SWNTs as a hydrogen evolution photocatalyst by laser irradiation in aromatic solvent.

Hydrogen evolution occurred in a deaerated benzene solution (2.5 mL) containing SWNTs (0.15 mg) under laser irradiation (λ =532 nm, 500 mW). The amount of hydrogen evolved reached 102 μmol and yield based on benzene used as a solvent was 0.40% by laser irradiation for 2 hours. The quantum yield of hydrogen evolution was determined as 0.34. When benzene was replaced by deuterated benzene, the deuterated hydrogen molecules such as HD and D_2 were evolved efficiently. This result suggests that the hydrogen source is benzene used as a solvent. Hydrogen was also evolved in substituted benzene such as toluene, 1,4-dimethylbenzene or benzonitrile as solvents. The evolved H_2 amounts were 66.0, 60.2 or 39.2 μmol by laser irradiation for 2 h, respectively. The products from benzene were determined by GC-MS and HPLC to be biphenyl and terphenyls. Thus, hydrogen was evolved via the condensation reaction of benzene in the photocatalytic reaction.

Scheme 1

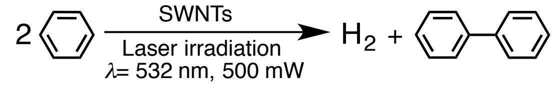

The initial rates of hydrogen evolution are proportional to the fourth power of laser intensity as shown in Figure 1. This result indicates that a multiphoton absorption process is involved in this photochemical reaction.

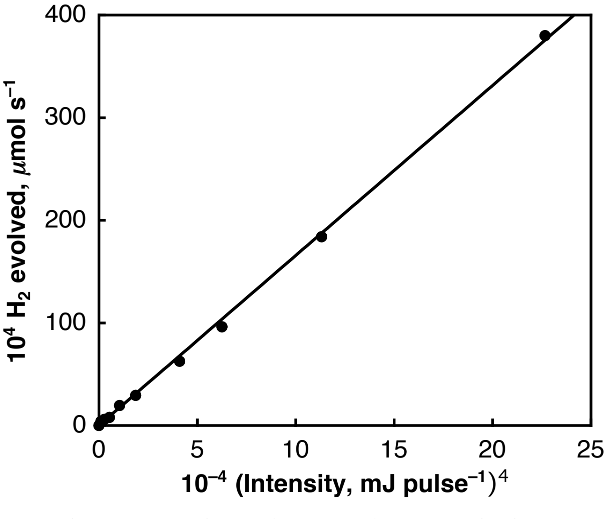

Figure 1. Plot of rate of H_2 evolution vs the fourth power of laser intensity in benzene containing SWNTs (2.5 mL, 0.15 mg) by laser irradiation (λ = 532 nm).

[1] Dilon, A. C. *et al. Nature* **1997**, *386*, 377.

Corresponding Author: S. Fukuzumi
Tel: +81-6-6879-7369, Fax: +81-6-6879-7370,
E-mail: fukuzumi@chem.eng.osaka-u.ac.jp

1P-19

High-throughput fabrication of carbon nanotube thin-film transistors with flexographic printing process: Fabrication of short channel top-gate devices

○Michihiko Maeda[1], Kentaro Higuchi[1], Shigeru Kishimoto[1], Yuta Nakajima[2],
Takuya Tomura[2], Masafumi Takesue[2], Katsuhiko Hata[2], and Yutaka Ohno[1]

[1] Department of Quantum Engineering, Nagoya University, Nagoya 464-8603, Japan
[2] Research and Development Center, Bando Chemical Industries, LTD., Kobe 650-0047, Japan

Among many kinds of thin-film transistors (TFTs), carbon nanotube (CNT) TFTs have attractive properties such as high mobility, flexibility, transparency, printability, and so on. In the previous work, we introduced flexographic printing technique, one of high speed printing methods, in the fabrication of CNT TFTs on a plastic film, and achieved a high mobility of 157 cm^2/Vs by the fully lithography-free and ambient-pressure processes. [1] In this work, we have improved the resolution of the printing technique to realize top-gate CNT TFTs with a short channel length of sub-10 μm.

The plate for high-resolution flexographic printing was made of PDMS with micro-fabrication process. Top-gate TFTs were fabricated on a polyethylene naphthalate (PEN) film with a thickness of 100 μm. First, a thin film of semiconductor CNTs was formed on the film by transfer process. The CNTs were patterned by printing resist ink subsequent etching with ambient pressure plasma with O_2/Ar. Then, the source and drain electrodes, gate insulator, and gate electrode were printed. Silver nanoparticle ink and polyimide ink were respectively used for the electrodes and insulator.

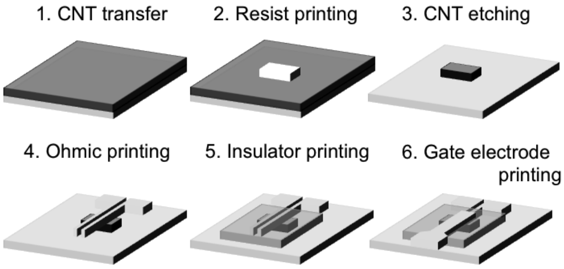

Fig. 1 Device fabrication process

Figure 2(a) shows the fabricated CNT TFTs. The channel length is about 8 μm as shown figure 2(b), which is about one-fourteenth of our previous device. [1]

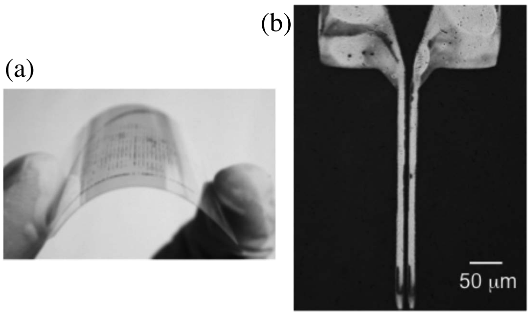

Fig. 2 (a) Printed CNT TFT on PEN substrate. (b) Printed source and drain electrodes with channel length of 8 μm.

This work was partially supported by ’08 NEDO Grant, ALCA-JST, SICORP-JST, and Grant-in-Aid of MEXT.

[1] K. Higuchi *et al*., *Appl. Phys. Express* **6**, 085101 (2013).

Corresponding Author: Y. Ohno
Tel: +81-52-789-5387, Fax: +81-52-789-5387
E-mail: yohno@nuee.nagoya-u.ac.jp

Evaluation of Dynamic Performance of CNT Random Network Transistors

Noriyuki Tonouchi[1,4], Hiroyuki Endoh[1,4], Takashi Manako[1,4]
Fumiyuki Nihey[2], Hideaki Numata[2], Tomoyuki Yokota[3], Tsuyoshi Sekitani[3], and Takao Someya[3,4]

[1] Smart Energy Research Laboratories, NEC Corporation, Tsukuba 305-8501, Japan
Phone: +81-29-850-1157 E-mail: n-tonouchi@ab.jp.nec.com
[2] Technology Research Association for Single Wall Carbon Nanotubes (TASC), Tsukuba 305-8565, Japan
[3] Department of Electrical Engineering, School of Engineering, The University of Tokyo, Tokyo 113-8656, Japan
[4]Institute for Nano Quantum Information Electronics, Tokyo 153-8505, Japan

1. Introduction

We have promoted research and development on carbon nanotube transistors (CNT-TFTs) as promising devices toward achieving applications for printed electronics [1–2]. CNTs have high electrical properties and the mobility of CNT-TFTs has achieved 1–10 cm^2/Vs or more even though their channels have been fabricated with printing processes [3–4]. Therefore, CNT-TFTs are expected to have the potential to achieve printed devices that are high performance such as those that require operating frequencies over 100 kHz (e.g., scanning line drivers for display panels). Until now, CNT-TFTs have been evaluated by only focusing on their static performance. Therefore, there have been few researchers who have actually evaluated their dynamic performance. In the present work, we evaluated the dynamic performance of CNT-TFTs whose channels had been fabricated with a printing process. We aimed at demonstrating switching action over 100 kHz.

2. Experiments and Results

First, we fabricated a CNT-TFT having vapor-deposited source-drain electrodes. Figure 1 has a cross-sectional view of the CNT-TFT. The width of the source-drain electrodes was 100 um. Generally, TFTs have parasitic gate capacitance due to the overlap between gate and source-drain electrodes. The parasitic capacitance conducts the displacement current, or the background noise superimposed on the on-off switching signal. Since the amplitude of the background noise has positive dependence on the gate frequency, the background masks the on-off signal of the CNT channel at higher frequency. We measured the amplitude of the background and found that it was 100-1000 times larger than that of the on-current of the CNT-TFT at 100 kHz. So no reliable verification of switching action could be achieved at the higher frequency. That is, verification of on-off action over 100 kHz requires an improved S/N ratio.

There are two main methods of improving the S/N ratio: (1) Reducing the gate capacitance; (2) Enhancing the on-current. We examined making the drain electrode narrower as a method of (1). We patterned the source-drain electrodes with super inkjet (SIJ) technology to make them narrower. The width of the electrodes was confirmed to be 2–3 µm from the SEM image. Compared to the case of the TFTs having vapor deposited electrodes, the amplitude of the background was suppressed to ~1/10. As a method of (2), we examined increasing CNT density. We fabricated the channel with CNT ink that had been treated to reduce the surfactant through dialysis to increase the CNT density. Reducing the surfactant enabled us to increase the relative content of CNTs. The on-current of the fabricated CNT-TFT was about 100 times larger than that of the CNT-TFT having vapor-deposited electrodes. Figure 2 shows the actual switching action of this improved CNT-TFT. Clear switching action can be identified even at 500 kHz. This study confirmed the superiority of CNTs as printable channel materials and suggested the possibility of pioneering fields of application for printed electronics by using CNT-TFTs.

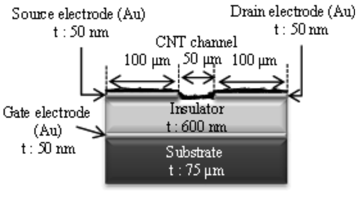

Fig. 1. Cross section of TFT

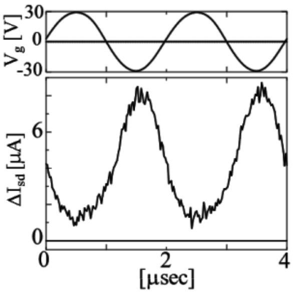

Fig. 2. Switching action at 500 kHz (SIJ)

References

[1] H. Numata *et al.*, *Appl. Phys. Express* **5** (2012) 055102.

[2] H. Endoh, *J.Photopoly.Sci.Tech* **25** (2012) 281.

[3] P. Beecher *et al.*, *J. Appl. Phys.* **102** (2007) 043710.

[4] T. Takenobu *et al.*, *Appl. Phys. Express* **2** (2009) 025005.

Preparation of Al-CNT Nanocomposites using Mechanical Alloying

○Takumi Goto, Kouki Terashima, Mitsuhiro Takeda, Masaru Sekido

Department of Material Science and Engineering, Sendai National College of Technology,
Natori 981-1239, Japan

Due to their combination of outstanding mechanical characteristics, extremely large interfacial contact area, high aspect ratio, and low mass density, CNTs are considered as the ideal reinforcement fillers for the nanocomposite materials. Among various nanocomposites CNT–metal matrix composites are expected to assume the role of structural materials in the next-generation. However, CNT–metal matrix composites are currently falling behind in bulk fabrication due to the difficulty of dispersing the CNTs. In this work we used mechanical alloying (MA) and spark plasma-sintering (SPS) technique to prepare Al-CNT nanocomposites with homogenous distribution and excellent dispersion of CNTs.

Briefly MWCNTs powder (0.5 -2.0 wt%) and Al powder were suspended in Acetone and sonicated for 30 min. After removing solvent the obtained powder was dried under reduced pressure for 12 h to give MWCNTs/Al powder with good dispersion. MWCNTs/Al powder was then placed into stainless steel mixing jars containing 25 stainless steel milling balls of 10 mm diameter (ball-to-powder weight ratio (BPR) = 10:1). The jars were filled with argon and were then agitated using a planetary ball mill at 300 rpm for 6 h. Microstructure characterizations were performed using scanning electron microscope (SEM).

The obtained MWCNTs/Al powder was sintered in a carbon mold using a spark plasma-sintering (SPS) device. The sintering conditions were maximum temperature 500 ^{o}C, holding time 20-30 min., and pressure of 10 MPa.

We will also report and discuss the improvement of tensile strength of Al-CNT nanocomposites, prepared by MA and SPS technique.

Corresponding Author: M. Sekido
Tel: +81-22-381-0329, Fax: +81-22-381-0329
E-mail: sekido@sendai-nct.ac.jp

Multi-walled carbon nanotubes and carbon black supported platinum nanoparticles for catalyst of polymer electrolyte membrane fuel cells

○ Zehui Yang [1], M. R. Berber[1], Tsuyohiko Fujigaya[1,2], and Naotoshi Nakashima[1,2,3]

[1] Department of Applied Chemistry, Graduate School of Engineering, Kyushu University, 744 Motooka, Nishi-ku, Fukuoka 819-0395, Japan
[2] International Institute for Carbon Neutral Energy Research (WPI-I2CNER), Kyushu University, 744 Motooka, Nishi-ku, Fukuoka 819-0395, Japan
[3] JST-CREST, 5 Sanbancho, Chiyoda-ku, Tokyo, 102-0075, Japan

Investigating alternating energy is one of the biggest challenges for the 21st century. Owing to high energy density, high efficiency and green emissions, polymer electrolyte membrane fuel cells (PEMFCs) are recognized as one of the promising solutions. Platinum (Pt) is selected as the catalyst due to the high catalytic activity among other metals and alloys. However, Pt nanoparticles still suffer from low durability due to the corrosion of carbon supports, Pt dissolution, Ostwald ripening, aggregation and migration. The low durability and high price blocks widespread commercialization of PEMFCs.

To reduce the cost and enlarge the catalytic activity, Pt loading on carbon supporting materials has been studied. Multi-walled carbon nanotubes (MWNTs) due to high electron conductivity and chemical stability are ideal supporting materials for Platinum. Carbon black (CB) has been widely used as the supporting material because of its low price. The pyridine-containing polybenzimidazole (PyPBI) can be used as a dispersant of CNTs to make them homogeneously dispersed. In this study, PyPBI wrapped CB and MWNTs were used as a hybrid support for the Pt-based PEMFCs catalyst.

Different ratios between the MWNTs and CB are investigated. Based on the durability measured by CV cycling and fuel cell performance, when the mount of MWNTs reaches to 10wt%, the durability and fuel cell performance are similar to that of 100wt%-MWNTs. Typical result is shown in Fig. 1.

Details will be reported at the meeting.

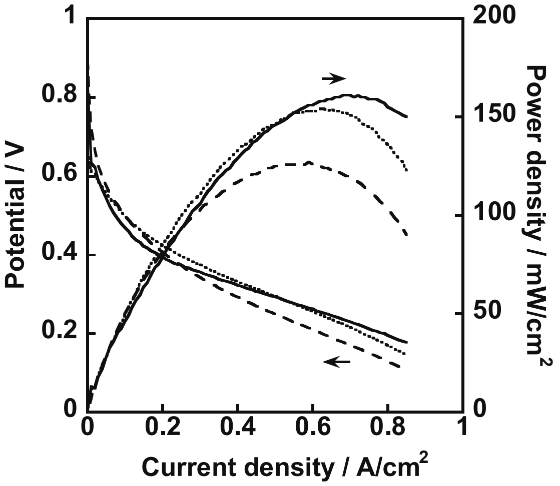

Figure 1. Polarization of I-V and power density curves of different MEAs for PyPBI/10%MWNTs-90%CB/Pt (dotted line), PyPBI/MWNTs/Pt (solid line), and PyPBI/CB/Pt (dashed line)

References

[1] N. Nakashima, et al., *Adv. Mater.* 25 (2013) 1666-1681.

[2] N. Nakashima, et al., *Sci. Rep.* 3 (2013) 1764.

Corresponding Author: N. Nakashima
TEL: 092-802-2840, FAX: 092-802-2840
E-mail:nakashima-tcm@mail.cstm.kyushu-u.ac.jp

1P-23

Low-voltage carrier injection into semiconductor thin film from CNT thin film utilizing field enhancement effect

○Tatsuya Yamada [1], Shigeru Kishimoto [1], and Yutaka Ohno [1]

[1] *Department of Quantum Engineering, Nagoya University, Nagoya 464-8603, Japan*

CNT thin films are attractive material for transparent conductors of various semiconductor devices such as OLEDs because of their flexibility and processability. In this work, we have investigated carrier injection from sparse CNT thin films into a semiconductor thin film by means of device simulation. As the result, we have found that it is possible to inject carriers at low voltage by utilizing field concentration onto CNTs.

Figure 1 shows a device structure examined in the simulation. CNTs were placed as the anode on the top surface of a *p*-type semiconductor thin film (E_g = 1.1e V, $N_A = 10^{17}$ cm^{-3}) with a thickness of 300 nm. Here, a simple metal wire with a diameter of 1 nm was assumed as the CNTs. The interface between the CNTs and semiconductor assumed to be a Schottky junction with a barrier height of 0.56 eV for a hole. A flat cathode electrode was placed on the bottom of the semiconductor layer. Ohmic contact was assumed for the cathode.

Figure 2 shows the hole current injected from the CNTs into the semiconductor film as a function of spacing between the CNTs (*Δ*) at a bias voltage of 1 V. Here, *Δ* = 0 corresponds to a plate electrode. The hole current increased with *Δ*, and showed a peak at around *Δ* = 125 nm. Figure 3 shows the calculated energy band structure at 1 V for two cases; the plate anode and the CNT anode with *Δ* = 125 nm. In the case of the CNT anode, the Schottky barrier was bent strongly, and the thickness of the barrier was decreased. This is because the electric field was concentrated to the thin CNT electrodes. As the consequence, the tunneling probability of holes was increased. The hole current increased about four orders of magnitude in the low voltage region as compared to the plate anode. For *Δ* > 125 nm, the current decreased due to a decrease in effective area of the anode electrode. By utilizing the field enhancement effect, it can be expected to reduce the operation voltage of devices such as OLEDs.

This work was partially supported by ALCA/JST, SICORP/JST, and Grant-in-Aid of MEXT.

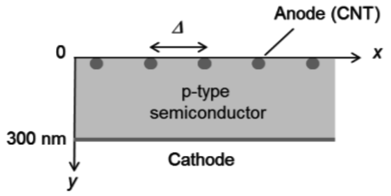

Fig. 1 Device structure examined in simulation.

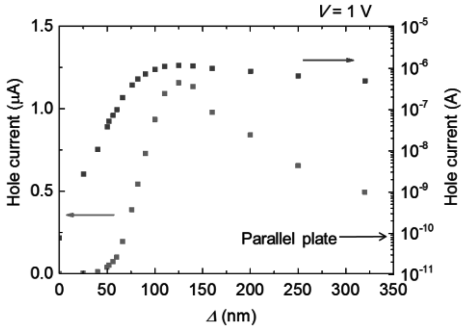

Fig. 2 Calculated hole current versus *Δ* at 1 V.

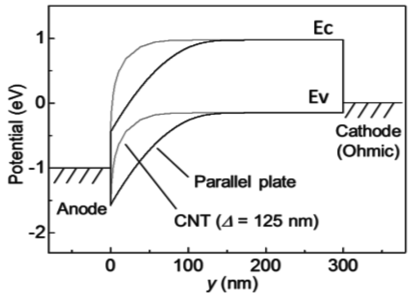

Fig. 3 Calculated energy band structures at 1 V for two cases; the plate anode and the CNT anode with *Δ* = 125 nm..

Corresponding Author: Y. Ohno
Tel: +81-52-789-5387, Fax: +81-52-789-5387,
E-mail: yohno@nuee.nagoya-u.ac.jp

1P-24

Highly durable membrane electrode assembly consists of poly(vinylphosphonic acid)-polybenzimidazole electrolyte and carbon nanotubes based-electrocatalyst

○Mohamed R. Berber[1,2], Tsuyohiko Fujigaya[1,3], Naotoshi Nakashima[1,3,4]

[1] *International Institute for Carbon Neutral Energy Research (WPI-I^{2}CNER),*
Kyushu University, Fukuoka 819-0395, Japan
[2]*Department of Chemistry, Faculty of Science, Tanta University,*
Tanta 31527, Egypt
[3]*Department of Applied Chemistry, Graduate School of Engineering,*
Kyushu University, 744 Motooka, Nishi-ku, Fukuoka 819-0395, Japan
[4]*JST-CREST, 5 Sanbancho, Chiyoda-ku, Tokyo, 102-0075, Japan*

Low durability of polymer electrolyte fuel cell (PEFC) is a major drawback that should be solved. Recent studies have revealed that leaching of liquid phosphoric acid (PA) from both polymer electrolyte membrane (e.g. polybenzimidazoles; PBIs) and catalyst layers causes inhomogeneous PA distribution and into membrane electrode assembly (MEA), leading to a deterioration of PEFC performance during long-term operation [1].

In this study, in order to prevent acid leaching from the high temperature PEFC system, we used poly(vinylphosphonic acid) (PVPA) in place of PA because PVPA is a polymeric acid and is stably bound to the PBIs via multipoint acid-base reactions [2]. Also, It forms a hydrogen-bonding network with the neighboring phosphonic acid groups [3]. Consequently, it forms an effective proton pathway after blending with PBI [4]. Typically in this study, we fabricated a novel fuel cell electrocatalyst by using carbon nanotubes (CNTs), PVPA-doped PBI and platinum (Pt) nanoparticles as an electron-conducting supporting material, electrolyte and metal catalyst, respectively (figure 1). The fabricated electrocatalyst was used beside a PVPA-PBI membrane to prepare the MEA. The assembled MEA was used to test the fuel cell performance and the durability at a non-humidified operating. The fuel cell performance of the assembled MEAs was measured at atmospheric pressure under flowing dry hydrogen (flow rate; 100 mL/min) and dry air (flow rate; 200 mL/min) at the anode and cathode, respectively. The polarization curves were recorded at 120° C under non-humidified operating conditions. Subsequently, the assembled MEA were subject to accelerating potential durability test.

Successfully, the assembled MEA showed a remarkable high durability (single cell test: >400,000 cycling) together with a high power density of 252 mW/cm^2 at 120˚C under a non-humidified condition. Such a high performance PEFC opens the door for the next-generation PEFC for “real world” use.

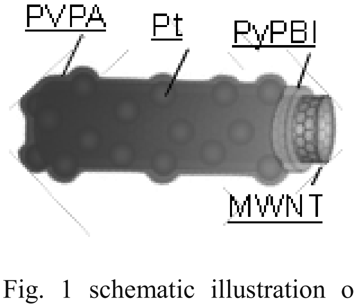

Fig. 1 schematic illustration of the prepared electrocatalyst

[1] Y. Oon *et al*. J. Power Sources **189**, 943(2009).

[2] Ü. Akbey *et al*, Aust. J. Chem. **62**, 848 (2009).

[3] Y. J. Lee *et al*. J. Phys. Chem. B **111**, 9711(2007).

[4] O. Acar *et al*. Int. J. Hydrogen Energy **34**, 2724(2009).

Corresponding Author: M. R. Berber
Tel: +81-92-802-2845, Fax: +81-92-802-2845,
E-mail: mrberber@mail.cstm.kyushu-u.ac.jp

1P-25

Single-Walled Carbon Nanotubes/Poly(Ionic Liquids) Nanocomposites for Extremely High Thermovoltage

○Motohiro Nakano, Yoshiyuki Nonoguchi, Takuya Nakashima, Tsuyoshi Kawai

Graduate School of Materials Science, Nara Institute of Science and Technology,
Nara 630-0192, Japan

Most flexible thermoelectric polymer composites with carbon nanotubes (CNTs) [1] have ever lacked practical Seebeck coefficient comparable to that of conventional inorganic materials. The effective procedure for enhancing the Seebeck coefficient has not yet been established. On the other hand, Aida et al. discovered that polymerizable ionic liquids (PILs) enable single-walled carbon nanotubes (SWNTs) to be exfoliated from their bundles, which formed highly-conducting polymer composites. [2] This well-dispersed SWNT material inspired us to investigate effects of the interaction between SWNT and PIL on their thermoelectric properties. We here-in report the thermoelectric properties of SWNT/PIL nanocomposites, using CNTs synthesized by supergrowth chemical vapor deposition (SG-CNT from AIST), and commercial ones purchased from KH-Chemicals Co., Ltd. (KH-CNT) and Southwest Nanotechnologies (CoMoCAT). PILs were synthesized following the modified procedure [2] except for MAEMAM [3] (Fig.1). These PILs and SWNTs were mixed with radical initiators at various concentrations and the mixtures were heated at 330 K for 2 hours, forming polymerized solids. We evaluated Seebeck coefficient and electrical conductivity of all the eighteen composites at 310 K. A SG-CNT/MAEMAM composite possessed an extremely high Seebeck coefficient (135 μV/K) at 310 K. This composite showed roughly 5-fold increase in Seebeck coefficient in comparison with previous CNT-based thermoelectric materials. We also found that the composite showed the highest Seebeck coefficient with 1% of weight fraction of SG-CNT. We will discuss temperature dependence of Seebeck coefficient and electrical conductivity.

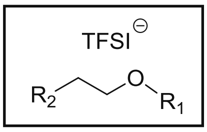

		R_1	
		Methacryloyl	**Acryloyl**
R_2	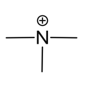	**MAEMAM**	**AEMAM**
	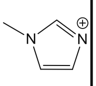	**MAEMIM**	**AEMIM**
	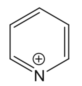	**MAEMPY**	**AEMPY**

Fig.1 Chemical structures of ionic liquid

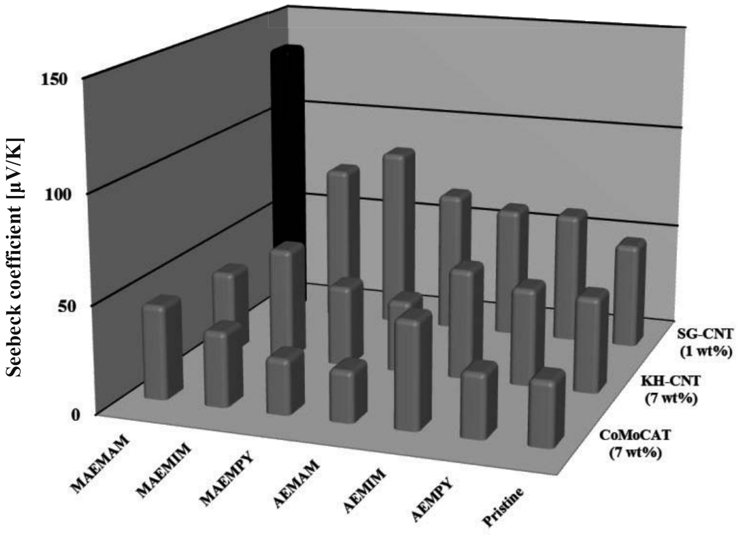

Fig.2 Seebeck coefficient of SWNT/PIL nanocomposites at 310 K

[1] J. C. Grunlan *et al.* Energy Technol. **1**, 265-272 (2013).

[2] T. Aida *et al.* Small **2**, 554 (2006).

[3] TREKSTAR® MOE-200 purchased from PIOTREK was used.

Corresponding Author: Y. Nonoguchi
E-mail: nonoguchi@ms.naist.jp

1P-26

Large-scale separation of eDIPS for application to TFTs

Shunjiro Fujii[1,2], Takeshi Tanaka[1,2], Tomoko Sugita[2], Satoshi Asano[2],
Masaharu Kiyomiya[2],Takeshi Saito[1,2], ○Hiromichi Kataura[1,2]

[1]*National Institute of Advanced Industrial Science and Technology (AIST)*
[2]*Technology Research Association for Single Wall Carbon Nanotubes (TASC)*

Semiconducting single-wall carbon nanotubes (s-SWCNTs) have a great potential as a channel source of thin film transistors (TFTs) because of their excellent electrical transport properties, for example, carrier mobility and high current carrying capacity. Recently, we achieved performance enhancement of solution-processed TFTs by using a network of s-SWCNTs obtained by gel separation method [1]. For further improvements of the performance, a use of higher quality s-SWCNTs is desirable. In this work, we separated eDIPS-SWCNTs [2] by gel column chromatography method [3] and fabricated TFTs using the separated high quality s-SWCNTs.

A liquid chromatography system equipped with a column filled with ~400 ml of dextran-based gel beads were used for large-scale separation. About 40 mg of SWCNTs were separated into metallic and s-SWCNTs in 2 hours. Figure 1 shows atomic force microscopy (AFM) image of the separated s-SWCNTs. The lengths of s-SWCNTs were 1-2 μm. TFTs using this s-SWCNTs exhibited high-performance transport characteristics. The on-off current ratio and the hole mobility calculated by a parallel plate model were larger than 10^5 and 100 cm^2/V, respectively. Figure 2 shows the output characteristics of the TFT. Detailed separation methods and device characteristics will be discussed.

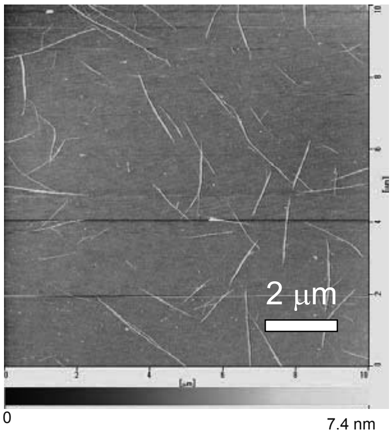

Fig.1 AFM image (10 x 10 μm^2) of s-SWCNTs.

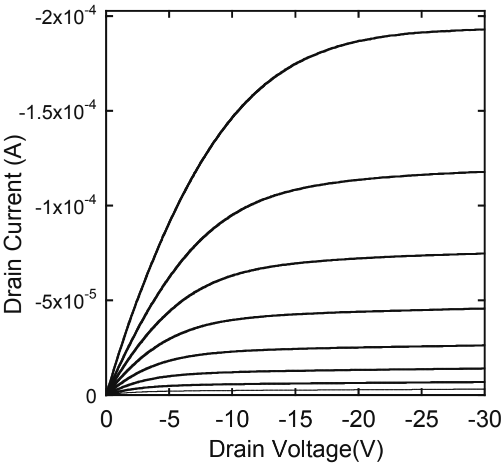

Fig.2 Output characteristics measured at gate voltages from −40 (top) in 2.5 V step.

[1] S. Fujii et al., Appl. Phys. Express (2009), 2, 071601.
[2] T. Saito et al., J. Nanosci. Nanotechnol. (2008), 8, 6153.
[3] T. Tanaka et al., Phys. Status Solidi RRL (2011), 5, 301.

Corresponding Author: Hiromichi Kataura **E-mail:** h-kataura@aist.go.jp, **Tel:** +81-29-861-2551

1P-27

Evaluation of the ratio of metal/semiconductive single-wall carbon nanotubes separated in two immiscible aqueous solution phases by utilizing Raman spectroscopy technique

Naoki Kanazawa[1], ○Shinzo Suzuki[1], Yu Tanaka[1], Akira Yamasaki[1],
Daiki Miyazaki[1], Akira Ono[2]

[1]Department of Physics, Kyoto Sangyo University, Kyoto 603-8555, Japan
[2]Department of Engineering, Kanagawa University, Yokohama 221-8686, Japan

In 2013, C.Y. Khripin et al. reported about spontaneous partition of single-wall carbon nanotubes (SWNTs) in polymer-modified aqueous solution phases [1], where metal/semiconductive SWNTs of large diameter (> 1.2 nm) are shown to be easily separated in two immiscible aqueous solution phases, i.e., polyethylene glycol (PEG) and dextran (DX) aqueous solution.

In this presentation, Raman spectroscopy technique was applied to each aqueous solution phase, in order to evaluate the ratio of metal / semiconductive SWNTs by changing excitation photon energy (532 nm and 633 nm). Briefly, mono-dispersed sodium cholate (SC) solution (2wt%) of SWNTs produced by arc-burning of Ni/Y-carbon composite rod in helium atmosphere was utilized for two immiscible aqueous solution, following the recipe by C.Y. Khripin et al. [1]. After recognizing that PEG sand DX solution phases show different colors because of the difference in the ratio of metal/semi-conductive SWNTs, Raman spectra of each phases were obtained by different excitation photon energy (532 nm and 633 nm).

Typical example of Raman spectra (G-band region) by excitation photon energy (532 nm and 633 nm) for PEG and DX solution phase were shown in Figures 1 and 2. It was clearly indicated that the ratio of semiconductive SWNTs to metallic ones was higher in PEG solution phase than that in DX solution phase.

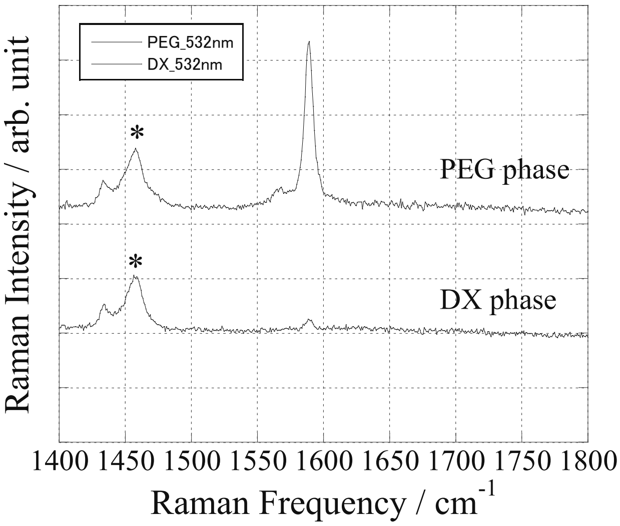

Figure 1. Raman spectra obtained by 532 nm photon energy (* indicates the reference signal due to the sample tube).

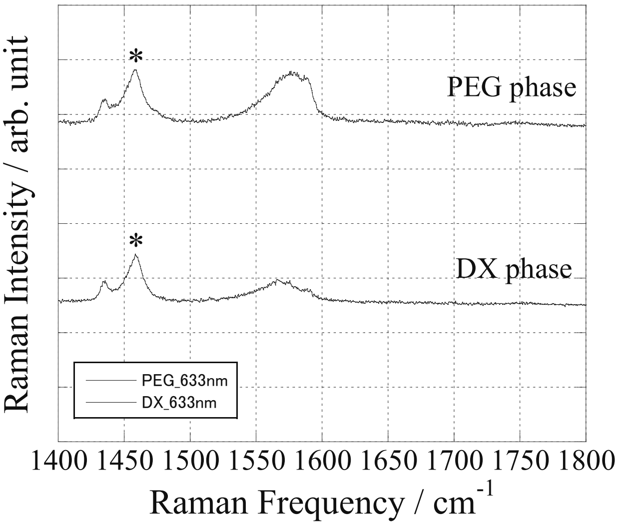

Figure 2. Raman spectra obtained by 633 nm photon energy (* indicates the reference signal due to the sample tube).

References:

[1] C.Y. Khripin et al., *J. Am. Chem. Soc.*, **135**, 6822-6825(2013).

Corresponding Author: Shinzo Suzuki
Tel: +81-75-705-1631, Fax: +81-75-705-1631,
E-mail: suzukish@cc.kyoto-su.ac.jp

1P-28

Single Chirality Separation and Optical Properties of Small-diameter Single-Wall Carbon Nanotubes

○Xiaojun. Wei[1], Yasuhiro. Ito[1], Takuya. Hirakawa[1], Atsushi. Hirano[1], Shunjiro. Fujii[1], Yuhei. Miyauchi[2,3], Kazunari. Matsuda[2], Takeshi. Tanaka[1] and Hiromichi. Kataura[1]

[1] Nanosystem Research Institute, AIST, Tsukuba, Ibaraki 305-8562, Japan
[2] Institute of Advanced Energy, Kyoto University, Uji, Kyoto 611-0011, Japan
[3]PRESTO, JST, Kawaguchi, Saitama 332-0012, Japan

Single-wall carbon nanotubes (SWCNTs) are one-dimensional nanostructures that offer great potential for application to novel optoelectronic devices due to large exciton binding energies. Because current SWCNTs products are mostly composed of various structures, structure sorting is necessary to obtain single chirality SWCNTs. Our group has successfully separated 13 different single-chirality SWCNTs using multicolumn gel chromatography method two years ago [1].

Recently, we have improved the multicolumn method and optimized it for the small diameter SWCNTs. In this work, (5,4) SWCNTs, which have the smaller diameter than C_{60} are successfully separated for the first time. In addition, high-purity (6,4) SWCNTs have also been successfully separated at room temperature using the same separation method. Here, the purity of (6,4) is much higher than that of our former separations by the temperature-controlled gel chromatography at 10 degree (66%) [2]. Moreover, both of (5,4) and (6,4) SWCNTs, show many bright photoluminescence (PL) peaks in an excitation-emission PL map (shown as Figure 1). All these peaks can be assigned to the emissions from only one type SWCNTs by considering oxide states probably produced in the heavy dispersion process before the separation [3].

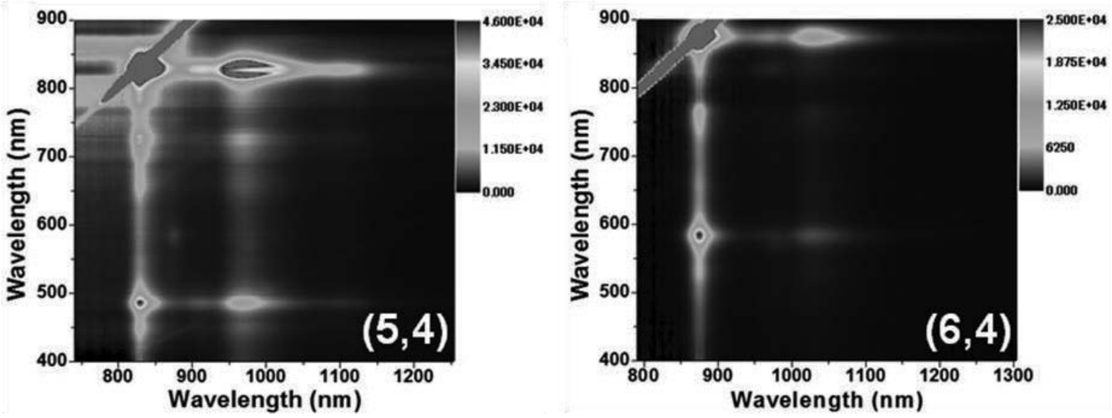

Figure 1. Contour maps of PL intensity of (5,4) SWCNTs (left) and (6,4) SWCNTs (right) as a function of the excitation and emission wavelength.

[1] H. Liu et al. Nat. Commun. **2**, 309 (2011).
[1] H. Liu et al. Nano Lett. **13**, 1996 (2013).
[3] Y. Miyauchi et al., Nat. Photonics **6**, 2013547 (2013).

Corresponding Author: H. Kataura
Tel: +81-29-861-2551, Fax: +81-29-861-2786, E-mail: h-kataura@aist.go.jp

1P-29

Fabrication of metal nanorods for the synthesis of short-carbon nanotubes

○Takao Sada[1], Tsuyohiko Fujigaya[1,2], Naotoshi Nakashima [1,2,3]

[1] Department of Applied Chemistry, Graduate School of Engineering, Kyushu University
Motooka, Fukuoka 819-0395, Japan, [2]WPI-I2CNER, Kyushu University,
[3]JST-CREST,5 Sanbancho, Chiyoda-ku, Tokyo, 102-0075, Japan

Carbon nanotubes (CNTs) are nanomaterials that possess remarkable electrical, mechanical and thermal properties and have been explored for biological applications [1]. One of the obstacles for the biological application of CNTs is the toxicity. The use of CNTs is currently considered with apprehension owing to their carcinogenic risks, especially come from their structural similarity to asbestos. To apply the CNTs to the biological applications, several groups have investigated the way to reduce their toxicity and reported long CNTs were found to trigger an inflammatory response [2]. Therefore, the demand for the length-controlled CNTs, especially short-CNTs is increasing. In this report, we describe the fabrication of metal nanorods as the new template catalyst for the synthesis of short-CNTs which is expected to be formed by the graphene around metal nanorods.

Fabrication of metal nanorods were conducted by the pulsed electrodepositon in anodic aluminum oxide (AAO) template thus forming Ni as the catalyst and Ag as the sacrificial layer alternatively with regulated pulse duration (τ_{Ni} = 10 s, τ_{Ag} = 120 s) to control respective segment length (**Fig. 1a**). The scanning transmission electron microscope (STEM) image and Energy Dispersive X-ray spectroscopy (EDX) analysis in **Figs. 1b, 1c and 1d** indicated that Ni-Ag nanowires with 75 ±9 nm in Ni segment were successively formed in single nanopore of AAO template. We have also confirmed Ni segment is easily controlled by the pulse duration. In the future, we are going to show the utility of the Ni nanorods as the metal catalyst for the synthesis of short-CNTs.

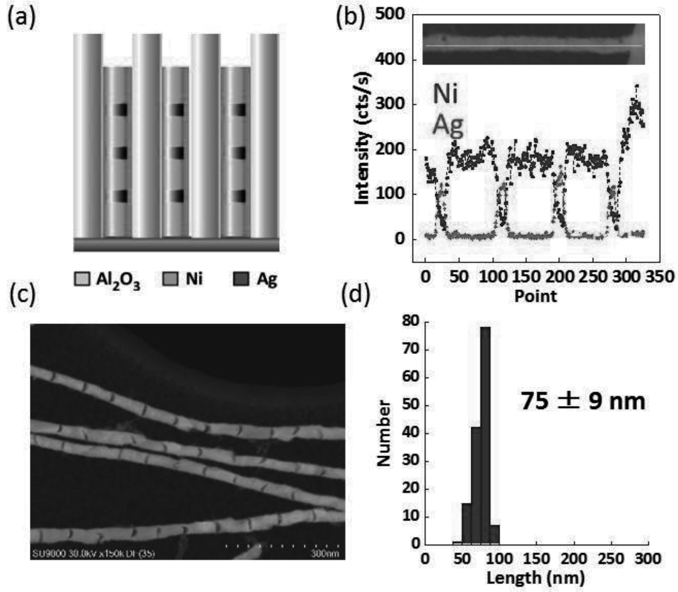

Fig. 1 (a) Schamatic illustration of the fabrication of Ni-Ag nanowires by pulsed electrodeposition. (b) STEM and corresponding Ni-Ag intensity profile along its growth direction. (c) STEM image of Ni-Ag nanowires after Ag etching. (d) Length histogram of Ni segment.

[1] H. Dai et al., *Nano Res.* **2009**, *2*, 85.
[2] H. Boucetta *et al.*, Angew. Chem. Int. Ed.. *2013*, **52**, 2274.

Corresponding Author: N. Nakashima
Tel: +81-92-802-2840, Fax: +881-92-802-2840,
E-mail: nakashima-tcm@mail.cstm.kyushu-u.ac.jp

1P-30

Growth of single-walled carbon nanotube from fullerene seeds by chemical vapor deposition and *in situ* scanning electron microscopy observation

○Huafeng Wang, Chisato Yamada, Kato Hiroki, Yoshikazu Homma

Department of Physics, Tokyo University of Science, 1-3 Kagurazaka, Shinjuku-ku, Tokyo, 162-8601, Japan

Chemical vapor deposition (CVD) method is proved to be a promising technique to get structure controlled, high quality nanotubes in a large-scale with low cost. Recently, growth of carbon nanotube (CNT) has been realized by using carbon seeds like nano-diamond, fullerene (C_{60}) fragments and nanotube segments [1-5]. This new route may produce high purity nanotube free from metal impurities, which will promote the application of nanotubes in future devices. In addition, researches on catalysts free nanotube seeds will contribute to understanding the growth mechanisms of CNT, so as to realize its controllable growth.

In this study, we perform conventional CVD (Fig. 1) to produce CNT from fullerene seeds. Various growth conditions including disperse solvent, substrates, pretreatment as well as growth conditions (temperature, pressure, gas flow) are investigated to evaluate the effects of these parameters on the formation of CNT. In addition, we also realize *in situ* nanotube growth (Fig. 2) from fullerene in scanning electron microscopy chamber, which render us to directly observe the whole nanotube formation process. On the basis of experimental analyses on conventional CVD and in-situ grown nanotube, we discuss the growth mechanisms of nanotube synthesized from fullerene.

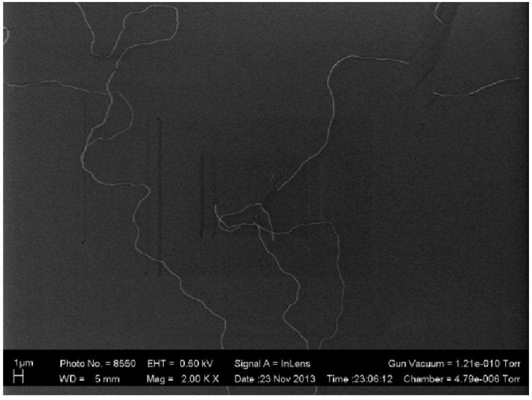

Fig.1 CVD grown nanotubes

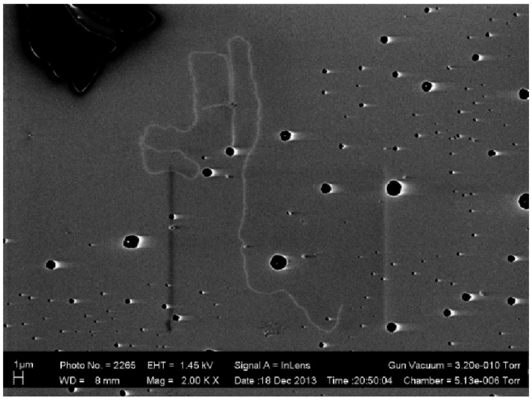

Fig.2 In-situ grown nanotubes

[1] Takagi, D. *et al. J. Am. Chem. Soc.* ***131***, 6922(2009).

[2] Yu, X. *et al. Nano Lett.* ***10***, 3343(2010).

[3] Ibrahim, I. *et al. ACS Nano* ***6***, 10825(2012).

[4] Yao, Y. *et al. Nano Lett.* ***9***, 1673(2009).

[5] Liu, J. *et al. Nat. Commun.* ***3***, 1199(2012).

Corresponding Author: Yoshikazu Homma
Tel: +81-3-5228-8244, Fax: +81-3-5261-1023
E-mail:homma@rs.kagu.tus.ac.jp

1P-31

Rapid separation of high-purity and micrometer-long semiconducting carbon nanotubes by gel filtration

○Boanerges THENDIE[1], Yasumitsu MIYATA[2,3], Haruka OMACHI[1], Ryo KITAURA[1], Yuhei MIYAUCHI[3,4], Kazunari MATSUDA[4], and Hisanori SHINOHARA[1]

[1]*Department of Chemistry and Institute for Advanced Research, Nagoya University,*
Nagoya, 464-8603, Japan
[2]*Department of Physics, Tokyo Metropolitan University, Tokyo, 192-0397, Japan*
[3]*JST, PRESTO, Tokyo, 102-0075, Japan*
[4]*Insititute of Advanced Energy, Kyoto University, Uji, Kyoto, 611-0011, Japan*

Single-wall carbon nanotubes (SWCNTs) hold promising applications for high performance electronic devices due to their excellent carrier mobility, flexibility, and solution processability. So far, realizing high performance nanotubes-based devices requires a sophisticated technique to prepare high purity and micrometer-length semiconducting SWCNTs. In the past, we have reported that the multi-stage gel filtration is capable to provide 99% high purity semiconducting and micrometer-long SWCNTs [1]. However, this multi-stage process is time-consuming (more than 24 hours per run) which limits the scalability of the method.

In the present study, we develop a fast, one-stage gel filtration method to obtain micrometer-long and high-purity semiconducting SWCNTs [2]. The present method utilizes fractionation process during the elution of semiconducting SWCNTs as illustrated in Fig. 1. The semiconducting SWCNTs fraction evaluated by optical absorption and Raman spectra shows the purity of semiconducting SWCNTs is as high as 99%, whereas the evaluation of SWCNTs length by photoluminescence imaging and atomic force microscopy provides the simultaneous length-based separation of micrometer-long SWCNTs.

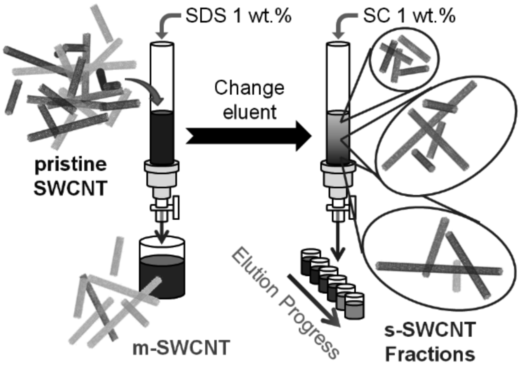

Figure 1 Schematic of the simultaneous single-stage separation of micrometer-long and high-purity semiconducting SWCNTs

[1] Y. Miyata *et al.* Nano Res. **4**, 963 (2011)

[2] B. Thendie *et al.* Appl. Phys. Express **6**, 065101 (2013)

Corresponding author: Hisanori Shinohara

Tel: (+81) 52-789-2482, **Fax:** (+81) 52-747-6442,

E-mail: noris@nagoya-u.ac.jp

1P-32

Efficiency Synthesis of Double Wall Carbon Nanotubes by Pressure Control of High-temperature Pulsed-arc Discharge

○Hayato Kikuchi[1], Katsuhide Terada[2], Toshiki Sugai [1]

[1] *Department of Chemistry, Toho University, Chiba 274-8510, Japan*
[2] *Faculty of Pharmaceutical Sciences, Toho University, Chiba 274-8510, Japan*

A high-temperature pulsed-arc discharge (HTPAD) has been developed to produce carbon nanotubes (CNTs). The system utilizes width controlled pulsed arc discharge for the vaporization of electrodes in a temperature controlled ambient gas. With this width and temperature control, novel materials have been produced such as high-quality double wall carbon nanotubes (DWCNTs)[1]. We have also optimized the production processes of CNTs by high-pressure discharge up to in 5 atm with controlling vaporization and condensation processes[2]. Here, we present TGA and TEM evaluation of product CNTs as well as Raman spectroscopy with getting optimal condition not only for SWCNTs but also for DWCNTs.

The system consists of a furnace with a ceramic tube inside, an Ar gas flow and pressure control system, an HV pulse voltage controller, and a water cooling trap. Electrodes made of graphite containing catalytic metals (Ni/Y 4.2/0.5 and 4.2/1.0 at. %:Toyo Tanso Co. Ltd.) were located in the ceramic tube. The pulsed arc discharges (0.6 ms, 50 Hz, and 100 A) vaporized the electrodes and produced CNTs in the high-temperature (1250 °C) and a wide pressure range of Ar (0.2-5 atm) in the ceramic tube. The products were collected on the trap and were characterized by Raman spectroscopy with excitation laser of 633 nm, TGA, and TEM.

Figure 1 shows the pressure dependence of concentration of CNTs by TGA. The obtained optimal pressure is 1.5 atm which is the same as that obtained with the Raman and TEM observations. The analysis on the optimal pressure of various production methods such as laser and steady arc methods have shown that the production processes are dominated by cooling and condensation processes[3]. Our optimal condition is exactly corresponding to those analyses[2], which shows that the cooling processes are also crucial for HTPAD.

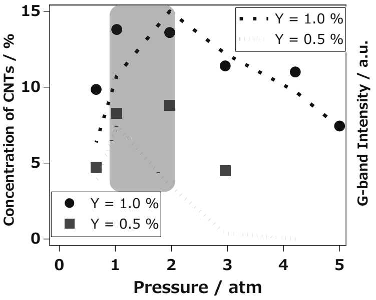

Fig. 1 Pressure Dependence of the Concentration of CNTs by TGA

Figure 2 shows the pressure dependence of the concentration of DWCNTs obtained by TEM and the speed of electrodes vaporization. Clearly, the lower the pressure, the high the concentration. The different pressure dependence shows that the production processes are dominated not by the cooling processes but by different processes. The correspondence of the concentration of DWCNTs and the speed of the electrodes vaporization suggests that the vaporization process is the crucial process on the production of DWCNTs.

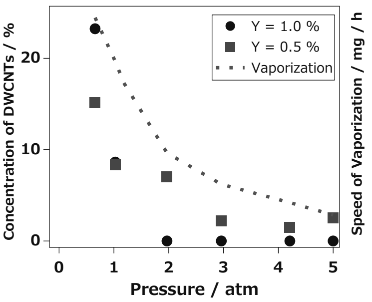

Fig. 2 Pressure Dependence of Concentration of DWCNTs

[1] T. Sugai *et al.*, *Nano Lett.* **3**, 769 (2003).
[2] H. Kikuchi *et al.* The 43th FNTG General Symposium. 1P-24.
[3] O. Jost, A. A. Gorbunov, J. Moller, W. Pompe X. Liu, P. Georgi, L. Dunsch, M. S. Golden, and J. Fink, *J. Phys. Chem.* B. **106**, 2875 (2002).

Corresponding Author: T. Sugai Tel: 047-472-4406 E-mail: sugai@chem.sci.toho-u.ac.jp

Synthesis and Evaluation of Single-Walled Carbon Nanotubes Using Metal Catalyst Ni-Y-Mo

○Bo Sun, Sakae Inoue, Tomoko Suzuki, Takayuki Yamamoto,
Chihiro Yanagi, Yoshinori Ando

Department of Materials Science and Engineering, Meijo University, Nagoya 468-8502, Japan

In the past decades, extensive works have been done in order to improve the purity and quality of single-walled carbon nanotubes (SWNTs) structure such as chirality, diameter by varying its growth conditions [1–3]. This paper focuses on the influence of Mo on the growth of SWNTs in arc discharge. Mo with different concentrations is incorporated in Ni-Y/He system. The yield, purity, ease of purification and diameter distribution of as-grown samples are characterized, and used to evaluate the effects of Mo. Based on analyses of yield and purity, we found the best concentration of Mo is 0.5 at% in Ni-Y/He system.

Figure 1 shows yield of SWNTs. For this system, the incorporation of Mo has dramatically increased the yield of soot in their best concentrations. Thermal gravimetric analysis showed that after purification, only negligible impurities remain in the sample for Ni-Y-Mo/He system. Figure 2 shows TGA plot of as-grown SWNT and purified SWNTs. Considering on these experimental results, we prove that Mo plays a positive role in arc discharge for the enhancement of SWNTs growth.

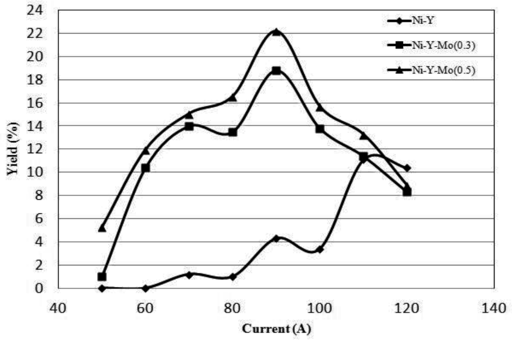

Fig. 1 Yield of SWNTs

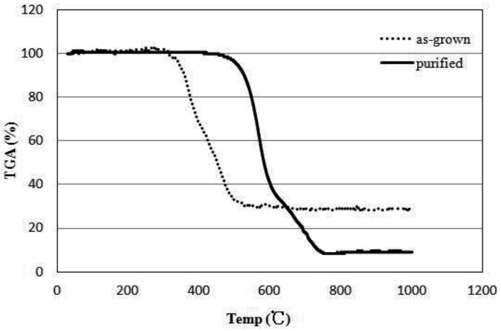

Fig. 2 TGA plot of as-grown and purified SWNTs

[1] C. Journet, W. K. Maser, P. Bernier, A. Loiseau, M. Lamyde la Chapelle, S. Lefrant, P. Deniard, R. Lee, and J. E. Fischer, *Nature* **388**, 756 (1997).

[2] X. Zhao, S. Inoue, M. Jinno, T. Suzuki, and Y. Ando, *Chem. Phys. Lett.* **373**, 266 (2003).

[3] Y. Ando, X. Zhao, K. Hirahara, K. Suenaga, S. Bandow, and S. Iijima, *Chem. Phys. Lett.* **323**, 580 (2000).

Corresponding Author: B. Sun
E-mail: louiskoo2518@hotmail.com

Studies on Chemical Reactions of Cobalt Clusters with Water and Oxygen by FT-ICR Mass Spectrometer

○Yuta Tobari[1], Kazuki Ogasawara[2], Shohei Chiashi[2], Shigeo Maruyama[2], Toshiki Sugai[1]

[1] *Department of Chemistry, Toho University, Chiba 274-8510 Japan*
[2] *Department of Mechanical Engineering, The University of Tokyo, Tokyo 113-8656, Japan*

Cobalt nano particles and clusters are a popular catalyst for carbon nanotube (CNT). However, reactions on Co clusters associated with CNT growth are not well known. To investigate these reactions, time of flight (TOF) and quadrupole mass spectrometers have been utilized as conventional methods but most of the studies are performed on hot (~2000 K) clusters with short term (~ms) observation, which is far from the realistic catalyzed reactions. Here we present studies on room temperature reactions of Co clusters with water and oxygen with long term (~10 s) observation by Fourier transform ion cyclotron resonance mass spectrometer (FT-ICR).

Experimental details have been described elsewhere [1]. Co clusters were produced by a laser vaporization cluster source and were introduced and trapped in a cell under a magnetic field of 6 T. The trapped clusters are thermalized in several seconds and are then exposed to water and dry air for several seconds. Finally ICR signals of product ions were observed and analyzed as mass spectra.

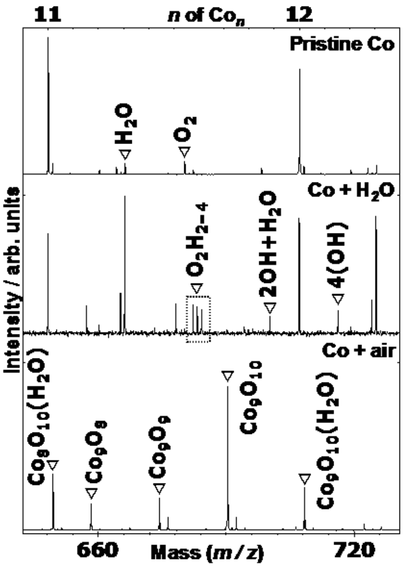

Fig. 1 Mass spectra of pristine and reacted Co clusters with H_2O & O_2.

Figure 1 shows mass spectra of pristine Co clusters and their reactants with water and dry air. Pristine Co clusters are observed with negligible contamination. In the water reactions, up to 4 adducts with dehydrogenation of $Co_n(OH)_m(H_2O)_l$ ($m+l=1\sim4$) are observed. Those multiple adducts have not been observed with TOF because of the hot production condition and the short term observation. Dehydrogenation is more significant as the number of water molecules increase. Tetra-water adducts are always more significant than tri-water adducts indicating that their stoichiometry is not $Co_n(H_2O)_2O_2$ but $Co_n(OH)_4$. On the contrary of the water adducts indicating weak interaction, the products with dry air are observed as Co oxide clusters of Co_nO_m ($n=m+1$ or $m+2$) with much stronger interaction between Co clusters and oxygen. In the hot TOF condition, much complicated and statistical distribution of n and m are observed [2]. In these oxide clusters, $Co_{13}O_8$ cluster is obtained as the same magic number cluster of those in the TOF hot condition [2]. Those results show the special stability of $Co_{13}O_8$ and much smaller stability of other Co_nO_m. The intensity of $Co_{13}O_8$ is much larger than that of pristine Co_{13} showing dissociation from larger oxide clusters of Co_nO_m ($n>13$) to $Co_{13}O_8$ [3]. Those salient differences between our results and those obtained with TOF show that our FT-ICR reaction condition is mild enough to have the final products with the highest stabilities. Those advantages of FT-ICR will contribute to reveal the catalyst reactions.

[1] S. Maruyama, *et al.*, Fullerene Sci. Technol. **7** (1999) 621. [2] Q. Sun, *et al.*, Phys. Rev. B **62** (2000) 8500.
[3] M. L. Anderson, *et al.*, J. Chem. Phys. **130** (2009) 064305.

Corresponding Author: T. Sugai, Tel: +81-47-472-4406, E-mail: sugai@chem.sci.toho-u.ac.jp

1P-35

Encapsulating Carborane within Aligned and Dense Carbon Nanotubes on SiC Substrate

○H. Fujita[1], W. Norimatsu[1], and M. Kusunoki[1,2]

[1] *Department of Applied Chemistry, Nagoya University, Nagoya 464-8603, Japan*
[2] *Eco Topia Science Institute, Nagoya University, Nagoya 464-8603, Japan*

Carbon nanotube (CNT) has been studied for various applications based on its specific properties since its discovery. Especially, encapsulation into CNTs has recently attracted a great attention for control of their properties. The encapsulation within CNTs has been developed from the first report of encapsulating fullerene which is called a peapod, and recently expands to various endohedral metallo-fullerene, metals, molecules and so on.

In this study, we focused on the boron cluster called carborane ($C_2B_{10}H_{12}$) as a new material instead of fullerene. The carborane has super aromatic series and cage type structures similar to fullerene and the constituent element is based on boron. It is well known that cluster materials inside the CNT could form one dimensional crystal and the carbon material such as the CNT and diamond becomes superconductive by doping boron [1][2]. We then expect that appearance of boron clusters into CNT's exhibits new properties. Here we report results about the carboranes encapsulated in the CNTs film on SiC substrate.

Firstly, we prepared the CNTs film about 160 nm thick synthesized by the SiC(000-1) surface decomposition [3]. The CNTs has a well aligned and highly dense structure, which might contribute to the formation of densely-aligned encapsulated CNTs. Secondly we opened the CNT's end-cap by oxidation using hydrogen peroxide solution. Finally we encapsulated carboranes into CNTs by exposing the CNTs film to the vapor of carboranes in the quartz tube. Observation of the CNTs film was carried out using transmission electron microscopy (TEM) and electron energy loss spectroscopy (EELS). Figure1 shows the CNTs film on SiC substrate after encapsulating carboranes into CNTs at 350 ˚C. Figure 1 (a) and (b) show that the CNTs were formed with a well aligned and highly dense film structure on SiC substrate. Figure 1(c) shows EELS boron K-edge mapping image in the area of Fig.1(b). That image indicates that many boron atoms existed in the CNTs film not that surface and lined along the CNTs axis. Furthermore, it was estimated from the intensity of each spectra in Fig.1(d) that the CNTs film included boron atoms about 4 at.% compared with carbon atoms.

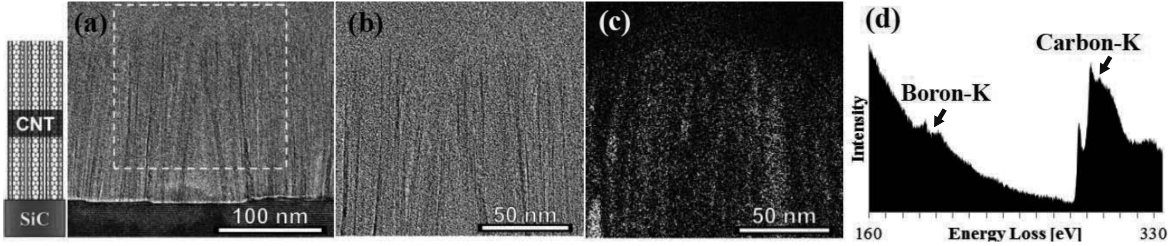

Fig.1(a) TEM image of the CNTs film on the SiC substrate and (b) the CNTs film within the white squire in (a), (c) boron K-edge mapping in the same area and (d) the EELS spectrum

[1] N, Murata *et al*, Phys. Rev. Lett. **101**, 027002(2008)
[2] M. Nesladek *et al*, Appl. Phys. Lett. **88**, 23211 (2006)
[3] M. Kusunoki *et al*, Appl. Phys. Lett. **77**, 531-533(2000)

Corresponding Author: H. Fujita
Tel: +81-52-789-5859, Fax: +81-52-789-5859,
E-mail: fujita.hayato@f.mbox.nagoya-u.ac.jp

1P-36

Synthesis of a carbon nanotube filled with solid-phase separating stainless alloy by liquid and solid interfacial arc discharge method

○Takuya Sagara [1], Satoshi Kurumi [1], Ken-ichi Matsuda [1], Kaoru Suzuki [1]

[1] *Department of Electrical Engineering CST, Nihon University, Tokyo 101-8308, Japan*

Metal-filled carbon nanotube (CNT) which is filled the hollow with various metal materials has been reported by S. Iijima and P. M. Ajayan [1]. In previous our work, we reported on controlling elongation and growth mechanism of Ni-filled CNT that is directly synthesized on Ni mesh by liquid and solid interfacial arc discharge method [2]. The method is based on liquid-phase deposition invented by M. Gamo-Nishitani *et al* [3]. Here we report on the structure of a CNT filled with stainless alloy separating solid-phase or crystalline phase by a similar technique.

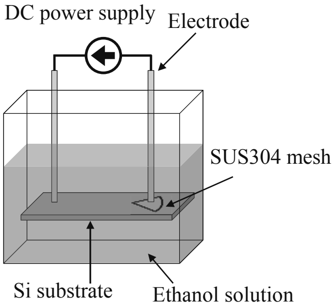

Fig.1 Schematic of experimental set-up

Figure 1 shows schematic diagram of liquid and solid interfacial arc discharge method. A sectorally processed stainless mesh (original diameter 3mm, 200 grid per an inch, SUS304) is set between Si substrate and cathode connected to a direct current power source (3.0 A, 70 – 80 V) as in fig.1. This electrically closed circuit is submerged in ethanol solution (99.5%). Then, arc discharge takes place between the SUS mesh of cathode and Fe rod of anode by applying direct current to the circuit. Figure 2 is the close-up photograph of cathode spot at the apex of the SUS mesh.

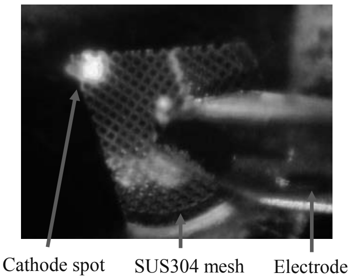

Fig.2 Appearance of cathode spot

Figure 3 (a) is the scanning transmission electron microscope dark field image of typical CNT filled with stainless alloy. White contrast appears in the part of CNT's hollow, which indicates evidence for filling. Figure 3 (b) - (d) are elemental mapping images with energy dispersive X-ray spectroscopy. These images showed the filler in the CNT is stainless alloy that consists of homogeneous Fe and Ni. However, difference in concentration of Cr is appears in fig.3 (d), and we suppose that solid-phase separation is attributed to this distribution of Cr.

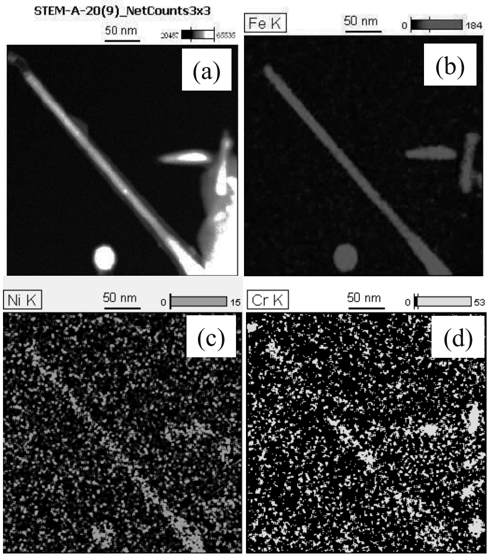

Fig.3 STEM and EDX elemental mapping images of a CNT filled with stainless alloy. (a) dark field image, and signal from: (b) Fe; (c) Ni; (d) Cr.

Acknowledgement

A part of this work was supported by "Nanotechnology Platform" (project No.12024046) of the Ministry of Education, Culture, Sports, Science and Technology (MEXT), Japan.

[1] P.M. Ajayan and S. Iijima, Nature **361**(1993) 333.
[2] T. Sagara *et al*. Appl. Surf. Sci. in press APSUSC-26712
[3] M. Nishitani-Gamo *et al*, Jpn. J. Appl. Phys. **46** (2007) 6329.

Corresponding Author: K. Suzuki
Tel: +81-3-3259-0770, Fax: +81-3-3259-0770,
E-mail: kaoru@ele.cst.nihon-u.ac.jp

1P-37

Containment method for transmission electron microscopy of gas molecules within the inner space of carbon nanotubes under high vacuum

○Keita Kobayashi [1], Takeshi Saito [2,3], Masaharu Kiyomiya [3], Hidehiro Yasuda [1]

[1] *Research Center for Ultra-High Voltage Electron Microscopy, Osaka University, Ibaraki, Osaka 567-0047, Japan*
[2] *Nanotube Research Center, National Institute of Advanced Industrial Science and Technology (AIST), Tsukuba, Ibaraki 305-8565, Japan*
[3] *Technology Research Association for Single Wall Carbon Nanotubes (TASC), Tsukuba, Ibaraki 305-8562, Japan*

The inner space of carbon nanotubes (CNTs) provides a suitable nanospace for molecules storage, and CNTs have thus been widely used as nanoscale test tubes for transmission electron microscopy (TEM) observation of isolated molecules and unstable low-dimensional crystals. The TEM observation of guest materials encapsulated within CNTs clarifies both the structure of the guest materials and their behavior within a confined nanospace, making this a powerful method for research on nanomaterials. However, since CNTs used as test tubes are prepared by removing the end-caps to provide a pathway for the guest molecules, containment of highly volatile molecules and gases in the inner space is problematic in the TEM specimen chamber, which is kept at high vacuum (~10^{-5} Pa). For this reason, TEM observation of gas molecules has not yet been reported, whereas the behavior and structure of various molecules (fullerenes [1], metal complexes [2], polycyclic aromatic hydrocarbons [3], etc [4].) have been observed directly by TEM using CNTs as test tubes. Therefore, the development of a novel method for the containment of gas molecules in CNTs during TEM observation is necessary for discovering the unique behavior and structures of such confined gas molecules. Against this background, we aimed to observe guest gas molecules encapsulated within CNTs by blocking the escape pathways. A typical EDX spectrum of Xe encapsulated in CNTs with blocked pathways shows a peak at 4.1 keV corresponding to the *Lα* line of Xe, which indicates that Xe gas was contained within the inner space of the CNTs even under high vacuum.

In this presentation, we will introduce the details of the method and discuss the unique behavior of gases confined within nanospaces.

This work was supported by KAKENHI (#25790003) from JSPS. KK thanks Prof. R. Kitaura and Prof. H. Shinohara for valuable discussion.

[1] R. Kitaura & H. Shinohara, Chem. Asian J. **1**, 646 (2006).
[2] L.-J. Li *et al.*, Nature Mater. **4**, 481 (2005).
[3] T. Okazaki *et al.*, Angew. Chem. Int. Ed. **50**, 4853 (2011).
[4] M. Koshino *et al.*, Science **316**, 853 (2007).

Corresponding Author: K. Kobayashi
Tel: +81-6-6879-7941, Fax: +81-6-6879-7942,
E-mail: kobayashi-z@uhvem.osaka-u.ac.jp

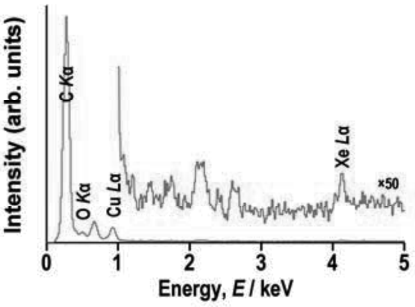

Fig.1 typical EDX spectrum of Xe encapsulated CNTs

1P-38

Light-assisted in-situ polymer formation on carbon nanohorns

Mei Yang[1], ○Minfang Zhang[1], Masao Kunioka[1], Sumio Iijima[1, 2], Masako Yudasaka[1]

[1] *National Institute of Advanced Industrial Science and technology 5-2, Tsukuba, Japan*
[2] *Department of Material Science and Engineering, Meijo University, Nagoya, Japan*

Carbon nanomaterials have attracted tremendous interest in the basic and application sciences. For example, carbon nanomaterials absorb light in a wide range from UV to IR and convert the light energy to thermal energy. The photothermal conversion has been shown to be useful for photothermal tumor therapy by animal tests [1]. Among the carbon nanomaterials, carbon nanohorns (CNHs) present higher photothermal conversion efficiency than other carbon nanomaterials, such as carbon nanotubes [2]. Here we report a method for in-situ polymer formation by using CNHs. In this method, by light irritation, CNHs worked as "molecular heater" to raise the local temperature, which helped selectively forming the polymers just on the surface of CNHs. This method may be quite useful for synthesis of nanocarbon-polymer composites and surface functionalization of carbon nanomaterials.

Polycaprolactone (PCL) is aliphatic polyester composed of hexanoate repeat units. It is an important biocompatible and biodegradable polymer. Due to its multiple biomedical applications, the synthesis of PCL or PCL/nanocarbon composites has received increased attention. In this study, irradiating NIR light (808nm) for 1 hour, the local temperature around CNH increased and the ring of cyclic monomer caprolactone was opened, leading to the polycaprolactone (PCL) formation on the CNHs surface. The number average molecular weight (M_n) and polydispersity (M_w / M_n) of the obtained PCL were 6982 and 1.235. As a control, without CNHs, the M_n of PCL is only 555.

Biological origin molecule of polydopamine (PDA) has served as a universal coating to nanoparticles for various biomedical applications. With the light irradiation, dopamine quickly self-assembled to the PDA and selectively coated the surface of CNHs. The coating amount can be controlled by the reaction time and light intensity.

All of these data suggested that the photothermal effect of CNHs is useful for polymer synthesis on the surface of carbon nanomaterials.

[1] M. Zhang *et al*. *Proc. Natl. Acad. Sci. U. S. A.* **105**, 14773 (2008).

[2] E. Miyako *et al*. *Proc. Natl. Acad. Sci. U. S. A.* **109**, 7523 (2012).

Corresponding Author: M. Zhang and M. Yudasaka.
TEL/Fax: +81-29-861- 6290
E-mail: m-zhang@aist.go.jp (M. Zhang), m-yudasaka@aist.go.jp (M. Yudasaka).

1P-39

Selective carboxylation of graphite-like thin sheet edges in carbon nanohorn aggregates

○Maki Nakamura [1], Michiko Irie [1], Ryota Yuge [2], Toshinari Ichihashi [2], Sumio Iijima [1,3], Masako Yudasaka [1]

[1] *National Institute of Advanced Industrial Science and Technology (AIST), Tsukuba 305-8565, Japan*
[2] *NEC Corporation, Tsukuba 305-8501, Japan*
[3] *Meijo University, Nagoya 468-8502, Japan*

Single-walled carbon nanohorns (CNHs) are expected to have many applications in the fields of electrochemistry, biomedicinal chemistry, and so on. Chemical functionalization of CNHs is important for their various applications. Especially, carboxylation is useful for changing hydrophobic CNHs to hydrophilic ones that are dispersible in aqueous solutions. Usually, *as-prepared* CNHs assemble by the thousands to form the spherical aggregates (~100 nm) containing graphite-like thin sheets (GLSs) [1]. We previously reported that several oxygenated groups, such as carboxyl, quinone, carbonyl, and hydroxyl groups were introduced into the CNH-GLS aggregates by the mild oxidation with hydrogen peroxide at room temperature for a certain period (from 1 hour to 56 days) [2,3]. In this report, we show that the GLS edges in CNH-GLS aggregates can be selectively carboxylated by 1 hour immersion in hydrogen peroxide at room temperature [4].

CNH-GLS aggregates were prepared by CO_2 laser ablation of graphite in Ar (~760 Torr) without auxiliary heating. For selective oxidation of the GLS edges, CNH-GLS aggregates were immersed in a 30% hydrogen peroxide aqueous solution for 1 hour at room temperature. After immersion, the oxidized CNH-GLS aggregates were filtered and washed with water. The types of the generated oxygenated groups were determined by using temperature-programmed desorption mass spectrometry (TG-MS). To visualize the location of carboxyl groups in the oxidized CNH-GLS aggregates, they were stained with Pt-ammine complexes, and observed using a transmission electron microscope (TEM) and a scanning transmission electron microscope (STEM).

According to the TG-MS results of the oxidized CNH-GLS aggregates, the presence of carboxyl groups was confirmed with the emission of $m/z = 44$ at 100-300 °C. In TEM and STEM observations, the Pt-ammine complexes that reacted with the carboxylic groups in the oxidized CNH-GLS aggregates were visible at the edges of GLSs, but not so on the basal planes of GLS and on CNHs. The selective carboxylation of GLS edges in CNH-GLS aggregates would enable unique chemical functionalization of CNH-GLS aggregates and could expand their application possibilities.

[1] M. Irie, M. Nakamura, M. Zhang, R. Yuge, S. Iijima, M. Yudasaka. Chem. Phys. Lett. **500**, 96 (2010).
[2] M. Nakamura et al. The 42th Fullerenes-Nanotubes-Graphene General Symposium, 2012.
[3] M. Nakamura, T. Kawai, R. Yuge, S. Bandow, S. Iijima, M. Yudasaka. Carbon in press.
[4] M. Nakamura, M. Irie, R. Yuge, T. Ichihashi, S. Iijima, M. Yudasaka. PCCP **15**, 16672 (2013).

Corresponding Author: M. Nakamura and M. Yudasaka
Tel: +81-29-861-4604, Fax: +81-29-861-6290,
E-mail: ma-ki-nakamura@aist.go.jp (M.N.) and m-yudasaka@aist.go.jp (M.Y.)

1P-40

Topological Controlled Synthesis of Graphene Sheet

Chozo Inoue,[1]
[1]*Professioal Engineer,(Department of Chemistry) ,Chigasaki city Kanagawa Japan*
E-mail:choinoue@nifty.com

1. Introduction.

There are many problems in the application of the graphene sheet. In order to enable an excellent alignment control, the development of a simple precursor to continue to grow into a sheet on the spot at the time of use is desirable. When synthesizing SWNT using a raw material decalin, sometimes graphene sheets extend laterally from the tube as a by-products . [1] By considering the mechanism of avoiding the winding of graphene, I found conditions under which the graphene grows into sheet. Using the raw material of armchair type and π-topological controlled catalysis of graphene edges, a two-step process were developed.

2. Experiment

Chemicals and feedstock are listed in comparative table 1. Zirconocene is a π-polymerization catalyst which is difficult to produce a CNT . Dibenzo-thiophene is the source of unit structure of the armchair type edge because having fixed rotational plane of the biphenyl structure by cross-linking of sulfur,. Paraffin was used for aliphatic carbon source, having higher boiling point than decaline.

Table1. Comparison of Catalyst, Radical-source, Raw material and Process Condition.

CNTprocess	Ferrocene	Thiophene	Benzene	1step
Graphene	Zirconocene	Dibenzothiophene	Paraffin	2step

① First step: .At 100 ℃ or more , dissolve the zirconocene and dibenzothiophene in paraffin. Stirring and changed the red purple color of the solution , the creamy solution to cool to room temperature.

② Second step: Schmear the cream thinly on a filter paper of quartz wool to facilitate sublimation .Then its slowly inserted into the electric furnace of 900 ℃ under a stream of argon. After the sublimation are finished, agglutinate graphene soot gather on the expanded graphite substrate placed at the exit. [3] Fig 1. SEM Photograph

3. Result and Discussion

These graphene soot can be dispersed to sheet easily in alcohol. This indicate to prevent the byproduct of CNT and the like, by setting to remain at the start point the impurities that can not be sublimated. Each step is monitored by Raman spectrum and was analyzed by SEM, TEM, STEM, EDX. [2] For future tasks, optical microscope should use to evaluate of graphene sheet. So nano-graphene precursor in the first stage is a PAH meso-phase having a terminal hydrogen, it is possible to align on device. Coating method is very important final step for the improvement of orientation and performance of the graphene sheet.

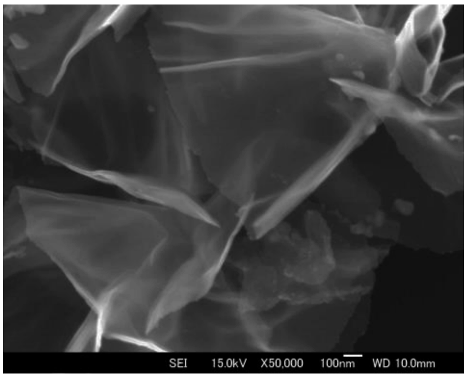

[1] Mauricio Terrones *et al,* Nano Lett., **2008**, 8 (9), pp 2773–2778
[2] Andrey L. Chuvilina *et al* , Carbon **47** (2009) 3099–3105
[3].C.Inoue *et al,* P2011-219372

1P-41

Direct growth of graphene on dielectric substrates by etching-precipitation method

○Masaki Kosaka[1,2], Kei Hasegawa [2], Suguru Noda [2]

[1] Department of Chemical System Engineering, The University of Tokyo, Japan
[2] Department of Applied Chemistry, Waseda University, Japan

Chemical vapor deposition (CVD) on catalyst metals is considered as the most promising method to synthesize graphene because of its potential for high scalability [1]. For many applications, it is necessary to fabricate graphene on dielectric substrates. However, wet transfer process easily causes impurities and damages to graphene. The synthesis of graphene with fair quality and uniformity directly on dielectric substrates is still challenging.

We have realized metal-free graphene directly on dielectric substrates by etching-precipitation method [2,3], in which carbon precipitates as graphene by removing the solvent metal by dry etching from carbon-metal solid solution on the substrates (Fig. 1).

In this work we used the Fe-C mixture film of various thickness (20-200 nm) sputter deposited on SiO_2/Si or quartz glass substrates. The samples were heated to 400-700 ^oC under 25 vol% H_2/ Ar at 100 Torr and kept for 10 min in the tubular reactor, and the etching of Fe was carried out under 0.05 vol% Cl_2/ Ar at the same temperature and 5 Torr for 1-90 min to yield graphene directly on the substrates. Typical results are shown in Fig. 2. The photograph of the sample shows the uniform gray color over the substrate, suggesting the uniform formation of graphene. Its optical transmittance was 86%, indicating the average layer number of 6~7. In the AFM image taken near the voids, the height difference between the graphene and void surfaces were ~ 2 nm, which is consistent with the layer number evaluated from the optical transparency. The Raman spectrum showed a G-band peak and a relatively small D-band peak with the G to D intensity ratio (I_G/I_D) of 20, suggesting the fair quality of this graphene. The plan-view SEM image had some contrast difference, suggesting some layer number distribution, and small holes suggesting some voids in the graphene film. From this image the grain size and graphene coverage were estimated to be 4~5 μm and over 99%, respectively. This film had a sheet resistance of 340~460 Ω/sq., corresponding to the volume resistivity of 70~90 μΩ cm which is similar to that of HOPG (20~50 μΩ cm). Our etching-precipitation method is a practical route to synthesize graphene directly on device substrates of arbitrary sizes.

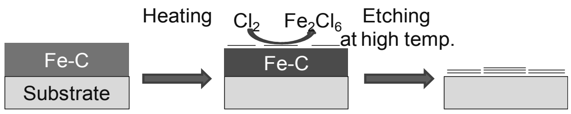

Fig.1 Schematic of etching-precipitation method

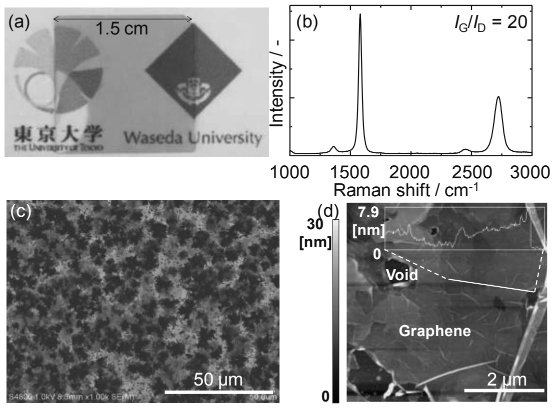

Fig. 2 (a) A photograph, (b) Raman spectrum, (c) SEM and (d) AFM image of the sample synthesized at 650 ^oC on a quartz substrate

[1] S.Bae, *et al.* Nat. Nanotechnol. **5**, 574 (2010).

[2] S. Takano and S. Noda, The 40th FNTG General Symposium, 2P-38 (2011).

[3] M. Kosaka, et al., The 44rd Fall Meeting of the Society of Chemical Engineers, Japan, G315 (2012)

*Tel&Fax: 03-5286-2769, E-mail: noda@waseda.jp

1P-42

CVD-growth of nitrogen-doped graphene using tetraphenyl porphyrin as a solid precursor

○Yuma Sugisaki, Ryo Kitaura*, Haruka Omachi and Hisanori Shinohara*

Department of Chemistry & Research Center for Materials Science, Nagoya University,
Nagoya 464-8602, Japan

Graphene, the two-dimensional monolayer form of sp^2-hybridized carbon, has attracted widerange interests due to its novel physical properties and promising applications in electronic devices and composite materials. While graphene can readily be p-doped by adsorbates, n-doped graphene, which is indispensable for device applications, is more difficult to achieve. Nitrogen doping is one of the most polular methods to dope electrons into graphene, but it is still a challenging topic to prepare large-area nitrogen-doped graphene with a controlled way. Here, we report the growth of large-area nitrogen-doped graphene using a chemical vapor deposition (CVD) with a solid precursor such as tetraphenyl porphyrin(TPP).

Figure 1 shows electron diffraction pattern and a corresponding TEM image of graphene using tetraphenyl porphyrin (TPP-G). 12 spots with 6-folded symmetry appears in the diffraction pattern, which clearly demonstrates a formation of hexagonal network of carbon. Figure 2 shows an intensity profile along the white line shown in Fig.1. The intensity ratio of two types of spots is 1:1, which is consistent with a formation of single-layer graphene. In the presentation, we will discuss details of synthesis and characterizations of structure and electronic properties of TPP-G.

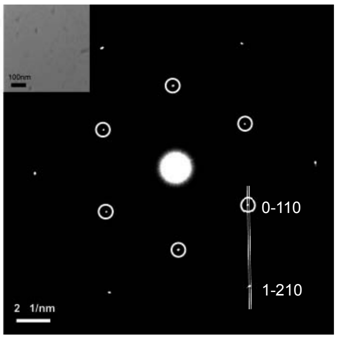

Fig.1 Electron diffraction pattern of TPP-G Inset : TEM image of TPP-G

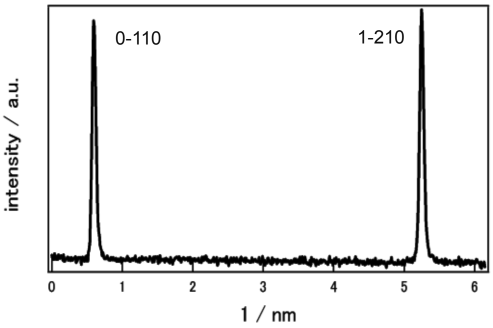

Fig.2 Intensity profile along the white line in Fig.1

Corresponding Author: Hisanori Shinohara
Tel: 052-789-2482, Fax: 052-747-6442
E-mail: r.kitaura@nagoya-u.jp and noris@nagoya-u.jp

1P-43

In situ doping of Electrochemical foliation- Mechanism of intercalation,exfoliation and doping

Shang-Lin Tsai[1], Mario Hofmann [2], Ya-Ping Hsieh[1]

[1]Graduate of Institute of Opto-Mechatronics, National Chung Cheng University, ROC.
[2] Department of Material Science and Engineering, National Cheng Kung University, ROC.

In the last few years graphene has become an important material in many application areas due to its unique properties such as transparency, high thermal conductivity, great mechanical resistance and excellent electronic conduction. Among all of these applications the use of graphene as a transparent optical conductor (TOC) has been considered the most promising.

To become a suitable replacement for current TOCs, a scalable production method and higher performance of graphene TOCs are required. Common fabrication methods rely on the chemical exfoliation of graphite which typically requires many complicated process steps and decreases the graphene quality.

Electrochemical exfoliation has been demonstrated to be a simple, low cost and fast route for synthesizing graphene. However, the reported quality and conductivity of exfoliated graphene has not met the criteria for transparent conductive thin film application and the mechanism of electrochemical exfoliation and intercalation is still not well understood.

We here present an approach to combine electrochemical exfoliation with simultaneous doping. A detailed analysis of the interaction between dopant and graphene was performed. Intercalation of dopant between graphene planes was confirmed through X-ray diffraction. X-ray photoelectron spectroscopic and EDS were used to characterize the effect of electrochemical parameters on the doping process. Raman analysis shows that under optimized exfoliation condition graphene could maintain its high quality while being highly doped.

This work opens a route to enhance the scalability and quality of graphene production which improves the commercial appeal of graphene for TOC applications.

Corresponding Author: Ya-Ping Hsieh
Tel: +886-52720411#23601
E-mail: yapinglab@gmail.com

1P-44

CVD Growth of Millimeter-Sized Graphene Grains on Heteroepitaxial Cu

Kenji Kawahara,[1] Tasuku Iwaizako,[2] Masaharu Tsuji,[1,2] and ○Hiroki Ago[1,2,3,*]

[1]*Institute for Materials Chemistry and Engineering, Kyushu University, Fukuoka 816-8580*
[2]*Graduate School of Engineering Sciences, Kyushu University, Fukuoka 816-8580*
[3]*PRESTO-JST*

Graphene has been attracting great interest as a new type of two-dimensional atomic sheet owing to its high carrier mobility, optical transparency, mechanical flexibility, and thermal conductivity, which promise applications in many electronic devices. Recent progress of chemical vapor deposition (CVD) growth offers a promising route to produce large-area graphene with low cost. To bring out the graphene's potential, the large-area and high-quality graphene growth is necessary. We have developed our original "heteroepitaxial CVD method" to grow high-quality single-layer graphene with controlled hexagon orientation [1-5]. In this method, the graphene hexagon orientation is defined by the surface lattice of heteroepitaxial metal films [4]. To realize the CVD growth of a single-crystalline graphene sheet, seamless connection of neighboring grains is important, but it is still under discussion [6]. Another approach is to increase the graphene's grain size to fully cover the Cu surface. Recently, a great progress has been achieved along this research direction [7,8].

In this presentation, we report our recent progress of large-area graphene grain growth on crystalline Cu films deposited on single crystalline substrates. Owing to the high Cu crystallinity and surface flatness, we can reproducibly synthesize mm-sized graphene grains on heteroepitaxial Cu films by ambient pressure CVD, as shown in Figure 1. We will also report transport properties of our CVD graphene. High performance electronic applications are expected for these large single-crystalline graphene grains.

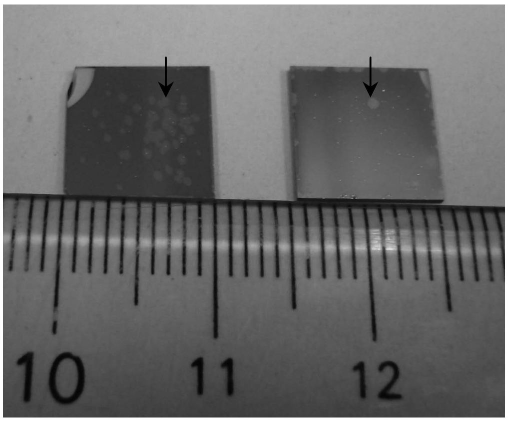

Figure 1 Photograph of mm-scale graphene grains on the epitaxial Cu films. Arrows indicate graphene grains visualized by weak oxidation of the Cu catalysts. Left substrate has a number of mm-sized grains, while right substrate has single mm-grain on the 1 cm□ Cu film.

References:
[1] H. Ago et al., *ACS Nano*, **4**, 7407 (2010). [2] B. Hu et al., *Carbon*, **50**, 57 (2012). [3] C. M. Orofeo et al., *Carbon*, 50, 2189 (2012)., [4] Y. Ogawa et al., *J. Phys. Chem. Lett.*, 3, 219 (2012). [5] H. Ago et al., *Appl. Phys. Exp.*, **6**, 75101 (2013). [6] Y. Ogawa et al., submitted. [7] Z. Yang et al., *ACS Nano*, **6**, 9110 (2012). [8] Y. Hao et al., *Science*, **342**, 720 (2013).

Acknowledgments:
This work was supported by JSPS-NEXT Funding Program (GR075).

Corresponding Author: Hiroki Ago (Tel&Fax: +81-92-583-7817, E-mail: ago@cm.kyushu-u.ac.jp)

1P-45

Quantum interference in a ballistic graphene *n-p-n* junction: from Fabry-Perot to edge channel interference

○Sei Morikawa[1], Satoru Masubuchi[1,2], Rai Moriya[1],
Kenji Watanabe[3], Takashi Taniguchi[3], Tomoki Machida[1,2]

[1] *Institute of Industrial Science, The University of Tokyo, Tokyo 153-8505, Japan*
[2] *Institute of Nano Quantum Information Electronics,*
The University of Tokyo, Tokyo 153-8505, Japan
[3] *National Institute for Material Science, Tsukuba 305-0044, Japan*

We studied transport properties of a ballistic graphene *n-p-n* junction. The graphene was sandwiched between two hexagonal boron-nitride (h-BN) crystals in order to eliminate the mobility degradation. By tuning the back gate and top gate bias voltages, a *n-p-n* junction with tunable polarity and doping levels (n_b-n_t-n_b, respectively) was formed [Fig. 1(a)] and it showed two types of characteristic quantum interference.

First, we studied the Fabry-Perot interference of charge carriers within the *n-p-n* cavity in low magnetic fields (B < 0.5 T) [Fig. 1(b,d)]. This observation indicates the charge carriers travelled ballistically and coherently in the cavity [1]. When a small magnetic field was applied, the oscillation phase was shifted by π, indicating the observation of Klein Tunneling, which is the intrinsic phenomenon of Dirac fermions.

Second, we studied the anomalous magnetoresistance oscillations in the quantum Hall regime [2]. Fig. 1(c) shows a color plot of two-terminal resistance R as a function of n_t and magnetic field B with fixed n_b. Aperiodic resistance oscillations as a function of B were emerged. These oscillations were neither periodic in $1/B$ (SdH oscillation) nor in B (AB oscillation), indicating the observation of novel quantum interference. We will discuss this result in terms of a new commensurability between the magnetic flux enclosed within the co-propagating edge channels and the flux quantum. This is the first observation of interference between the edge channels along *p-n* interfaces [Fig. 1(e)].

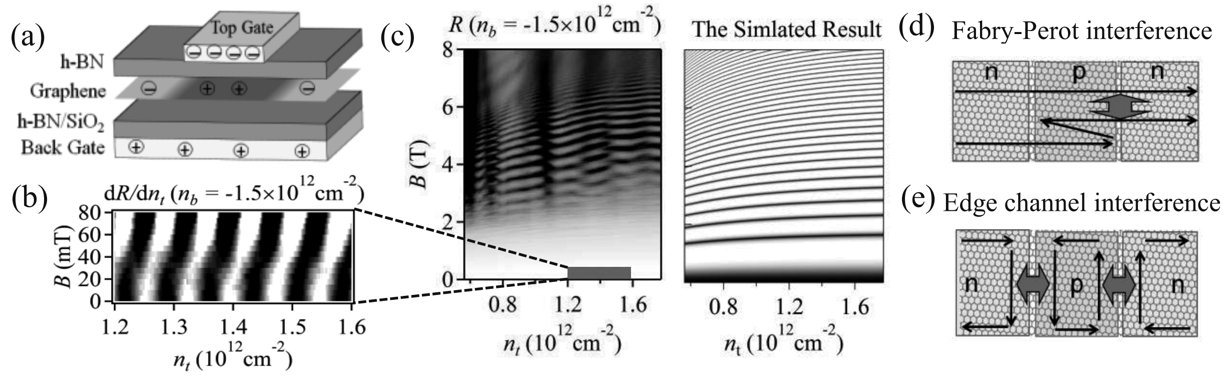

Fig. 1: (a) A schematic of our h-BN/Graphene/h-BN device. (b) The Fabry-Perot interference in low magnetic fields. (c) The edge channel interference in the quantum Hall regime. The experimental result (left) shows good agreement with the simulated result (right). (d,e) Schematics of the two types of interference.

[1] S. Masubuchi, S. Morikawa *et al.*, Jpn. J. Appl. Phys. **52**, 110105 (2013).

[2] S. Morikawa *et al.*, in preparation.

Corresponding Author: S. Morikawa

Tel: +81-3-5452-6158, Fax: +81-3-5452-6157, E-mail: morikawa@iis.u-tokyo.ac.jp

1P-46

Exciton-Exciton Annihilation in Monolayer Transition-Metal Dichalcogenides

○Satoru Konabe[1,2] and Susumu Okada[1,2]

[1]Graduate School of Pure and Applied Sciences, University of Tsukuba, Tsukuba, Ibaraki 305-8571, Japan
[2]Japan Science and Technology Agency, CREST, 5 Sanbancho, Chiyoda, Tokyo 102-0075, Japan

Monolayer transition metal dichalcogenides (TMDs) are atomically thin layered materials, which have been attracting much interest because of their remarkable electronic and optical properties [1–3]. TMDs are direct-gap semiconductors with the energy gaps within the range of visible light. Interestingly, TMDs show peculiar valley-dependent optical selection rules; the circular polarized light can selectively excite electrons in one of the two valleys. These valley-related phenomena make TMDs possible candidates for emerging materials for spintronics and valleytronics devices. In addition to these striking properties, many-body effects play a crucial role in TMDs since the screening effect is less effective in TMDs due to their atomically thin structures, resulting in enhanced Coulomb effects. Generally, the strong Coulomb interaction profoundly affects the excited state dynamics in low-dimensional nanomaterials and induces the interesting nonlinear phenomena.

In the present paper, we theoretically investigate the optically excited states in TMD and their dynamical properties focusing on the exciton-exciton annihilation by the Auger recombination process in TMDs. Solving the Bethe-Salpeter equation based on the effective-mass theory, we first calculate the absorption spectra of TMDs, which shows the good agreement with both the experimental observation and the previous theoretical calculations. We then evaluate the exciton-exciton annihilation rate by the exciton Auger recombination process using the Fermi's golden rule with the obtained exciton states.

References:
[1] A. Splendiani *et al*. Nano Lett. **10**, 1271 (2010).
[2] K. F. Mak *et al*. Phys. Rev. Lett. **105**, 136805 (2010).
[3] Q. H. Wang *et al*. Nat. Nanotechnol. **7**, 699 (2012).

Corresponding Author: Satoru Konabe
E-mail: konabe@comas.frsc.tsukuba.ac.jp
Tel: +81-2-9853-5600 ext.8233

1P-47

Edge-Roughness Effect on Electronic Transport in Semiconductor Graphene Nanoribbons

○Kengo Takashima[1], Hiromu Fujii[1], Takahiro Yamamoto[1,2]
[1]*Dept. of Electrical Engineering, Tokyo Univ. of Science, Niijuku-ku, Tokyo 125-8585, Japan*
[2]*Dept. of Liberal Arts, Tokyo Univ. of Science, Niijuku-ku, Tokyo 125-8585, Japan*

Graphene is expected to be a channel material of field effect transistors (FETs) because of their high carrier mobility. However no band gap of the graphene is a serious problem for its FET application. One possible way to overcome the gap-opening problem is to process it in the form of a nanometer width ribbon, referred as graphene nanoribbons (GNRs). They have been successfully applied to FETs with high on-off ratio. However, the GNR-based FETs have not yet provided the best performance. A recent experiment reported that the resistance of GNRs increases exponentially with their length even at the room temperature [1]. This non-Ohmic behavior is due to the edge-roughness of GNRs. The effects of edge-roughness become more remarkable when the ribbon width becomes narrower in the future. However the electronic transport properties of such narrow GNRs have not been clarified yet.

In this study, we have computationally investigated the coherent electronic transport in narrow edge-disordered armchair GNRs (ED-AGNRs) using the nonequilibrium Green's function method combined with a tight-binding model. In our model, the edge roughness is modeled by removing pairs of carbon atoms at the armchair-type edges and ED-AGNR is connected to semi-infinite armchair GNR leads without disorder. We calculated the conductance with various edge-disorder configurations with changing the electron energy from -2eV to 2eV, the amount of edge carbon-pair vacancies from 4% to 30% and the ribbon-width from 0.74nm to 2.95nm.

We confirmed that the averaged conductance of ED-AGNRs decreased exponentially with their lengths, which is consistent with a previous experimental report [2]. We also examined (i) a relation between the localization length ξ and the edge-vacancy concentration, and (ii) the ribbon-width dependence of ξ. As is expected, ξ increases with decreasing the edge-vacancy concentration and with increasing the ribbon width. Furthermore, we found ξ for holes is longer than that for electrons, i.e., the electrons tend to be more localized than holes. The electron-hole symmetry breaking on the localization will be discussed in detail at the symposium.

[1] Xu *et al.*, Nano Lett. **11**, 1082 (2011).
[2] K. Takashima and T. Yamamoto (submitted)

Corresponding Authors: Takahiro Yamamoto
TEL&FAX: +81-3-5213-0990
E-mail: takahiro@rs.tus.ac.jp

1P-48

Temperature dependence of polarization-resolved photoluminescence in monolayer WSe_2

○Lizhong Zhou[1], Yuhei Miyauchi[1, 2], Shinichiro Mouri[1], Minglin Toh[3], Goki Eda[3]
and Kazunari Matsuda[1]

[1]Institute of Advanced Energy, Kyoto University, Uji, Kyoto 611-0011, Japan
[2]Japan Science and Technology Agency, PRESTO, 4-1-8 Honcho Kawaguchi, Saitama 332-0012, Japan
[3]Department of Physics, National University of Singapore, 2 Science Drive 3, Singapore 117542

Atomically-thin transition metal dichalcogenides (TMDs) such as MoS_2 and WSe_2 have attracted much attention as novel 2D semiconductors with remarkable physical properties [1-3]. In contrast to graphene with no band gap and centrosymmetric structure, monolayers of the TMDs are non-centrosymmetric materials with a direct band-gap located at the energy-degenerate K and K' valleys in momentum space. The structural inversion asymmetry in the 1L(monolayer)-TMDs gives rise to coupling of electron spin and valley degree of freedom; this characteristic enables valley-selective optical excitation in these materials using circular-polarized incident photons [1]. Therefore, the 1L-TMDs are promising materials for "Valleytronics", future optoelectronics technology using valley degree of freedom of electrons.

Here we study temperature dependence of polarized photoluminescence (PL) in 1L-WSe_2 [2] to understand spin-valley relaxation mechanism between the degenerate K and K' valleys. In the experiment, circular polarization of the incident photons was set to be σ^+ polarization (corresponding to selective excitation of K' valley), and σ^+ and σ^- components of the PL signals were separately detected. Figure 1 shows the polarization-resolved PL spectra at 15 K. The PL intensity of the σ^+ emission is larger than that of σ^- emission under the σ^+ excitation condition, suggesting spin-valley polarization in 1L-WSe_2 at 15 K. Temperature dependence of the observed valley polarization and its mechanism will be discussed.

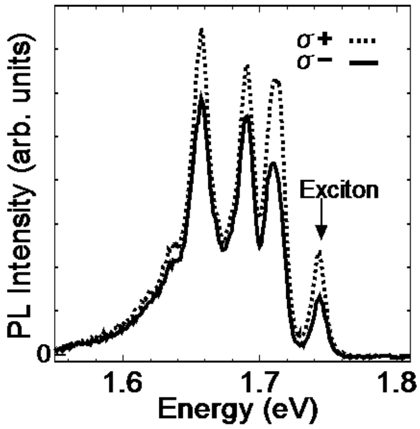

Fig.1 Polarization-resolved PL spectra of 1L-WSe_2 at 15 K.

[1] K. F. Mak *et al.*, Nature Nanotech. **7**, 494 (2012).

[2] W. Zhao *et al.*, ACS Nano **7**, 791 (2013).

[3] S. Mouri, Y. Miyauchi, and K. Matsuda, Nano Lett. **13**, 5944 (2013).

Corresponding Author: L. Zhou
E-mail: zhou.lizhong.46a@st.kyoto-u.ac.jp

1P-49

Nonlinear Photoluminescence Properties in Monolayer Transition Metal Dichalchogenides

Shinichiro Mouri[1], Lizhong Zhou[1], Yuka Tsuboi[1], Yuhei Miyauchi[1,2], Minglin Toh[3], Satoru Konabe[4], Goki Eda[3], Susumu Okada[4], and Kazunari Matsuda[1]

[1]Institute of Advanced Energy, Kyoto University, Uji, Kyoto 611-0011, Japan
[2]Japan Science and Technology Agency, PRESTO, 4-1-8 Honcho Kawaguchi, Saitama 332-0012, Japan
[3] Department of Physics, National University of Singapore, 2 Science Drive 3, Singapore
[4]Graduate School of Pure and Applied Sciences, University of Tsukuba, Tsukuba, Ibaraki 305-8571, Japan

Monolayer transition metal dichalcogenides (TMDs) have been attracted much attention as a novel two-dimensional direct band gap semiconductor [1], and are also a promising candidate to realize the ultra-thin opto-electronic devices [2]. Strong Coulomb interactions due to the quantum confinement effect in ultra-thin materials would give rise to intriguing many-body effects among optically generated carriers [3,4]. In this study, we investigated the exciton-exciton interactions in TMDs through optical nonlinearity and exciton dynamics.

Figure 1 (a) shows the photoluminescence (PL) spectra of monolayer (1L) WSe_2 with increasing excitation power density. The peak around 1.66 eV is originated from exciton (X) PL. As shown in the inset of Fig. 1 (a), the integrated exciton PL intensity is gradually saturated with increasing excitation power density. Exciton PL decay profiles at each excitation power density are plotted in Fig. 2. The exciton recombination time of 1L-WSe_2 is estimated as ~3 ns from the data of weak excitation region (0.0085 $\mu J/\mu m^2$). On the other hand, rapid decay component (<500 ps) due to exciton-exciton annihilation (EEA) becomes dominant with increasing excitation power density. From these results, we will discuss the detail mechanism of exciton-exciton scattering in TMDs based on the Monte-Calro simulation and the EEA rate calculated using Bethe-Salpeter-equations.

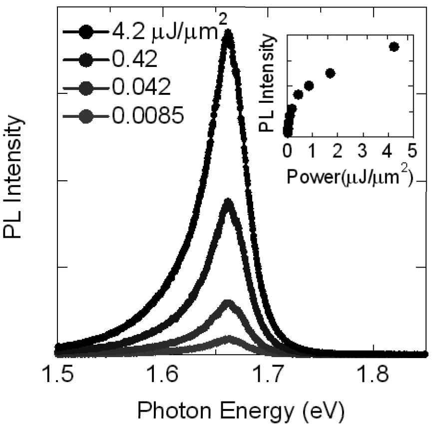

Fig. 1 Excitation power density dependent PL spectra of 1L-WSe_2.

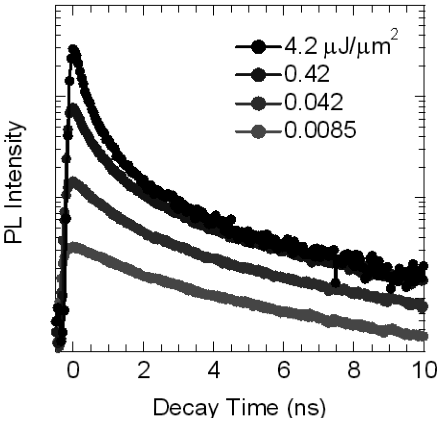

Fig.2 Decay profile of exciton PL of 1L-WSe_2 at each exciton power.

[1] A. Splendiani *et.al. Nano Lett.* **10**, 1271 (2010).

[2] Q. H. Wang *et.al. Nat. Nanotechnol.* **7**, 699 (2012).

[3] K. F. Mak *et.al. Nat. Mater.* **12,** 207 **(**2012**)**.

[4] S. Mouri *et.al. Nano Lett.* **13**, 5944 (2013).

Corresponding Author: Shinichiro Mouri
Tel: +81-774-38-3463,
Fax: +81-774-38-3467,
E-mail: iguchan@iae.kyoto-u.ac.jp

1P-50

Photoluminescence Imaging of Monolayer MoS_2 Synthesized by Chemical Vapor Deposition Method

○Yuka Tsuboi[1], Daichi Kozawa[1], Yuhei Miyauchi[1,2], Shinichiro Mouri[1],
Kazunari Matsuda[1]

[1]Institute of Advanced Energy, Kyoto University, Uji, Kyoto 611-0011, Japan
[2]Japan Science and Technology Agency, PRESTO, 4-1-8 Honcho Kawaguchi, Saitama 332-0012, Japan

Two-dimensional transition metal dichalcogenide, MX_2 (M=Mo,W, S=S,Se) has been extensively studied from the viewpoint of fundamental physics and optoelectronic applications. The atomically-thin monolayer MoS_2 is a direct band-gap semiconductor showing photoluminescence (PL). Very recently, the fabrications of large scale monolayer MoS_2 by chemical vapor deposition (CVD) have been reported [1]. However, the PL properties of these CVD grown MoS_2 have not been fully understood. In this study, we investigated PL properties of monolayer MoS_2 synthesized by CVD.

Monolayer MoS_2 with a triangle shape on SiO_2 substrate was fabricated by CVD method [1]. The fabricated monolayer MoS_2 shows PL around 1.8 eV [2]. The obtained PL images in the insets of Figure 1(a) and 1(b) clearly show the triangular shapes reflecting the shape of monolayer MoS_2. There are two types of triangle MoS_2 flakes in the spatial PL mapping; one shows stronger PL at the edge of triangle flake in Fig. 1(a) and the other shows that at the inside of flake in Fig. 1(b). The PL spectra at various positions of the triangular flakes are also shown. It is found that PL peak energy in Fig. 1(a) slightly changes. We will discuss the physical mechanism of difference of PL properties depending on the flakes based on detail PL imaging measurement.

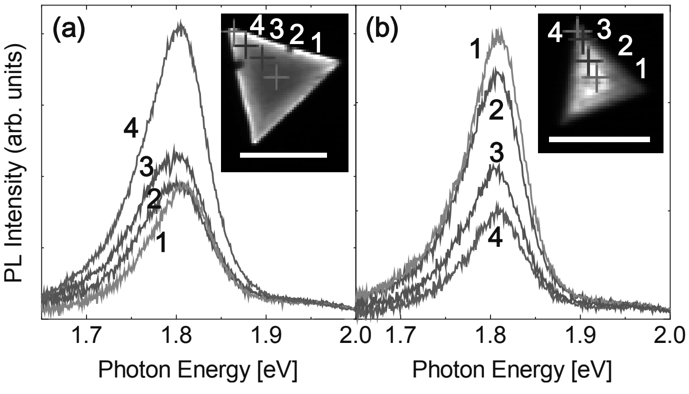

Fig. 1(a),(b) Normalized PL spectra measured at various points of the flakes. The insets show the PL images of monolayer MoS_2 flake (scale bar: 10 μm).

[1] C. Cong, J. Shang, X. Wu, *et al.*, arXiv:1312.1418 (2013).
[2] S. Mouri, Y. Miyauchi, and K. Matsuda, Nano Lett. **13**, 5944, (2013).

Corresponding Author: Y. Tsuboi
Tel: +81-774-38-3465
Fax: +81-774-38-3467
E-mail:tsuboi.yuka.72w@st.kyoto-u.ac.jp

2P-1

Investigation of molecular dynamics of fullernol solids by ^{2}H NMR spectroscopy

○Yoshiaki Sano[1], Keisuke Baba [2], Hironori Ogata [1,2]
[1]*Graduate School of Engineering, Hosei University, Tokyo 184-8584, Japan*
[2]*Department of Faculty of Biosci. and Applied Chem.,Hosei University,Tokyo184-8584, Japa*n

Fullerenols (Polyhydroxylated Fullerene: $C_{60}(OH)_x$) have been a subject of intense research in many fields with the claim of possible applications in a variety of areas, including optoelectronics, medical therapeutics, biotechnology, chemical mechanical polishing, and fuel cells, owing to their high solubility in a large variety of solvents (depending on the number of hydroxyl groups, x). It was reported that $C_{60}(OH)_n$ (n~12) show proton conductivity and their applications for the proton conducting membrane of a polymer electrolyte fuel cell (PEFC) is proposed. However, their proton conduction mechanism has not been thoroughly studied yet. We previously reported the proton dynamics in both $C_{60}(OH)_{13.5}$ and $C_{60}(OH)_{38.7}(O)_{1.6}$ solids by means of ^{1}H-solid-state NMR[4] and it was clarified that the formation of both interamolecular and intermolecular hydrogen-bond networks had a large influence on their proton dynamics at low temperature. In this study, we investigated to get more detailed proton dynamics by using ^{2}H-NMR of deuterated fullerenols.

The detailed results about their proton dynamics will be presented.

References:
[1] Hinokuma *et. al., Chem. Phys. Lett.,* 341, 442 (2001)
[2] Chiang *et al.*, Org. Chem. **59**, 3960 (1994).
[3] Kokubo *et al.*, Nano Res., **4,** 204 (2011)
[4]K.Baba et al, Proc.of the 44th Fullerene-Nanotubes-Graphene General Symposium(1-5).

Corresponding Author: H. Ogata
Tel: +81-42-387-6229, Fax: +81-42-387-6229,
E-mail: hogata@hosei.ac.jp

2P-2

Synthesis of a Novel Open-cage C_{60} Derivative with a Ketolactam Moiety

○Yoshifumi Hashikawa[1], Michihisa Murata[1], Atsushi Wakamiya[1], Yasujiro Murata[1,2]

[1] Institute for Chemical Research, Kyoto University, Uji, Kyoto 611-0011, Japan
[2] JST, PRESTO, 4-1-8 Honcho, Kawaguchi, Saitama 332-0012, Japan

Open-cage fullerene derivatives[1] have been attracting considerable attention because they are interesting molecules for host-guest chemistry and can be used as precursors for endohedral fullerenes encapsulating an atom or small molecules. However, reports on their synthesis are still limited. We have previously synthesized several open-cage C_{60} derivatives, which can encapsulate a He atom, H_2 molecules, and an H_2O molecule.[2] Ketolactam **1**, one of the reported open-cage C_{60} derivatives,[3] is known as a precursor for azafullerenes such as $(C_{59}N)_2$.[4] However, the size of the opening is too small for insertion of even a He atom. Herein, we studied its reaction in order to enlarge the opening.

Scheme 1

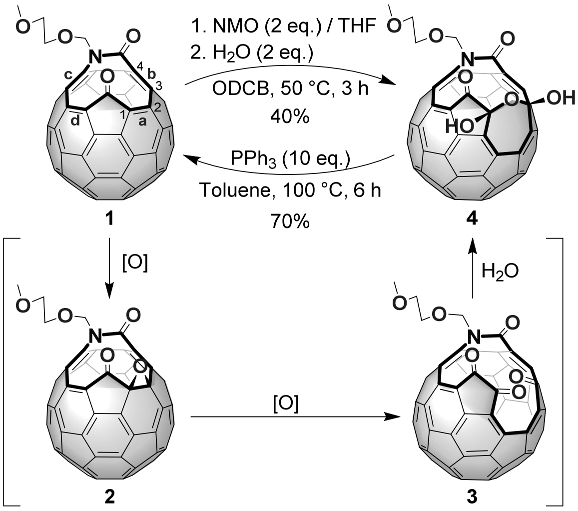

Novel open-cage C_{60} derivative **4** was obtained in 40% yield by the reaction of **1** with *N*-methylmorpholine *N*-oxide (NMO) in *o*-dichlorobenzene (ODCB) in the presence of a small amount of water (Scheme 1). The structural assignments of **4** were conducted by APCI MS, ^1H and ^{13}C NMR, UV-vis, and IR spectra, in addition to theoretical calculations. It is supposed that the epoxidation of **1**, as the possible first step of this reaction, takes place at one of the C=C double bonds **a**, **b**, **c**, or **d**. The theoretical calculations at the B3LYP/6-31G* level of theory demonstrated that the LUMO is relatively localized at the butadiene unit (C1=C2–C3=C4) including bonds **a** and **b**, and that epoxide **2** formed by reacting on **a** is 9.0 kcal/mol more stable than another epoxide formed by reacting on **b**. Then, compound **2** is thought to react with the second NMO to give **3**, which affords **4** by the addition of an H_2O molecule.[5]

The chemical reactivity of **4** was studied. The reaction of **4** with 20-fold trifluoroacetic anhydride at room temperature for 3 h gave tetraketo derivative **3**. In addition, **4** was converted to original **1** in 70% yield by treatment with triphenylphosphine in toluene. Structures and encapsulation behaviors of these open-cage C_{60} derivatives will be presented in detail.

[1] Vougioukalakis, G. C.; Roubelakis, M. M.; Orfanopoulos, M. *Chem. Soc. Rev.* **2010**, *39*, 817.
[2] Murata, M.; Murata, Y.; Komatsu, K. In *Organic Nanomaterials: Synthesis, Characterization, and Device Applications*; Torres, T., Bottari, G., Eds.; John Wiley & Sons: West Sussex, U.K, 2013, pp 225–239.
[3] Hummelen, J. C.; Prato, M.; Wudl, F. *J. Am. Chem. Soc.* **1995**, *117*, 7003.
[4] Hummelen, J. C.; Knight, B.; Pavlovich, J.; González, R.; Wudl, F. *Science* **1995**, *269*, 1554.
[5] Kurotobi, K.; Murata, Y. *Science* **2011**, *333*, 613.

Corresponding Author: Y. Murata
Tel: +81 774-38-3172, Fax: +81 774-38-3178,
E-mail: yasujiro@scl.kyoto-u.ac.jp

2P-3

A Novel Ligand-free ZnO Particle for Fullerene:Polymer Inverted Organic Solar Cell

○ Il Jeon[1], James W. Ryan[1], Kee Sheng Yeo[1], Tafu Nakazaki[2], Yuichi Negishi[2] and Yutaka Matsuo[1]

[1] Department of Chemistry, The University of Tokyo, Tokyo 113-0033, Japan
[2] Department of Applied Chemistry, Tokyo University of Science, Tokyo 162-8601, Japan.

Organic solar cells are drawing much attention as the next-generation solar cells on account of their cost effectiveness, lightweight, and flexibility with its high power conversion efficiency. [1] Its shortcoming of low stability is now resolved by applying the inverted structure. [2] Recently, zinc oxide (ZnO) nanoparticles have been a popular choice for use as interlayers in organic thin film solar cells, due to its favorable energy levels, as well as its solution-processability. The ZnO nanoparticles not only possess a work function that matches well with acceptor materials (e.g. PCBM)[3] but also exhibit high electron mobility. In addition, ZnO is not as dependent on UV light activation like in the case of TiO_2.[4] Unlike conventional ZnO thin film fabrication, where high energy and high temperature are required, ZnO nanoparticles can be applied to device with much mild conditions. However, current ZnO nanoparticles synthesis needs ligands to stabilize them and in turn, requires higher temperature around 150 ˚C to remove the insulating ligand remnants. In our research we introduce a novel ZnO nanoparticle synthesis, which is ligand free and consequently leading to ZnO film with no annealing temperature required, making the flexible device application more facile.

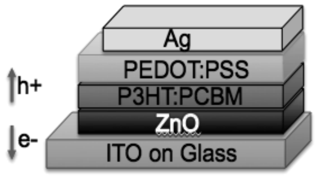

Fig. 1. Inverted Organic Solar Cell with ZnO layer

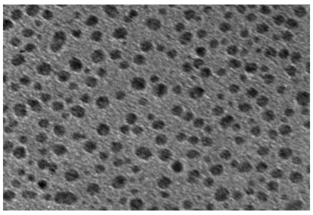

Fig. 2.TEM image at 150,000x magnification

For generation of ZnO, following the heating of zinc acetate precursor in amino-ethanol under reflux, the reaction mixture is centrifuged, to separate the precipitate that contains larger ZnO particles. The supernatant in this case will contain well-dispersed ZnO nanoparticles of average size of 2.5 nm, as observed via TEM. (Fig. 2) The experimental results compared to the conventional sol-gel method are given in Table 1.

Table 1. Optimal OSC Device performance both ZnO sol-gel (ref.) and ZnO nano particles based devices according to their annealing temperatures

ECL	Annealing Temperature	V_{OC} (V)	J_{SC} (mA/cm^2)	FF	Rs(Ω)	Rsh(Ω)	PCE (%)
ZnO sol-gel	200 °C	0.60	9.42	0.56	5.71	2.23E+04	3.2
ZnO sol-gel	No Anneal	0.01	0.03	0.25	280	3.54E+02	0.0
ZnO np	No Anneal	0.61	9.08	0.56	8.29	1.66E+04	3.1
ZnO np	120 °C	0.62	9.13	0.53	8.43	1.54E+04	3.0
ZnO np	150 °C	0.62	8.65	0.53	8.35	1.27E+04	2.9
ZnO np	180 °C	0.61	7.98	0.45	9.77	1.22E+04	2.2
ZnO np	210 °C	0.59	6.91	0.34	20.11	1.12E+04	1.4

[1] X. Yang *et al., Adv. Mater.* **24** 1202 (2012), [2] A.K.K. Kyaw *et al., Appl. Phys. Lett.* **93** 2211071 (2008), [3] L. Dou *et al., Nature Photon.* **6**, 180 (2012), [4] J. You *et al., Adv. Mater.* **24**, 5267 (2012)

Corresponding Author: Professor Y. Matsuo
Tel: +81-3-5841-1476
E-mail: matsuo@chem.s.u-tokyo.ac.jp

2P-4

Synthesis of Penta(aryl)[60]fullerene Cobalt Dithiolene Complexes for Organic Solar Cells

○Keisuke Ogumi, Takafumi Nakagawa, Yutaka Matsuo

Department of Chemistry, The University of Tokyo, Tokyo 113-0033, Japan

Introduction

The transition metal fullerene complexes frequently have been studied because of their interesting chemical properties. Cobalt trisulfide fullerene complex **1** had 4-membered ring from cobalt and trisulfide [1]. This organometallic ring exhibited an aromatic 6π-electron system. Thus, this complex possessed antithetical properties, the stability from aromaticity and the reactivity from distortion of 4-membered ring. This complex also showed distinctive structure which has bowl-shape derived from fullerene and five substituents. Cobalt trisulfide fullerene complex **1** was consequently prominent starting material because of specific reactivity and structure [2].

This work

Novel cobalt dithiolene complexes **2**-**8** were obtained from starting material penta(aryl)[60]fullerene cobalt trisulfide complex and corresponding disulfides through a process of S–S bond cleavage and C–H bond activation (Scheme 1). Their electrochemical properties were tuned by the dithiolene ligand moiety (Figure 1).

Complexes **2**-**8** showed long wavelength absorption and the stability due to aromaticity in pentagonal cobalt dithiolene rings. These properties suggested complexes **2**-**8** were suitable materials for organic solar cells. Photovoltaic devices using complexes **2**-**8** acted as electron acceptors in organic solar cells. AFM observations revealed that the dithiolene ligand moiety influenced on film morphology and device performance. Complex **8** having bulky naphthalene dithiolene ligand moiety gave 0.59% PCE. These complexes will expand organometallic fullerene chemistry in organic solar cells.

Scheme 1. Synthesis of cobalt dithiolene complexes.

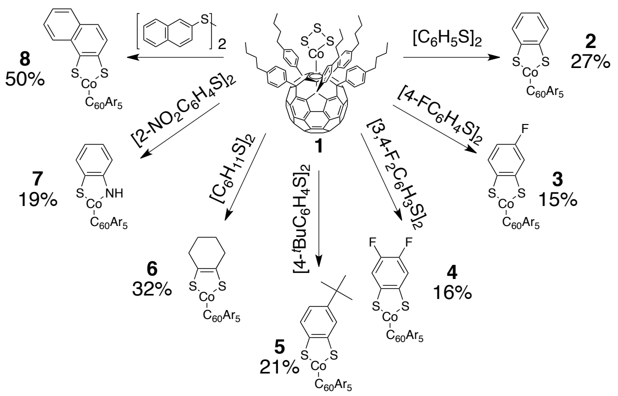

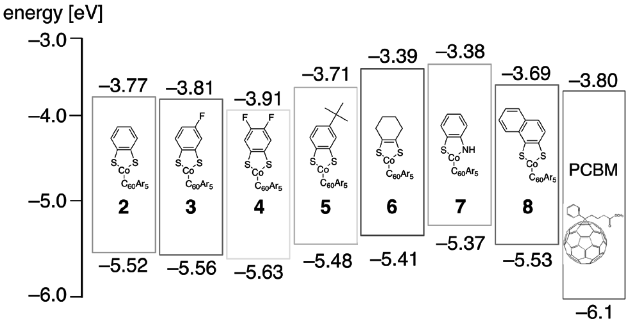

Figure 1. HOMO-LUMO levels of **2**-**8**.

[1] M. Maruyama. *et al. J. Am. Chem. Soc.* **2011**, *133*, 6890–6893.

[2] M. Maruyama. *et al. Angew. Chem. Int. Ed.* **2013**, *52*, 3015–3018.

Corresponding Author: Y. Matsuo

Tel: 03-5841-1476, Fax: 03-5841-1476, E-mail: matsuo@chem.s.u-tokyo.ac.jp

Characterization of surface layer of C_{60} thin-film polymerized by optical vortex

○Wataru Akiyama[1], Daiki Momiyama[1], Naoto Toriumi[1], Naoto Nakamura[1],
Katsuhiko Miyamoto[1], Takashige Omatsu[1,2], Jonathan P. Bird[3], Yuichi Ochiai[1],
and Nobuyuki Aoki[1,4]

[1] *Graduate School of Advanced Integration Science, Chiba University,*
Chiba, 263-8522 Japan
[2] *JST-CREST, 4-1-8 Honcho Kawaguchi, Saitama 332-0012, Japan*
[3] *Department of Electrical Engineering, University at Buffalo, SUNY, Buffalo, NY 14260-1920, USA*
[4] *JST-PREST, 4-1-8 Honcho Kawaguchi, Saitama 332-0012, Japan*

Recently, a state of the art photo-polymerization of a C_{60} thin film has been realized by irradiation of topological laser beam namely optical vortex (OV). Since the beam has a helical wavefront and a torque appears along the tangential direction, a confinement force can be expected along the peripheral direction of the beam and the polymerization takes a progress with a compressive photon-pressure under a high-beam-power density. Therefore, it can be expected to achieve unusual photo-polymerization mechanism in a C_{60} thin film. Moreover, combining with circular polarization, total angular momentum of light can be controlled [1].

In our study, thermally evaporated C_{60} thin film was deposited 100 nm on a SiO_2 layer on top of a heavily doped Si substrate. A continuous-wave laser beam (λ = 532 nm) was used for the optical source. The OV was produced by using a spiral phase plate and irradiated onto the sample through an objective lens. The photo-polymerization was done at high-vacuum condition.

In the observation of the surface of the C_{60} thin film by atomic force microscope, very thin layers having a thickness of 5~6 nm covering the grains of C_{60} were observed after the OV irradiation. Taking care of the fact, in-situ transport characteristics (top-contact condition) were observed in a vacuum probe station after the irradiation of the OV. The transfer characteristic after a dose of 30 MJ/cm^2 shows a linear current-voltage characteristic and no dependence on the sweep of the back gate voltage, which is different from the usual semiconducting characteristic of a C_{60} photo-polymer. It suggests that a metallic layer might be realized on the top of the thin-film after the heavy dose of OV irradiation.

[1] T. Omatsu *et al.*, Opt. Express **18** (2010) 17967.

Corresponding Author: W. Akiyama
Tel: +81-43-290-3430, Fax: +81-43-290-3427,
E-mail: adsa3781@chiba-u.jp

2P-6

Extraction and Isolation of Missing Small-Bandgap Metallofullerenes through Exterior Functionalization

○Zhiyong Wang, Yusuke Nakanishi, Shoko Noda, Hiroyuki Niwa, Jinying Zhang, Ryo Kitaura, Hisanori Shinohara

Department of Chemistry and Institute for Advanced Research, Nagoya University, Nagoya 464-8602, Japan

C_{60} and C_{70} are the most stable members in the fullerene family. However, the corresponding endohedral fullerenes M@C_{60} and M@C_{70} (M = rare-earth metal) are missing in conventional extract of arc-produced fullerene soot. Besides M@C_{60} and M@C_{70}, there are a large number of other missing, the so-called small-bandgap (or small HOMO-LUMO gap) metallofullerenes such as M@C_{72}, M@C_{74}, etc. These metallofullerenes are chemically unstable due to their open-shell electronic configurations or small bandgaps, and they tend to form insoluble polymerized solids in the raw soot.

Here, we report in situ exterior functionalization of the small-bandgap metallofullerenes using a modified arc-discharge method [1]. Solid polytetrafluoroethene (PTFE) is used as a source for the functional groups. A series of trifluoromethyl derivatives of small-bandgap metallofullerenes M@$C_{2n}(CF_3)_m$ ($2n$ = 60, 70, 72 or 74; m = 1 or 3) are formed effectively. Surprisingly, these derivatives, including those of M@C_{60} and M@C_{70}, are totally soluble and stable in conventional fullerene solvents (Fig. 1). A C_{70}-based metallofullerene (Y@C_{70}) is solvent extracted and isolated for the first time ever since the first macroscopic synthesis of metallofullerenes in 1991. Theoretical calculations demonstrate that trifluoromethyl functionalization of Y@C_{70} induces a large bandgap opening and thereby gives rise to a stable metallofullerene.

This method can be applied to any rare-earth metals. Similar results have been obtained in the present laboratory for metals of Y, La, Gd, and Dy.

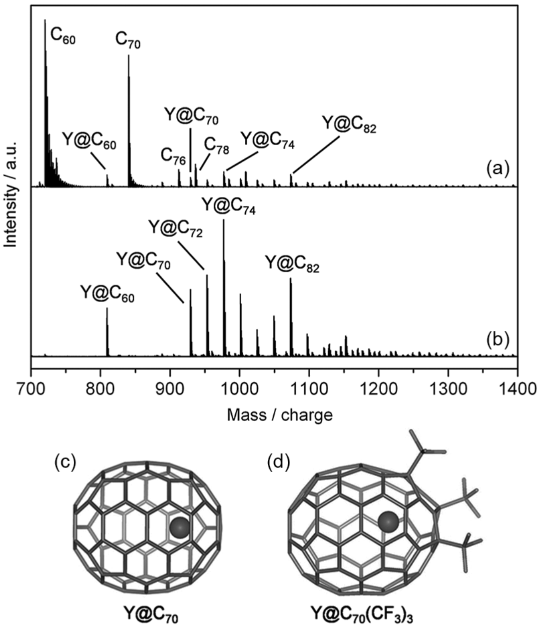

Fig. 1. Laser desorption time-of-flight mass spectra for (a) *o*-xylene extracted mixture and (b) separated metallofullerenes (the observed Y@C_{2n} ions are actually fragments of Y@$C_{2n}(CF_3)_m$). DFT-optimized molecular structures of (c) Y@C_{70} and (d) Y@$C_{70}(CF_3)_3$.

[1] Z. Y. Wang *et al.* Angew. Chem. Int. Ed. **52**, 11770-11774 (2013).

Corresponding Author: H. Shinohara
Fax: +81-52-747-6442,
E-mail: noris@nagoya-u.jp

2P-7

Supercapacitor using Lithium-Ion Endohedral Metallofullerene

○Eunsang Kwon[1], Ken-ichirou Komatsu[1], Yoichi Yamada[2], Yuri Hasegawa[2], Sho Sato[2], Seiji Sakai[3], Kazuhiko Kawachi[4], Kuniyoshi Yokoo[4], Shoichi Ono[4], Yasuhiko Kasama[4], Shinobu Aoyagi[5], Tomoaki Endo[6], Tomoyuki Ogawa[7], Migaku Takahashi[7]

[1] Research and Analytical center for Giant Molecules, Graduate School of Science, Tohoku University, Sendai, 980-8578, Japan
[2] Institute of Applied Physics, University of Tsukuba. 1-1-1 Tennodai, Tsukuba, Ibaraki, 305-8573, Japan
[3] Advanced Science Research Center, Japan Atomic Energy Agency, Japan
[4] Idea International Co., Ltd, 981-0922, Japan
[5] Nagoya City University, Nagoya 467-8601, Japan
[6] Sendai National College of Technology, 981-1239, Japan
[7] NICHe, Tohoku University, Sendai 980-8579, Japan

Since the synthesis and characterization of lithium cation endohedral metallofullerene (lic fullerene) [1], several investigations have been performed on the application of the “lic fullerene” to the functional materials [2]. However, there has been no study on the application of the “lic fullerene” to the energy storage systems.

In the present work, we investigated the energy storage characteristics of $Li^+@C_{60}$ capacitor. The ortho-dichlorobenzene (*o*-DCB) solution of $Li^+@C_{60}\cdot PF_6^-$ in different concentrations, ranging from 0.1 to 1.0 mmol/L, and interdigital Au electrode (Fig. 1) were used for the measurements. The *o*-DCB solution of $TBA^+\cdot PF_6^-$ was used for comparison under the same experimental conditions.

As shown in Fig. 2, the energy stored by $Li^+@C_{60}$/*o*-DCB capacitor was greater by several times than that stored by TBA^+/*o*-DCB capacitor under the same conditions. This result indicated that TBA^+ ions undergo solvation and the size of the solvated TBA^+ would be larger than that of $Li^+@C_{60}$ ions. Moreover, the charging speed of $Li^+@C_{60}$/*o*-DCB capacitor was faster than that of TBA^+/*o*-DCB capacitor. This would originate from the shape of $Li^+@C_{60}$ ion having a spherical structure.

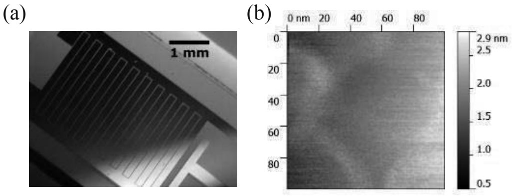

Fig. 1. (a) A photograph of an interdigital Au electrode. (b) AFM image of the $Au(111)/\alpha\text{-}Al_2O_3(0001)$ electrode showing surface roughness of Au.

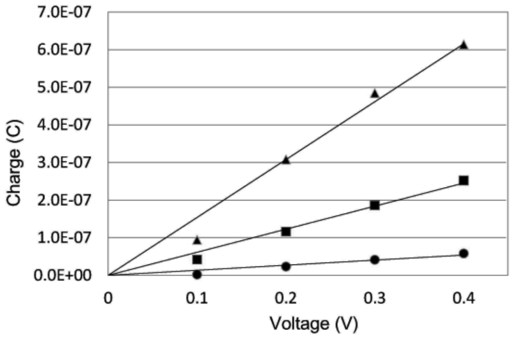

Fig. 2. Charge versus voltage plot of $Li^+@C_{60}\cdot PF_6^-$/*o*-DCB (1.0 mmol/L) capacitor (triangles), $TBA^+\cdot PF_6^-$/*o*-DCB (1.0 mmol/L) capacitor (squares) and *o*-DCB (circles).

[1] S. Aoyagi *et al*., Nature Chemistry, **2**, 678 (2010). [2] For recent reports, see: K. Ohkubo *et al*., Chem. Commun., **49**, 7376 (2013); K. Kokubo *et al*. Nanoscale, **5**, 2317 (2013); K. Ohkubo *et al*. Chemical Science, **4**, 1451 (2013).

Corresponding Author: E. Kwon
Tel: +81-22-795-6752, Fax: +81-22-795-6752, E-mail: ekwon@m.tohoku.ac.jp

2P-8

Spin-state Tuning of Deca-Methyl C_{60} by an Electric Field

○Kohei Narita and Susumu Okada

Graduate School of Pure and Applied Sciences, University of Tsukuba
1-1-1 Tennodai, Tsukuba, Ibaraki 305-8571, Japan

Electronic structure of carbon allotropes with the three-fold coordination depends on their morphology, dimensionality, size, and boundary condition. Indeed, chemical modifications on fullerenes result in interesting π electron systems on the spherical networks. For instance, deca-organo C_{60} possesses interesting geometric and electronic structures arisen from chemical modification on C_{60} by ten aromatic molecules [1]. Attached aromatic molecules divide spherical π electron system into three parts: a short armchair nanotube and two pentagonal rings surrounded by molecules. According to these two pentagonal rings, this C_{60} derivative has two radical spins localized at these pentagonal rings, which are coupled in an anti-parallel manner in their ground state [2]. In this work, we explore the possibility of the spin-state tuning of the radical spins in deca-methyl C_{60} by an external electric field in the framework of first-principles electronic structure calculations.

By applying the normal electric field to the pentagonal rings surrounded by the methyl groups, we find that the energy difference between the total energies of the parallel and antiparallel spin states gradually decrease with increase of the electric field (Fig. 1). Finally, at the electric field of 0.07 V/A, the total energy of the parallel state is the same as that of the antiparallel arrangement indicating that the spin-flip process occurs in terms of the external electric field. In sharp contrast, such spin-flip process does not occur under the parallel electric field to the pentagonal rings possessing radical spins. Based on the result, we conclude the possibility of magnetic-state tuning of the radical spin in deca-methyl C_{60} by the electric field..

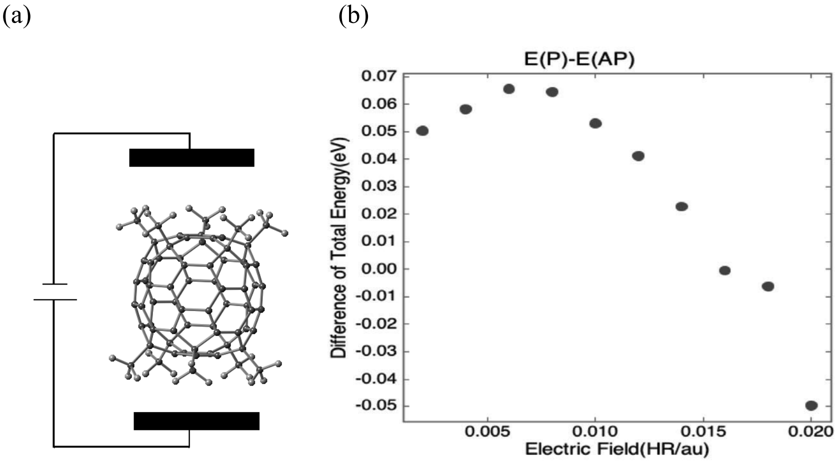

Fig. 1 (a) Geometric structure of deca-methyl C_{60} sandwiched by two electrons. (b) Energy difference between the total energies of the parallel and antiparallel spin configuration.

References

[1] E. Nakamura, et al. J. Am. Chem. Soc. **125** (2003) 2834.
[2] H. Nitta et al. Appl. Phys. Express. **6** (2013) 045102

Corresponding Author: K. Narita
Tel: +81-29-853-5921, Fax: +81-29-853-5924,
E-mail: sokada@comas.frsc.tsukuba.ac.jp

2P-9

Geometric and electronic structures of two-dimensionally polymerized C_{32}

○Mina Maruyama and Susumu Okada

Graduate School of Pure and Applied Sciences, University of Tsukuba, Tennodai, Tsukuba 305-8577, Japan

Fullerenes are kwon to form covalent networks of C atoms with one-, two-, and three-dimension in which the fullerenes are tightly bound each other via covalent bonds between adjacent molecules by introducing the four-fold coordinated C atom. According to the intermolecular covalent bonds, these condensed phases of fullerenes could be classified as a novel carbon allotropes consisting of both sp^2 (three-fold coordinated) and sp^3 (four-fold coordinated) C atoms. Electronic structures of these sp^2 - sp^3 hybrid carbon allotropes strongly depend on their dimensionality and morphologies leading to peculiar electronic structure at/around Fermi level. Among the possible fullerenes, small fullerenes whose cluster sizes are smaller than C_{60} are also regarded as possible constituent units for such covalent networks of sp^2 and sp^3 carbon atoms because of their remarkable chemical reactivity arising from the large curvatures. Indeed, in our previous calculations, we demonstrated that the C_{26} and C_{28} fullerenes form two and three-dimensional covalent networks, respectively, as their stable condensed forms with interesting diversity in their electronic structures. In the present work, we theoretically design two-dimensional covalent networks with hexagonal symmetry comprising small fullerene C_{32} with D_{3h} symmetry based on the first-principles total-energy calculations in the framework of the density functional theory (DFT).

Figure 1 (a) shows an optimized structure of two-dimensionally polymerized C_{32}. As shown in figure, C_{32} forms a two-dimensional honeycomb network with covalent bond between C_{32} as in the case of graphene sheet. We find that polymerized C_{32} is a semiconductor with a direct energy gap of 1.3 eV. For this sheet, we examine the possibility of molecular doping of the other small fullerene C_{36} [Fig. 1 (b)]. The doped structure is energetically stable and is a metal with relatively small dispersion band at the Fermi level.

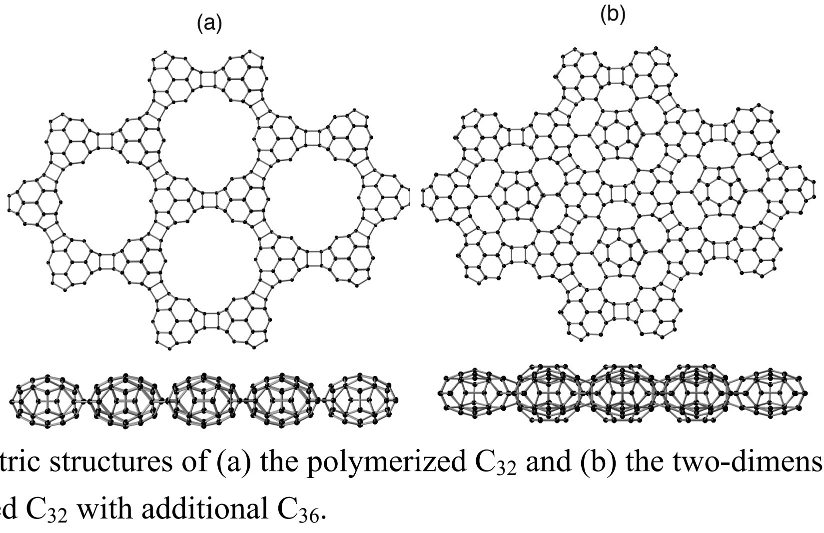

Fig. 1 Geometric structures of (a) the polymerized C_{32} and (b) the two-dimensional network of polymerized C_{32} with additional C_{36}.

Corresponding Author: M.Maruyama
Tel: +81-29-853-5600, Fax: +81-29-853-5924,
E-mail: mmaruyama@comas.frsc.tsukuba.ac.jp

2P-10

Electronic structure change of single-walled carbon nanotube by X-ray irradiation

○Toshiya Murakami[1], Yuki Yamamoto[1], Mitsuaki Matsuda[1], Kenji Kisoda[2],
Hiroshi Nishigaki[3], Noriyuki Hasuike[3], Hiroshi Harima[3], Chihiro Itoh[1]

[1]Department of Materials Science and Chemistry, Wakayama University, Wakayama, 640-8510, Japan
[2]Department of Physics, Wakayama University, Wakayama, 640-8510, Japan
[3]Department of Electronic, Kyoto Institute of Technology, Kyoto, 606-8585, Japan

Because of strong correlation of the electronic structure with geometric structure of single-walled carbon nanotubes (SWNTs), structural modification by ionizing radiation can be utilized as a tool to modify the SWNT's electronic structure. We have shown that X-ray irradiation gives rise to the formation of vacancy and interstitial pairs (Frenkel defects) in SWNTs, which eventually leads to their structural change.[1] The formation efficiency and thermal stability of X-ray-induced defects were shown to depend on the number and helicity of layer of tubes.[2] However, the irradiation effects on the SWNT's electronic structure has been left to be ambiguous. In this report, we have shown the results of the multi-probe resonant Raman spectra of the X-ray-irradiated SWNTs and discuss the irradiation effect on the electronic structure of SWNT.

SWNTs grown by chemical vapor deposition were irradiated by X-ray (Kα line of Mg) in vacuum. Resonant Raman spectra were measured with the excitation wavelengths of 532, 561, 568, 647, and 660 nm.

Figure 1(a) shows the radial breathing modes (RBMs) in Raman spectra of the SWNTs before X-ray irradiation. Figure 2 is an RBM map of pristine SWNT drawn based on the experimental spectra shown in Fig. 1 with simulating the spectral features according to the previous reports. The resonant Raman spectra of the X-ray-induced samples can be reproduced from Fig. 2 by considering that the optical transition energy contributing the resonance is reduced by 0.05 eV by the X-ray irradiation. The simulated resonant Raman spectra thus obtained are shown by dotted curves in Fig. 3. This result is consistent with the results of optical absorption measurements. On the basis of these results, we have concluded that the X-ray irradiation modifies electronic structure of SWNTs.

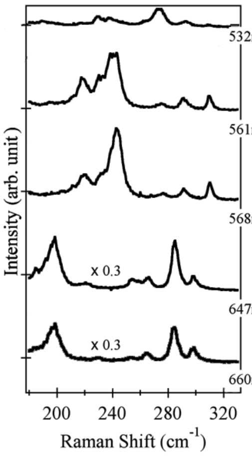

Fig. 1 Raman spectra of pristine SWNT

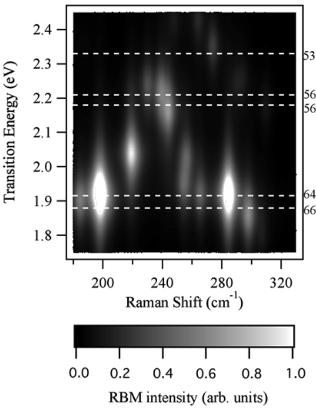

Fig. 2 Raman map of pristine SWNT

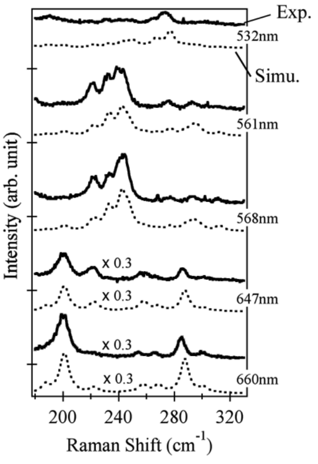

Fig. 3 Raman spectra of irradiated SWNT

[1] Murakami, *et. al.*, Eur. Phys. J. B **86**,187 (2013) [2] Murakami, *et. al.*, J. Appl. Phys. **114**, 114311 (2013)

Corresponding Author: T. Murakami, Tel: +81-73-457-8532, E-mail: murakami@sys.wakayama-u.ac.jp

Anharmonic effects on phonons in single-walled carbon nanotubes

○Masashi Mizuno,[1] Riichiro Saito[1]

[1] *Department of Physics, Tohoku University, Sendai 980-8578, Japan*

Graphene and carbon nanotubes are promising materials for their outstanding physical properties, *i.e.*, thermal conductivity, *etc*. [1]. However, the analytical forms of these properties are not well understood yet [2-4]. To calculate thermal conductivity accurately, we have to take anharmonicity (cubic or higher order terms) of interatomic potential [5,6] into account [7], so the problem is non-linear. With anharmonicity, phonon states are no longer the eigenstates of crystal and phonons have finite lifetimes, which make the thermal conductivity a finite value. The main purpose of this research is to understand anharmonic effects on phonons in carbon nanotubes for getting better understanding of thermal conductivity and line broadening in phonon spectra.

There are two approaches for this study: classical and quantum method. Classical way is solving the classical equations of motions for crystal atoms numerically and applying Fourier analysis to observe phonons' behavior. Quantum way is to treat anharmonic interactions as perturbations, but this research is at an early stage now.

From study on classical one-dimensional chain with anharmonic potential, it is found that the frequencies and wavenumbers of scattered phonons are mixing of those of initial phonons, and these mixing rules can be found formally in equations of motions as cross-terms.

Also looking at the shape of the potential, it is found that the hexagonal lattice is relevant to anharmonicity especially for bond-stretching mode, which determines the mean free paths of in-plane phonons. Therefore, thermal conductivity may depend on crystal direction or chirality of a carbon nanotube. In the presentation, we show how to make anharmonic potential terms and some preliminary calculations.

[1] R. Saito, *et al.*, *Physical Properties of Carbon Nanotubes*, Imperial College Press, London (1998).

[2] J. Shiomi, *et al.*, Int. J. Thermophys. **31**, 1945–1951 (2008).

[3] L. Paulatto, *et al.*, Phys. Rev. B. **87**, 214303 (2013).

[4] Chen S, *et al.*, Nat. Mater. **11**, 203 (2012).

[5] L. Lindsay, *et al.*, Phys. Rev. B **81**, 205441 (2010).

[6] V. K. Tewary, *et al.*, Phys. Rev. B **79**, 075442 (2009).

[7] G. P. Srivastava, *The Physics of Phonons*, Taylor & Francis, New York (1990).

Corresponding Author: M. Mizuno
E-mail: mizuno@flex.phys.tohoku.ac.jp

2P-12

The Analysis of Exchange Reactions of Sodium Cholate and Double-Stranded DNA on Single -Walled CNTs

○Akiko Tsuzuki[1] and Naotoshi Nakashima[1,2,3]

[1]Department of Applied Chemistry, Graduate School of Engineering, Kyushu University, 744 Motooka, Nishi-ku Fukuoka, [2] WPI I2CNER, [3] JST-CREST,

Deoxyribonucleic acid (DNA) is one of the well-known solubilizers of single-walled carbon nanotubes (SWNT). The DNA-SWNT hybrids have attracted much research. There are many applications of the hybrids. Bio-sensors, electron transfer, length fractionation, and chirality separation of SNWTs are the typical examples. Previously, we reported quantitative evaluation of the exchange reactions between sodium cholate (SC) and single-stranded DNA (ssDNA) on SWNTs [1,2]. In this work, the interaction of ssDNA and double-stranded DNA (dsDNA) on SWNTs was studied.

CNTs were solubilized by sonication in a SC solution (2 mM). After centrifugation (120,000 ×g, 3 h), the supernatant was used as a solubilized-CNT solution. Two ssDNA solutions, NF-κB decoy sense that have such nucleotide sequence, 5’-CCTTGAAGGGATTTCCCTCC-3', and NF-κB decoy anti-sense which have the complementary sequence of NF-κB decoy sense, were mixed and stored for one hour at 80 °C to prepare dsDNA. The CNT solution with TE buffer was mized with various concentrations of DNAs (20-mers, $d(A)_{20}$, $d(T)_{20}$, $d(G)_{20}$,$d(C)_{20}$, NF-κB decoy sense, NF-κB decoy anti-sense, 0-800 μM, and dsDNA of NF-κB decoy, 0-400 μM). The solutions were stored for three days at a temperature of 15, 20, 25, 30, 35, or 40 °C, and then absorption spectra were measured using a UV-vis spectroscopy with a temperature controller. The equilibrium constants ($K\alpha$), enthalpy change (ΔH), and entropy change (ΔS) of the solubilizer exchanges were evaluated.

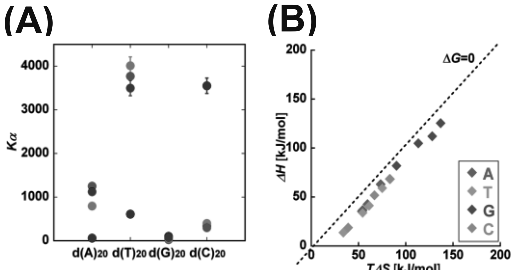

Figure 1 Equilibrium constants (A) and thermodynamic parameters (B) of exchanges of SC for the $d(A)_{20}$, $d(T)_{20}$, $d(G)_{20}$, $d(C)_{20}$.

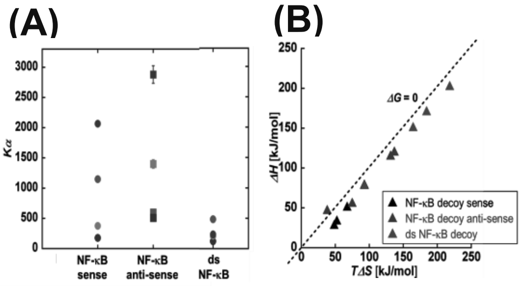

Figure 2 Equilibrium constants (A) and thermodynamic parameters (B) of the exchanges of SC for the double stranded (ds) NF-κB and its single strands.

Figure 1-(A) and Figure 2-(A) indicate the value of $K\alpha$ against each of the kinds of nucleobases, and Figure 1-(B) and Figure 2-(B) indicate the value of ΔH against the values of $T\Delta S$ (T = 298 K) which of the exchange reaction. We found the behavior of this reaction can be seen from these data, d(G)20 and dsDNA (NF-κB decoy) is similar. We have already done also discussed about the discussion of this, on the behavior of the other.

[1] Y. Kato, Y. Niidome, N. Nakashima, *Chem. Lett.*, **2011**, 40, 730.
[2] Y. Kato, A. Inoue, Y. Niidome, N. Nakashima, *Scientific Reports*, **2012** 2,733.

Corresponding Author: N. Nakashima
Tel: +81-92-802-2841, Fax: +81-92-802-2841
E-mail: nakashima-tcm@mail.cstm.kyushu-u.ac.jp

Chirality Dependence of Quantum Thermal Transport in Carbon Nanotubes at Low Temperatures: A First-Principles Study

○Tomoyuki Hata, Hiroki Kawai, Tatsuhiko Ohto, Koichi Yamashita

Department of Chemical System Engineering, The University of Tokyo, Tokyo 113-8656, Japan

I. OBJECTIVE

Understanding the structural dependency of the physical properties of low dimensional systems is one of the challenges in the design of potential material. Single-walled carbon nanotubes (SWCNTs) are among the most promising candidates for materials of nano-electronic devices because of their high thermal conductivity. We investigate the thermal properties of single-walled carbon nanotubes (SWCNTs), focusing the chirality dependency.

II. COMPUTATIONAL DETAILS

For calculations of thermal properties, the nonequilibrium Green's function (NEGF) method based on lattice dynamics is chosen in this work. This method includes the quantum nature of phonons adequately and reliable at the low temperatures where the thermal conductances have quantized plateau.

Moreover, to evaluate the transmission coefficients and the thermal conductances from the perspective of the coupling properties of each normal mode, we project the dynamical matrix renormalized by the interactions with the semi-infinite leads onto the normal mode basis of the center region. This allows us to evaluate the effect of the coupling and the energy shift from the phonon-phonon interaction [1].

III. RESULTS AND DISCUSSION

We applied our methods to three SWCNTs with different chiralities (3, 3), (5, 0) and (4, 2) (Fig. 1), and found the thermal conductance varies significantly with the chirality, at both low and high temperatures (Fig. 2) [2,3]. Such differences are attributed to the dependence on the chirality of the frequency of optical modes and phonon-phonon interaction with the semi-infinite leads.

Our result indicates that high optical mode frequency and weak phonon coupling on the SWCNT (3, 3) are the origin of slow rise of the thermal conductance at low temperature. On the other hand, the suppression of the (5, 0) thermal conductance at high temperature results from the fact that the transmission coefficient is reduced greatly in the vicinity of 50-70 meV.

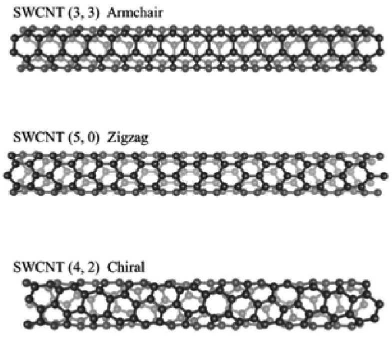

Fig. 1 Atomic structures of SWCNTs

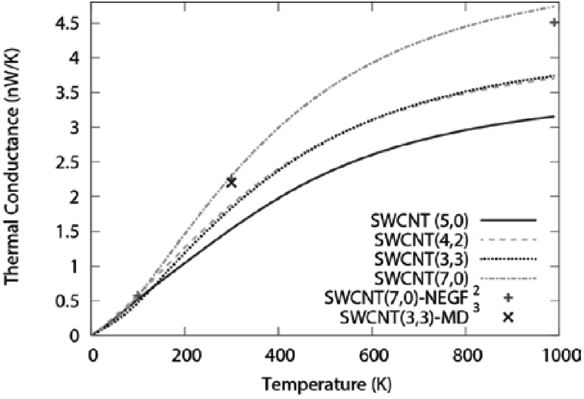

Fig. 2 Thermal conductances of SWCNTs

[1] T. Hata, *et al*. J. Chem. Phys. **139**, 044711 (2013)

[2] N. Mingo, *et al*. Phys. Rev. B 77, 033418 (2008)

[3] T. Yamamoto, *et al*. Appl. Phys. Express **2**, 095003 (2009)

Corresponding Author: K. Yamashita
Tel: +81-3−5841-7228, Fax: +81-3−3818-5012,
E-mail: yamasita@chemsys.t.u-tokyo.ac.jp

2P-14

Li-ion battery electrode property of anthraquinone molecules encapsulated in single-walled carbon nanotubes

○S. Kawasaki, T. Matsuura, K. Tashiro, H. Song

Nagoya Institute of Technology
Gokiso,Showa, Nagoya 466-8555, Japan

Li-ion battery (LIB) whose energy density is the highest among the secondary batteries has been widely used for cell phones, notebook computers and so on. Recently it has come to be used for electric vehicles including plug-in hybrid cars. However, it should be noted that LIB is facing today serious problems related to safety concerns and resource costs. The latter problem is caused by the use of what we call "rare metals" in the cathode active materials such as $LiCoO_2$ and $LiNiO_2$.

Organic electrode active materials are expected for the replacement of the expensive rare metal oxides. However, it is generally very difficult for LIB using the organic electrode active materials to show good cyclability because organic materials tend to dissolve in the electrolyte during charge-discharge cycles. If the dissolution can be restricted, we could obtain cheap and flexible LIBs. For that purpose we tried to use organic electrode active materials encapsulated in single-walled carbon nanotubes. Here, we show the electrode property of anthraquinone molecules encapsulated in SWCNTs.

The encapsulation of anthraquinone was carried out by exposing the SWCNT sample to anthraquinone gas in an evacuated glass tube. The open-end SWCNT sample and the organic molecule powder sample in the evacuated glass tube were heated at 200ºC for 10 hours. After the heat-treatment, the SWCNT sample was washed several times with ethanol in order to remove the physically adsorbed organic molecules on the SWCNT surface. The encapsulation was confirmed by XRD and N_2 adsorption experiments. For the electrochemical measurements, we prepared a test cell consisting of the SWCNT working electrode and Li metal counter electrodes. A mixture of ethylene-carbonate: diethyl-carbonate = 1:1 containing 1 M $LiClO_4$ was used as the electrolyte solution. Charge-discharge measurements were performed in an Ar drybox in a potential range of 1.5-3.2 V vs. Li/Li^+.

As shown in Fig. 1, the capacity drop by cycling is effectively restricted by the use of SWCNTs.

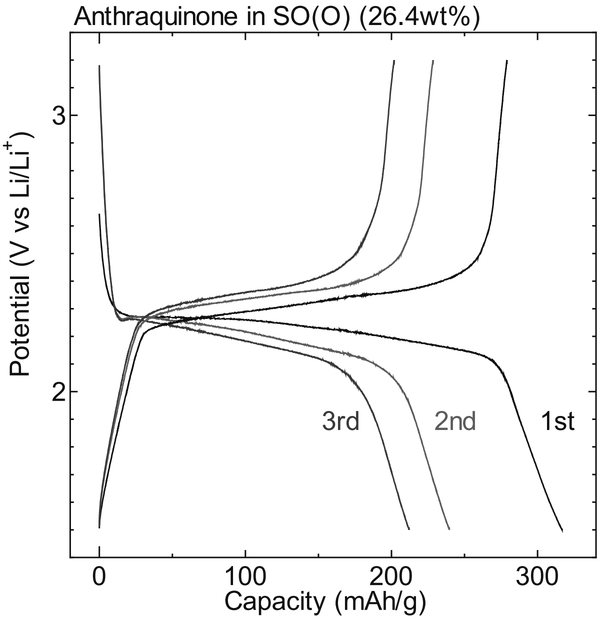

Fig.1 Charge-discharge curves of anthraquinone encapsulated in SWCNTs.

2P-15

Diameter dependence of RBM frequency of SWNTs in water vapor

○Naoki Homma[1], Shohei Chiashi[2], Yoshikazu Homma[1], and Takahiro Yamamoto[3]

[1]*Dept. of Physics, Tokyo University of Science, Shinjuku, Tokyo 162-8601, Japan*
[2]*Dept. of Mechanical Engineering, The University of Tokyo, Bunkyo, Tokyo 113-8656, Japan*
[3]*Dept. of Liberal Arts, Tokyo University of Science, Katsushika, Tokyo 125-8585, Japan*

Radial breathing mode (RBM) is one of the most important vibrational modes of single-walled carbon nanotubes (SWNTs), because the measurement of RBM frequency ω_{RBM} enables us to uniquely assign the chirality of an individual SWNT by combining it with the theory of resonant transitions.

In FNTG44, we reported the molecular dynamics (MD) simulation on (i) the distribution structure of water molecules around an SWNT and (ii) ω_{RBM} of SWNTs in water vapor [1]. The water molecules are condensed around an SWNT surface due to the van der Waals interactions between water molecules and an SWNT. The condensed water molecules formed the hydrogen-bond network parallel to the SWNT surface and eventually they construct a few-layer structure. In addition, we showed that the diameter dependence of ω_{RBM} of thin SWNTs with the tube diameter d_t~1nm is approximately represented as $\omega_{\mathrm{RBM}}=A/d_t+B$ referred to as the $1/d_t$ law, where A and B are estimated as A=227.9 cm^{-1}nm and B=7.5±2.5 cm^{-1} by MD simulation.

In this symposium, we report tube-diameter dependence of ω_{RBM} in a wider range of d_t up to 2 nm on SWNTs in water vapor. In the wider range, the tube-diameter dependence of ω_{RBM} no longer obeys the $1/d_t$ law, but it can be well fitted by $\omega_{\mathrm{RBM}}=\frac{A}{d_t}\sqrt{1+C_e d_t^2}$. In our simulation, the environment parameter C_e was estimated as C_e=0.057±0.005nm^{-2} for the wider range of d_t<2nm. Table 1 shows various values of C_e for carbon nanotubes in different environments [2].

Table 1. Environment parameter C_e [2].

C_e (nm^{-2})	Sample
0.05	HiPCO@SDS
0.059	Alcohol-assisted CVD
0.065	SWNT@SiO$_2$
0.067	Free-standing
0.057	SWNT in water vapor (This work)

[1] N. Homma, *et al.*, Abstract book of 44th FNG symposium, p.22.
[2] A. Jorio, R. Saito, G. Dresselhaus, M. S. Dresselhaus. "*Raman Spectroscopy in Graphene Related Systems*" Wiley-VCH (2011), pp.205, and references therein.

Corresponding Author: Takahiro Yamamoto,
Tel&FAX: +81-3-5876-1486,
E-mail: takahiro@rs.tus.ac.jp

2P-16

Optical Detection of DNA Hybridization and Denaturation on Single-Walled Carbon Nanotube Surface

○Yusuke Ito, Masahiro Ito, Daisuke Nii, Hiroki Kato, Kazuo Umemura, Yoshikazu Homma.

Department of Physics, Tokyo University of Science, Tokyo 162-8601, Japan

DNA is one of the functional dispersant of single-walled carbon nanotubes (SWNTs) [1,2]. The combination of DNA and SWNT (DNA-SWNT) is expected to have application for a biosensor. For example, Heller *et al.* revealed a conformation change of the DNA from B-type to Z-type adsorbed on the SWNT surface by photoluminescence (PL) spectroscopy [3].

Double stranded DNA (dsDNA) transforms single stranded DNA (ssDNA) when heated approximately 94°C in solution. Gradually decreasing the temperature causes transition from ssDNA to dsDNA. However, ssDNA does not transform dsDNA when rapidly cooled. These reactions are known as hybridization (ssDNA to dsDNA) and denaturation (dsDNA to ssDNA). In this study, we investigated hybridization and denaturation of DNA adsorbed on SWNT surface by PL spectroscopy.

First, we investigated hybridization on SWNT. The combination of oligo(dT)$_{30}$ and SWNT (T30-DNA-SWNT) is prepared, and then T30-DNA-SWNT and oligo(dA)$_{30}$ are mixed in solution and heated to cause the hybridization. Schematic illustration of experimental procedure and PL spectrum of each process are shown in Fig. 1 and Fig. 2. The redshift of PL spectra is attributed to the change of dielectric constant surrounding SWNT, i.e. hybridization occurred on SWNT surface. Then, we investigated denaturation of dsDNA on SWNT. The dsDNA derived from salmon testes was used. The combination of dsDNA and SWNT in solution was heated to cause denaturation and rapidly cooled to prevent hybridization. In this case, any change of PL spectrum was not observed. This result shows existence of strong interaction between DNA and SWNT surface. This interaction inhibits detachment of DNA from the SWNT surface.

In conclusion, we revealed that the transition of DNA between ssDNA and dsDNA on SWNT is non-reversible. Based on these results, we will discuss mechanism and structure of DNA adsorption on SWNT surface.

[1] N. Nakashima, *et al.*: Chem. Lett. **32** (2003) 456. [2] M. Zheng, *et al.*: Nature Mater. **2** (2003) 338.
[3] D. Heller, *et al.*: Science. **311** (2006) 508.

Corresponding Author: Yoshikazu Homma
Tel: +81-3-3260-4271 (ext. 2298), Fax: +81-3-5261-1023,
E-mail: homma@rs.tus.ac.jp

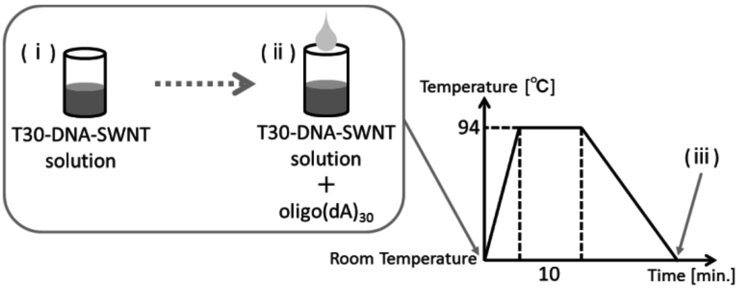

Fig. 1. schematic illustration of experiment.

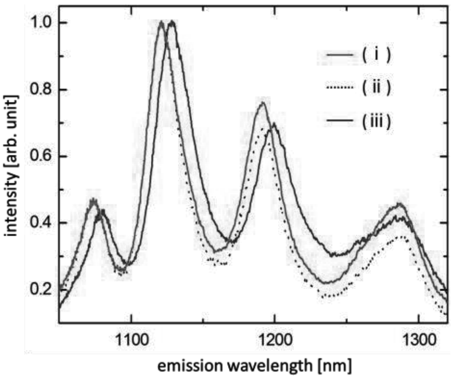

Fig. 2. PL spectrum of each process.

2P-17

Observation of a gate-induced photoluminescence peak in individual carbon nanotubes

○Y. Ueda, M. Yoshida, A. Ishii, T. Uda, Y. K. Kato

Institute of Engineering Innovation, The University of Tokyo, Tokyo 113-8656, Japan

We perform photoluminescence spectroscopy on individual air-suspended carbon nanotubes within field effect transistor structures [1,2]. The devices are fabricated by etching trenches on Si substrates with a 100-nm-thick oxide layer, and Ti/Pt are deposited as electrodes. Single-walled carbon nanotubes are grown by chemical vapor deposition, and we perform photoluminescence microscopy at room temperature under high vacuum. Photoluminescence imaging and excitation microscopy are used to identify individual nanotubes, and spectra are collected as a function of gate voltage. As the gate voltage is increased, we find that a new peak appears at an energy lower than the bright exciton emission, consistent with the expected behavior for trion luminescence.

Work supported by KAKENHI, KDDI Foundation, and the Photon Frontier Network Program of MEXT, Japan.

[1] S. Yasukochi, T. Murai, S. Moritsubo, T. Shimada, S. Chiashi, S. Maruyama, and Y. K. Kato, Phys. Rev. B **84**, 121409(R) (2011).
[2] Y. Kumamoto, M. Yoshida, A. Ishii, A. Yokoyama, T. Shimada, and Y. K. Kato, arXiv:1307.5159 (2013).

Corresponding Author: Y. K. Kato
Tel: +81-3-5841-7702, Fax: +81-3-5841-7772
E-mail: ykato@sogo.t.u-tokyo.ac.jp

Thermal Properties of SWNT Forest with Various Volume Fraction

○JinHyeok Cha[1], Kei Hasegawa[2], Shohei Chiashi[1], Asuka Miura[1], Jeonyoon Lee[3], Brian L Wardle[3], Suguru Noda[2], Junichiro Shiomi[1], Shigeo Maruyama[1]

[1] Department of Mechanical Engineering, The University of Tokyo, Tokyo 113-8656, Japan
[2] Department of Applied Chemistry, Waseda University, Tokyo 169-8555, Japan
[3] Department of Aeronautics and Astronautics, Massachusetts Institute of Technology, Cambridge, MA 02139, U.S.A.

Needs of a material for thermal management in reduced-sized electronic devices drive single-walled carbon nanotubes (SWNTs) to be one of the most expected materials due to the outstanding flexibility and thermal conductivity [1]. Therefore, many numerical and experimental studies to understand thermal property of SWNTs have been reported to be used in the applications.

In present study, we have investigate thermal diffusivity and thermal conductivity of mm-long SWNT forest [2] with various volume fraction using laser flash technique. Our primary aim here is to understand thermal properties of SWNT forest, and to identify the difference from that of an individual SWNT which potentially explains lower thermal property than expected when composing forest.

Figure 1 shows the *densification* process of SWNT forest that various volume fraction [3] of mm-long vertically aligned SWNT forest [2] were obtained by mechanical squeezing. We measured the thermal diffusivity of SWNT forests and calculate thermal conductivity using additional information such as density and specific heat of the forest. Through the estimation of numbers of SWNTs in the forest and the density of SWNTs, we derived the apparent thermal conductivity equivalent to a single SWNT. The result reveals that thermal diffusivity and thermal conductivity of SWNT forest increased with at high volume fraction of the SWNT forest, which is considered to give additional channels for thermal transport. In particular, apparent thermal conductivity equivalent to a single SWNT is found to be greater at higher volume fraction. We potentially considered that densification of the forest made an interstitial distance between SWNTs, hence the thermal boundary resistance between them is relieved.

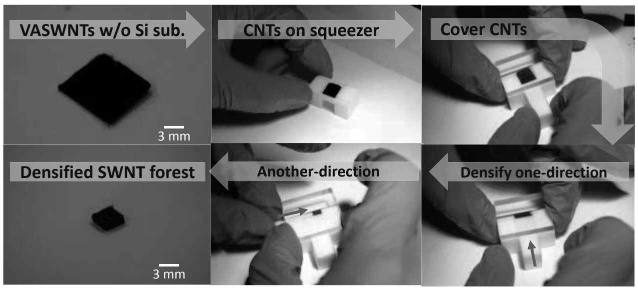

Fig. 1 Densification process of vertically aligned SWNT forest by mechanical squeezing.

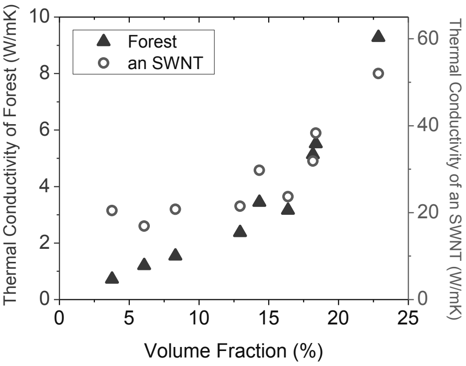

Fig. 2 Thermal conductivity of SWNT forest and the calculated thermal conductivity equivalent to a single SWNT.

[1] Y. Won *et al.*, PNAS, **110**, 20426 (2013).
[2] K. Hasegawa *et al.*, ACS Nano **5**, 975-84 (2011).
[3] B. L. Wardle *et al.*, Adv. Mater. **20**, 2707-2714 (2008).

Corresponding Author: S. Maruyama
Tel: +81-3-5841-6408, Fax: +81-3-5841-6408, E-mail: maruyama@photon.t.u-tokyo.ac.jp

2P-19

In-plane conductivity of dense carbon nanotube forest on semi-insulating silicon carbide

○Masafumi Inaba[1], Chih-Yu Lee[1], Kazuma Suzuki[1], Megumi Shibuya[1], Atsushi Hiraiwa[1],
Yoshiho Masuda[2], Wataru Norimatsu[2], Michiko Kusunoki[2], Hiroshi Kawarada[1]
[1] Graduate School of Advanced Science and Engineering, Waseda University, Tokyo 169-8555, Japan
[2] Eco Topia Science Institute, Nagoya University, Aichi 464-8603, Japan

Carbon nanotube forest formed by silicon carbide surface decomposition method (CNT on SiC) consists of nearly ideally close-packed CNTs with a surface density of ~10^{13} cm^{-2}[1]. Generally, CNT conducts in its on-axis direction, yet such highly dense CNT forest may cause high in-plane direction conductivity. Previously, we revealed the Schottky barrier height of CNT/SiC interface for CNT new application as heat dissipating ohmic electrode of SiC power devices[2]. Here we report on the in-plane conductivity evaluation of CNT forest on semi-insulating SiC.

On-axis C-face (000-1) of semi-insulating SiC substrates (< 10^{-8} S/cm) were annealed at 1500~1600 °C in vacuum (~10^{-3} Pa). The in-plane conductivity was measured by van der Pauw method. Fig.1 shows (a) the schematic image of sheet conductivity measurement and (b) its equivalent circuit. Four parts which may contribute to CNTs on SiC in-plane conductivity are considered, CNT caps, CNT bulk, CNT/SiC interface, and SiC bulk. To determine which part(s) is/are dominant in conduction, CNT lengths were varied by controlling decomposition time to change CNT bulk conductivity.

Fig.2 shows the relationship between CNT on SiC sheet conductivity and CNT length. The slope corresponds to the CNT bulk conduction. The in-plane CNT bulk conduction is calculated to be ~50 S/cm. The intercept of Fig.2 corresponds to the conduction of the others. The SiC bulk conduction is negligible, since the conductivity of initial SiC substrate is extremely as low as 10^{-7} S/cm. The conductivity of CNT/SiC interface was checked by removing CNTs and is also sufficiently small. Therefore, the intercept indicates the sheet conductivity of CNT caps as ~7×10^{-4} S/sq. If the thickness of CNT caps is presumed to be 5 nm, the room temperature conductivity is evaluated to be ~1.4×10^{3} S/cm.

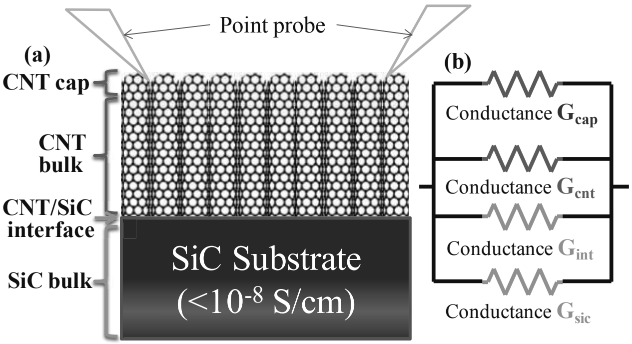

Fig. 1 (a) Schematic image of sheet conductivity measurement and (b) its equivalent circuit

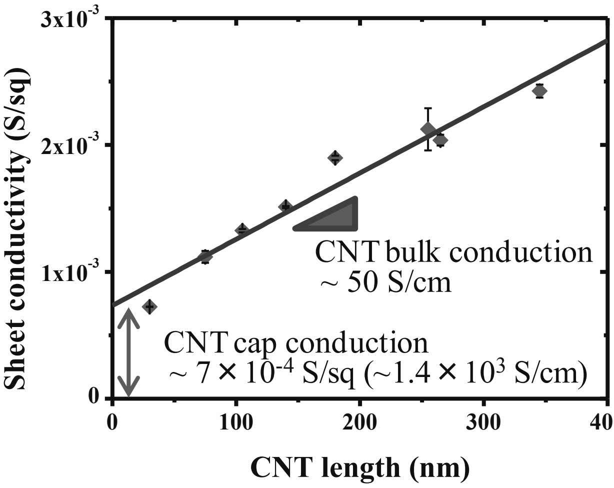

Fig. 2 Relationship between CNT sheet conductivity and CNT length

[1] M. Kusunoki et al., Appl. Phys. Lett.77, 531 (2000)
[2] M. Inaba, H. Kawarada et al., to be submitted

Corresponding Author: M. Inaba
Tel&Fax: +81-3-5286-3391
E-mail: inaba-ma@ruri.waseda.jp

Systematic Conversion of Single Walled Carbon Nanotubes into n-type Thermoelectric Materials by Molecular Dopants

○Yoshiyuki Nonoguchi[1], Kenji Ohashi[1], Tsuyoshi Kawai[1]

[1] *Graduate School of Materials Science,Nara Institute of Science and Technology,*
Ikoma, Nara 630-0192, Japan

Thermoelectrics is a challenging issue for modern and future energy conversion and recovery technology. Carbon nanotubes are promising active thermoelectic materials owing to their narrow band-gap energy and high charge carrier mobility, and they can be integrated into flexible thermoelectrics that can recover any waste heat. Pristine single walled carbon nanotubes (SWNTs) exhibit p-type majority charge carriers because of oxygen impurity, and few examples of their controlled n-type doping has been exploited.[1] We here report air-stable n-type SWNTs with a variety of weak electron donors in the range of HOMO level between ca. -4.4 eV and ca. -5.6 eV, in which partial uphill electron injection from the dopant to the conduction band of single walled carbon nanotubes is dominant.[2]

We demonstrated that a Seebeck coefficient of pristine SWNT buckyapers (+49 μV/K) can be drastically converted into negative values by doping SWNT buckypapers with a wide range of electron donors. All the dopants altered the Seebeck coefficients ranging from +90 μV/K to -80 μV/K. Among them, a lot of dopants listed in Fig.1 successfully switched the majority carriers of SWNT materials from p- to n-type (Fig.2). We assumed that this conversion was due to charge transfer doping from Lewis bases to SWNTs. This methodology was not limited for previously-known dopants such as PEI, and versatile electron donors are here available to dope SWNTs into n-type materials. To generalize these phenomenon, we obtained the trend of highest occupied molecular orbital (HOMO) of dopants for n-type doping of SWNT materials. Dopants with HOMO energy above roughly -5.6 eV against the vacuum level successfully altered the sense of majority carriers from holes in pristine SWNTs to electrons.

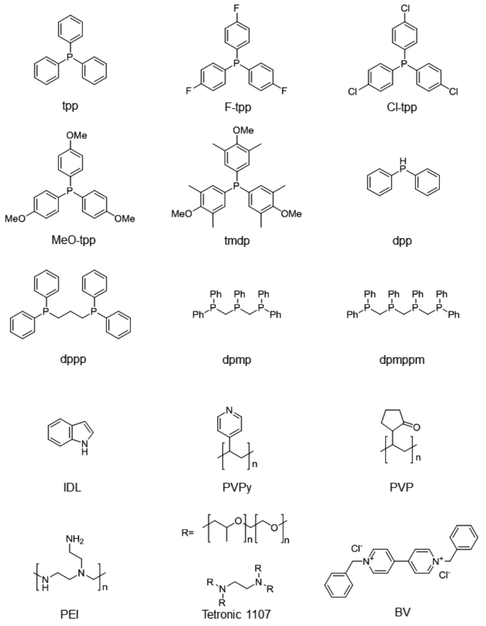

Fig.1 Dopants for n-type SWNTs

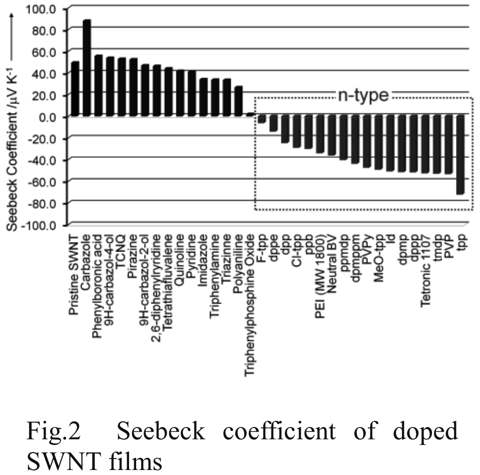

Fig.2 Seebeck coefficient of doped SWNT films

[1] H. Dai *et al.* J. Am. Chem. Soc. **123**, 11512 (2001).
[2] Y. Nonoguchi *et al.* Sci. Rep. **3**, 3344 (2013).

Corresponding Author: Y. Nonoguchi
Tel: +81-743-72-6028, Fax: +81-743-72-6179,
E-mail: nonoguchi@ms.naist.jp

2P-21

Evaluation of the contact resistivity and Schottky barrier height at carbon nanotubes/silicon carbide interface

○Kazuma Suzuki[1], Masafumi Inaba[1], Megumi Shibuya[1], Lee Chih Yu[1],
Miho Myodo[1], Atsushi Hiraiwa[1], Yoshiho Masuda[2],
Wataru Norimatsu[2], Michiko Kusunoki[2], Hiroshi Kawarada [1]
[1] *School of Science and Engineering, Waseda University, Tokyo 169-8555, Japan*
[2] *Eco topia Science Institute, Nagoya University, Aichi 464-8603, Japan*

1. CNT on SiC

Carbon nanotube forest synthesized with silicon carbide surface decomposition method (CNT on SiC)[1][2] exhibits the most densely packed CNT forest (~10^{13} cm^{-2}) and is suitable for electrodes with high current density durability. CNTs can be important material for SiC, which is promising materials of power semiconductors, in cooperation with its high thermal conductivity. It is necessary for application as electrodes to evaluate the contact resistivity.

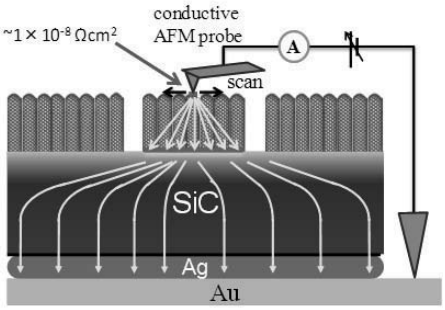

Fig.1 Schematic image of current paths in CNT/SiC system

2. The contact resistivity at CNT/SiC interface

As shown in Fig.1, lateral conduction also coexists in the CNT on SiC because of its high tube density. To restrict the contact area of CNT forest on SiC, electrically isolated areas was formed with focused ion beam schematically shown in Fig.1. The electric properties of isolated areas with different size were measured by conductive AFM to obtain size dependence of total resistance composed of top and bottom contact resistances and CNT intrinsic resistance. Fig. 2 shows the relationship between reciprocal conduction area and total resistance of the measurement system (Fig.1) at each donor density. Since the contact resistance of CNT/SiC interface is inversely proportional to the conduction area, the slope of the graph corresponds to the contact resistivity. In addition, contact resistivity decreases as donor density of SiC substrate increases.

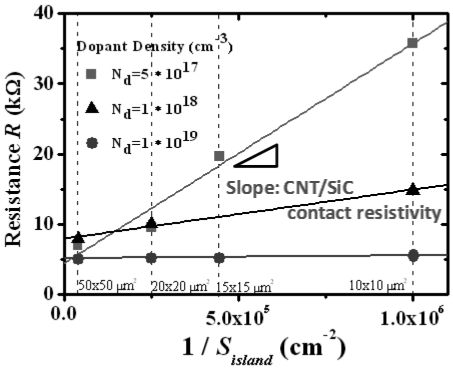

Fig.2 Relationship between reciprocal conduction area and total resistance

3. Schottky barrier height at CNT/SiC interface

Fig. 3 shows the results of plotting the contact resistivity of the each donor density(5×10^{17} cm^{-3}, 1×10^{18} cm^{-3}, 1×10^{19} cm^{-3}) SiC. Each curve is the theoretical relationship between donor density and contact resistivity of the metal and 4H-SiC when Schottky barrier height varies from 0.3 to 1.5 eV. Contact resistivity of donor density of 5×10^{17} cm^{-3}, 1×10^{18} cm^{-3} corresponds to Schottky barrier height of 0.5 ~ 0.6 eV. At donor density of 1×10^{19} cm^{-3}, however, lower contact resitivity than 2×10^{-4} Ωcm^2 is difficult to measure in the present technique, the estimated Schottky barrier height deduced from the contact resistivity was 0.8 eV. The real contact resistivity at donor density of 1×10^{19} cm^{-3} might be lower than this value.

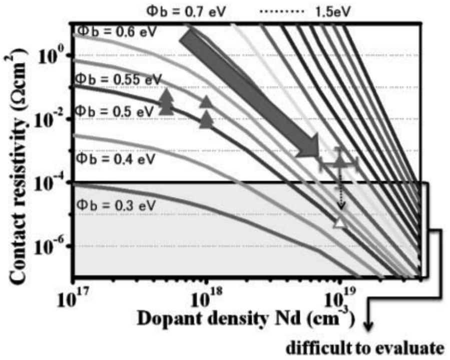

Fig.3 Relationship of the dopant density and the contact resistivity

[1] M. Kusunoki *et al., Appl. Phys. Lett.*77, 531 (2000)

[2] M. Kusunoki *et al., Appl. Phys. Lett.* 87, 103105 (2005)

Corresponding Author: K. Suzuki

Tel: 03-5286-3391, Fax: 03-5286-3391, E-mail: gloria-274@asagi.waseda.jp

2P-22

Infra-Red Light Sensor using High-Purity Semiconducting Single-Wall Carbon Nanotube Networks

○Hikaru Kudo[1], Seiya Kaji[1], Hideki Kawai[1], Taishi Takenobu[2], Kazuhiro Yanagi[1]

1. Department of Physics, Tokyo Metropolitan University, Tokyo 192-0397, Japan
2. Waseda University, Tokyo 169-8555, Japan

There is a lot of demand for un-cooled infrared (IR) light image sensors for security and health industries. Micro-bolometers are the most popular high-performance un-cooled far-IR detectors and are widely used for night-vision cameras, and thermography applications. However, they are considerably expensive due to their fabrication costs. A diaphragm structures with vacuum thermal isolation is used in the cell, which requires complicated semiconductor MEMS processes and vacuum packaging, and this makes it very difficult to reduce costs. Therefore, there is a large demand for IR detection sensors which are fabricated through other const effective processes. Single-wall carbon nanotubes (SWCNTs) have IR optical absorption. Thus the uses of SWCNTs for IR detection have been proposed. The value of temperature coefficient ratio (TCR) is a very important parameter to evaluate the performance of bolometer. In the mixture of metallic and semiconducting SWCNTs, previous study has revealed almost zero TCR value at room temperature,[1,2] suggesting that SWCNTs in their mixture state cannot be used as un-cooled IR detectors. However, in high-purity semiconducting SWCNTs networks, a large temperature dependence is expected.[2] Here we clarified that the high-purity single-chiral SWCNTs has - 2.6% K^{-1} TCR value (Figure 1), which is the larger than typical VOx bolometer, and was the largest TCR value in SWCNTs. We clarified the TCR value can be controlled through carrier injection using ion gel. We demonstrated IR detection using semiconducting SWCNTs fabricated on plastic substrate. Figure 2 shows 28% of resistance change under IR radiation from black body source at temperature of 150 ℃ (in this situation, peak emission wavelength is 7μm). Our sensors displayed approximately 1 % of resistance changes to the IR radiation from our body, suggesting semiconducting SWCNTs are useful for un-cooled IR sensors.

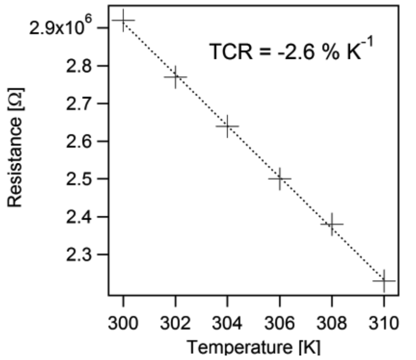

Figure 1 Temperature dependence of resistance of semiconducting SWCNTs networks.

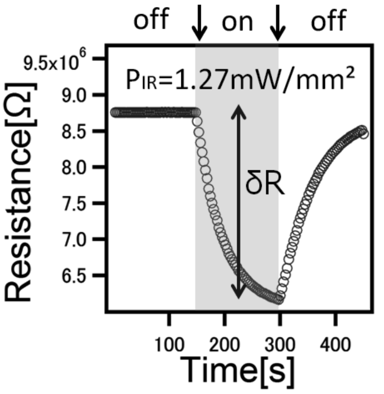

Figure 2 IR responses of semiconducting SWCNTs networks

Acknowledgment:
KY thanks for discussion with Dr. Narita (NEC) and Komatsubara (Nippon Avionics Co.). This work is partially supported by JST A-step program.

Reference:
[1]Itkis et al., Science 312, 413 (2006)
[2]Yanagi et al., ACS Nano 4, 4027 (2010)

Corresponding Author: Kazuhiro Yanagi
Tel: +81-42-677-2494
E-mail: yanagi-kazuhiro@tmu.ac.jp

2P-23

Operation Speed Improvement of Carbon Nanotube Integrated Circuits on Plastic Substrate

○Toshitada Sanzen[1], Antti Kaskela[2], Patrik Laiho[2], Albert G. Nasibulin[2],
Shigeru Kishimoto[1], Esko I. Kauppinen[2], and Yutaka Ohno[1]

[1] *Department of Quantum Engineering, Nagoya University, Nagoya 464-8603, Japan*
[2] *Department of Applied Physics, Aalto University, Espoo, Finland*

Carbon nanotube thin-film transistors (CNT TFTs) are expected to realize high-performance flexible devices. In the previous works, we realized CNT TFTs and integrated circuits (ICs) on a flexible plastic substrate [1,2]. However, the speed of the previous ICs, which was evaluated using a ring oscillator, was lower than that expected from the carrier mobility. It was considered that the parasitic overlap capacitances between the gate and source/drain electrodes degraded the switching speed of the inverters. In this work, we report the improvement of operation speed by reducing the overlap capacitances. The operation speed has been enhanced by reducing the overlap capacitances by a factor of 7.4. We have also measured the gate capacitances of the devices to discuss the effect of parasitic capacitances on the operation speed.

We fabricated three types of 21-stage ring oscillators consisting of bottom-gate TFTs (a) with 20-μm overlaps (same as the previous work), (b) with 2-μm overlaps, and (c) without overlap on PEN substrates as shown in Fig. 1. Conventional photolithography-based processes were used for the fabrication. A 40-nm-thick Al_2O_3 insulator was deposited by an atomic layer deposition technique. A CNT thin film was grown by floating-catalyst chemical vapor deposition, collected on a membrane filter, and transferred on the substrate as our previous works. Chemical doping with F_4TCNQ was carried out to adjust the logic threshold voltage and reduce parasitic resistances of the non-overlap regions in device (c).

Figure 2(a)-(c) show the photograph of the fabricated devices, the micrograph, and the output wave form of the ring oscillator with device (c). The oscillation frequencies (*f*) were 1.4, 3.6, and 10 kHz for devices (a), (b), and (c), respectively. Corresponding delay times ($\tau = 1/2Nf$, $N = 21$ stages) were 17, 6.6, and 2.3 μs, respectively. The switching speed was enhanced by a factor of 7.4 by reducing the parasitic overlap capacitances. The results will be discussed on the basis of the results of capacitance-voltage measurements in the TFTs.

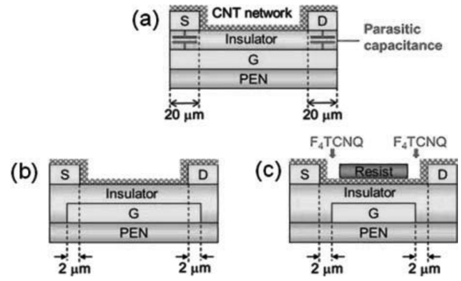

Fig.1 Schematic device structures (a) with 20-μm overlaps, (b) with 2-μm overlaps, and (c) without overlap.

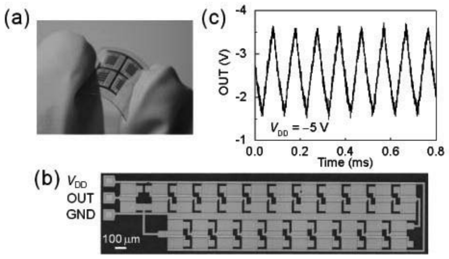

Fig.2 (a) Photograph of devices on PEN substrate. (b), (c) Optical micrograph and output wave form of a ring oscillator with device (c).

[1] D.-M. Sun *et.al.*, Nature Nanotech. **6**, 156 (2011).

Corresponding Author: Y. Ohno
Tel: +81-52-789-5387, Fax: +81-52-789-5387,
E-mail: yohno@nuee.nagoya-u.ac.jp

2P-24

Photovoltaic features of p-n homo-junction with position selective Cs encapsulated single-walled carbon nanotubes thin films

○Yoshihiro Abiko, Toshiaki Kato, Toshiki Akama, Rikizo Hatakeyama, Toshiro Kaneko

Department of Electronic Engineering, Tohoku University, Sendai, 980-8579, Japan

Single-walled carbon nanotube (SWNT) is one of the most attractive material for future high performance solar cells due to their flexible filament-like structure, high carrier mobility, tunable bandgap energy by controlling the diameter. In addition, multiple exciton generation (MEG) in SWNT has demonstrated experimentally and theoretically [1, 2]. For the fabrication of p-n homo-junction based SWNTs thin film, it is necessary to fabricate both p- and n-type SWNTs thin film. It is well known that pristine SWNTs shows p-type transport property. Recently, we have demonstrated very stable n-type SWNTs-thin film transistors (TFTs) by Cs encapsulation into SWNTs by a plasma ion irradiation method [3].

Here we report the fabrication of p-n homo-junction based on position selective Cs encapsulated SWNTs thin film. The half channel area of a pristine SWNTs-TFT fabricated by a conventional photolithography technique is covered with polymer to prevent Cs plasma irradiation and position selective Cs encapsulation is realized. Cs encapsulation is carried out by the plasma ion irradiation method. Finally, Cs irradiated SWNTs thin film is rinsed by purified water to remove the Cs atoms adsorbing on the outside of SWNTs. In this study, the electrical transport properties are investigated without or with light illumination using a solar simulator.

It is found that the clear rectifying drain-source current (I_{DS}) vs. drain-source voltage (V_{DS}) characteristics can be observed after the position selective Cs encapsulation into SWNTs thin film. Furthermore, a short-circuit current and an open-circuit voltage can be detected under light illumination using a solar simulator, as shown in Fig. 1. This indicates that p-n homo-junction based on SWNTs thin film can be applicable to solar cells. Our finding is important as a crucial step for the fabrication of high performance SWNTs solar cells.

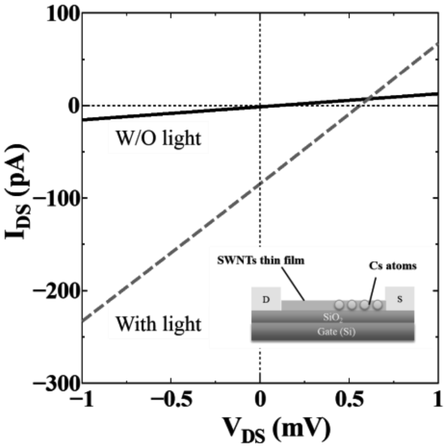

Fig.1 I_{DS}-V_{DS} characteristics of position selective Cs encapsulated SWNTs thin film without and with light illumination.

[1] S. Konabe and S. Okada, Phys. Rev. Lett. **108** (2012) 227401.
[2] N. M. Gabor *et al.*, Science **325** (2009) 1367.
[3] R. Hatakeyama *et al.*, J. Phys. D: Appl. Phys. **44** (2011) 174004.

Corresponding Author: Y. Abiko
Tel: +81-22-795-7046, Fax: +81-22-263-9225,
E-mail: abiko12@ecei.tohoku.ac.jp

2P-25

Molecular recognition on surfaces of metallic and semiconducting single-walled carbon nanotubes

○Wenxin Huang[1], Tsuyohiko Fujigaya[1,2], and Naotoshi Nakashima[1,2,3]

[1]Department of Applied Chemistry, Graduate School of Engineering, Kyushu University,
744 Motooka, Fukuoka 819-0395, Japan
[2]World Premier International (WPI), International Institute for Carbon-Neutral Energy
Research, Kyushu University 744 Motooka, Nishi-ku, Fukuoka 819-0395, Japan
[3]Japan Science and Technology Agency, CREST, 5 Sanbancho, Chiyoda-ku, Tokyo,
102-0075, Japan

Introduction

Single-walled carbon nanotubes (SWNTs) are produced as a mixture of metallic SWNTs (m-SWNTs) and semiconducting SWNTs (s-SWNTs). Since both of them are promising materials especially for electronics in next generation, their separation (MS separation) is necessary. Up to date, many MS separation methods such as gel chromatography and selective oxidation have been reported. However, these methods involve problems that are either time consuming or causing damages to SWNTs. It is expected the process become very simple if only dispersion process realizes the MS separation. For that purpose, the first requisite is to find out the molecule that can recognize the m- or s-SWNTs. In this study, we utilized the newly developed affinity chromatography technique [1] to search for a type of molecule that can make MS separation possible by solubilization, in which m- or s-SWNT were employed as a stationary phase. As analytes, polyaromatic hydrocarbons were used to obtain the preliminary data.

Experiment

As a stationary phase, m-SWNTs are coated on silica gel. The silica gel coated with m-SWNTs was fabricated by a simple mixing of m-SWNTs (0.733 mg NanoIntegris) dispersed in *N*-methyl-2-pyrrolidinone (NMP) at a concentration of 0.01 mg mL^{-1} (73.3 mL) and amino-functionalized silica gel (NH$_2$-silica) with a 3.5 μm diameter (733 mg). Green blue power was collected after filtration. The m-SWNT-silica-gel slurry prepared from m-SWNT-silica (323 mg) was packed in a 2.1 mm × 125 mm empty column (CE-402, Waters) using a slurry packing apparatus (Model 124A, Chemco Scientific) to fabricate a packed column (m-column). The column having s-SWNTs as a stationary phase (s-column) was made in similar fashion using s-SWNTs instead of m-SWNTs.

Results and discussion

Fig. 1 shows the chromatographs for polyaromatic hydrocarbons obtained from m- (Fig. 1A) and s-columns (Fig. 1B) using tetrahydrofuran (THF) as an eluent. Four samples showed different retention times depending on the magnitude of the interaction. Interestingly, we found the elution orders of the four samples in m- and s-columns are identical (Fig.1). The result suggests that these molecules showed no clear recognition for m- or s-SWNTs, which agreed well with the general understanding for these molecules showing no MS separation ability.

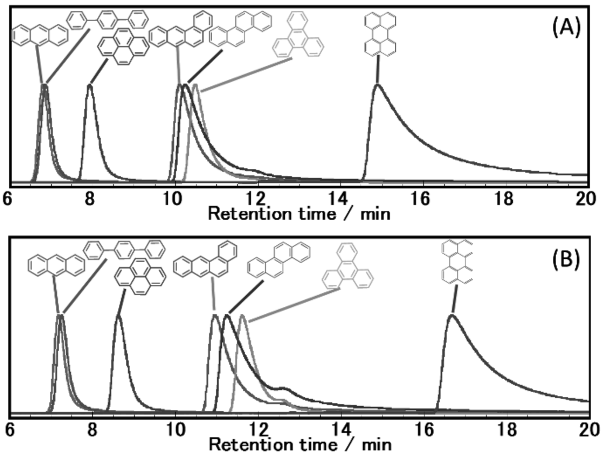

Fig. 1 Chromatograms of PAHs using (A) m- and (B) s-SWNT-silica as stationary phases at flow rates of 0.1 mL min^{-1}; eluent: THF.

[1] J. Yoo et al., *Nanoscale* **2011**, *3*, 2517.

Corresponding Author: Naotoshi Nakashima
E-mail: nakashima-tcm@mail.cstm.kyushu-u.ac.jp
Tel & Fax: +81-92-802-2842

High Photovoltaic Performance of MoO_3-doped Single-walled Carbon Nanotube/Si Solar Cells

Feijiu Wang[1], Daichi Kozawa[1], Yuhei Miyauchi[1,2],
Shinichiro Mouri[1], Yutaka Ohno[3], and Kazunari Matsuda[1]

[1]Institute of Advanced Energy, Kyoto University, Uji, Kyoto 611-0011, Japan
[2]Japan Science and Technology Agency, PRESTO, 4-1-8 Honcho Kawaguchi, Saitama 332-0012, Japan
[3]Department of Quantum Engineering, Nagoya University, Furocho, Chikusa-ku, Nagoya 464-8603, Japan

Single-walled carbon nanotubes (SWNT) have attracted a great deal of attention for photovoltaic applications due to their excellent physical and electronic properties. Recently, the heterostructures of SWNT and Si has been extensively studied for photovoltaic cells [1]. It was found that the key to realize the highly efficient solar cell is the use of high quality and doped SWNTs network film [2-4]. In this study, we have fabricated the SWNTs/Si solar cells using the high quality and MoO_3 doped SWNTs network film and evaluated the photovoltaic properties of the cells.

The high quality SWNTs network films fabricated by the floating catalytic CVD method were used for the cells. The dotted line and solid line of Figure 1 show the current density voltage (J-V) characteristics of pristine SWNT/Si and MoO_3-doped SWNT/Si heterojunction solar cells, respectively. From the J-V curve of pristine SWNT/Si solar cell, the conversion efficiency (η), current density (J_{sc}), fill factor (FF) and open circuit voltage (V_{oc}) are 11.1%, 27.9 mA/cm^2, 69% and 0.57 V, respectively. In contrast, the photovoltaic properties are much enhanced in MoO_3-doped SWNT/Si solar cell. The high values of J_{sc} (=38.4 mA/cm^2), V_{oc} (=0.59 V), and FF (=0.59 V) cause very high value of photovoltaic conversion efficiency of 17.6 %. The obtained value of 17.6 % is the highest one in the carbon nanotube based solar cells. The physical mechanism of drastic enhancement of photovoltaic properties in MoO_3-doped SWNT/Si will be discussed.

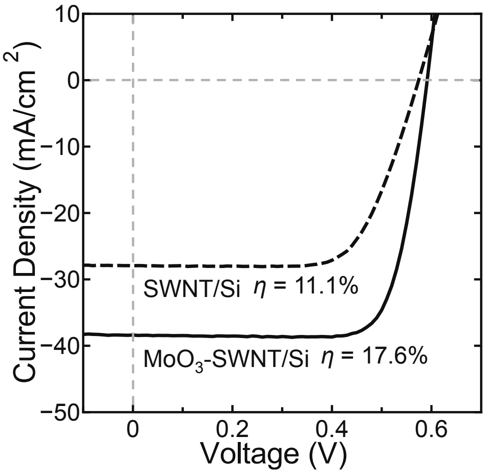

Fig. 1: J–V curves of SWNTs/Si solar cell before and after coating MoO_3

[1] D. D. Tune *et al.*, Adv. Energy Mater. **2**, 1043 (2012).
[2] D. Kozawa *et al.*, Appl. Phys. Express **5,** 042304 (2012).
[3] F. Wang *et al.*, Appl. Phys. Express **6,** 102301 (2013).
[4] F. Wang *et al.*, submitted for publication.

Corresponding Author: Feijiu Wang
Tel: +81-774-38-3465, Fax: +81-774-38-3460
E-mail: wang.feijiu.75w@st.kyoto-u.ac.jp

2P-27

Solubility control of SWCNT by using photofunctional dispersants

○Yoko Matsuzawa, Yuko Takada, Hideyuki Kihara, Masaru Yoshida

Nanosystem Research Institute,
National Institute of Advanced Industrial Science and Technology,
Tsukuba 305-8656, Japan

Solubilization of the single-walled carbon nanotubes (SWCNTs) is important for fundamental studies and industrial applications of SWCNTs. Especially, precise tuning of the dispersibility of the SWCNTs is necessary in advanced applications including switching devices, sensors, and drug delivery systems.

Recently, we have reported dispersibility tuning of SWCNTs by applying photochemical reaction of a water-soluble stilbene **1** as a dispersant [1]. Due to the rigid and nearly coplanar structure of **1**, it can interact with the SWCNTs via π–π interactions, resulting in a stable dispersion of the SWCNTs in water without bundling. In contrast, the photocyclized product **2** having a highly twisted and bent structure is unfavorable for the π–π interactions with the SWCNTs. Since such drastic change in the molecular structure of the dispersant affects the affinity between the dispersant and the SWCNT surfaces, on-off switching of the dispersibility control of the SWCNTs has been successfully demonstrated by in-situ photoreaction of the **1**/SWCNTs dispersion. Further, it has been found that the photofunctional dispersant **1** is useful for purification of raw-SWCNT by combination procedure with high-speed centrifugation [2].

In this study, we have investigated photochemical reaction of the dispersant **1** in **1**/SWCNTs hybrid films. The films were prepared by casting of the **1**/SWCNT dispersion on fused silica. Upon UV-light irradiation, photoreaction of **1** progressed even in the hybrid films, and we found that the solubility of the SWCNT films was altered by the photoirradiation. The **1**/SWCNTs hybrid films without photoirradiation easily dissolved into water. In contrast, the UV-exposed films remained on the glass substrate, while only photoreacted dispersant **2** was rinsed off from the SWCNT surface using water.

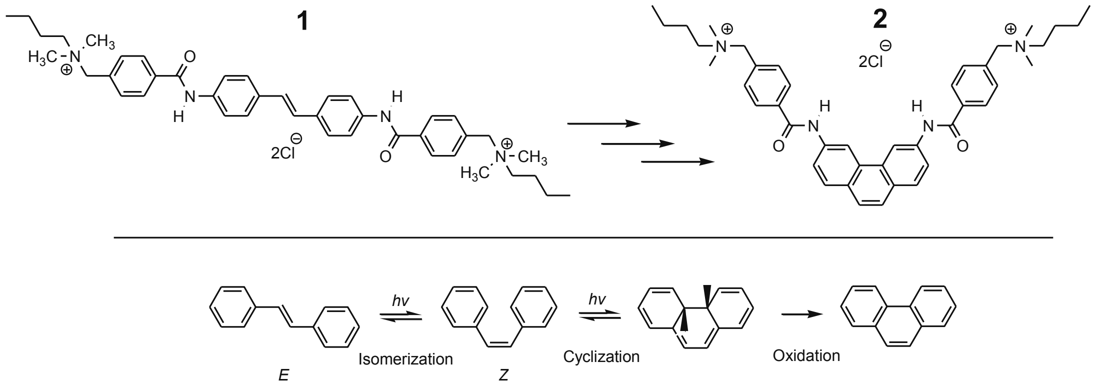

Fig.1 Structures of the photoresponsive dispersant (up). Photoreaction of stilbene (bottom).

[1] Y. Matsuzawa et al., *Adv. Mater.*, **23**, 3922 (2011)
[2] Y. Matsuzawa et al., *J. Phys. Chem. C* submitted.

Corresponding Author: Yoko Matsuzawa
Tel: +81-29-861-2958, Fax: +81-29-861-4673
E-mail: yoko-matsuzawa@aist.go.jp

2P-28

Growth of CNTs using the dip coat method as the catalyst support

Keisuke Fujii, Yoshinori Ando, Masato Ohkohchi

Dept. of Materials Science and Engineering, Meijo University, Nagoya, Japan

Dip coat method [1] is well known as a simple method for supporting the catalyst. This method only includes pulling the substrate that is placed in the catalyst solution. So, no special equipment is needed in the process, and it is possible to reduce the waste of the catalyst.

In this experiment, Fe / Co was used as the catalyst, and camphor [2] was used as the carbon source. The catalyst was supported on the substrate by dip coat method (drawing speed 3cm/min). Carbon nanotubes (CNTs) were grown up using chemical vapor deposition (CVD). Camphor was sublimed at 200℃ in an electric furnace, and the temperature of the substrate was set to 750℃.

In the experiments by the dip coat method, CNTs which are arranged on the entire surface of the substrate have been synthesized (Fig.1). The G/D ratio obtained from Raman measurements was 1.26. CNTs did not sometimes grow up even if the experiments had been done under the same conditions. Formation of the liquid film on the substrate is to be influenced by slight fluctuations of the vibration, temperature, and humidity. Dip coat method has so poor reproducibility, further improvement is needed.

[1] F. Iskandar, M. Abdullah, H. Yoden, K. Okuyama, J. Sol-Gel Sci. Tech.: 29, 41-47 (2004)

[2]M. Kumar, Y. Ando, J. Physics: Conference Series 61, 643–646 (2007)

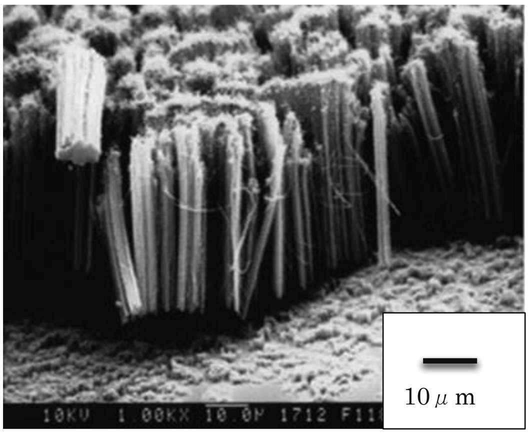

Fig 1 SEM image of the oriented carbon nanotubes

Corresponding Author: K. Fujii
E-mail: 133434028@ccalumni.meijo-u.ac.jp

2P-29

Chiral selective solubilization of single-walled carbon nanotubes using flavin and isoalloxazine derivatives

Masashi Fukuzawa[1], Fumiyuki Toshimitsu[1], Yuichi Kato[1], Naotoshi Nakashima[1, 2, 3]

[1] Department of Applied Chemistry, Kyushu University, Fukuoka 819-0395, Japan
[2] WPI-I^{2}CNER, Kyushu University, Fukuoka 819-0395, Japan
[3] JST-CREST, Chiyoda-ku, Tokyo 102-0075, Japan

SWNTs are classified into metallic or semiconducting tubes according to their chirality. However, the coexistence of tubes with various chiralities in the raw SWNT material interferes fundamental researches and development of devices. Despite several technical methods have been developed for the separation, the development of a new powerful separation method is still a great challenge.

Here we report a selective recognition and extraction of semiconducting SWNTs (s-SWNTs) using flavin and isoalloxazine derivatives. We previously revealed that **dmC12** (Fig. 1), the compound that has been reported to disperse SWNTs [1], can selectively solubilize s-SWNTs [2]. In order to explore the origin of such chiral selectivity, we here synthesized several flavin and isoalloxazine derivatives (Fig. 1), and examined their s-SWNTs solubilization ability. Fig. 2 shows the absorption spectra of the HiPco-SWNTs dissolved in toluene using such derivatives, in which we observe that **dmC12**, **dmC18** and **7mC12** are able to solubilize s-SWNTs selectively. On the other hand, **C12** and ***N*mdmC12** did not solubilize any SWNTs. These results strongly suggested that the imidyl hydrogen and methyl group(s) on the aromatic rings are essential for selective solubilization/extraction of the s-SWNTs. A possible mechanism for such selective dissolution/separation will be presented at the meeting.

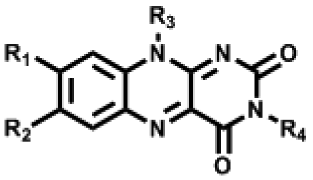

R_1, R_2, R_3, R_4 =
a) Me, Me, $C_{12}H_{25}$, H (**dmC12**)
b) H, H, $C_{12}H_{25}$, H (**C12**)
c) Me, Me, $C_{18}H_{37}$, H (**dmC18**)
d) H, Me, $C_{12}H_{25}$, H (**7mC12**)
e) Me, Me, $C_{12}H_{25}$, Me (***N*mdmC12**)

Fig. 1 Chemical structures of flavin and isoalloxazine derivatives.

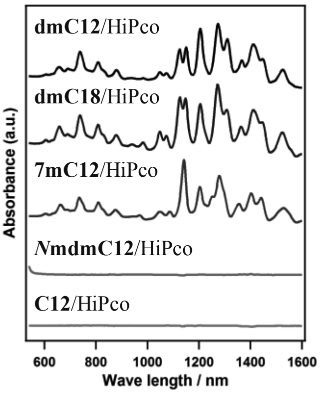

Fig. 2 Vis-near IR absorption spectra of SWNTs dissolved by flavin and isoalloxazine deraivatives.

[1] F. Papadimitrakopoulos *et al*., Science. **323**, 1319 (2009).

[2] Y. Kato *et al*., the 44th FNTG symposium, **2P-25** (2013).

Corresponding Author: N. Nakashima
Tel: +81-92-802-2840, Fax: +81-92-802-2840;
E-mail: nakashima-tcm@mail.cstm.kyushu-u.ac.jp

2P-30

Self-assembly of Highly Aligned Metallic/Semiconducting SWCNTs using Crystal Templates

○H. Kawai[1], K. Hasegawa[1], Y. Naitou[2], Y. Takagi[3], Y. Wada[3], T. Takenobu[3], K. Yanagi[1]

[1] Tokyo Metropolitan Univ., [2]AIST, [3]Waseda Univ.

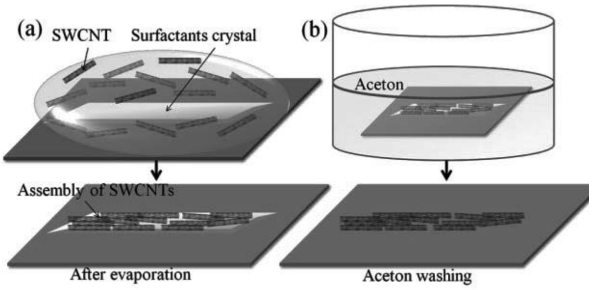

Fig. 1 (a) Assembly process of aligned SWCNT
(b) Removal of the surfactans crystal

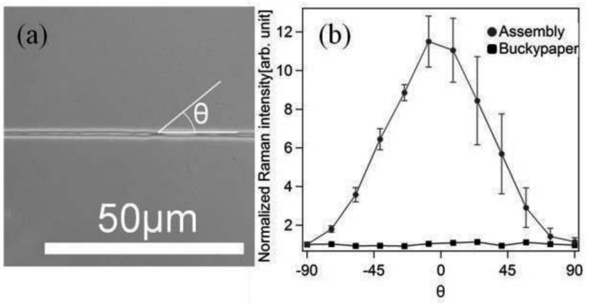

Fig. 2 (a) Metallurgical microscope image of assembly of SWCNTs after washing.(b) Polarized micro-Raman measurement.

Single Wall Carbon Nanotubes (SWCNTs) have various electronic structures depending on their chirality. Recent progress of separation technique enables us to extract metallic, semiconducting and single chiral state of SWCNTs from the mixed state sample. It is expected that fabrication of devices exploiting their intrinsic excellent electrical transport property. However, typical devices fabricated as random networks in which the SWCNTs are randomly oriented and connected. Random interfaces work as scattering centers, thereby localizing conducting carriers thus, the device performance of such networks is inferior to that expected in a single rope of SWCNTs. Therefore, controlling the alignment of SWCNTs is an essential step to achieving superior macroscopic device performance. We previously reported string-like assembly of aligned SWCNT in a single-chiral state, which induced by self assemble process in temperature controlled solution of SWCNTs, and the assembly exhibit good field effect performance[1].

In this study, we introduce another unique technique to control alignment of SWCNTs, which utilize self-assemble processes of SWCNTs upon the crystal surfaces of surfactants. Fig. 1 illustrates our method for assembling SWCNTs on the surfaces of needle-like crystals of deoxycholate (DOC). SWCNTs dispersed in solution with surfactants were dropped on the needle, and SWCNTs were self-assembled on the crystal surfaces during the gradual evaporation of the solutions. Then the surfactant crystals were removed by soaking the substrate in aceton for 20h, as a result aligned SWCNT assemblies were left on the substrates. Micro -Raman measurement and scanning electron microscopy (SEM) measurements clearly show that the SWCNTs were highly aligned parallel to needle axis in the assembly. Angle distribution evaluated from SEM image indicates about 65% of SWCNTs are aligned parallel to needle axis within ±5°and about 85% are aligned within ±10°, which is better alignment than that we previously reported and on the same level with aligned SWCNTs horizontally grown on specific substrate.

[1]Kawai et al., Appl. Phys. Express **6** (2013) 065103.

Corresponding Author: K. Yanagi
Tel: +81-42-677-2494, Fax: +81-42-677-2483, E-mail: yanagi-kazuhiro@tmu.ac.jp

2P-31

Chirality selective desorption of SWCNTs using mixed surfactant gel column chromatography

○Yohei Yomogida, Mayumi Tsuzuki, Atsushi Hirano, Shunjiro Fujii, Takeshi Tanaka,
Hiromichi Kataura

Nanosystem Research Institute, National Institute of Advanced Industrial Science and Technology, Ibaraki 305-8562, Japan

Single-wall carbon nanotubes (SWCNTs) show great promises of future applications in electronics and optoelectronics. Because the band structure of SWCNT is highly depending on its structure, chirality separation from the structure-mixed raw soot is very important for both fundamental research and further application of SWCNTs. Recently, we have developed a multicolumn gel chromatography method for single chirality separation that is based on the chirality-dependent interaction between sodium dodecyl sulfate (SDS)-wrapped SWCNTs and the gel.[1] In this method, however, we had to prepare a huge amount of SWCNT solution to get a tiny amount of single-chirality SWCNTs. To accelerate SWCNT research, we still need more effective separation method for the single-chiralities.

To improve the selectivity, in this work, we tried small amount of sodium deoxycholate (DOC) as a co-surfactant that is well known to be effective for diameter selective desorption in agarose gel chromatography. [2] Figure 1 shows typical optical absorption spectra of SWCNTs obtained by stepwise elution changing DOC concentration from 0.04 to 0.12 wt%, in addition to 1 wt% SDS aqueous solution. These spectra clearly show chirality selective desorption. The second upper spectrum shows prominent (6,5) peak while the upper and lower most spectra never show (6,5) peak. This strong selectivity is very useful for large scale chirality sorting despite less selectivity in large diameter part (1100 - 1300 nm). We can combine another diameter sorting process to get single chirality SWCNTs.

This work was supported by KAKENHI No. 25220602.

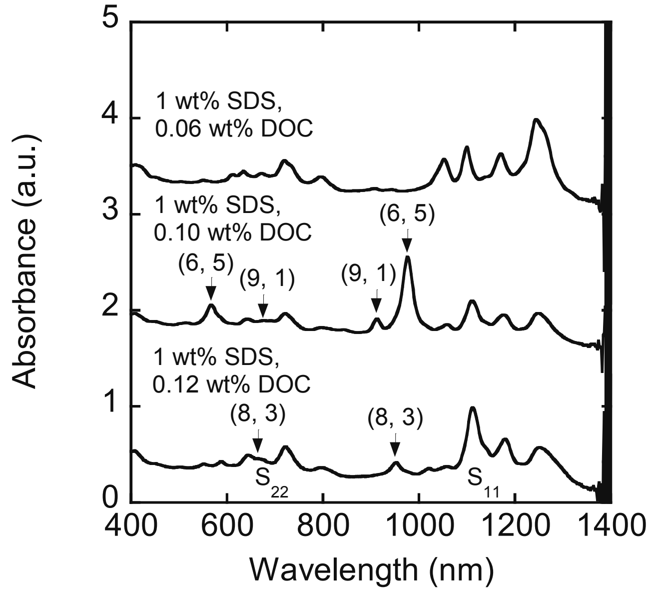

Fig. 1 Optical absorption spectra of the SWCNTs eluted from gel columns by the stepwise elution with various DOC concentrations in the presence of 1 wt% SDS

[1] H. Liu *et al.* Nat. Commun. **2**, 309 (2011).
[2] H. Liu *et al.* J. Phys. Chem. C **247**, 9270 (2010).

Corresponding Author: Hiromichi Kataura,
Tel: +81-29-861-2551, Fax: +81-29-861-2786
E-mail: h-kataura@aist.go.jp

2P-32

FT-ICR Study of Chemical Reaction of Cobalt Clusters with Acetonitrile

○Kazuki Ogasawara [1], Yuta Tobari [2], Shohei Chiashi [1], Toshiki Sugai [2], Shigeo Maruyama [1]

[1] *Department of Mechanical Engineering, The University of Tokyo, Tokyo 113-8656, Japan*
[2] *Department of Chemistry, Toho University, Chiba 274-8510, Japan*

The chemical vapor deposition (CVD) method is currently regarded as one of the most expected techniques for the industrial or commercial production of single walled carbon nanotubes (SWNTs). In CVD method, SWNTs grow from carbon source molecules such as CH_4 or alcohol on nanoscale catalytic metal particles, therefore understanding surface chemical reaction is critically important. Recently, Thurakitseree et al.[1] reported that changing the carbon feedstock from pure ethanol to a few % mixture of acetonitrile (CH_3CN) in ethanol during CVD drastically reduces the average diameter of the SWNTs from approximately 2 to 1 nm, and the feedstock-dependent change is reversible and repeatable. The role of nitrogen in reducing the diameter is suggested to be the surface impeding of SWNT formation, which causes the growth mode change from 'Octopus' to 'VLS (vapor-liquid-solid)', but the detailed mechanism of the surface impeding is still not clear.

In this work, chemical reaction of small cobalt cluster cation with acetonitrile was observed by Fourier Transform Ion Cyclotron Resonance (FT-ICR) mass spectrometer [2,3]. Cobalt clusters composed of 7-17 atoms were directly trapped within the FT-ICR cell. Subsequently, acetonitrile was introduced into the ICR cell via pulsed leak valve. Figure 1 shows the typical mass spectrum of the reaction products from Co_{11}^{+} clusters. Dotted line indicates simple chemisorption of acetonitrile, and we can also observe dehydrogenated chemisorption such as $+(CCN)_2$ or $+(CCN)_2(HCCN)$. Figure 2 shows the Co cluster size dependence of the reaction products. Co_{n}^{+} clusters smaller than Co_{10}^{+} show no dehydrogenate reaction and the chemisorption rate monotonically increases with cluster size. On the other hand, Co_{n}^{+} clusters larger than Co_{10}^{+} shows almost the same dehydrogenate rate and hence the chemisorption rate. The efficient full dehydrogenate process leading to $+(CCN)_2$ will be discussed.

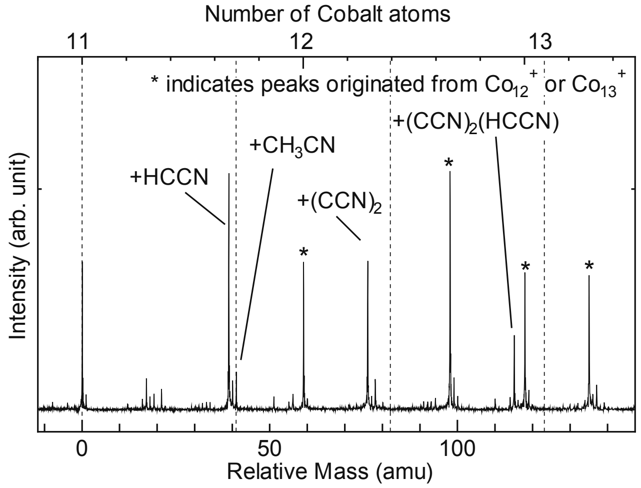

Fig. 1 Chemisorption on Co clusters of 11 atoms.

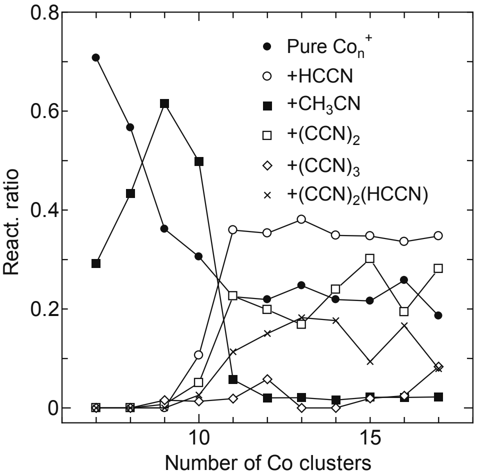

Fig.2 Cluster size dependence of the reaction products.

[1] T. Thurakitseree *et al.*, ACS Nano, 7 (2013), 2205./[2] S. Maruyama *et al.*, Rev. Sci. Instrum., 61 (1990), 3686./[3] S. Inoue, S. Maruyama, Jpn. J. Appl. Phys., 47 (2008) 1931.

Corresponding Author: S. Maruyama, Tel: +81-3-5841-6421, Fax: +81-3-5841-6983,
E-mail: maruyama@photon.t.u-tokyo.ac.jp

Synthesis and TEM-based Structural Characterization of C_{60}-Flattened CNT Nanopeapods

○Qing Wang[1], Ryo Kitaura[1*], Yuta Yamamoto[2], Shigeo Arai[2], Hisanori Shinohara[1*]

[1]Department of Chemistry & Institute for Advanced Research, Nagoya University, Nagoya 464-8602, Japan
[2]High Voltage Electron Microscope Laboratory, Ecotopia Science Institute, Nagoya University, Nagoya 464-8602, Japan

The fully flattened carbon nanotube (FNT), a graphene nanoribbon analogue, provides a unique low-dimensional nanospace with an extremely wide dumbbell-like cross section that is significantly different from that of carbon nanotubes [1]. This new type of nanospace provides the ability to align atoms or molecules in not only one-dimensional but also two-dimensional way, creating a brand new class of FNTs-based hybrid nanostructures such as FNT nanopeapods. In this study, we report synthesis of FNTs-based C_{60} nanopeapods and their structure characterization using transmission electron microscopy (TEM).

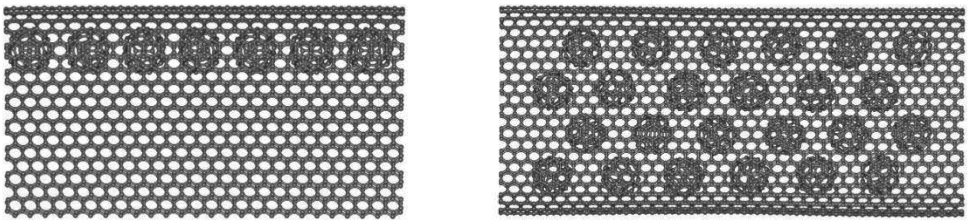

Fig.1 Structure models of one-dimensional (left) and two-dimensional (right) packing of C_{60} molecules inside of FNTs

TEM images and electron energy loss spectroscopy (EELS) spectra of FNT show a clear-cut evidence of the hollow space at the edges. The encapsulation of C_{60} molecules into the edge space provides new hybrid material (C_{60}@FNT) with one-dimensional C_{60} alignment at the edge. In addition, we also synthesized C_{60}@FNT that possesses two-dimensional packing of C_{60}. These structures were characterized by TEM observation and image simulation based on the multi-slice method. While the observed one-dimensional C_{60} chains along the edges of FNTs are almost identical to that already reported for C_{60}-peapods, the two-dimensional packing of C_{60} molecules in FNT has been revealed for the first time in the present study. Further investigation on structure and properties of C_{60}@FNTs is currently underway and will be presented in future.

[1] D. H. Choi *et al*. Scientific Reports **3** 1617 (2013).

Corresponding Author: Ryo Kitaura and Hisanori Shinohara
TEL: (+81) 52-789-2482, FAX: (+81) 52-789-6442,
E-mails: r.kitaura@nagoya-u.jp and noris@ nagoya-u.jp

2P-34

Modulating the Electronic Properties of Multimeric Thiophene Oligomers by Utilizing Carbon Nanotube Confinement

○Takashi Yumura[1], Hiroki Yamashita [1]

[1] *Department of Chemistry and Materials Technology, Kyoto Institute of Technology,*
Matsugasaki, Sakyo-ku, Kyoto, 606-8585, Japan

We investigated the arrangement of methyl-terminated terthiophenes inside a nanotube by using density functional theory (DFT) including dispersion corrections. The DFT calculations aim at obtaining atomistic information of thiophene oligomers inside nanotubes, which were reported experimentally [1]. After conducting DFT calculations, a variety of arrangements of the inner terthiophene chains was found, depending on host-tube diameters and the number of chains [2,3]. Because of the various inner thiophene arrangements, the terthiophene chains interact differently. The interactions are stronger in a smaller nanotube compared to within a larger nanotube, indicating importance of nanotube confinements to the interchain couplings. The interchain interactions split the orbitals of the multimeric terthiophene chains, which are built from single-chain frontier orbitals, to broaden their energy levels. Therefore, nanotube confinements are key factors in determining the energy levels of the frontier orbitals of contained multimeric terthiophenes. As a result, their electronic transitions are affected by the encapsulation into a restricted nanotube space. According to time-dependent DFT calculations, a specific electronic transition occurs from a HOMO-built orbital to a LUMO-built orbital. The broadening of the orbital energies by the aggregation of terthiophene chains in a nanotube leads to a widened range of excitation energies (E_x) in their electronic transitions relative to the single-chain. With respect to the strongest transition of multimeric terthiophenes, the excitation energy is enhanced by confinement to a nanotube. The E_x enhancement within a smaller nanotube is more significant than within a larger nanotube due to the stronger interchain interactions in a smaller nanotube. Therefore, it is proposed from the DFT calculations that nanotube confinements can modulate electronic and absorption properties of multimeric terthiophene chains by changing the interchain interactions.

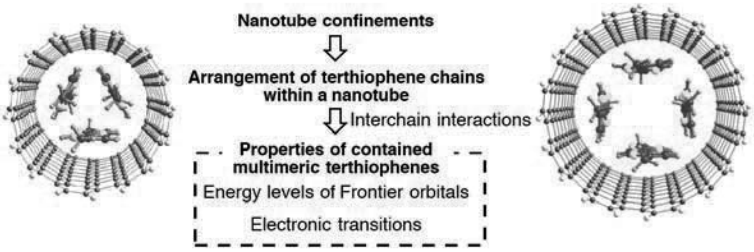

Fig. 1 Modulating the electronic properties of thiophene multimers by utilizing carbon nanotube confinement.

[1] (a) M. A. Loi *et al.*, Adv. Mater. **22**, 1635 (2010). (b) L. Alvarez *et al.*, J. Phys. Chem. C **115**, 11898 (2011).
[2] H. Yamashita and T. Yumura, J. Phys. Chem. C **116**, 9681 (2012).
[3] T. Yumura and H. Yamashita, submitted for publication.

Corresponding Author: Takashi Yumura
Tel: +81-75-724-7571, Fax: +81-75-724-7571
E-mail: yumura@chem.kit.ac.jp

2P-35

Energetics and Electronic Structures of Carbon Nanotubes Encapsulating Polycyclic Aromatic Hydrocarbon Molecules

○Shota Kigure and Susumu Okada

Graduate School of Pure and Applied Sciences, University of Tsukuba,
1-1-1 Tennodai, Tsukuba, Ibaraki 305-8571, Japan

Single-walled carbon nanotubes (SWCNTs) can accommodate molecules or atoms within their interior space. Tubular space inside CNT with the nanoscale diameter leads to unusual ordered arrangements of encapsulated molecules and atoms. Indeed, C_{60}s form one-dimensional van-deer Waals chain inside the CNTs with interesting electronic properties those are not expected from the simple sum of the constituent units [1]. Recently, polycyclic aromatic hydrocarbon (PAH) molecule, coronene, is also encapsulated into the SWCNT in which the coronene molecules are coaxially aligned along the tube axis [2]. In this work, we aim to elucidate the energetics and electronic properties of PAH molecules (coronene, sumanene, and coranulene) encapsulated into SWCNT based on density functional theory with local density approximation.

Figure 1 shows an energy gain upon the encapsulation of PAH molecules inside the SWCNTs as a function of the tube diameter. We found these molecules can be encapsulated within SWCNTs with appropriate diameter: Optimum tubes for encapsulation is (17,0)CNT for sumanene and coranulene, while the tube is (19,0)CNT for coronene, depending on the diameter of these PAH molecules. The calculated encapsulating energies for the optimum structures are about 1 eV per molecules irrespective to the molecule species. The large encapsulation energy is ascribed to the substantial interaction between CH bond of PAH molecules and π states of CNT. Indeed, the energy depends on the number of CH bonds of PAH molecules. We also check the stable mutual angle associated to the tube axis and find that the encapsulated PAH molecules are not tilted for the case of coranulene and sumanen in contrast to the coronene inside the CNT.

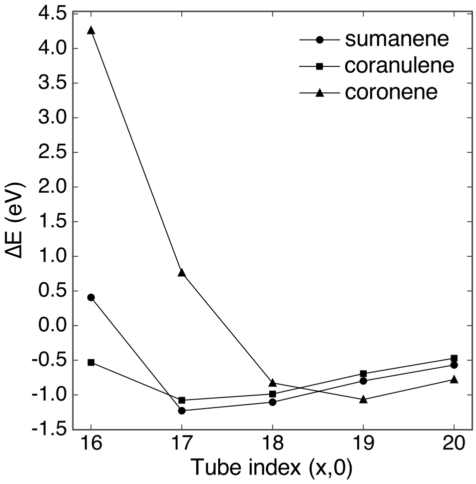

Figure.1 Encapsulation energy (ΔE) of PAH within (n,0) CNT(n = 16~20).

[1] S. Okada *et al*. Phys. Rev. Lett. **86**, 3835 (2001)
[2] T. Okazaki *et al*. Angew. Chem. Int. Ed. **50**, 4853 (2011)

Corresponding Author: S. Kigure
Tel: +81-29-853-8233, Fax: +81-29-853-5924,
E-mail: skigure@comas.frsc.tsukuba.ac.jp

Functionalization of Carbon Nanohorns for Targeted Photo-Thermal Cancer Therapy

○Minfang Zhang[1]*, Mei Yang[1], Wuxio Ding[1], Sumio Iijima [1, 2], Masako Yudasaka[1]*

[1] *National Institute of Advanced Industrial Science and technology 5-2, Tsukuba*
[2] *Department of Material Science and Engineering, Meijo University, Nagoya*

Carbon nanomaterials such as nanotubes and nanohorns have been extensively investigated for applications in drug delivery system and photo-thermal cancer therapy. Recently, the functionalization of single-wall carbon nanotubes (SWNTs) by coating with 90 kDa amphiphilic poly(maleic anhydride-alt-1-octadecene)-methoxy poly(ethylene glycol) (C_{18}-PMH-mPEG) have shown a longer blood circulation and higher tumor accumulation due to EPR effect in vivo [1]. The modification of SWNTs with a targeting agent, epidermal growth factor (EGF) exhibited high active targeting efficiency to squamous cancer cells that overexpress EGFR [2]. Herein, we multiply functionalized carbon nanohorns (CNHs) with C_{18}-PMH-mPEG and EGF to realize a targeted photo thermal cancer therapy.

CNHs labelled by Gd_2O_3 particles [3] were non-covalently coated with C_{18}-PMH-mPEG and DSPE-PEG-EGF (named as p-CNH-EGF) as reported previously [1-2]. Gd_2O_3@CNHs coated only with C_{18}-PMH-mPEG (p-CNHs) was also used for control. The obtained samples were dispersed in phosphate buffered saline and intravenously injected into mice that had subcutaneously transplanted tumor. After samples injection for 24 h, the tumor on the flank of each mouse was irradiated with 808-nm laser for about 5 min every day for 7 days. The laser irradiation markedly suppressed the tumor growth of mice with p-CNHs-EGF injected. These results indicated that the EGF modification had efficiency on targeted photo-thermal cancer therapy. However, the quantity of p-CNHs-EGF and p-CNHs in tumors were similar, about 2% of injection dose. This means that the quantity was not the reason for the high anti-tumor effect of p-CNHs-EGF. We infer that the accumulation site of p-CNHs-EGF in tumor might be different from that of p-CNHs, thereby caused the different effects of photo-thermal therapy.

[1] J.T. Robinson, et al. *J. Am. Chem. Soc.* 134, 10664 (2012).

[2] A. A. Bhirde, et al. *ACS Nano* 3, 307 (2009).

[3] J. Miyawaki et al. *ACS Nano* 3, 1399 (2009)

Corresponding Author: M. Zhang and M. Yudasaka.
TEL/Fax: +81-29-861- 6290
E-mail: m-zhang@aist.go.jp (M. Zhang), m-yudasaka@aist.go.jp (M. Yudasaka).

2P-37

Quick charge/discharge properties of Li-ion battery using carbon-coated composites of graphites, vapor grown carbon fibers, and carbon nanohorns

○Ryota Yuge, Noriyuki Tamura, Takashi Manako, Kaichiro Nakano, and Kentaro Nakahara

Smart Energy Research Laboratories, NEC Corporation, Tsukuba 305-8501, Japan

The lithium-ion battery (LIB) is the most remarkable rechargeable battery for portable electronics, electric vehicles (EVs), and plug-in hybrid electric vehicles (HEVs) [1]. Recently, their applications in EVs and HEVs have been demanded especially, leading to increases in battery size and capacity [2-3]. The demand for quicker charging of EVs has been increased drastically for very long charge time. Therefore, the LIB operating at high-rates needs to be developed to realize the above industrial applications [4-5]. In this study, we tried to prepare novel composites of graphite, vapor grown carbon fibers (VGCFs), and carbon nanohorns (CNHs) covered by carbon films (C-graphite/VGCF/CNH) for quick charge-discharge of LIB. We also investigated the relationship between the structure of C-graphite/VGCF/CNH and electrochemical rate-properties.

Graphite (1g), VGCFs (20 mg), and CNHs (20 mg) were dispersed in ethanol (40 ml) and stirred at room temperature for about 10 min. The mixture was filtered, and black powder was obtained on the filter paper (graphite/VGCF/CNH). The mixture of graphite, vapor grown carbon fibers (VGCFs), and carbon nanohorns (CNHs) was heat-treated in Ar atmosphere and carbon-coated by using a chemical vapor deposition (CVD) method.

Scanning electron microscopy observation showed that the graphite and/or VGCF in C-graphite/VGCF/CNH had a smoother and rounder surface structure than those of graphite/VGCF/CNH. Thermogravimetric analysis also indicated that carbon film formed by the CVD method combusted at 550ºC and the quantity of carbon film was about 4 wt%. The C-rate properties of half-cell for C-graphite/VGCF/CNH were superior to those for the mixture of graphite, VGCF, and CNHs (C-graphite/VGCF/CNH (discharge) : 3C/0.1C, 85%, graphite/VGCF/CNH (discharge) : 3C/0.1C, 50%), accelerating a promising application for quick charge-discharge of LIB. The details are shown in the presentation.

[1] M. Endo *et al*. Carbon **38**, 183 (2000).

[2] Y. E. Hyung *et al*. J. Power Sources **81-82**, 842 (1999).

[3] T. Horiba *et al*. J. Power Sources **97-98** 719 (2001).

[4] H. Fujimoto, J. Power Source **195**, 5019 (2010).

[5] R. Krishnan et al. Nano Lett. **11**, 377 (2011).

Corresponding Author: R. Yuge

Tel: +81-29-850-1566, Fax: +81-29-856-6137

E-mail: r-yuge@bk.jp.nec.com

Synthesis and TEM structural characterizations of AgI nanowires formed inside carbon nanospace

○Shihono Naruse[1], Ryo Kitaura[1,*], Suguru Noda[2], Hisanori Shinohara[1,*]

[1] *Department of Chemistry & Institute for Advanced Research,*
Nagoya University, Nagoya 464-8602, Japan
[2] *Department of Applied Chemistry & School of Advanced Science and Engineering,*
Waseda University, Tokyo 169-8555, Japan

α-phase of silver iodide (α-AgI) is one of the most promising candidates for solid-state electrolytes for various electrochemical devices due to its superionic conductivity. α-AgI cannot exist, however, below 420 K, thereby limiting their applications. Recently, it was reported that AgI nanoparticles with a diameter of 10 nm can retain α-phase even at 313 K, where size and morphology of AgI presumably play an important role in this α-AgI stabilization [1]. Low-dimensional AgI nanostructures thus can act as a superionic conductor at room temperature that is potentially important in the field of electrochemical devices.

To synthesize low-dimensional AgI nanostructures, we have used one-dimensional (1D) nanospace of carbon nanotubes (CNTs). CNTs have unique 1D nanospace ranging in diameter from 0.4 to 50 nm, which can stabilize otherwise unstable phases of nanomaterials. Here, we present a high yield synthesis and TEM structural characterization of AgI nanowires that are formed in nanospace of CNTs with various diameters.

We have synthesized AgI nanowire encapsulated in CNTs (hereafter designated as AgI@CNTs) by the sublimation method reported previously [2]. Figures 1 (a) and (b) show low-magnification high resolution transmission electron microscope (HR-TEM) images of CNTs and AgI@MWCNTs [3]. In contrast to empty CNTs, the image of AgI@MWCNTs clearly shows dark areas overlapping with the CNTs. An estimated filling ratio of AgI is as high as ca. 80 %. Figure (c) shows high magnification HR-TEM images of AgI nanowire synthesized wthin MWCNT with an inner diameter of 9.0 nm. The figure clearly shows dark spots aligned in the MWCNT in a perfectly regulated fashion.

In the presentation, we will discuss the details on the synthesis of various AgI nanowires and characterizations of their structure using HR-TEM and HAADF observations.

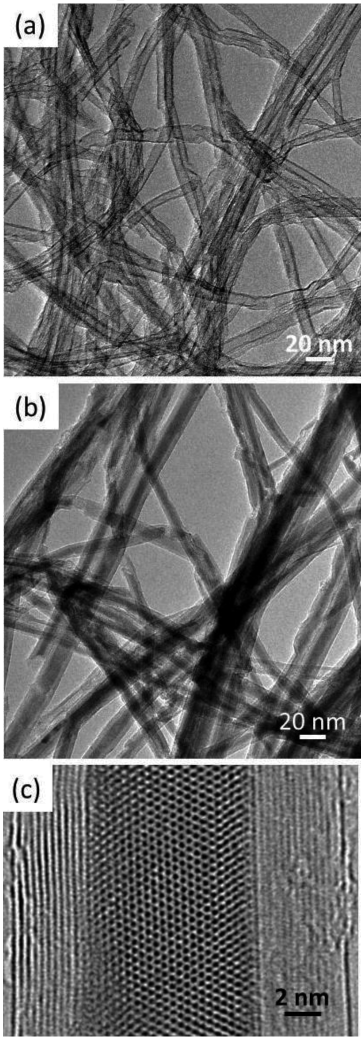

Fig. 1 HR-TEM images of
(a) empty MWCNTs
(b) (c) AgI@MWCNTs

[1] R. Makiura, et al., ***Nature.Mater.*** 8, 476 (2009).
[2] R. Kitaura, et al., ***Angew.Chem.Int.Ed.*** 48, 8298 (2009).
[3] R. Kitaura, et al., ***Nano Res.*** 1, 152 (2008).

Corresponding Author: Hisanori Shinohara
TEL: (+81)52-789-2482, **FAX:** (+81)52-747-6442, **E-mail:** r.kitaura@nagoya-u.jp, noris@ nagoya-u.ac.jp

2P-39

High-yielding synthesis of graphene by supuercritical fluid

○Nobuto Oka [1], Takaaki Tomai [1], Itaru Honma [1]

[1] *Institute of Multidisciplinary Research for Advanced Materials, Tohoku University,*
Sendai 980-8577, Japan

Graphene is a monolayer of sp^2-bonded carbon atoms arranged in a dense honeycomb crystal structure, which exhibits remarkable electronic, optical, thermal, and mechanical properties. These absorbing properties make graphene the most promising candidate for various applications in many fields, such as electronic and optical devices, and energy storage in batteries. A mass production technique of high-quality graphene is indispensable for many of these applications. Recently, we have reported a novel supercritical fluid (SCF) method for the exfoliation of graphite to obtain high quality and high yield graphene sheets [1-3]. SCF has unique characteristics such as a low interfacial tension, excellent surface wetting, and high diffusion coefficients. Solvent molecules in SCF state diffuse between the graphene layers in bulk graphite and expand the interlayer distance. Consequently, graphene sheets are exfoliated from graphite crystals.

In this study, the flow-through reactor for graphite flakes dispersed in ethanol has been developed for the purpose of mass production and much higher yield, as shown in fig. 1 [4]. A repeat of specific temperature profile, temperature rise and rapid quench, leads to better synthetic efficiency of graphene, amounting to improvement by one digit or more as compared to before. On the other, the conventional chemical exfoliation method, known as modified Hummers' method, is widely used as the mass production technique. It involves an oxidation process, resulting in the formation of defective graphene sheets. The supercritical fluid exfoliation method, developed in this study, denotes the direct conversion from graphite crystals into much less defective graphene since this method does not require the oxidation process. This mass production technique of high-quality graphene should contribute to the desirable growth of various industrial applications.

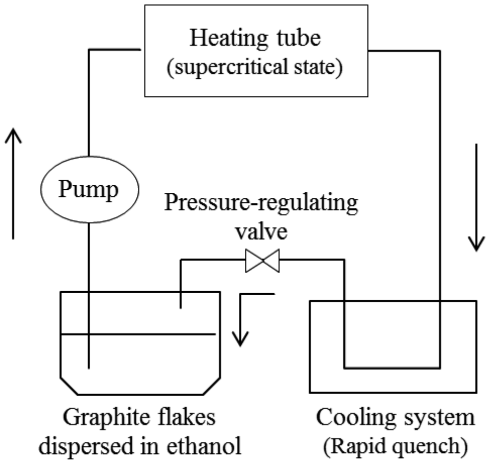

Fig.1 Schematic diagram of flow-through supercritical fluid method

[1] D. Rangappa, K. Sone, M. Wang, U. K. Gautam, D. Golberg, H. Itoh, M. Ichihara and I. Honma, *Chem. Eur. J.* **16**, 6488- 6494 (2010).

[2] J.-H. Jang, D. Rangappa, Y.-U. Kwon and I. Honma, *J. Mater. Chem.* **21**, 3462-3466 (2011).

[3] T. Tomai, Y. Kawaguchi and I. Honma, *Appl. Phys. Lett.* **100**, 233110 - 233110-4 (2012).

[4] http://www.sdk.co.jp/assets/files/news/2013/sdkrelease20130110.pdf

Corresponding Author: N. Oka, I. Honma
Tel: +81-22-217-5816, Fax: +81-22-217-5828,
E-mail: n.oka@tagen.tohoku.ac.jp,
i.honma@tagen.tohoku.ac.jp

2P-40

Fabrication of wide terraces on SiC (0001) for pit-free graphene growth in Ar atmosphere

○Wang Chenxing, Hitoshi Nakahara, Koji Asaka, and Yahachi Saito

Department of Quantum Engineering, Nagoya University, Furo-cho, Nagoya 464-8603, Japan

According to the current experimental studies on thermal decomposition of SiC (0001) surfaces, morphology of SiC substrate surfaces after graphene growth depends on annealing conditions, such as inert gases and their pressure, and annealing temperature and duration. In the present study, the SiC substrates are annealed at various temperatures and at various pressures of argon (Ar) atmosphere, and the processes of annealing the SiC substrates are investigated by *in situ* scanning tunneling microscope (STM) to reveal the most appropriate annealing condition for forming wide terraces and pit-free graphene on SiC.

Before the forming of graphene layers on SiC surfaces, the terraces keep growing due to the step bunching. Figure 1 shows the temporal evolutions of the average width of terraces at different temperatures at 0.1 atm of Ar atmosphere, and the largest increasing rate of terrace widths was observed at 1400℃. In the annealing processes at 0.5 and 1atm of Ar atmosphere, the largest increasing rate of terrace widths was also observed at 1400℃. The temperature appropriate for promoting step bunching was found to be 1400℃, while Ar pressure did not show any significant effect on this process.

On the other hand, we observed that Ar pressure played an important role for suppressing the formation of pits after graphene growth. The density of pits decreases dramatically with increasing the pressure of Ar atmosphere. Figure 2 shows a STM image of graphene on SiC substrate which was heated at 1400℃ for an hour, and then graphene was grown at 1 atm of Ar atmosphere. The uniform graphene covered almost the whole surface of the 4-μm-width terrace without the growth of pits.

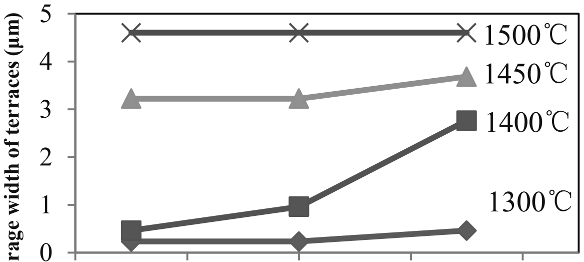

Fig. 1 Average width of terraces versus annealing time for various annealing temperatures. Ar pressure during annealing was 0.1 atm.

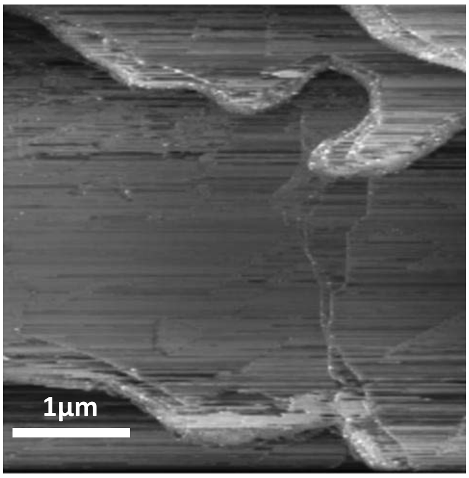

Fig. 2 STM image of graphene grown on SiC surface. The substrate was annealed at 1400℃ for an hour, and then graphene was grown at 1 atm of Ar atmosphere.

Corresponding Author: Wang Chenxing
Tel: +81-52-789-3714, Fax: +81-52-789-3703,
E-mail: cx-wang@surf.nuqe.nagoya-u.ac.jp

2P-41

In situ observation of graphene formation on polycrystalline Cu

○Huafeng Wang[1], Pei Zhao[2], Shohei Chiashi[2], Shigeo Maruyama[2], Yoshikazu Homma[1]

[1] Department of Physics, Tokyo University of Science, Tokyo, 162-8601, Japan
[2]Department of Mechanical Engineering, The University of Tokyo, Tokyo 113-8656, Japan

With the progress on the researches on graphene, its many distinguished properties have been studied. But there are still some fundamental questions which should be answered before the application of graphene. Undoubtedly, the controllable growth of graphene is one of these tasks. Mono-layer and multi-layer graphene have been synthesized by using Cu, Ni and etc. Among these substrates, Cu with low carbon solubility is proved to be suitable for graphene formation [1-2]. Although graphene can be easily obtained on Cu substrate, it seems difficult to control its quality, which depends on many parameters such as temperature, pressure, carbon source, percentage of hydrogen etc. To produce as large as possible single-crystal graphene and finally control its growth, observation of formation process and understanding of its mechanisms are indispensable. In situ scanning tunneling microscopy (STM) analyses have showed this process at atomic scale [3]. But this technique is limited by its relatively small detect area. Complementary to STM, in situ scanning electron microscopy (SEM) observation provides a larger field of view, which may help us to better understand the growth mechanisms [4].

In this study, we perform graphene growth in SEM chamber, and conduct *in situ* observation on its formation. By changing the growth conditions, mono-layer and multi-layer graphene with various structures are obtained on the polycrystalline Cu substrate. At the same time, some key issues concerning with graphene formation such as temperature, evaporation of Cu, carbon source and so on are systematically investigated. The whole graphene formation process on Cu substrate is demonstrated. After transferring the *in situ* grown graphene on SiO_2/Si substrate, the effects of experimental parameters on the morphology and quality of graphene are studied.

[1] Li, X. *et al*. *Science* ***324***, 1312 (2009).

[2] Reina, A. *et al*. *Nano Lett.* ***9***, 30(2009).

[3] Niu, T.; Zhou, M.; Zhang, J.; Feng, Y.; Chen, W. *J. Am. Chem. Soc.* ***135***, 8409 (2013).

[4] Kidambi, P. R. *et al*. *Nano Lett.* ***13***, 4769 (2013).

Corresponding Author: Yoshikazu Homma
Tel: +81-3-5228-8244, Fax: +81-3-5261-1023
E-mail:homma@rs.kagu.tus.ac.jp

2P-42

Interface structures between graphene and SiC formed in the nitrogen atmosphere

○Yoshiho Masuda, Wataru Norimatsu and Michiko kusunoki

[1] *Department of Applied Chemistry, Nagoya University, Nagoya 464-8603, japan*
[2] *Eco Topia Science Institute, Nagoya University, Nagoya 464-8603, Japan*

Introduction

Epitaxial graphene on silicon carbide (SiC) is synthesized by Si sublimation of the SiC substrates in a vacuum at high temperature, which is a very promising method for homogeneous large scale production with a high crystalline quality [1]. In particular, higher quality graphene was obtained when the decomposition process is progressed in the Ar atmosphere, which suppresses the sublimation of Si [2]. However, the carrier mobility of graphene grown on SiC (0001) is reduced by the influence of the SiC substrate. So, it is important to modify the interface structure between graphene and SiC for obtaining the higher mobility. In this study, we aimed to grow homogeneous graphene in the atmosphere of ~~an~~other inert gas, N_2, and investigated its interface structure.

Experimental Procedures

Single-crystal wafers of 6H-SiC (0001) were heated to 1600~1800 °C and held at this temperature in the mixed gas of N_2 and Ar. For comparison, the substrates were also heated in the Ar atmosphere. The observations were carried out using Topcon EM-200B and ARM200F-type transmission electron microscopes.

Results and Discussion

After heated at 1700 °C in the mixed gas of N_2 and Ar, few layers graphene was formed on SiC surface. Interestingly, periodic contrasts were also observed at the interface between the graphene and the SiC substrate [Figure 1(a)], which had never been observed for graphene formed in the Ar atmosphere [Figure 1(b)]. And we also discovered that two types of nitrided interface structure were formed by decomposed SiC in the presence of nitrogen gas. In the presentation, we will report the origin of the periodic contrasts and introduce these two types of nitrided structures.

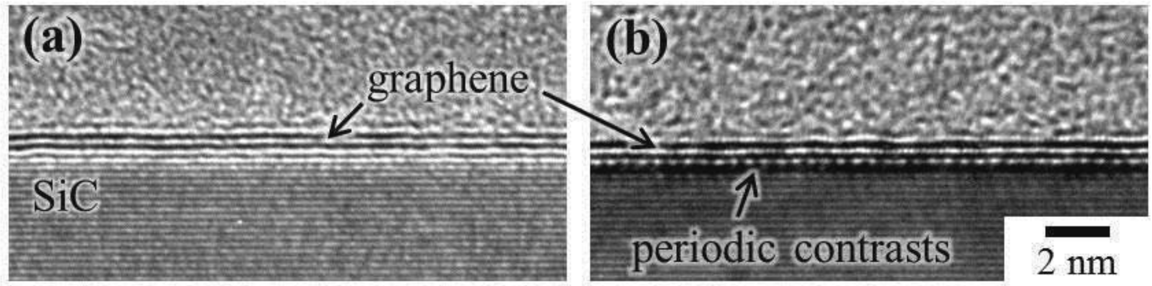

Figure 1 TEM images of graphene formed in (a) the Ar and (b) the mixed gas of N_2 and Ar.

[1] W. Norimatsu and M. Kusunoki. Phys. Rev. B 81, 161410 (2010).
[2] K. V. Emtsev *et al*. Phys. Rev. B 77, 155303 (2008).

Tel: +81-52-789-5859, Fax: +81-52-789-5859,
E-mail: masuda.yoshiho@a.mbox.nagoya-u.ac.jp

2P-43

Preparation of multilayer graphene nanoribbons on very narrow graphene templates of unzipped DWCNTs

○H. Kitakawa[1], R. Negishi[1], H. Tanaka[2], M. Fukumori[2], T. Ogawa[2], Y. Kobayashi[1]
[1]*Department of applied physics, Osaka University, Suita 565-0871, Japan*
[2]*Department of Chemistry, Osaka University, Toyonaka 560-0043, Japan*
Corresponding Author: E-mail: negishi@ap.eng.osaka-u.ac.jp

Multilayer graphene nanoribbons (M-GNRs) with weak interlayer coupling such as turbostratic structures are promising candidates for channel materials in field effect transistors (FETs) because the multilayer channels lead to high-current gain [1] in addition to band gap opening between graphene Dirac cones due to the electron confinement. M-GNRs can be synthesized by unzipping multi-wall carbon nanotubes (CNTs), but their width becomes relatively large [2]. As a result, it is difficult to observe the band gap opening and control the layer numbers. In this work, we report the M-GNR synthesis by graphene growth on narrow double-layer GNRs with several nanometers width, which are prepared by unzipping double-wall CNTs (DWCNTs).

GNRs as growth templates were obtained from unzipping of DWCNTs [3]. Graphene layers were grown by chemical vapor deposition (CVD) using a furnace with three temperature zones, in which temperatures for carbon feedstock decomposition and graphene growth can be controlled individually[4]. The temperatures used for thermal decomposition and graphene growth were 900 ºC and 720-735 ºC, respectively. Thickness of the grown graphene was evaluated by atomic force microscopy (AFM).

Figure 1 shows the AFM images obtained from the GNR (a) before and (b) after CVD growth, and (c) height profiles of the GNR along L-L'. Before the growth, the layer numbers of the GNR estimated from the AFM image is mono or bilayer [3]. The height of the GNR increases from ~0.7 to ~1.7 nm after growth. This result indicates that the multilayer GNR with 2~3 layers is formed by the growth. Figure 2 shows the height and width distributions of the GNR before and after growth. The median height and width of M-GNRs increase from 1.2 to 1.6 nm and 25 to 50 nm after growth, respectively. These results indicate that the growth rate at edge sites is higher than that at terrace sites of GNR templates, and that the edge sites are active sites for adsorption of carbon species compared with terrace sites. In addition to that, the surface roughness on the GNR is not changed before and after growth, and is atomically flat. This result means that the growth of graphene layers is proceeded via layer-by-layer mode, and is consistent with the graphene layer growth on the graphene prepared by mechanical exfoliation[4]. More works are necessary for elucidation of the growth mechanism of the M-GNRs to control the layer number and width.

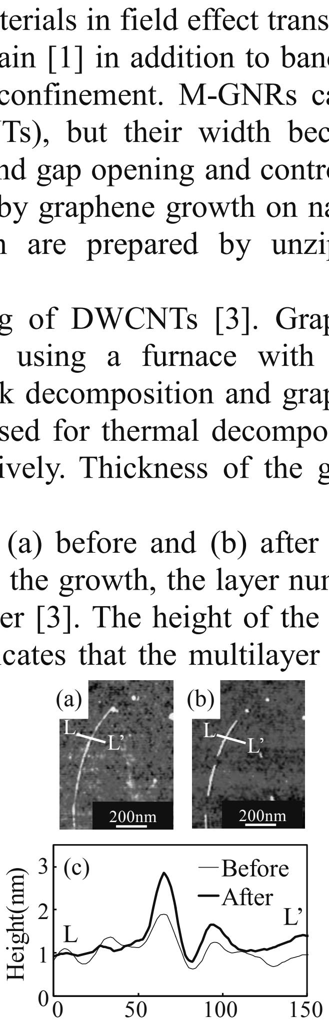

Fig.1 AFM images of GNR (a) before and (b) after growth. (c) Height profiles along L-L'.

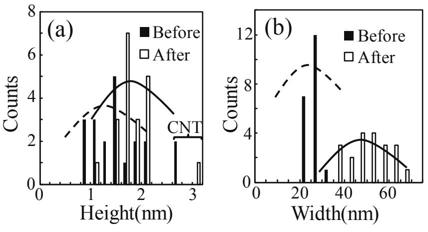

Fig.2 (a)Height and (b)width distributions of GNRs before and after growth estimated from AFM observations.

References: [1] Y. Ouyang, et al., Nano Research **3** (2010)8. [2] S. R. Dhakate et al., Carbon **49** (2011) 4170. [3] X. Li, et al., Science **319** (2008)1229. [4] R. Negishi, et al., Thin Solid Films **519** (2011)6447.

Acknowledgement: Authors would like to thank Prof. K. Matsumoto (Osaka Univ.) for supporting AFM measurements.

2P-44

Flexible transistor and inverter of large-area WSe_2 thin film

○Kazuma Funahashi[1], Jiang Pu [1], Lain-Jong Li [2], Yoshihiro Iwasa [3,4], Taishi Takenobu [1,5]

[1] *Department of Applied Physics, Waseda University, Shinguku 169-8555, Japan*
[2] *Institute of Atomic and Molecular Sciences, Academia Sinica, Taipei 11529, Taiwan*
[3] *Department of Applied Physics, The University of Tokyo, Tokyo 113-8656, Japan*
[4] *RIKEN Center for Emergent Matter Science (CEMS), Wako 351-0198, Japan*
[5] *Kagami Memorial Laboratory, Waseda University, Tokyo 169-0051, Japan*

Atomically thin films of transition metal dichalcogenides (TMDCs) are promising candidates for flexible devices complementing graphene due to their extraordinary properties such as high on/off switching ratio, sizable bandgap, and flexibility. Actually, highly flexible transistors based on molybdenum disulfide (MoS_2), one of the TMDCs, have been reported [1-3] and proved the usefulness of TMDCs in flexible electronics. Although logic circuit (*e.g.* CMOS inverter) is strongly required for further application, commonly-used MoS_2 is not suitable because of their n-type unipolar conduction. For logic application, p-type or ambipolar flexible transistors are additionally necessary. Therefore, in this study, we focus on tungsten diselenide (WSe_2) which is known as ambipolar TMDC semiconductor [4]. Using chemically grown WSe_2 and electrolyte-gating method, we fabricate flexible ambipolar transistors and CMOS-like inverters.

WSe_2 thin film was synthesized by chemical vapor deposition [4] and was transferred onto flexible polyimide substrate. We fabricated WSe_2 electric double layer transistors (EDLTs) using flexible gate insulator, ion gel, and they showed ambipolar operation as reported [4]. This realization of WSe_2 ambipolar transistors allowed us the development of CMOS-like inverters because the inverters can be achieved by combining two identical ambipolar transistors together, as shown in Fig. 1 [5]. We applied this method into WSe_2 ambipolar flexible transistors and realized flexible inverters (Fig. 2). The device revealed gain ~17, which is sufficient to drive next stage components in a logic circuit.

In summary, we have demonstrated flexible inverter based on WSe_2 ambipolar EDLTs, which is important first step for the next-generation flexible devices.

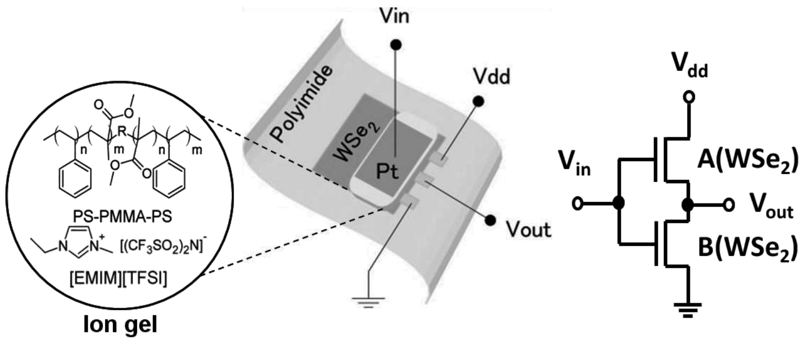

Fig.1 Schematics of WSe_2 flexible inverter (left) and equivalent circuit (right)

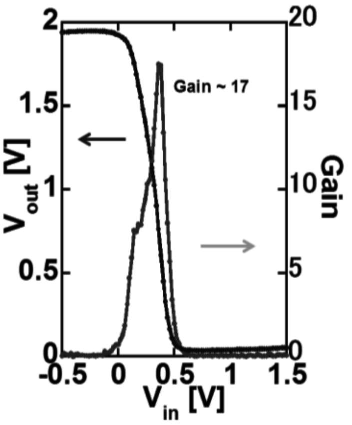

Fig.2 Inverter characteristic

[1] J. Pu, T. Takenobu *et al*. Nano Lett. 12(8), 4013–4017 (2012), [2] G. H. Lee *et al*, ACS Nano 7(9), 7931–7936 (2013),
[3] H. Y. Chang *et al*, ACS Nano 7(6), 5446–5452 (2013), [4] J. K. Huang, J. Pu, T. Takenobu *et al*., ACS Nano, DOI: 10.1021/nn405719x,
[5] E. J. Meijer *et al*, Nat. Mater. 2, 678–682(2003)

Corresponding Author: Taishi Takenobu, Tel&Fax: +81-3-5286-2981, E-mail: takenobu@waseda.jp

2P-45

Controlled doping in densely aligned graphene nanoribbons by covalent functionalization

○Pablo Solís-Fernández,[1] Mark A. Bissett,[1] Masaharu Tsuji,[1] Hiroki Ago[1,2]

[1] Institute for Materials Chemistry and Engineering (IMCE), Kyushu University, Kasuga Park 6-1, Fukuoka 816-8580, Japan
[2] JST-PRESTO

The excellent properties of graphene potentially make it a good candidate for a vast number of applications. Particularly, graphene is expected to be well suited for high performance electronics. However, some issues must still be addressed, including the lack of a bandgap in the electronic structure of the graphene. One of the proposed ways to open the bandgap is by patterning graphene into a one-dimensional shape, known as graphene nanoribbons (GNRs). Recently we have shown the production of dense arrays of aligned GNRs (see the inset of Fig. 1) [1]. Nanoribbons were produced by substrate-controlled etching of graphene with Ni nanoparticles at high temperatures and in the presence of hydrogen. For many applications it is necessary to control the electrical properties of graphene, such as the level of doping, to specific values. For this purpose, chemical functionalization has been shown to be very effective [2].

In the present work, we have studied the behavior of our GNRs under chemical functionalization with two different diazonium salts, 4-nitrobenzenediazonium tetrafluoroborate (4-NBD) and 4-methoxybenzediazonium tetrafluoroborate (4-MBD). Functionalization proceeds by the covalent attachment of the diazonium groups to the GNRs. Due to the different aryl molecules, both p- and n-type doping are expected for 4-NBD and 4-MBD functionalized GNRs respectively. The degree of functionalization can be determined by the position and relative intensities of the 2D and G Raman bands. We found our GNRs to be much more reactive than pristine graphene, most probably due to the presence of exposed edges. As shown in Fig. 1, the change of the 2D band shift with functionalization time is opposite for the two diazonium salts. The observed trends seem to corroborate the anticipated p-type (n-type) doped character of the GNRs functionalized with 4-NBD (4-MBD). Thus, this method will allow for a controlled tuning of the transport type to either p- or n-type by adjusting the functionalization time and diazonium salt employed. Our finding is expected to contribute to the developing of CMOS devices based on aligned nanoribbons.

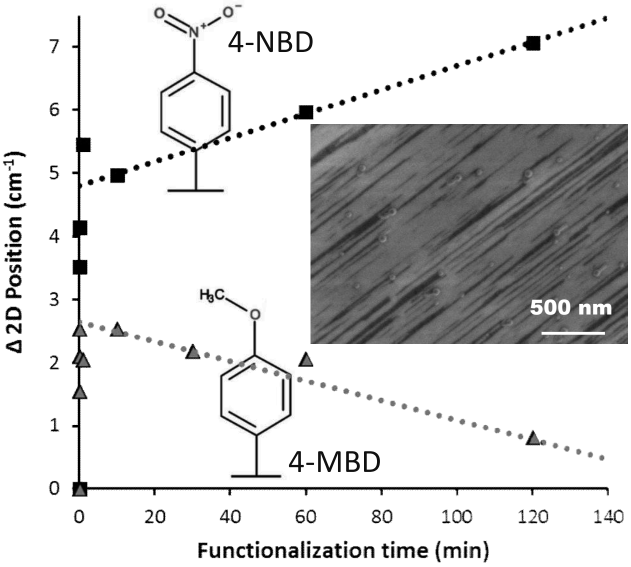

Fig.1 Change of the Raman 2D band shift of GNRs functionalized with 4-NBD and 4-MBD. Inset: SEM image of the GNRs.

[1] P. Solís-Fernández *et al.* Adv. Mat. **25**, 6562 (2013).
[2] M.A. Bisset *et al.* ACS Nano **7**, 10335 (2013).

Corresponding Author: H. Ago
Tel: +81-92-583-7817, Fax: +81-92-583-7817,
E-mail: ago@cm.kyushu-u.ac.jp

2P-46

Mechanism of photoluminescence in graphene oxide

○Hiroyuki Yokoi[1,2], Takaaki Taniguchi[1,2], Michio Koinuma[1,2], Yasumichi Matsumoto[1,2]

[1] Graduate School of Science and Technology, Kumamoto University, Kumamoto, 860-8555, Japan
[2] JST, CREST, K's Gobancho 6F, 7 Gobancho, Chiyoda-ku, Tokyo, 102-0076, Japan

Graphene oxide (GO) is graphene-like material which can be produced through oxidation of graphite. Carbon atoms in the basal plane or on the edges of GO are partially modified with functional groups containing oxygen. One of the interesting features of this material is to exhibit photoluminescence (PL) in a wide spectral range between near-infrared and blue depending on the degree of oxidation or reduction [1]. A lot of researches have been conducted to investigate the PL properties and mechanisms. However, the PL mechanisms have not been clarified fully yet. In a recent model, for example, it is thought that excitation occurs between π–π* bands, and that red and blue emissions are induced through defect levels induced by modification with functional groups and quantum levels in *sp*^{2} quantum dot produced by reduction, respectively [1]. However, it is inexplicable with this model that PL excitation spectra for red and blue emissions are different.

In this work, we aim to clarify the PL mechanisms through ab initio calculations with realistic structural models for GO, where an *sp*^{2} quantum dot is embedded in fully epoxidated area. We arranged the relative configuration of the epoxy groups as stably as possible [2]. In the calculations of structure relaxation and electronic states, we have employed the Vienna Ab Initio Simulation Package (VASP) [3]. Figure 1 shows the electronic structure of a GO sheet with a coronene-type *sp*^{2} quantum dot (Region A in Fig. 2). HOMO and LUMO were π and π* states localized in the quantum dot. We have found that a state locating at around 1.2 eV above LUMO spreads both in the quantum dot and in the specific epoxidation structure, where all epoxides are arranged outward from a six-membered carbon ring as shown in Fig. 2. This structure appears in the fully epoxidated area inevitably. We have considered that it could work as an excitation site in the blue emission. We will also report a model for the red emission, and experimental results to examine these models.

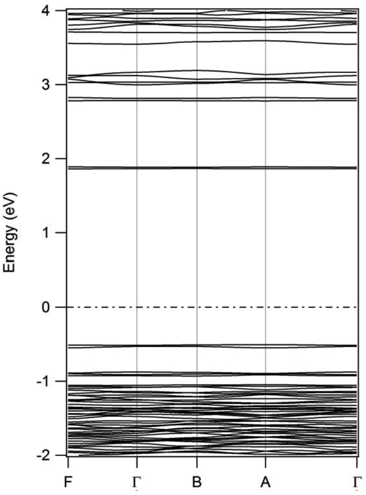

Fig. 1 Band structure of GO with a coronene-type sp2 quantum dot.

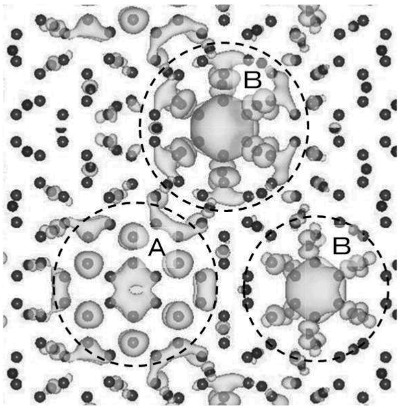

Fig. 2 The employed structure model and partial charge density of a state above LUMO by 1.2 eV. A: quantum dot area; B: six-membered ring area where epoxides are arranged outward.

[1] C.-T. Chien *et al.* Angew. Chem. Int. Ed. **51**, 6662 (2012).
[2] G. Kresse and J. Furthmüller, Phys. Rev. B **54**, 11169 (1996).
[3] M.-T. Nguyen *et al.* Phys. Rev. B **86**, 115406 (2012).

Corresponding Author: H. Yokoi
Tel: +81-96-342-3727, Fax: +81-96-342-3710,
E-mail: yokoihr@kumamoto-u.ac.jp

2P-47

Mechanisms of Near-Infrared Photoluminescence from Graphene Oxides

○Daichi Kozawa[1], Yuhei Miyauchi[1,2], Shinichiro Mouri[1], Masao Ichida[3],
and Kazunari Matsuda[1]

[1] *Institute of Advanced Energy, Kyoto University, Uji, Kyoto 611-0011, Japan*
[2] *Japan Science and Technology Agency, PRESTO, 4-1-8 Honcho Kawaguchi, Saitama 332-0012, Japan*
[3] *Faculty of Science and Engineering, Konan University, 8-9-1 Okamoto, Higashi-Nada-ku, Kobe 658-8501, Japan*

Graphene oxide (GO) is one of the graphene related materials, and has attracted interests because of a finite band gap[1]. The availability of oxidation and reduction for GO enables tunable photoluminescence (PL) in the broad range of UV–visible–near-infrared (NIR) as a result of the inhomogeneous structure. In our previous study, it has been revealed that UV and visible PL from GO originate from the quasi-molecular-like small sp^2 fragments embedded in GO[2]. However, the physical mechanism of NIR PL in GO has been still controversial. In this study, we have investigated mechanisms of NIR PL from GO produced by modified Hummer's method using steady-state and time-resolved spectroscopy.

Figure 1 shows PL spectra of GO in aqueous solution with excitation at various photon energies from 1.8 to 2.5 eV, where the arrows indicate the excitation photon energies. The PL spectrum of GO shows a broad emission peak in NIR region (~1.7 eV), and the gradual blueshift and broadening of emission peaks are observed with increasing the excitation energy, which is also observed in the PLE map as shown in the inset of Figure 1. We attribute the NIR PL to the electron-hole pair recombination in various size and shape of graphene nanodisc (sp^2 carbon cluster) states embedded in GO, in which the nanodisc states have various band gap corresponding to their structures.

To further verify the mechanisms of the NIR PL, we conducted time-resolved PL measurements. The longer PL decay time and build-up are observed at lower emission energy. This result suggests that the energy transfer from small to adjacent larger carbon cluster states embedded in a GO. These provide us further insights into tunable optical properties toward GO-based optoelectronic devices.

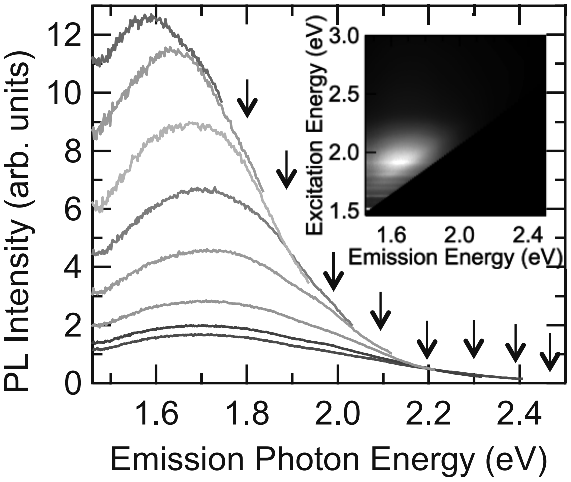

Fig. 1 PL spectra with various excitation energies of GO in aqueous solution. The arrow indicate the excitation energy for each PL spectrum. The inset shows PLE map.

References

[1] Eda, G.; Fanchini, G.; Chhowalla, M., *Nat. Nanotechnol.* **2008**, 3, 270-274.

[2] Kozawa, D.; Miyauchi, Y.; Mouri, S.; Matsuda, K., *J. Phys. Chem. Lett.* **2013**, 4, 2035-2040.

Corresponding Author: D. Kozawa
Tel: +81-774-38-3465, Fax: +81-774-38-3467,
E-mail: d-kozawa@iae.kyoto-u.ac.jp

Molecular dynamics simulation for water molecules between two graphene layers

○Riichiro Saito[1], Masashi Mizuno[1]

[1] *Department of Physics, Tohoku University, 980-8578, Japan*

Water molecules in nano carbon materials show an interesting behavior which is not observed in conventional ice. A famous example is the water molecules confined in single wall carbon nanotubes (SWNTs) which is called ice nanotube in which melting temperature and lattice structure of ice depend on the diameter or chirality of SWNTs [1,2,3]. The change of physical properties in the ice nanotube is understood by (1) the confinement of molecules in nano-meter size and (2) interaction between carbon and water molecules. Here we would like to discuss water molecules confined in two graphene layers. Compared with ice nanotubes, the confinement of water molecules in the direction of graphene plane can be relaxing by increasing the inter-layer spacing, while we expect some pressure in the direction perpendicular to graphene plane by van der Waals interaction between the two graphene layers. However, a qualitative understanding for water molecules between two graphene layers is not easily obtained by some analytical discussion or phenomenological theory. In order to get a realistic picture of motion of water molecules and carbon atoms at a give temperature, we performed molecular dynamics simulation using a package so called LAMMPS. LAMMPS is open and free software working on Linux machine and LAMMPS is widely used not only in physics but also polymer science or even biology. Here we will show some preliminary results by animation and show what is happening in the system. It should be noted that we just start this project and that we would like to discuss with many people for possible direction of the research.

The authors acknowledges Prof. R. Kitaura, Nagoya University for important discussion of this subjects and MEXT grant (SATL, No. 25107005).

References:

[1] K. Koga *et al.*, Nature 412, 802 (2001).
[2] Y. Maniwa *et al.* JPSJ 71, 2863 (2002).
[3] D. Takigawa *et al.* PNAS 105, 39 (2008).

Corresponding Author: R. Saito
Tel: +81-22-795-7754, Fax: +81-22-795-6447,
E-mail: rsaito@flex.phys.tohoku.ac.jp

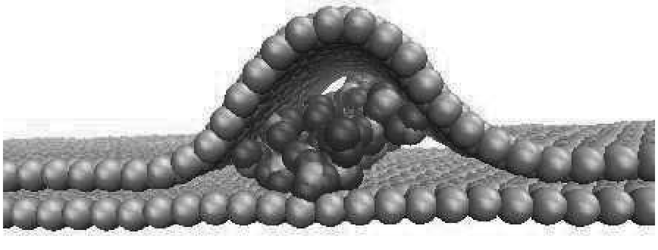

Water molecules between two graphene layers at 100K by LAMMPS simulation. Because of the periodic boundary condition, the bottom layer does not deform.

2P-49

Formation of fullerenes and polyynes by graphite laser ablation in ambient gases

○Yurika Abe, Hitomi Endo, Yohji Achiba, Haruo Shiromaru

Department of Chemistry, Tokyo Metropolitan University, Hachioji, 192-0397, Japan

Carbon clusters formed by laser ablation of graphite are sorted into three main structural categories, namely linear chains, monocyclic rings, and fullerenes. In the present study, we examined macroscopic production of linear chains and fullerenes by laser ablation of a graphite disk in argon gas flow at room temperature, in which the formers were in fact obtained as the polyynes. Laser ablation was performed in a glass tube with a cone-shaped exit for argon gas, which carried the ablation products to a cold organic solvent in a glass bottle. Then, soluble products were analyzed by UV absorption.

A typical UV spectrum of the hexane solution prepared by ablation at the graphite surface parallel to the gas flow is shown in Fig.1, together with that of pure C_{60} solution. As can be seen in the figure, a characteristic band of C_{60} appears around 330nm, indicating formation of considerable amount of soluble C_{60}. Among strong unassigned absorption bands, characteristic peaks of polyynes are also identified. It shows coexistence of linear-form carbons and fullerenes in the cluster source. When the ablation surface was set so as to let the clusters to be ejected toward the exit, polyynes were preferentially produced, as demonstrated by the spectrum A in Fig.2.

It should be noted that the addition of a hydrocarbon (propane) to the ambient argon gas drastically enhances the polyyne yield as shown in the figure. It offers clear evidence that these polyynes are produced by gas-phase reactions.

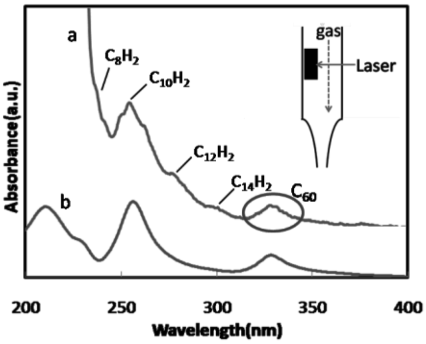

Fig. 1 (a) Absorption spectrum of hexane solution prepared by 30 min. irradiation of 300mJ/pulse ns laser. Assignment is indicated in the figure. (b) Absorption spectrum of hexane solution of pure C_{60}.

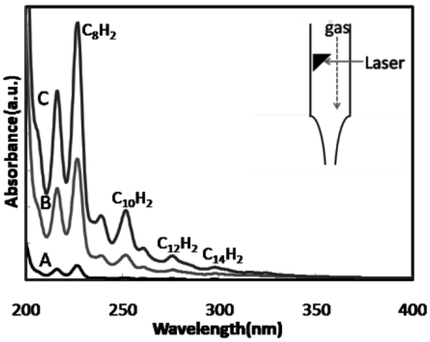

Fig. 2 Absorption spectra of hexane solution prepared by 10 min. irradiation of 150mJ/pulse ns laser. The ambient gases are (A) pure argon, (B) with propane, (C) with higher flow rate of propane.

Corresponding Author: H. Shiromaru
Tel: +81-42-677-1111, Fax: +81-42-677-2525,
E-mail: shiromaru-haruo@tmu.ac.jp

2P-50

Vibronic interaction in the forbidden transition of polyyne molecules

○Tomonari Wakabayashi

Department of Chemistry, Kinki University, Higashi-Osaka 577-8502, Japan

The π-π^* excitation in a conjugate linear polyyne molecule gives rise to three excited states. The electric-dipole transition from the ground state is fully allowed for the one, but symmetry forbidden for the other two. However, vibronic coupling allows the latter two some transitions weakly. In order to understand spectral features appearing in the vibronic transition, symmetry considerations are useful. Using Herzberg-Teller expansion, matrix elements in the vibronic coupling scheme were examined for the symmetry-forbidden transition. As an example, we chose the HOMO-LUMO excitation for hydrogen-end-capped polyyne molecules, $H(C\equiv C)_nH$ ($n\geq2$), and compared the results to the observed absorption and emission spectra [1].

Pronounced features in the absorption and emission spectra were those comprising a vibrational progression for a totally symmetric vibrational mode of σ_g, while the inducing mode was π_g. Depending on the direction for the transition dipole, or the symmetry of the intermediate state for the intensity borrowing, the number of vibrational quanta necessary for inducing the vibraonic transitions is different. This is crucial for locating the missing origin for the forbidden transition. Symmetry considerations are made to discuss the assignment of the missing origin in the forbidden transition for the centrosymmetric linear polyyne molecule [2].

[1] T. Wakabayashi, H. Nagayama, K. Daigoku, Y. Kiyooka, K. Hashimoto: Laser induced emission spectra of polyyne molecules $C_{2n}H_2$ (n=5-8), Chem. Phys. Lett. **446**, 65-70 (2007).

[2] T. Wakabayashi, Y. Wada, N. Iwahara, T. Sato: Vibronic bands in the HOMO-LUMO excitation of linear polyyne molecules, J. Phys. Conf. Ser. **428**, 012004 (2013).

Corresponding Author: T. Wakabayashi
Tel: +81-6-4307-3408, Fax: +81-6-6723-2721,
E-mail: wakaba@chem.kindai.ac.jp

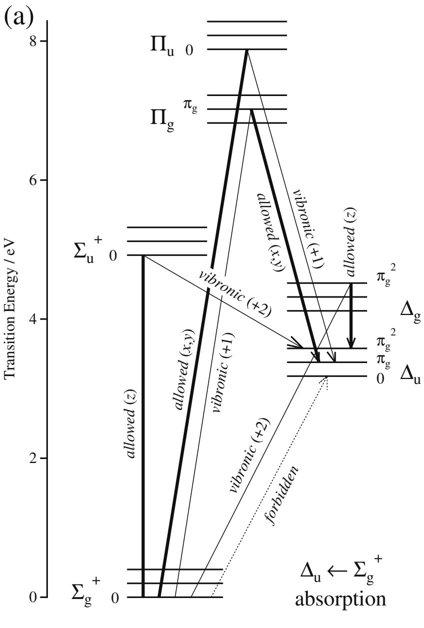

Fig. 1. Schematic diagram for vibronic transitions in polyyne molecules, showing intermediate states.

3P-1

Thermal Bis-silylation, Carbosilylation, and Bis-germylation of Fullerenes

○Daiki Inaba[1], Kazuya Minami[1], Kyosuke Miyabe[1], Ryosuke Iida[1], Masahiro Kako[1],
Yutaka Maeda[2], Michio Yamada[2], Tadashi Hasegawa[2], Takeshi Akasaka[3]

[1]Department of Engineering Science, The University of Electro-Communications, Chofu, Tokyo 182-8585, Japan
[2]Department of Chemistry, Tokyo Gakugei University, Koganei, Tokyo 184-8501, Japan
[3]Life Science Center of Tsukuba Advanced Research Alliance, University of Tsukuba, Tsukuba, Ibaraki, 305-8577, Japan

Chemical functionalization of fullerenes has been attracting much attention from both mechanistic and synthetic viewpoints. Introduction of heteroatoms such as electropositive silicon has been known to an effective method to modify the electronic characteristics of hollow fullerenes and endohedral metallofullerenes. The facile silylation reactions of fullerenes have been described using reactive silicon compounds such as silylenes, disiliranes, and silyl radicals. Electrochemical analyses and theoretical calculations have disclosed that the silylated fullerene derivatives have more negative charge on the cage than the parent fullerenes. Such derivatization of fullerenes would contribute to the application of fullerenes as functional materials. For example, a silirane derivative of C_{60} with a higher LUMO is expected to be a promising compound to increase the open-circuit voltage of organic solar cells. However, silylation of C_{60} and C_{70} have been limited to photolytic reactions using ultraviolet irradiation and nucleophilic addition of anionic silicon reagents, in which degradations of silylated products take place disadvantageously under those conditions.

Therefore, alternative procedures for silylation of fullerenes are desirable for development of various silylated fullerene-based materials. Recently, thermal addition of endohedral metallofullerenes with disiliranes, siliranes, and silylenes have been demonstrated to afford the corresponding silylated derivatives.[1-3] In addition, thermal reactions of C_{60} with siliranes have been reported by employing thermally generated silylenes as the silylating reagent. As our continuing research of functionalization of fullerenes, we have conducted the bis-silylation and bis-germylation of C_{60} and C_{70} under non-photolytic conditions. Although the silylene addition and bis-silylation of C_{70} under photolytic conditions have been described previously, such examples are rather sparse. Herein we report the thermal reactions of C_{60} and C_{70} with disilirane, digermirane, and siliranes, indicating that bis-silylation, bis-germylation, silylene addition, and carbosilylation of C_{60} and C_{70} proceed at higher temperatures without photoirradiation.(Schemes 1, 2)

Scheme 1.

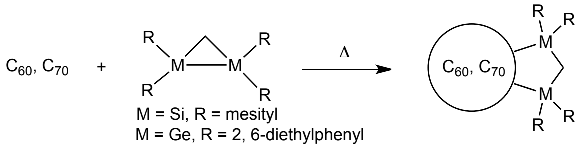

Scheme 2.

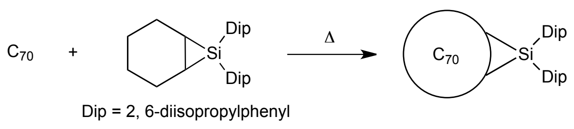

[1] Y.Iiduka *et al. J. Am. Chem. Soc.* **127**, 9956–9957(2005). [2] M. Yamada *et al. J. Am. Chem. Soc.* **127**, 14570–114571(2005). [3] M. Yamada *et al. J. Am. Chem. Soc.* **132**, 17953–17960(2011). [4] K. Sato *et al. J. Am. Chem. Soc.* **134**, 16033–16039(2012).

Corresponding Author: Masahiro Kako Tel: +81-42-442-5570 E-mail: kako@e-one.uec.ac.jp

3P-2

Synthesis of [60]Fullerene Derivative with 1,3-Dipolar Cycloaddition as a Novel Structure for Bulk-Heterojunction Photovoltaic Cells

○Hisashi Tokutomi[1], Masaru Sekido[2]

[1] Division of Production System and Design Engineering, Advanced Engineering Course, Sendai National College of Technology, Natori, 981-1239, Japan.
[2] Department of Materials and Environmental Engineering, Sendai National College of Technology, Natori, 981-1239, Japan.

Bulk-Heterojunction (BHJ) solar cell is expected to be the lightweight, flexible, and potential low cost solar cell. To overcome low power conversion efficiency of BHJ solar cell caused by lower crystal orientation, [1] novel structure of BHJ solar cell model for high crystal orientation using Linked C_{60} (L-C_{60}) is designed (Figure 1).

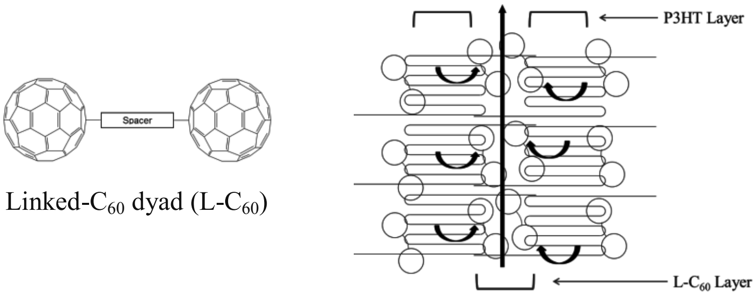

Linked-C_{60} dyad (L-C_{60})

Figure 1. Novel structure of BHJ solar cell model (Wide arrow is electron transfer way).

L-C_{60} is the C_{60} dyads containing sebacoyl carbon chain and AS (aniline and sebacoyl carbon chain) as a spacer. L-C_{60} is expected to interact with the crystal part of P3HT (poly(3-hexylthiophene-2,5-diyl)) to help its crystal orientation to give high power conversion efficiency. AS spacer was synthesized by using aniline and sebacoyl chloride (29% isolated yield). Functionalized-C_{60} (F-C_{60}) was synthesized by Prato reaction [2.3] (24% isolated yield) and F-C_{60} was then reacted with AS spacer to form L-C_{60} (64% reacted yield). Figure 2 is ^{1}H NMR shift of AS spacer and reacted compound. According to ^{1}H NMR spectrum, the peak of AS spacer was observed at reacted compound. Since non-reacted AS spacer was washed by acetone, AS Spacer and F-C_{60} was stacked by π-π stacking. By using the developed methods is also applicable to synthesize other C_{60} dyads containing various spacers.

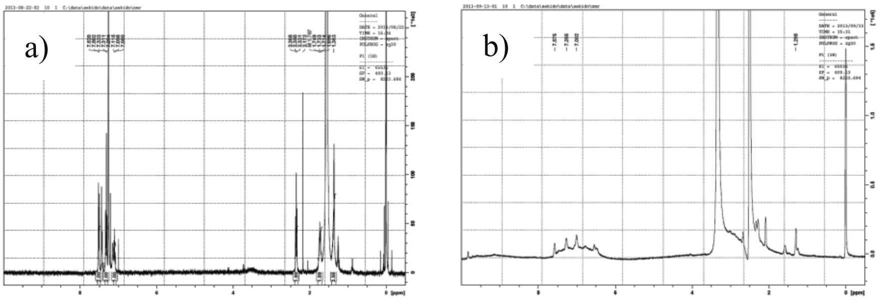

Figure 2. ^{1}H NMR shift of AS spacer (a) and reacted compound (b)

[1] *Chem. Mater.* **2010**, 22, 5371-5376.
[2] *J. Am. Chem. Soc.* **1993**, 115, 9798-9799.
[3] *J. Am. Chem. Soc.* **2008**, 130, 8733-8740.

Corresponding Author: H. Tokutomi
Tel: +81-22-381-0329, Fax: +81-22-381-0329
E-mail: a1301019@sendai-nct.jp

3P-3

Electrochemical synthesis of Li@C_{60} supraatom

○Hiroshi Ueno [1], Naohiko Ikuma [1], Kei Ohkubo [2], Hiroshi Moriyama [3], Shunichi Fukuzumi [2,4],
Ken Kokubo [1]

[1] *Division of Applied Chemistry, Graduate School of Engineering, Osaka University,*
2-1 Yamadaoka, Suita, Osaka 565-0871, Japan.
[2] *Department of Material and Life Science, Graduate School of Engineering, Osaka University, and ALCA, Japan Science and Technology (JST), Suita, Osaka 565-0871, Japan*
[3] *Department of Chemistry, Faculty of Science, Toho University, 2-2-1 Miyama, Funabashi, Chiba 274-8510, Japan*
[4] *Department of Bioinspired Science, Ewha Womans University, Seoul 120-750, Korea*

The ionic nature of $Li^+@C_{60}$ is one of the remarkable characteristics among all reported endohedral metallofullerenes [1,2]. The ionic property makes it an open possibility to apply as electrolyte in suitable organic solvents such as *o*-dichlorobenzene (*o*-DCB) and benzonitrile, and we have succeeded in the electrochemical synthesis of Li^+-encapsulated C_{60} radical anion without any supporting electrolytes [3]. However, the isolation and characterization of the obtained $Li^+@C_{60}^{\bullet-}$ were still insufficient for its further application due to its lower concentration and difficulty in isolation process. On the other hand, counter anion-exchanging is one of the chemical modifications of $Li^+@C_{60}$ salts to give higher solubility in several organic solvents [4]. Such improved solubility can lead $Li^+@C_{60}$ to more applicable solution processes including our electrochemical application. As a continuing interest of our studies on the ionic properties of $Li^+@C_{60}$ salts, we herein report the ionic conductivity of several $Li^+@C_{60}$ salts, electrochemical synthesis, and complete isolation of $Li^+@C_{60}^{\bullet-}$ based on the large solubility difference between $Li^+@C_{60}$ salts and $Li^+@C_{60}^{\bullet-}$.

All measured samples showed enough high ionic conductivity for electrochemical reduction of $Li^+@C_{60}$ cation. On the synthesis of $Li^+@C_{60}^{\bullet-}$ using CH_2Cl_2 solution of $[Li^+@C_{60}](NTf_2^-)$*, only the product was deposited on the surface of cathode due to the lower solubility of the product for the solvent used (Figure 1). Through NIR, EPR, NMR, and Raman spectroscopy, the deposited sample was fully characterized as Li-encapsulated fullerene Li@C_{60} ($Li^+@C_{60}^{\bullet-}$) supraatom which is far different from the starting $Li^+@C_{60}$ salt having an external counter anion.

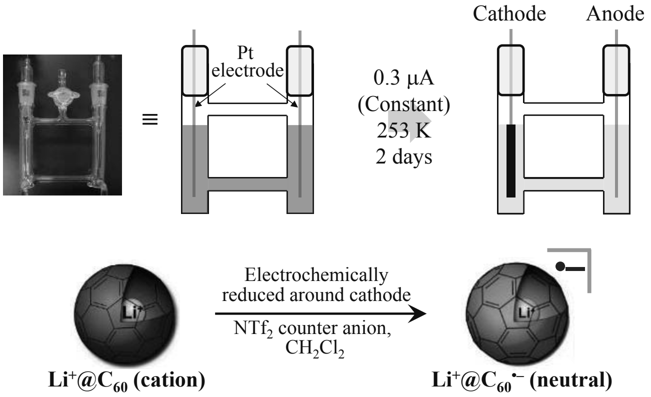

Figure 1. Pattern diagram of the electrochemical reduction of $[Li^+@C_{60}]$ cation in CH_2Cl_2.

* NTf_2^-; bis(trifluoromethylsulfonyl)imide anion ($N(SO_2CF_3)_2^-$)

[1] Sawa, H. and Tobita, H. *et al. Nat. Chem.* **2010**, *2*, 678. [2] Aoyagi, S. *et al. Angew. Chem. Int. Ed.* **2012**, *51*, 3377. [3] Kokubo, K. *et al. Chem. Commun.* **2013**, *49,* 7376. [4] Matsuo, Y. *et al. The 45th Fullerenes-Nanotubes-Graphene general Symposium* (2013) 2P-36.

Corresponding Author: K. Kokubo
Tel: +81-6-6879-4592, Fax: +81-6-6879-4593, E-mail: kokubo@chem.eng.osaka-u.ac.jp

3P-4

Separation of a missing small-bandgaped metallofullerene $Gd@C_{60}$ by *in situ* trifluoromethylation

○Hiroyuki Niwa, Yusuke Nakanishi, Zhiyong Wang, Ryo Kitaura,
Haruka Omachi and Hisanori Shinohara*

Department of Chemistry & Institute for Advanced Research, Nagoya University, Nagoya 464-8602, Japan.

Ever since the first mass spectroscopic observation of $La@C_{60}$ in 1985[1], many attempts to solvent-extract, separate and purify $M@C_{60}$ (M = Ca, Er, Eu etc.) have been reported [e.g., Ogawa *et al. JACS* on $Er@C_{60}$[2]]. However, even today, the final purification and isolation (i.e., more than 99 % purity) of $M@C_{60}$ have not yet been done. Because of their high reactivity due to their small-bandgap or the radical property, $M@C_{60}$ is entirely insoluble in common organic solvents. Recently, our group have reported a brand-new stabilization method of small-bandgap metallofullerenes such as $M@C_{2n}$ ($2n$ = 70–74) by *in situ* trifluoromethylation[3].

Herein, we report the first synthesis and separation of pertrifluoromethylated $Gd@C_{60}$ derivatives. DC arc-discharge was carried out with a Gd/graphite composite rod as positive electrodes and polytetrafluoroethylene (PTFE) situated below the arc-discharge region[3]. The LD-TOF mass spectra of the crude extract shows that the generation of $Gd@C_{60}$ and/or its derivatives (Fig 1a). After the separation of the crude extract by the $TiCl_4$ treatment[4,5] and recycle HPLC, enhanced peaks of $Gd@C_{60}(CF_3)_4$ and $Gd@C_{60}(CF_3)_5$ were observed by MALDI-TOF-MS mass spectral analysis (Fig. 1b). DFT calculations on the causes of the electronic stability of trifluoromethylated $Gd@C_{60}$ will also be presented.

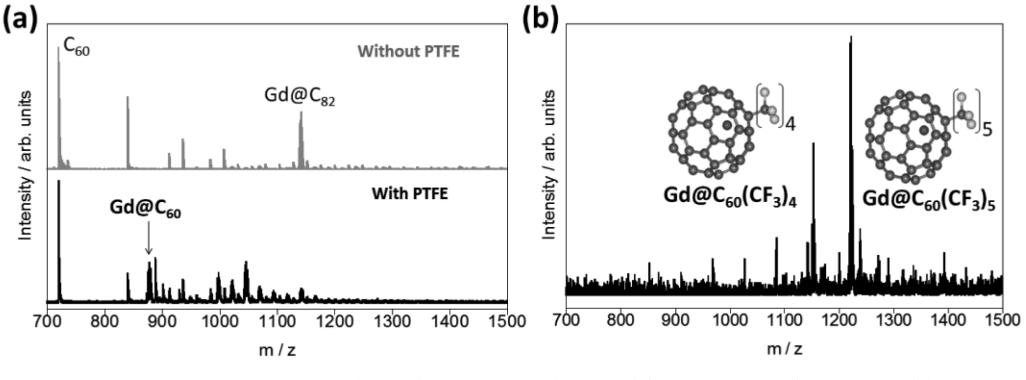

Fig. 1 (a) LD-TOF mass spectra of crude extracts (top: without PTFE, bottom: with PTFE) (b) MALDI-TOF mass spectra after separation.

[1] J. R. Heath *et al.,* ***J. Am. Chem. Soc.,*** 107, 7779 (1985) [2] T. Ogawa *et al.,* ***J. Am. Chem. Soc.,*** 122, 3538 (2000). [3] Z.Wang *et al.,* ***Angew. Chem., Int. Ed.,*** 52, 11770 (2013). [4] K. Akiyama *et al.,* ***J. Am. Chem. Soc.,*** 134, 9762 (2012). [5] Z. Wang *et al.,* ***J. Phys. Chem. C*** 116, 25563 (2012).

Corresponding Author: Hisanori Shinohara
Tel: +81-52-789-2482, Fax: +81-52-747-6442, E-mail: noris@nagoya-u.jp

3P-5

Spontaneous exciton dissociation in carbon nanotubes

Y. Kumamoto, M. Yoshida, A. Ishii, A. Yokoyama, ○T. Shimada, Y. K. Kato

Institute of Engineering Innovation, The University of Tokyo, Tokyo 113-8656, Japan

Simultaneous photoluminescence and photocurrent measurements on individual single-walled carbon nanotubes reveal spontaneous dissociation of excitons into free electron-hole pairs [1]. A simple model is constructed to consistently describe the excitation power and voltage dependence of the photoluminescence and photocurrent. Using this model, we find that a significant fraction of excitons are dissociating before recombination. Furthermore, the combination of optical and electrical signals also allows for extraction of the absorption cross section and the oscillator strength. Our observations explain the reasons for photoconductivity measurements in single-walled carbon nanotubes being straightforward despite the large exciton binding energies.

Work supported by KAKENHI, SCOPE, KDDI Foundation, and the Photon Frontier Network Program of MEXT, Japan.

[1] Y. Kumamoto, M. Yoshida, A. Ishii, A. Yokoyama, T. Shimada, and Y. K. Kato, arXiv:1307.5159 (2013).

Corresponding Author: Y. K. Kato
Tel: +81-3-5841-7702, Fax: +81-3-5841-7772
E-mail: ykato@sogo.t.u-tokyo.ac.jp

3P-6

Quantum interference effect in Raman spectra of metallic nanotubes and graphene

○ Eddwi H. Hasdeo, Ahmad R.T. Nugraha, and Riichiro Saito
Department of Physics, Tohoku University, Sendai 980-8578, Japan

In graphene and metallic single wall carbon nanotubes (m-SWNTs), the existence of gapless linear energy bands (Dirac cones) modify the G band (in-plane optical phonon modes) Raman spectra. One of the well-known phenomena is the Kohn anomaly effect, in which the phonon energy (lifetime) becomes lower (shorter) due to the interaction between the G phonon and an electron-hole pair in the linear energy band [1]. The other phenomenon is the asymmetric spectral shape of the G band, also known as Breit-Wigner-Fano (BWF) line shape, which long been observed in m-SWNTs [2] and recently observed in graphene as a function of Fermi energy [3]. This BWF lineshape asymmetry is still not well explained theoretically. In this presentation, we explain the origin of BWF line shape by means of quantum interference of phonon G band spectra and electronic Raman spectra (ERS). The ERS are electronic spectra whose origin comes from an electron-hole pair excitation in the Dirac cone [4].

In the case of m-SWNTs, the exciton-exciton interaction between a photo-excited exciton and an exciton in the linear band is relevant to the ERS. We calculated ERS spectra as a function of laser excitation energy which schematically reproduces the experimental BWF spectral shape. We found that the direct Coulomb interaction between the two excitons surprisingly vanishes at q=0 because of the symmetry of the two sub-lattices of SWNTs unit cell even though the Coulomb interaction at q=0 is generally considered to be a maximum [5]. In the case of graphene, we use the same method to obtain the electron-electron interaction matrix element and we will present the G band asymmetry as a function of Fermi energy. We also predict that the radial breathing phonon mode (RBM) spectra in m-SWNTs exhibit the opposite BWF asymmetry to that of the G band, by showing the laser energy dependence of RBM spectra.

[1] “Raman spectroscopy in graphene related systems”, A. Jorio et al, Wiley (2011)
[2] S. D. M. Brown et al., Phys. Rev. B 63, 155414, (2001)
[3] D. Yoon et al., Carbon, 61, 373-378, (2013)
[4] H. Farhat et al., Phys. Rev. Lett. 107, 157401 (2011).
[5] E. H. Hasdeo et al.Phys. Rev. B 88, 115107, (2013).

Corresponding Author: E. H. Hasdeo
TEL: +81-22-795-6442, FAX: +81-22-795-6447, E-mail: hasdeo@flex.phys.tohoku.ac.jp

3P-7

Observation of Upconversion Photoluminescence from Single-walled Carbon Nanotubes

○Naoto Akizuki [1], Yuhei Miyauchi [1, 2], Shinichiro Mouri [1], and Kazunari Matsuda [1]

[1] *Institute of Advanced Energy, Kyoto University, Uji, Kyoto 611-0011, Japan*
[2] *Japan Science and Technology Agency, PRESTO, 4-1-8 Honcho, Kawaguchi, Saitama 332-0012, Japan*

Photoluminescence (PL) properties of single-walled carbon nanotubes (SWNTs) have been intensively studied over the past decade because of their potential applications in optoelectronics and bioimaging, as well as for exploring fundamental exciton physics in one-dimensional electronic systems [1]. Here, we report a novel PL property in SWNTs: ability to emit PL by photoexcitation with lower energy photons than those of the emission, which is called upconversion PL (UCPL). UCPL has been attracting much interest related to optical manipulation of phonons in solid, high efficiency solar cells, and bioimaging. Our findings will thus provide a new dimension for the optical application of SWNTs.

The SWNTs were dispersed with 0.2 wt% SDBS in D_2O. Figure 1 shows PL spectra of SWNTs around (6,5) E_{11} exciton peak observed under excitation with higher (2.18 eV, dotted line, normal PL) and lower (1.13 eV, solid line, UCPL) energy photons than (6,5) E_{11} exciton energy (1.26 eV). There are distinct peaks at the photon energy close to (6,5) E_{11} in the both PL spectra. Excitation density dependence of the UCPL intensity is shown in the inset of Fig. 1. The UCPL intensity depends on the excitation density nearly linearly under weak excitation conditions; this result rules out the possibility that the observed UCPL originates from a two photon excitation process that should show a quadratic dependence. On the basis of the observations of temperature and excitation photon energy dependence, the UCPL is attributed to the excitation processes mediated by large energy optical phonons in SWNTs. We will discuss the detailed mechanism of the UCPL, and the further enhancement of the UCPL intensity by introducing lower energy local states in SWNTs.

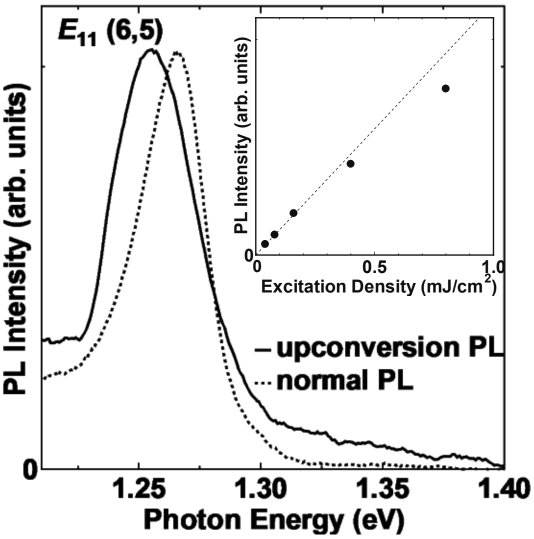

Fig. 1. PL spectra with the excitation photon energy of 2.18 eV (dotted line) and 1.13 eV (solid line) normalized at E_{11} intensity. Upconversion PL spectrum was measured under the pulsed excitation density of 0.13 mJ/cm^2. The inset shows the excitation density dependence of the UCPL intensity.

[1]Y. Miyauchi, J. Mater. Chem. C 1, 6499 (2013)

Corresponding Author: N. Akizuki
Tel: +81-774-38-3465,
E-mail: akizuki.naoto.88x@st.kyoto-u.ac.jp

3P-8

Electronic structures of CNT with a defect under carrier accumulations

○U Ishiyama, Susumu Okada

Graduate School of Pure and Applied Sciences, University of Tsukuba, Tennodai, Tsukuba 305-8577, Japan

Carbon nanotubes (CNTs) are attracting much attention due to its possible application for semiconductor electronic devices in the post-silicon era. It has been shown experimentally that CNTs work as a conducting channel of field-effect transistors(FETs). However, the operating mechanism of the CNT-FET is not fully understood. In particular, it is still unclear how the defects introduced into CNT affect on the electronic properties of CNT under charge accumulation being one of important issues for device applications. In this work, we aim to elucidate the fundamental electronic properties of CNT with an atomic defect under the charge accumulation by the electrode.

All calculations are performed by using the density functional theory. To express the exchange correlation potential among interacting electrons, we apply the local density approximation. We use an ultrasoft pseudopotential to describe the interaction between valence electrons and ions. The effective screening medium (ESM) method is applied to investigate electronic properties of CNT with carriers under the electric field in the framework of the first-principles calculations. Here, we use the (10,0) CNT with a monatomic defect per triple periodicities of CNT along its axis. To simulate the CNT-FET device, we consider the model system shown in Fig. 1, in which CNT is located above the planar electrode simulated by the effective screening medium mimicking the ideal metal electrode.

Figure 2 shows the calculated electrostatic potential of (10,0) CNT with an atomic defect and excess electrons of 0.5e. As shown in Fig. 2, substantial potential modulation occurs around the defect: the potential possesses peak around the defect indicating the electric field concentration around the defect. By evaluating the distribution of the accumulated electrons, we found that the accumulated electrons are mainly distributed around the atomic defect. Therefore, the electric field concentration is ascribed to the carrier concentration around the defect.

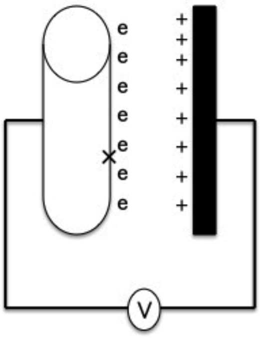

Fig. 1 A structural model of nanotubes under the electric field.

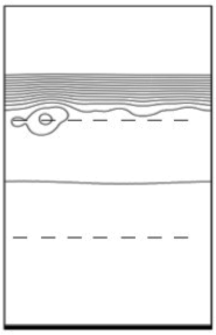

Fig. 2 Electrostatic potential of CNT with an atomic defect under the electric field. Dotted lines denote a wall of CNT.

Corresponding Author: U Ishiyama
Tel: +81-29-853-5600 (ext. 8233), Fax: +81-29-853-5924,
E-mail: sokada@comas.frsc.tsukuba.ac.jp

3P-9

Metal Deposition Effects on Photoluminescence and Raman Scattering Spectra of Suspended Single-walled Carbon Nanotubes

○Akihiko Ozao[1], Shohei Chiashi[2], Genta Yamaguchi[1], Yoshikazu Homma[1]

[1] *Department of Physics, Tokyo University of Science, Tokyo, 162-8601, Japan*
[2] *Department of Mechanical Engineering, The University of Tokyo, Tokyo, 113-8656, Japan*

Photoluminescence (PL) of single-walled carbon nanotubes (SWCNTs) are known to be sensitive to the environment, such as gas, surfactants and dispersants adsorbed on them [1, 2, 3]. However, the effect of metal deposited on SWCNTs has not been analyzed in detail. In this work, we observed the effects of gold and iron deposition on suspended SWCNTs using PL spectroscopy and Raman scattering spectroscopy.

The suspended SWCNTs were grown on a patterned quartz substrate and metals were deposited by vacuum deposition. PL spectra and Raman scattering spectra were obtained before and after the deposition. The deposition and optical measurements were repeated alternately. With depositing metals, PL emission energy shifted depending on the chirality of SWCNT (Fig. 1). Also, the G-band of Raman scattering spectrum, which represents in-plane vibration mode of graphene, down-shifted after deposition. Those PL emission energy shift and G-band down-shift are likely to be caused by axial deformation of SWCNTs due to gold and iron particle formation. And the strain was estimated about 0.1 - 1% (Fig. 2).

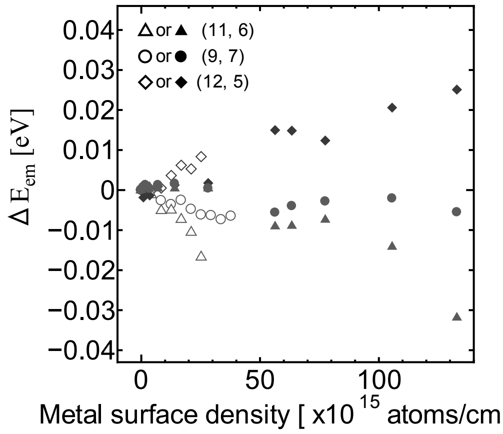

Fig. 1 Metal surface density dependence of PL emission energy shift (ΔE_{em}). Open circles and filled circles are the result of gold deposition and iron deposition, respectively.

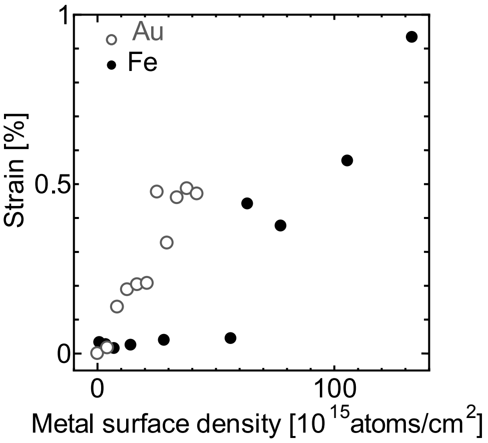

Fig. 2 Estimated strain in SWCNTs as a function of metal surface density.

[1] J. Lefebvre, *et al.*, Appl. Phys. A, **78**, 1107 (2004).
[2] S. Chiashi, *et al.*, Nano Lett., **8**, 3097 (2008).
[3] T. Hertel, *et al.*, Nano Lett., **5**, 511 (2005).

Corresponding Author: Y. Homma
Tel: +81-3-5228-8244, Fax: +81-3-5261-1023,
E-mail: homma@rs.tus.ac.jp

3P-10

NMR study of ^{13}C enriched single-wall carbon nanotubes

○Noboru Serita[1], Yusuke Nakai[1], Yasumitsu Miyata[1,2], Yutaka Maniwa[1],
and Takeshi Saito[3,4]

[1] *Department of Physics, Tokyo Metropolitan University, Hachioji, 192-0397, Japan*
[2] *JST, PRESTO, Kawaguchi, 332-0012, Japan*
[3] *Nanotube Research Center, National Institute of Advanced Industrial Science and Technology (AIST),*
[4] *Technology Research Association for Single Wall Carbon Nanotubes (TASC)*

The bond length between the nearest neighbor carbon atoms (C-C bond length) is an important parameter for the understanding of the physical properties of carbon materials. Although the precise C-C bond lengths of single-wall carbon nanotubes (SWCNTs) have been remained unclear, recent X-ray diffraction measurements revealed the C-C bond lengths of highly-enriched (6, 5) SWCNTs [1]. NMR also has been a useful probe of structural characterization. For instance, the bond length of C_{60} was successfully determined through NMR [2]. The C-C bond length can be estimated from ^{13}C-^{13}C magnetic dipolar coupling that affects ^{13}C NMR spectra. Since the natural abundance of ^{13}C isotope that has a spin I = 1/2 is only 1.1%, it is necessary to enrich ^{13}C isotopes for the investigation of the C-C bond length through the dipolar coupling.

We prepared ^{13}C enriched SWCNTs synthesized by the enhanced direct injection pyrolytic synthesis (e-DIPS) method [3]. By using a density gradient ultracentrifugation method, we removed magnetic impurities from our sample. The obtained ^{13}C-NMR spectra cannot be described only by the usual sp^2 hybridized orbital [4], but appear to require ^{13}C-^{13}C dipolar interaction as well. In this presentation, we report our experimental data in detail and discuss the origin of the ^{13}C NMR spectra.

[1] R. Mitsuyama *et al*., submitted.
[2] C. S. Yannoni *et al*, J. Am. Chem. Soc., **113**, 3190 (1991)
[3] T. Saito *et al*., J. Nanosci. Nanotech. **8**, 6153 (2009).
[4] K. Matsuda *et al*., J. Phys. Soc. Jpn. **82**, 015001 (2012).

Corresponding Author: Y. Nakai
Tel: +81-42-677-2498, Fax: +81-42-677-2483, E-mail: nakai@tmu.ac.jp

3P-11

Numerical study of electronic states in double-walled carbon nanotubes ---Formation of metallic bands by covalent bridge between tubes---

Yuhei Natsume

Department of Physics, Chiba University, Chiba 263-8522, Japan

Band structure calculation has been made for double-walled carbon nanotubes (DWCNT) by Atomistix ToolKit [1].

Tough the interaction between tubes is attributed to Van der Waals forces, the covalent bridge appears in Bloch states at Fermi surfaces. As a result, we get the metallic bands in DW CNT, even for cases where DWCNT is composed of inner and outer CNT's with energy gaps [2]. In short, the Fermi surfaces are induced from bonding-aintibonding splitting between CNT's. Such the splitting occurs both for LUMO's and HOMO's.

As a typical example of numerical calculation, we show the electron density for covalent bands in 2s and 2p levels in Fig.1, where semiconducting (8,0) CNT is surrounded by semiconducting (13,0) CNT. The ratio of radiuses is 1.62. The axis of tubes are the z-direction. As far as the distribution of total density, the Van der Waals interaction plays an important role. For overall properties, the states of inner CNT are independent of those of outer CNT.

In contrast, Bloch states at Fermi levels present quite different features as shown in Fig.2. In fact, we find the bridge between inner CNT and outer CNT, which has covalent characters. We would like to emphasize that multiwalled CNT's have a strong tendency to acquire metallic properties.

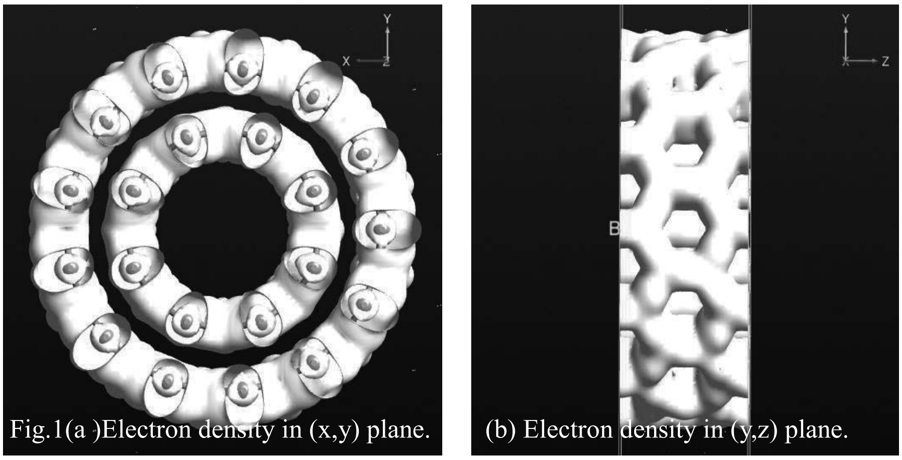

Fig.1(a)Electron density in (x,y) plane. (b) Electron density in (y,z) plane.

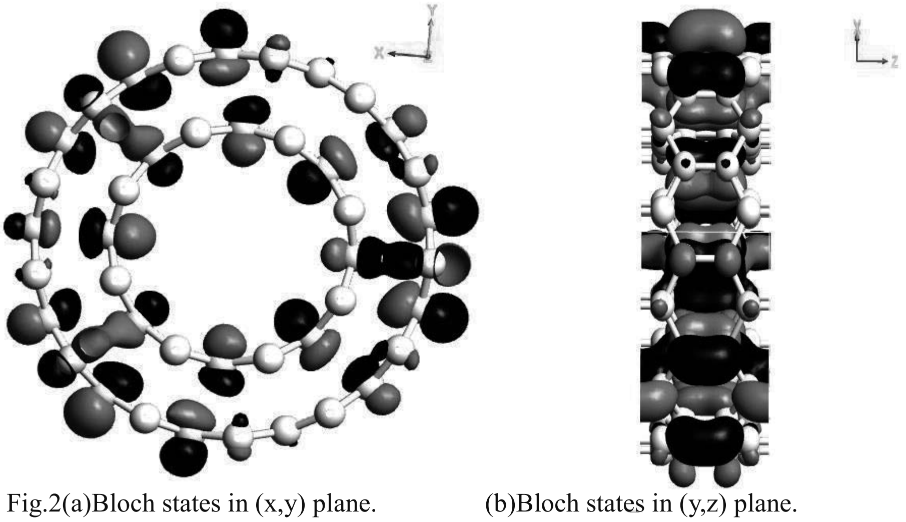

Fig.2(a)Bloch states in (x,y) plane. (b)Bloch states in (y,z) plane.

[1]Atomistix ToolKit & Virtual NanoLab, Quantum Wise Japan, Shinjyuku, Tokyo, Japan http://www.quantumwise.co.jp/
[2] H.-S.Philip Wong and Deji Akinwande,"Carbon Nanotube and Graphene Devise Physics", (Cambridge University Press, 2011).

Corresponding Author:
Y. Natsume
Tel: +81-43-204-6260,
Fax:+81-43-204-6261
natsume@faculty.chiba-u.jp

3P-12

Electronic Structure of Carbon and BN Nanotubes: A Comparative First Principles Study

○Yuya Uchida, Takashi Koretsune, and Susumu Saito

Department of Physics, Tokyo Institute of Technology,
2-12-1 Oh-Okayama, Meguro-ku, Tokyo 152-8551, Japan

Carbon nanotubes have been intensively studied both theoretically and experimentally for last two decades due to its characteristic electronic properties. Because of the large unit cell sizes of general chiral nanotubes, the detailed electronic and geometric structures were not understood well. In our previous research, we have studied the electronic and geometric structures of carbon nanotubes with various chiralities systematically for the first time using the helical symmetry[1].

In this study, we report the electronic structures of BN nanotubes with various chiralities obtained by the local density approximation in real-space density functional theory(DFT). By extending the helical-symmetry DFT program for carbon nanotubes to BN nanotubes, we now can investigate BN nanotubes of all chiralities with small unit cell including only two atoms. We study the carbon and BN nanotubes comparatively(Fig.1), and discuss the chirality dependence of the electronic properties of BN nanotubes.

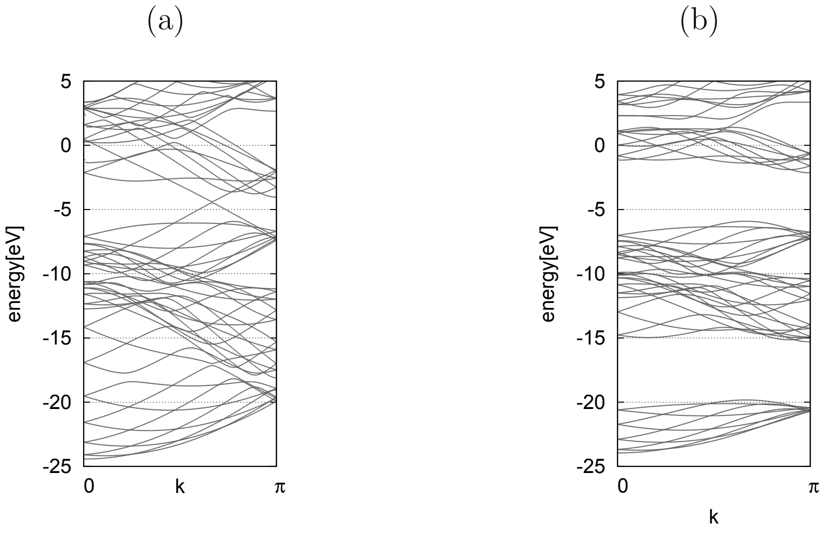

Figure 1: Band structures of (a)(9,0)Carbon nanotube and (b)(9,0)BN nanotube

[1]K. Kato, T. Koretsune, and S. Saito, Physical Review B **85** 115448 (2012).

Corresponding Author: S. Saito
E-mail: y-uchida@stat.phys.titech.ac.jp

3P-13

Photoconductivity spectroscopy of individual suspended carbon nanotubes

T. Uda, Y. Kumamoto, M. Yoshida, A. Ishii, Y. K. Kato

Institute of Engineering Innovation, The University of Tokyo, Tokyo 113-8656, Japan

To investigate photoconductivity of chirality-identified carbon nanotubes, we have fabricated field-effect transistors with individual air-suspended nanotubes [1]. Trenches are etched into SiO_2/Si substrates, and Pt/Ti are deposited on both sides of the trenches. By ethanol chemical vapor deposition, carbon nanotubes are grown over the trenches. We have also constructed a system which can simultaneously measure photocurrent and photoluminescence excitation spectra [2]. Nanotubes are excited with a wavelength-tunable continuous wave Ti:sapphire laser, and photoluminescence is detected by an InGaAs photodiode array attached to a spectrometer. Photoluminescence imaging and excitation spectroscopy allows us to locate the nanotubes and identify their chirality. For photocurrent microscopy, excitation laser is modulated by an optical chopper and a lock-in amplifier is used for detection.

Work supported by KAKENHI, KDDI Foundation, and the Photon Frontier Network Program of MEXT, Japan.

[1] S. Yasukochi, T. Murai, S. Moritsubo, T. Shimada, S. Chiashi, S.Maruyama, and Y. K. Kato, Phys. Rev. B **84**, 121409 (2011).
[2] Y. Kumamoto, M. Yoshida, A. Ishii, A. Yokoyama, T. Shimada, and Y. K. Kato, arXiv:1307.5159 (2013).

Corresponding Author: Y. K. Kato
Tel: +81-3-5841-7702, Fax: +81-3-5841-7772
E-mail: ykato@sogo.t.u-tokyo.ac.jp

3P-14

Environment-Friendly Functionalization Method to Obtain Water-Dispersible Carbon Nanotubes

Mohammad Jellur Rahman[1], ○Tetsu Mieno[1,2]

[1]Graduate School of Science and Technology, Shizuoka University, Shizuoka 422-8529, Japan
[2]Department of Physics, Shizuoka University, Shizuoka 422-8529, Japan

Carbon nanotubes (CNTs) are promising candidates for microelectronics, polymer composites, biochemistry, pharmaceuticals, and medical engineering, due to their unique mechanical and electrical properties [1,2]. To realize the applications strategic approaches toward their stable dispersion in liquids are necessary. For this, usually harsh chemical processes are followed, which degrade their properties and are not environmentally safe [3]. Therefore, enhancement of dispersibility preserving their properties is a crucial issue. We have developed an easy and environment-friendly method to functionalize both single-walled and multiwalled CNTs (SWNTs and MWNTs) using citric-acid-assisted RF oxygen plasma treatment, which is less destructive to their structure. Pristine SWNTs and MWNTs are pretreated in pure ethanol and dried under reduced pressure. Then, they are wetted by citric acid solution and placed in a RF (13.56 MHz) plasma chamber. Finally, oxygen plasma reaction is operated on the wet CNTs under optimum condition. The resultant CNTs can be easily dispersed in pure water owing to the attachment of a large number of carboxyl groups onto their surfaces. Dispersibility is observed by the UV-visible spectroscopy, precipitation tests, and transmission electron microscopy. Successful attachment of the carboxyl groups is confirmed by the Fourier transform infrared spectroscopy and thermogravimetric analysis. Preservation of the structural quality is verified by Raman spectroscopy, which suggests the preservation of their basic properties. These water-dispersible CNTs are good candidates for electronic coating industries, composite technology and biomedical engineering.

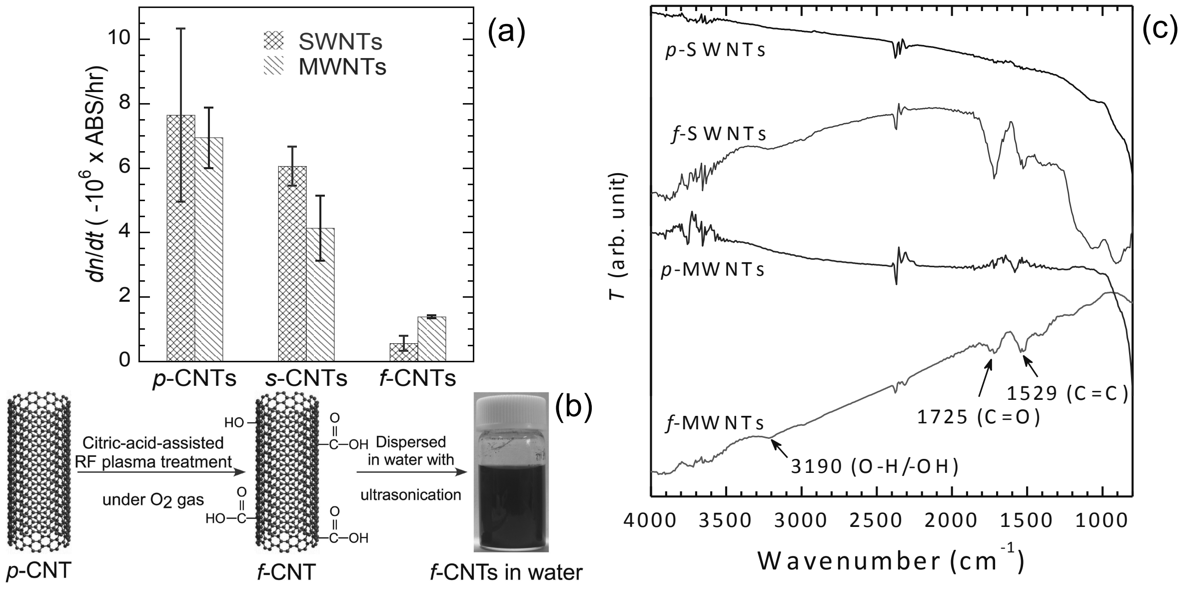

Fig.1 (a) Settling speed, *dn*/*dt*, calculated from the Abs (250 nm) versus time graphs for the pristine CNTs (*p*-CNTs), sonicated CNTs (*s*-CNTs), and functionalized CNTs (*f*-CNTs). (c) Schematic of the production of stable suspension. (a) FT-IR spectra of the pristine and functionalized SWNTs and MWNTs.

[1] M. F. L. De Volder, *et al.* Science **339**, 535 (2013). [2] M. Endo, *et al.* in *Carbon nanotubes-Topics in Applied Physics*, (Springer, Heidelberg, 2008). [3] A. Hirsch, O. Vostrowsky, Top. Curr. Chem. **245**, 193 (2005).
Corresponding Author: T. Mieno, Tel. and Fax: + 81-54-238-4750, E-mail: sptmien@ipc.shizuoka.ac.jp

3P-15

A Test for the growth of single-wall carbon nanotubes on the porous glass (PG) sheet by ACCVD technique

Kyohei Nagao[1], ○Shinzo Suzuki[1], Shinji Ogami[1], Yosuke Ito[1],
Hiroshi Nagasawa[2], Yohji Achiba[3]

[1]*Department of Physics, Kyoto Sangyo University, Kyoto 603-8555, Japan*
[2]*Nano-support Co., Ltd., Kanagawa 251-0024, Japan*
[3]*Department of Chemistry, Tokyo Metropolitan University, Tokyo 192-0397, Japan*

Abstract:

ACCVD technique has been widely used in the field of single-wall carbon nanotube (SWNT) growth, partly because that the ambient temperature suitable for the formation of SWNTs is relatively lower (typically, less than 800°C), and the purity of SWNTs in as-grown material is better than those obtained by other technique, e.g. arc-burning procedure.

In 2005, Aoki et al., reported about the formation of SWNTs in the porous glass (PG) material by using ACCVD technique [1], where a kind of metal particles (e.g. Co particles) were deposited on the PG material before ethanol was introduced as carbon source for making SWNTs in the PG material. The advantage of using PG material is that, it is very easy to make any kind of shape (rod, sheet.., etc.) made of PG, which implies that the as-grown PG-SWNT complex itself is expected to be used as an optical or other kind of device.

In this presentation, in order to investigate the growth of SWNTs on the porous glass sheet by PG-ACCVD technique, four different kinds of PG-sheet were prepared (shown in Figure 1), where each average pore size (diameter) is controlled to 10nm, 30nm, 50nm, and 100nm, respectively. After optimizing the condition for the PG-ACCVD process in our apparatus, a test for the growth of SWNTs is planned.

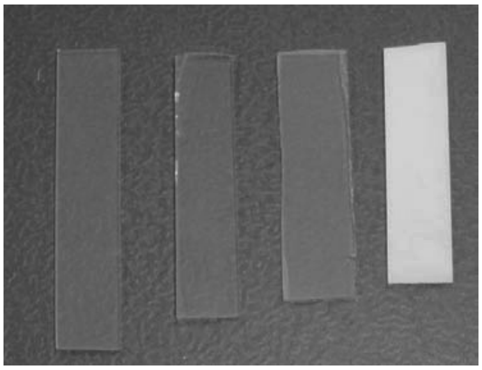

Figure 1. Four different kinds of PG-sheet (8mm width, 1mm thickness), where the average pore-size is 10nm, 30nm, 50nm, and 100nm (from the left to the right).

References:

[1] Y. Aoki, S. Suzuki. S. Okubo. H. Kataura, H. Nagasawa, and Y. Achiba, *Chem. Lett.*, **34**, 562(2005).

Corresponding Author: Shinzo Suzuki
Tel: +81-75-705-1631, Fax: +81-75-705-1631,
E-mail: suzukish@cc.kyoto-su.ac.jp

3P-16

Molecular recognition on external grooves of bundled surfaces of single-walled carbon nanotubes

○Tsuyohiko Fujigaya[1,2], JongTae Yoo[1], and Naotoshi Nakashima[1,2,3]

[1]Department of Applied Chemistry, Graduate School of Engineering, Kyushu University, 744 Motooka, Fukuoka 819-0395, Japan
[2]World Premier International (WPI), International Institute for Carbon-Neutral Energy Research, Kyushu University 744 Motooka, Nishi-ku, Fukuoka 819-0395, Japan
[3]Japan Science and Technology Agency, CREST, 5 Sanbancho, Chiyoda-ku, Tokyo, 102-0075, Japan

Recently, one-dimensional nano-spaces in the bundle of single-walled carbon nanotubes (SWNTs) such as interstitial channel and external groove attract attentions in experimentally and theoretically due to their intense van der Waals interaction with molecules. Here, we investigated an effect of SWNT bundle for SWNT-molecular interaction using the affinity chromatography [1] incorporating SWNT bundles as a stationary phase.

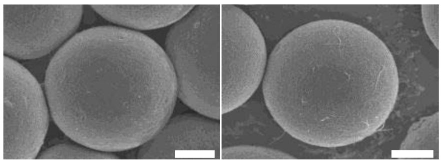

Fig. 1 SEM images of silica gel coated by (A) isolated and (B) bundled SWNTs. Scale bars: 1 μm.

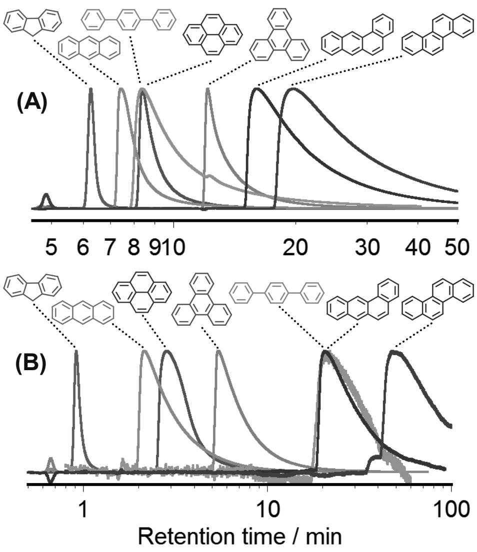

Fig. 2 Chromatograms of PAHs using (A) isolated and (B) bundled SWNTs as stationary phase at flow rates of (A) 0.1 and (B) 0.7 mL/min.

In a preparation of the stationary phase, different concentrations of SWNT dispersions in 1-methyl-2- pyrrolidinone (NMP) were mixed with silica sphere and the precipitates were collected [2]. As shown in SEM images, bundled structures of SWNTs were observed on the silica surface prepared from higher concentration (**Fig. 1B**), while such a structure was hardly seen on that from lower one (**Fig. 1A**).

Quite interestingly, we noticed the changes of the order of retentions between isolated and bundled SWNTs caused by the unusual behavior of *p*-terphenyl in the chromatograms (**Fig. 2**) and the result suggests the specific recognition of bundled SWNTs for *p*-terphenyl. We consider that *p*-terphenyl strongly interacts with the one-dimensional external groove in the SWNT bundle due to its structure. Also diameter dependency of the degree of groove recognition was observed [3].We believe that this unique aspect will provide a promising feature for new applications of SWNTs.

[1] J. Yoo et al., *Nanoscale* **2011**, *3*, 2517.
[2] T. Fujigaya et al., *Carbon* **2011**, *49*, 468.
[3] J. Yoo et al., *Nanoscale* **2013**, *5,* 7419.

Corresponding Author: Naotoshi Nakashima
E-mail: nakashima-tcm@mail.cstm.kyushu-u.ac.jp
Tel & Fax: +81-92-802-2842

3P-17

Fabrication and Properties of Functionalized Multiwall Carbon Nanotube/ PA-6 Composite

○Yoshimi Muraoka, Hiroki Sato, Masaru Sekido

Department of Material Science and Engineering, Sendai National College of Technology, Natori 981-1239, Japan

Due to their combination of outstanding mechanical characteristics, extremely large inter-facial contact area, high aspect ratio, and low mass density, CNTs are considered as the ideal reinforcement fillers for the nanocomposite materials. The challenges for the development of high-performance CNTs/polymer nanocomposites are homogeneous dispersion of CNTs in polymeric matrix. For this purpose we have developed simple solution-evaporation method using functionalized Multiwall Carabon Natotubes(MWCNTs) followed by mechanically melt-compounding for the fabrication of composites.

MWCNTs were functionalized by using 1,3-dipolar cycloaddition reaction to obtain water-soluble functionalized MWCNTs. MWCNTs (200 mg) were mixed with N-methylglycine (2.0 g) and 3,4-dihydroxybenzaldehyde (2.0 g) in DMF (500 mL) and the reaction mixture was stirred at 120 ^{o}C for 5 days. After removing DMF under reduced pressure remaining precipitate was washed with water and acetone to give functionalized MWCNTs. The obtained functionalized MWCNTs were used as filler for the nanocomposites without further purification.

MWCNTs/nylon-6 (PA6) nanocomposites have been prepared by simple melt-compounding and tensile strength was compared with various loading of MWCNTs. In the present study we report the effect of MWCNTs and functionalized MWCNTs loading for the improvement of mechanical properties of nanocomposites.

Corresponding Author: M. Sekido
Tel: +81-22-381-0329, Fax: +81-22-381-0329
E-mail: sekido@sendai-nct.ac.jp

Printed SWCNT thin film CMOS inverters based on chemically doped ion gels

○Yoshifumi Wada [1], Ryota Inukai [1], Taiyo Fujimoto [1], Hiroki Hamahata[1], Satoki Matsuzaki [1], Kazuhiro Yanagi [2] and Taishi Takenobu [1,3]

[1] *Department of Applied physics, Waseda University, Tokyo 169-8555, Japan*
[2] *Department of Physics, Tokyo Metropolitan University, Tokyo 192-0397, Japan*
[3]*Kgami Memorial Laboratry, Waseda University, Tokyo 169-0051, Japan*

Single-walled carbon nanotubes (SWCNTs) have been of high interest due to their excellent performance such as high mobility, flexibility and printability. Recently, SWCNT thin films, the random networks of SWCNT, open the route for the application as printable semiconductors.[1] Though there was problem of trade-off with on/off ratio and current density, electrolyte-gated transistors (EGTs) of SWCNT thin film realized ambipolar switching with high on/off ratio ($>10^5$) in low voltage (<2V).[2] Importantly, SWCNT thin film EGTs are achievable using ion gels, which is one of the printable solid electrolytes. Thus, it is expectable to fabricate low-voltage logic circuit with printing method. The first step to logic circuit is the fabrication of CMOS inverters. To fabricate a CMOS inverter, both p- and n-type transistors are needed. Because SWCNT thin film EGTs are ambipolar characteristics, the point to control polarity is turn-on voltage, which is controllable by the chemical doping using donative organic molecules.[3] However, the combinations of donative organic molecules and ion gels for EGTs have not been reported.

Here, we fabricated CMOS inverters based on n-type and ambipolar SWCNT thin film EGTs (Fig.1). First, SWCNT thin films were fabricated by ink-jet printing method. Then, Au/Ni electrodes were fabricated by vacuum evaporation as source and drain electrode. Ion gels were fabricated on a SWCNT thin film by drop-cast method. After dropping ion gels, Au foil was placed on ion gel as gate electrode. To change turn-on voltage of EGTs, we added polyethylenimine (PEI) as donative polymer of ion gel. By adding PEI to ion gels, we could change turn-on voltage of EGTs. Finally we fabricated CMOS inverters and obtained low-voltage (1.5V) operation with maximum gain of 28 (Fig.2). This method has potential to achieve vacuum-process-free logic circuits with applying metallic SWCNT thin-film electrodes.

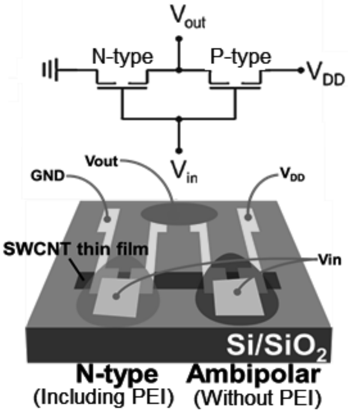

Fig.1 SWCNT thin film CMOS inverter based on EGTs

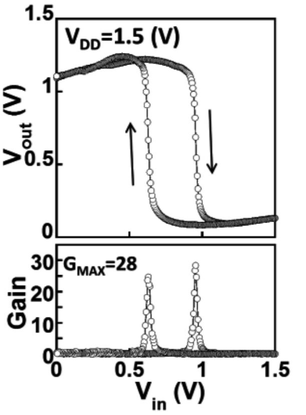

Fig.2 Transfer characteristics of SWCNT thin film inverter

[1] H. Okimoto *et al*. J.J.Appl. Phys. 48, 06FF03 (2009).
[2] M. Ha *et al.* Nano Lett. 13, 954 (2013)
[3] R. Shimizu *et al.* Appl. Phys. Express 5, 125102 (2012)

Corresponding Author: T. Takenobu
Tel: +81-3-5286-2981, Fax: +81-3-5286-2981,
E-mail: takenobu@waseda.jp

3P-19

Surface modification of multi-walled carbon nanotubes with benzyl radical derivatives generated by photo-irradiation

○Tomoya Takada[1], Batbuyan Munkh-od [1], Shigeaki Abe [2]

[1] *Department of Materials Chemistry, Asahikawa national College of Technology, Asahikawa 071-8142, Japan*
[2] *Graduate School of Dental Medicine, Hokkaido University, Sapporo 060-8586, Japan*

Surface modification of carbon nanotubes (CNTs) is an essential subject for their industrial application, since homogeneous dispersion of CNTs in solvents are effectively enhanced by appropriate surface modification. In addition, functional groups introduced by surface modification of CNTs act as reaction sites for subsequent bond formation with, for example, other organic molecules and polymers. Many methods for the surface modification have been reported previously. However, modification methods employing photochemical reactions have been scarcely studied. In this work, a simple method for the surface modification of CNTs with radicals formed by photo-irradiation was developed. Benzyl radical derivatives were employed in this study; these radical derivatives can be smoothly generated by bond cleavage of benzyl halide derivatives. In general, CNTs are capable of capturing radicals through covalent bonds (Fig. 1). Therefore, applying the photochemical radical generation, development of a novel one-pot surface modification method of CNTs is expected.

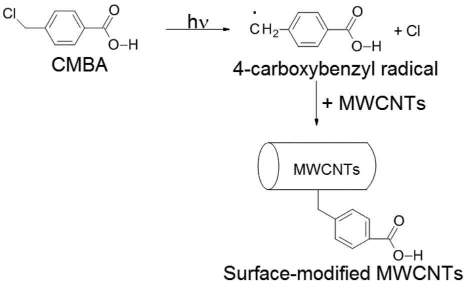

Fig. 1 Scheme of the surface modification in this work

As a radical source, 4-(chloromethyl)benzoic acid (CMBA, Wako Chemicals, Co. Ltd.) was used in this work. CMBA and multi-walled carbon nanotubes (MWCNTs, diameter 10-30 nm, Wako Chemicals, Co. Ltd.) were added into dimethylformamide (DMF) and then dispersed by sonication. Light from an Xe lamp (wavelength 300-600nm) was irradiated to the mixture at room temperature for 24 hours. During the irradiation, oxygen in the mixture solution was purged with Ar gas. MWCNTs after the irradiation were filtered, washed and dried in the air. Amount of the 4-carboxyl benzyl radicals introduced on the MWCNTs surface was determined by conventional acid-base back titration; carboxyl groups attached on MWCNTs were neutralized with sodium hydroxide (NaOH) aqueous solution, and the amount of residual NaOH was then measured by titration with hydrochloric acid (HCl).

On the basis of the back titration results, partial neutralization of NaOH aqueous solution caused by carboxybenzyl groups introduced on MWCNTs was confirmed. In addition, dispersibility of the modified MWCNTs in water was drastically improved compared to that of pristine MWCNTs. These results indicate that carboxybenzyl groups generated by photo-induced C-Cl bond cleavages are successfully attached to the MWCNTs surface. Other results (for example, effect of the addition of triphenylamine as an electron generator) will also be shown in the symposium. This work has been supported by JSPS KAKENHI (Grant-in-Aid for Scientific Research (C)) No. 25420814.

Corresponding Author: T. Takada
Tel/Fax: +81-166-55-8036 , E-mail: takada@asahikawa-nct.ac.jp

3P-20

“Laminated” ion-gel film as high capacitance insulator for carbon-nanotube transistor

○Taiyo Fujimoto [1], Ryo Shimizu [1], Yuki Takagi [1], Yoshifumi Wada [1], Kazuhiro Yanagi [2],
Taishi Takenobu [1,3]

[1] *Department of Applied Physics, Waseda University, Shinjuku 169-8555, Japan*
[2] *Department of Physics, Tokyo Metropolitan University, Hachioji 192-0397, Japan*
[3] *Kagami Memorial Laboratory, Waseda University, Tokyo 169-0051, Japan*

Ion gel, which is a mixture of ionic liquid and organic polymer is promising candidates for gate dielectrics of field effect transistor due to exceptionally large specific capacitances [1]. Recently, low voltage operation of carbon-nanotube transistors based on the ion gel has been already performed [2] and proved the usefulness of ion gel in reduction in consumed electric power. Realization of three-dimensional integrated circuits has strongly been desired in order to improve both functionality and energy efficiency. However, still, ion gel is not suitable for insulator of three-dimensional integrated circuits, because specially controlled deposition of ion-gel films with arbitrary film thickness has not been established. Therefore, in this study, we focus on the "laminating" method, in which ion gel is deposited on plastic substrate and, then, whole films are laminated on semiconducting carbon nanotube films for fabricating transistors.

Figure 1 shows a schematic illustration of fabrication process by the laminate method. Semiconducting single-walled carbon nanotube (S-SWCNT) thin film was formed on Si/SiO_2 substrate by inkjet printing and Au was evaporated as source, drain and side-gate electrodes. On the other hand, ion gel was spin coated on polyimide substrate and cut into enough size to be used as insulator of transistors. Finally, ion gel was laminated to Si/SiO_2 substrates. As shown in transfer characteristics of Fig. 2, the fabricated nanotube transistor showed ambipolar transport with low-operation voltage, suggesting the effectiveness of laminating method.

In summary, we succeeded in both specially controlled deposition of ion-gel films with arbitrary film thickness and the fabrication of ambipolar nanotube transistors, which is important first step for the three-dimensional ion-gel devices.

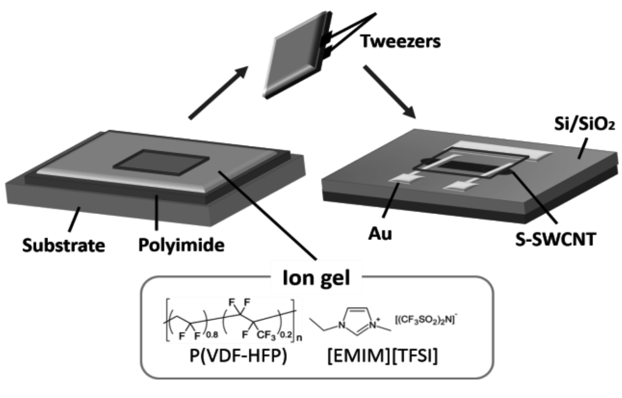

Fig.1 Schematics of side-gated EDLT fabricated by the laminate method

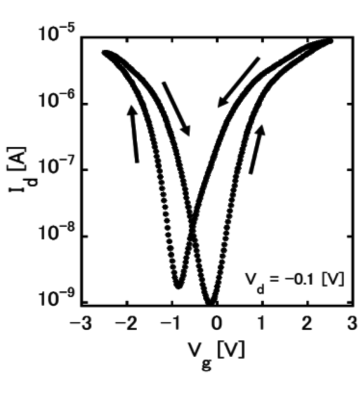

Fig.2 Transfer characteristic

[1] J. Lee *et al, J. Am. Chem. Soc.* **2007** , *129* , 4532 ., [2] M. Ha *et al,* Nano Lett. 2013, 13, 954.,
Corresponding Author: Taishi Takenobu, Tel&Fax: +81-3-5286-2981, E-mail: takenobu@waseda.jp

3P-21

Polyglycerol-functionalized single-walled carbon nanotubes for drug loading and delivery

○Hongmei Qin, Li Zhao, Keisuke Nakamura, Takahide Kimura and Naoki Komatsu

Department of Chemistry, Shiga University of Medical Science, Seta, Otsu 520-2192, Japan

A variety of nanoparticles have been investigated as a nonviral vector in drug and gene delivery systems. Among these nanoparticles, single-walled carbon nanotubes (SWNTs) have attracted a great deal of attention because of their large specific surface area and hydrophibic nature. In addition, various functions can be added to SWNTs through organic reactions on the SWNT surface and edges. Recently, we have found that polyglycerol (PG) can graft onto nanoparticles (nanodiamond [1], ZnO [2] and Fe_3O_4 [3]) and afford very good hydrophilicity and biocompatibility. In this study, we apply this methodology to the synthesis of PG-functionalized SWNTs (SWNT-PG).

After mixed acid treatment, the resulting SWNTs containing carboxyl groups at the edges were allowed to react with glycidol to give SWNT-PG through ring opening polymerization. The SWNT-PG exhibited good solubility and stability not only in water (>15.9 mg/mL), but also phosphate buffer saline (PBS) (>10.5 mg/mL), making the in vivo use of SWNT more promising in biomedical applications. In addition, a large hydrophobic sidewall surface area is expected to provide high loading capacity of aromatic molecules including a cancer drug, doxorubicin (DOX), through π-π stacking and hydrophobic interaction. After simple mixing of the SWNT-PG solution with DOX at pH 8 overnight, SWNT-PG-DOX complexes was formed and free, unbound DOX in solution was removed by washing. DOX-loading on SWNTs were confirmed by the red-shift of the absorption around 480nm (Fig 1a) and the quenching of fluorescence (Fig 1b).

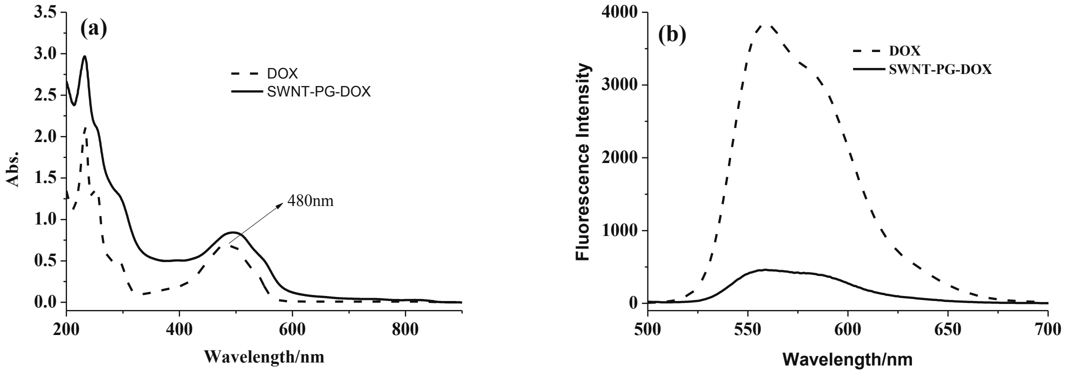

Fig. 1. Absorption (a) and fluorescence (b) spectra of free DOX and SWNT-PG-DOX with the same DOX concentration (excitation at 480 nm).

[1] L.Zhao, N. Komatsu, et al. Angrew. Chem. Int, Ed., 50, 1388-1392 (2011)

[2] L.Zhao, N. Komatsu, et al. J. Indian Chem. Soc., 88, 1787-1790 (2011)

[3] L.Zhao, N. Komatsu, et al. Adv. Funct. Mater., 22, 5107-5117 (2012)

Corresponding Author: Naoki Komatsu

Tel: +81-77-548-2102, Fax: +81-77-548-2405, E-mail: nkomatsu@belle.shiga-med.ac.jp

3P-22

Simple and loss-free printing of carbon nanotubes for flexible electronics

○Hiroyuki Shirae, Dong Young Kim, Kei Hasegawa, and Suguru Noda*

Department of Applied Chemistry, Waseda University, Tokyo 169-8555, Japan

Carbon nanotubes (CNTs) are an attractive candidate material for electrodes and wirings in flexible electronic devices owing to their fair electric conductivity, excellent stability in ambient, flexibility, and compatibility with printing processes. Their uniform films with excellent conductivities have been realized through mild dispersion followed by centrifugation and printing, however a significant fraction of expensive CNTs are wasted during centrifugation. Moreover, in the fabrication of patterned electrodes/wirings, photo- or electron-beam lithography is often applied to the uniform films, which causes additional loss of CNTs. Toward the practical application of CNTs to flexible electronics, simple and loss-free printing of conductive CNT films is highly demanded.

In this work, we propose and examine a repetitive dispersion-centrifugation process, which minimize the damage to CNTs via mild dispersion and the material loss of CNTs via reuse of undispersed CNTs. We also propose and examine a filtration process using a metal mask with a membrane filter, which yields patterned CNT films with minimal material loss.

We used the sub-millimeter-long few-wall carbon nanotubes (FWCNTs) synthesized by our fluidized-bed chemical vapor deposition process at a high carbon yield ~ 70% [1]. FWCNTs were added at 0.01 wt% to the 0.5 wt% aqueous solution of sodium dodecylbenzenesulfonate (SDBS). Ultrasonication (40 W, 40 kHz) was applied for 3 min to the solution in iced water bath and then centrifugation was applied to the solution at 3500 rpm for 10 min. Supernatant (1/4 of the solution) was taken out and the same amount of the SDBS aqueous solution was added to the solution. A CNT film was made from the sampled supernatant via vacuum filtration over a polytetrafluoroethylene (PTFE) membrane filter and washed with hot water. These processes are repeated for ~ 10 cycles and the weight and conductivity of the film were evaluated for each cycle.

By using a metal mask during vacuum filtration, CNT line patterns were easily formed on the filter, which were then transferred to polyethylene terephthalate (PET) films (Fig. 1). Without using the metal mask, uniform CNT films were easily formed on the filter, which can be self-supporting (Fig. 2). Uniform CNT films with steady weight and conductivity were formed from the 3rd to 11th cycles via repetitive dispersion-centrifugation process (Fig. 3).

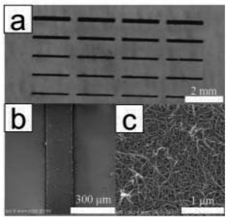

Fig. 1 Photo (a) and SEM images (b,c) of CNT lines on PET.

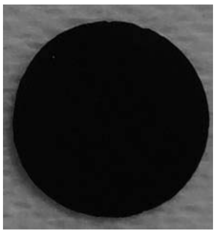

Fig. 2 A photo of a self-supporting CNT film.

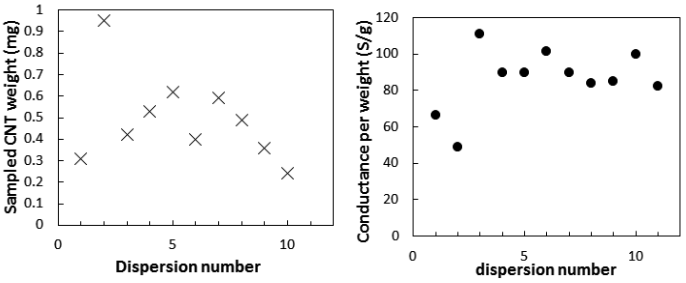

Fig. 3 Weight (left) and normalized conductance (right) of uniform CNT films prepared at different cycles.

[1] D.Y. Kim, et al., *Carbon* **49**, 1972 (2011).

Corresponding Author: S. Noda, Tel&Fax: +81-3-5286-2769, E-mail: noda@waseda.jp

3P-23

Chemical Vapor Deposition of MoS_2 on Carbon Nanotube for Organic Thin Film Solar Cells

○Il Jeon,[1] Dai Kutsuzawa,[2] Yu Hashimoto,[2] Takashi Yanase,[2] Taro Nagahama,[2]
Toshihiro Shimada,[2] and Yutaka Matsuo[1]

[1]*Department of Chemistry, School of Science, The University of Tokyo, 7-3-1 Hongo, Bunkyo-ku, Tokyo 113-0033, Japan*
[2]*Division of Materials Chemistry, Faculty of Engineering, Hokkaido University, Kita-ku, Sapporo 060-8628, Japan*

Making bulk heterojunction using high mobility n-type semiconductors is one of the challenges in fabricating high performance organic thin film solar cells. One strategy is to use inorganic nanowires as n-type semiconductors because they will show high charge mobility with morphology suitable for the bulk heterojunction. However, this approach has not been successful so far because of the transport barriers and charge traps present on the surface of the nanowires[1]. In this work, we attempted growing nanowires of layered semiconductor MoS_2, which can be used as an n-type semiconductor. Since the layered materials do not have dangling bonds on the surface, the charge traps will not be present on the surface in principle. Since there are layered materials with a variety of constituent elements, we can tune their LUMO levels by choosing suitable materials[2]. In order to control the morphology of MoS_2, we have used atmospheric chemical vapor deposition using MoO_3 and S as sources on bundles of single wall carbon nanotubes (SWCNT).

Figure 1 shows the TEM image, local Auger electron spectrum (AES) and Raman spectra of MoS_2 grown on SWCNT. Hexagonal plates are surrounding SWCNTs, which were identified as MoS_2 by AES and Raman. The MoS_2-covered SWCNT was dispersed in ethanol and was scattered on TiO_2 nanocrystal layer / ITO. P-type semiconductor P3HT was spin-coated on it and its power conversion efficiency ( ) was measured. A sample with pristine SWCNT without MoS_2 was prepared for comparison. As a result, we obtained =0.46% for a cell containing MoS_2-SWCNT and =0% for SWCNT.

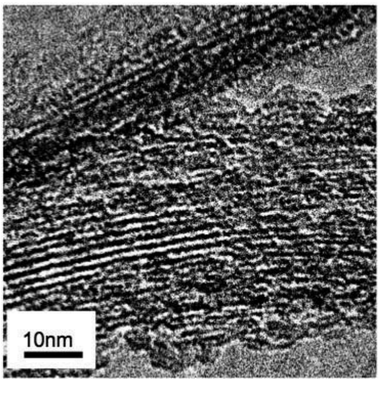

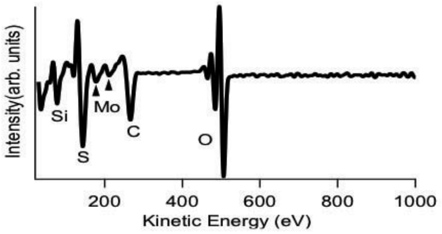

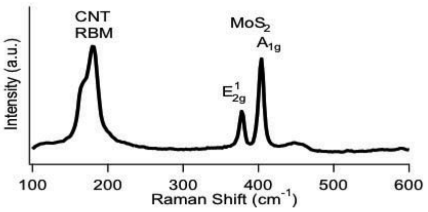

[1] K. Takanezawa, K. Tajima, K. Hashimoto, Appl. Phys. Lett. 93, 063308 (2008).
[2] T. Shimada, F. S. Ohuchi, B. A. Parkinson, Jpn. J. Appl. Phys. 33, 2696 (1994).

Corresponding Author: Y. Matsuo & T. Shimada
TEL/FAX: +81-3-5841-1476; TEL/FAX: +81-11-706-6576
E-mail: matsuo@chem.s.u-tokyo.ac.jp, shimadat@eng.hokudai.ac.jp

3P-24

Dispersion of SWCNTs in Wrapping of Belt-Type π-Conjugated Polymer

Wataru Sagawa[1], ○Masahiro Takahashi[1], Keiki Kishikawa1[1], Shigeo Kohmoto[1]

[1] *Faculty of Engineering, Chiba University, Chiba, 263-8522, Japan*

Scheme 1 Wrappings of CNT and fullerene with belt-type π-conjugated polymer.

By making multiple π conjugated systems connect with controlling the joint direction by an ethynyl group, we aimed at construction of the "belt type π conjugated polymer" which can transform the mainl chain into a two-dimensional plan. The following advantages are acquired, when a complex is formed so that this macromolecule may wrap in CNT, fullerene, etc. (i) Since the flexible region of the macromolecule is restricted, the rise of delta S is suppressed. (ii) Since multiple π-π interactions (large delta H) are created by cylindrical π conjugation face, efficiently inclusion (big delta G) is expected (Scheme 1).

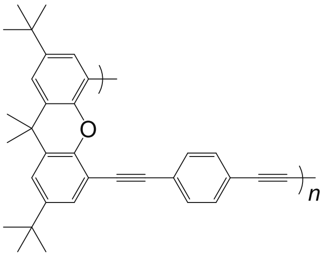

Fig. 1 Structure of polymer **1**.

Table 1. Properties of Polymer **1**.

$\overline{M}_{\mathrm{w}}$ [a)]	PDI[a)]	*n*
2.6×10^{3}	1.6	5.8

a) Measured by GPC with polystyrene standards.

Alternating copolymerization of the diethynylbenzene was carried out to diiodoxanthene by the Sonogashira coupling reaction, and Polymer 1 was obtained as yellow powder of the weight average molecular weight 2,600 (Fig.1, Table 1). Ultrasonic churning of CoMoCAT(1 mg), and Polymer 1(10 mg) was carried out in THF(10mL), and dark black dispersion was obtained. Even if it centrifuged this SWNTs dispersed solution (10,000G, 10 min), the supernatant liquid solution has held the distributed state of dark black. From the UV/*vis* spectrum, characteristics absorption of SWNTs without chiral selectivity was observed (Fig.2). With the model compound corresponding to the monomer of this Polymer 1, although dispersion of SWNTs was tried under the same conditions, it was hardly able to disperse. By repeating π conjugated polymer to a belt type, it has attained distributing powerful CNT.

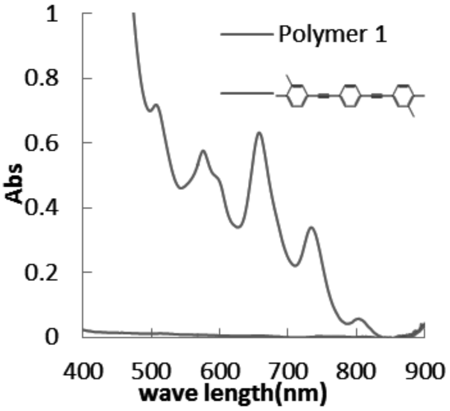

Fig. 2 UV/*vis* spectrum of Dispersed CNT with polymer **1** and monomeric unit.

Corresponding Author: M. Takahashi
Tel:+81-43-290-3397, Fax:+81-43-290-3401, E-mail: masahiro@faculty.chiba-u.jp

3P-25

Chirality purification of DNA-wrapped single-walled carbon nanotubes toward thin film transistors

○Yuki Kuwahara[1,2], Fumiyuki Nihey[2,3], Shigekazu Ohmori[2], Takeshi Saito[1,2]

[1] *National Institute of Advances Industrial Science and Technology (AIST),*
Tsukuba 305-8565, Japan
[3]*Technology Research Association for Single Wall Carbon Nanotubes (TASC),*
Tsukuba 305-8565, Japan
[2]*NEC Corporation, Tsukuba 305-8501, Japan*

It is well known that single-walled carbon nanotubes wrapped with DNA (DNA-SWCNTs) based on the non-covalent interaction can be sorted by single-chiralities of SWCNTs by using specific DNA sequence and ion exchange chromatography (IEX) technique [1]. In our previous works, we had reported the effective way to fabricate SWCNT thin film transistors (SWCNT-TFTs) by preparing homogeneous network of DNA-SWCNTs without the process of extracting semiconducting SWCNTs [2]. This method needs optimally adjusting the SWCNT density to be around the percolation threshold, because of the existing metallic SWCNTs. Because the increase in the ratio of semiconducting SWCNTs results in the increase in the SWCNT density of the percolation threshold, the development of DNA-SWCNTs with a semiconducting single-chirality is important for the upgrade of SWCNT-TFT performances.

In this study, we purified CoMoCAT and eDIPS [3] SWCNTs by IEX for the fabrication of SWCNT-TFTs using purified DNA-SWCNTs.

Acknowledgment: This work was supported by Iketani Science and Technology Foundation. A part of this work was conducted at the Nano-Processing Facility, supported by IBEC Innovation Platform, AIST and "Nanotechnology Network Japan" of the Ministry of Education, Culture, Sports, Science and Technology (MEXT), Japan.

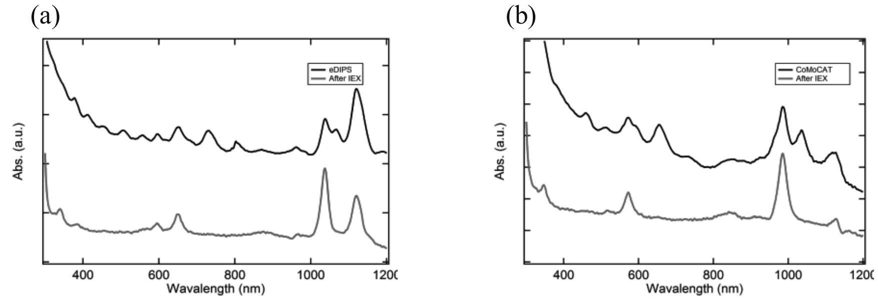

Fig.1 Absorption spectra of DNA-SWCNTs before and after IEX.
(a) eDIPS, (b)CoMoCAT

[1] X. Tu *et al.*, Nature. **460**, 250 (2009).
[2] Y. Asada *et al.*, Adv. Mater. **23**, 4631 (2011).
[3] T. Saito *et al.*, Nanosci. Nanotechnol. **8**, 6153 (2008).

Corresponding Author: Takeshi Saito
Tel: +81-29-861-4863, Fax: +81-29-861-4413,
E-mail: takeshi-saito@aist.go.jp

3P-26

Effects of pulse conditions on growth of (6,5) enriched single-walled carbon nanotubes under pulse plasma CVD

○Bin Xu, Toshiaki Kato, Koshi Murakoshi, and Toshiro Kaneko

Department of Electronic Engineering, Tohoku University, Sendai, 980-8579 Japan

Single-walled carbon nanotubes (SWNTs) have very unique one dimension structure which leads to many novel characteristics like high mechanical strength, enhanced optical absorption, high current density, and so on. Since the electronic and optical properties of SWNTs are mostly decided by their chirality, chirality-controlled SWNTs synthesis is one of the major challenges in nanotube science and applications. Plasma CVD that has a relative low reaction temperature and can precisely control the synthesis time are often used to synthesize nano carbon materials [1-3]. By using plasma CVD, we have realized synthesis of SWNTs with narrow-chirality distribution [4,5].

In our previous study, the correlation between the incubation time and SWNTs chirality distribution was investigated. We found that SWNTs with only small diameter and narrow-chirality distribution can be grown by using short time plasma CVD [4]. To increase the SWNTs quantity, we improved the previous method and introduced a novel method, which is pulse plasma CVD. SWNTs synthesized by pulse plasma CVD can be with large quantity as well as narrow-chirality distribution.

For the synthesis of SWNTs with higher purity, we also tried to elucidate the effects of pulse parameters such as on and off times on the growth of narrow chirality-distributed SWNTs. The chirality distribution of SWNTs becomes narrower with an increase in off time (Fig.1), which can be explained by the combination of the incubation time difference between small and large diameter SWNTs and changes of catalyst particle size due to Ostwald ripening.

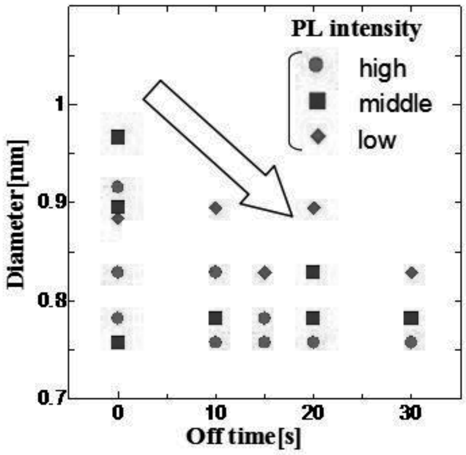

Fig.1: Diameter distribution of SWNTs with the variation of off time

[1] T. Kato, L. Jiao, X. Wang, H. Wang, X. Li, L. Zhang, R. Hatakeyama, and H. Dai : Small **7,** 574 (2011).

[2] T. Kato and R. Hatakeyama: ASC Nano **6,** 8508 (2012).

[3] T. Kato and R. Hatakeyama: Nature Nanotechnology **7,** 651 (2012).

[4] T. Kato and R. Hatakeyama: ACS Nano **4,** 7395 (2010).

[5] Z. Ghorannevis, T. Kato, T. Kaneko, and R. Hatakeyama: J. Am. Chem. Soc. **132,** 9570 (2010).

Corresponding Author: B. Xu
Tel: 022-795-7046, Fax: 022-263-9225,
E-mail: xu12@ecei.tohoku.ac.jp

3P-27

Selective recognition of semiconducting single-walled carbon nanotubes with large diameters by using polyfluorenes carrying mono-alkyl chain

○Takahiro Fukumaru[1], Fumiyuki Toshimitsu[1], Tsuyohiko Fujigaya[1,2], Naotoshi Nakashima[1,2,3]

[1]Department of Applied Chemistry, Graduate School of Engineering, Kyushu University, 744 Motooka, Fukuoka 819-0395, Japan
2 WPI-I2CNER, Kyushu University, 744 Motooka, Fukuoka 819-0395, Japan
[3]Japan Science and Technology Agency, CREST, 5 Sanbancho, Chiyoda-ku, Tokyo, 102-0075, Japan

For the fundamental nanotubes science as well as fabrication of high-performance single-walled carbon nanotubes (SWNTs) devices, sorted SWNTs with a specific chirality are strongly demanded. One of the most promising approaches is to design and synthesize a molecule that enables to selectively recognize/extract SWNTs. Poly(9,9-dioctyl-fluorene-2,7-diyl) (**2C8-PFO**, in Fig. 1, left)[**1**] are attractive molecules because they recognize and extract only semiconducting SWNTs, while the mechanism is still unclear. Here we focused on the alkyl chain number on the PFOs to understand the mechanism. We synthesized polyfluorene carrying mono-octyl moiety (poly(9-octyl-9*H*-fuluorene-2,7-diyl (**C8H-PFO** in Fig. 1, right), and characterized its selective recognition/extraction ability toward SWNTs.

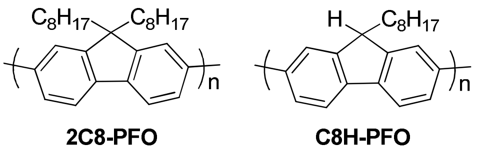

Fig. 1 Chemical structures of poly(9,9-dioctyl-fluorene-2,7-diyl) (**2C8-PFO**) (left) and poly(9-octyl-9*H*-fuluorene-2,7-diyl) (**C8H-PFO**) (right).

C8H-PFO was synthesized by Yamamoto coupling of fluorene monomer carrying Br-terminated mono-octyl moiety.

Fig. 2 shows the 2D-PL mapping of the SWNT solution in toluene with **C8H-PFO** (C8H-PFO-SWNTs, left) and **2C8-PFO** (2C8-PFO-SWNTs, right) for comparison. In the case of C8H-PFO-SWNTs, little bit larger diameter SWNTs (0.9 – 1.1 nm) were extracted and many (*n*,*m*)SWNTs such as (9,5)SWNT (chiral angle: 20.66 °) and (10,5)SWNT (chiral angle: 19.16 °) were observed, which indicated that **C8H-PFO** recognized larger diameter semiconducting SWNTs with broad chiral angle (>20 °). In other words, the second alkyl chain in fluorene unit enabled both the chiral angle selection and diameter selection for semiconducting SWNTs. Molecular mechanics simulation was revealed that **C8H-PFO** showed superior diameter selective recognition to **2C8-PFO**.

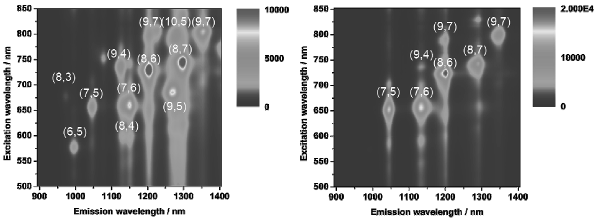

Fig. 2 2D-PL maps of C8H-PFO-SWNTs (left) and 2C8-PFO-SWNTs (right) for comparison.

[1] A. Nish *et al. Nat. Nanotechnol.* **2**, 640 (2007).

Corresponding Author: N. Nakashima
Tel: +81-92-802-2840, Fax: +81-92-802-2840,
E-mail: nakashima-tcm@mail.cstm.kyushu-u.ac.jp

3P-28

Cloning Growth of Single-Walled Carbon Nanotubes from Activated Nanotube Edges

○Takanori Umino, Taiki Inoue, Shohei Chiashi and Shigeo Maruyama

Department of Mechanical Engineering, The University of Tokyo, Tokyo 113-8656, Japan

The chirality controlled synthesis is one of the most important topics in the research of single-walled carbon nanotubes (SWNTs). Recently, metal-catalyst free chemical vapor deposition (CVD) growth of SWNTs from nanotube edges (also referred to as "cloning") has been reported [1, 2]. Although this technique is promising for chirality controlled synthesis [2], further improvement of the yield is required.

Here, we performed CVD growth of SWNTs from nanotube edges to understand the mechanism and improve the growth yield. Firstly, horizontally aligned SWNTs were grown from patterned Fe catalysts on quartz substrates and partially removed by photolithography and O_2 plasma treatment. Figure 1 (a) shows a scanning electron microscopy (SEM) image of patterned SWNTs. The samples were then placed in a CVD chamber and annealed in air at 200 °C, followed by water vapor exposure at 800 or 900 °C. In these processes, nanotube edges were activated as the template for the growth of SWNTs. Finally, CVD growth was performed at 800, 850, or 900 °C using ethanol gas as the carbon feedstock. As shown in Fig. 1 (b), SWNTs were grown from some of the nanotube edges. Although the occurrence ratio of SWNT growth to original nanotube edges was less than 1 % in the case of one cycle of activation and growth, the yield of SWNTs gradually increased by repeating the cycles. In Raman scattering spectra, G-band and D-band were obtained from SWNTs grown from nanotube edges. Atomic force microscopy observation revealed the SWNT diameters of the grown parts and the original parts were almost same.

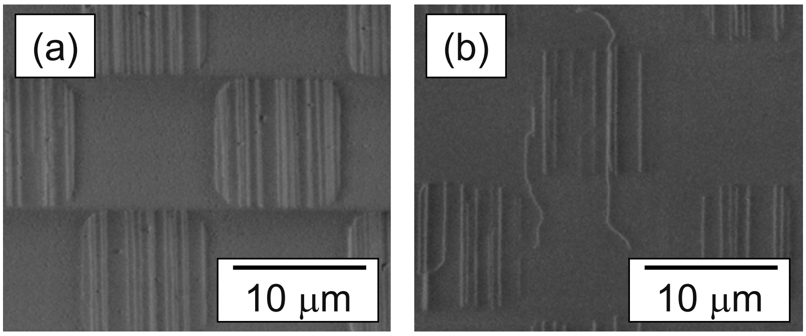

Fig. 1 SEM images of (a) partially etched SWNTs for the growth template and (b) the sample after the growth process.

[1] Y. Yao, et al., *Nano Lett.*, **9** (2009) 1673.
[2] J. Liu, et al., *Nat. Commun.*, **3** (2012) 1199.

Corresponding Author: Shigeo Maruyama
TEL: +81-3-5841-6421
FAX: +81-3-5800-6983
E-mail:maruyama@photon.t.u-tokyo.ac.jp

3P-29

Growth of high-density carbon nanotube arrays toward thermal interface materials

○Nuri Na[1,2], Kei Hasegawa[2], Suguru Noda[2,*]

[1] Department of Chemical System Engineering, The University of Tokyo, Japan
[2] Department of Applied Chemistry, Waseda University, Tokyo 169-8555, Japan

Carbon nanotubes (CNTs) are a candidate for future thermal interface materials (TIMs) owing to their high thermal conductivity (3000 W/m K) and mechanical flexibility. However, typical CNT arrays grown by conventional chemical vapor deposition (CVD) method have thermal conductivity far below the expected values because of their porous structure (> 90% porosity) and high thermal resistances at the contact with opposing substrates. Therefore, in this work, we target at high-density CNT arrays with uniform height for TIM applications.

Two approaches are possible in preparing CNT arrays on metal foils; one is transfer of CNT arrays grown on oxide substrates to the foils and the other is direct growth of CNT arrays on the foils. We deposited Ni, Co, or Fe catalyst on TiN or Al_2O_3 underlayer by sputtering, annealed them with pure H_2 at 500-700 °C, and then carried out CVD by feeding C_2H_2 at a pressure of 3-300 mTorr. We evaluated the height and density of CNTs by scanning electron microscopy (SEM) with by energy dispersive X-ray spectroscopy.

The height and density of CNT arrays changed largely with a trade-off relationship, depending on the catalyst and underlayer used. Fig. 1 shows the typical CNT arrays grown by Ni particles on $TiN/SiO_2/Si$, which had a density as high as 2.6×10^{12} cm^{-2} prior to CVD. At a high C_2H_2 pressure of 30 mTorr, CNT arrays initially had a high density (0.7 g cm^{-3} for 0.5 µm-tall arrays) but abruptly lost the density due to the rapid catalyst deactivation. Whereas at a low C_2H_2 pressure of 3 mTorr, CNT arrays had a moderate and constant density (0.4 g cm^{-3}). We then examined the two step growth where the CNT nucleation was enhanced by feeding C_2H_2 at 30 mTorr for the initial 20 s and then the CNT growth was sustained by feeding C_2H_2 at 3 mTorr for 1-60 min. This method yielded CNT arrays with a steady density as high as 0.5 g cm^{-3} with a uniform height (Fig 1e). Careful control over nucleation and growth of CNT array are keys to tailor CNT structure for application to TIMs.

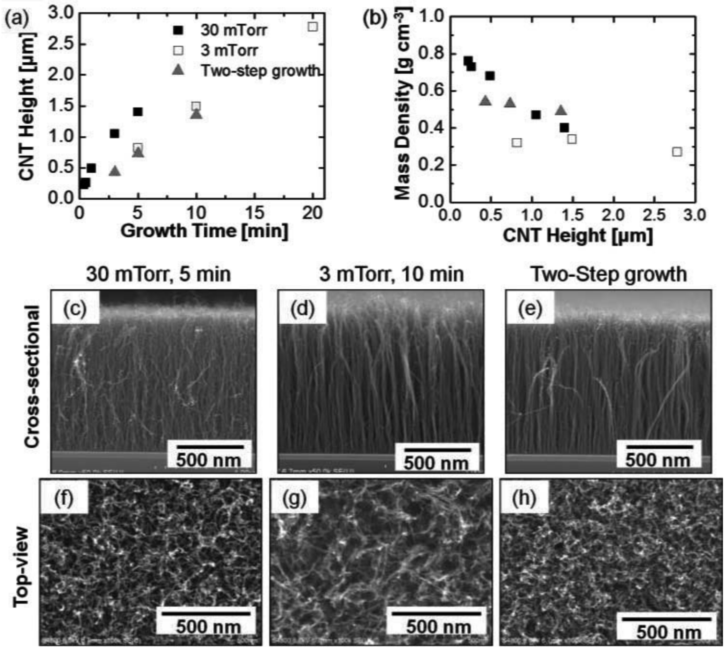

Fig 1. (a) CNT height vs. growth time, (b) mass density vs. CNT height. Cross-sectional (c-e) and top-view (f-h) SEM images of CNT arrays grown at constant C_2H_2 partial pressures (3, 30 mTorr) and by the two-step growth method.

*Corresponding Author: Suguru Noda, Tel&Fax: +81-3-5286-2769, E-mail: noda@waseda.jp

3P-30

Selective Growth of Single-Walled Carbon Nanotubes with Specific Diameter and Chirality by Irradiating Free Electron Laser during Growth

○Keisuke Yoshida[1], Takumi Sagara[1], Yusaku Tsuda[1], Koji Ishii[2], Kenichi Yamakawa[1],
Hirofumi Yajima[2], Nobuyuki Iwata[1] and Hiroshi Yamamoto[1]

[1] *Department of Electronics & Computer Science,College of Science & Technology, Nihon University, 7-24-1 Narashinodai, Funabashi, Chiba 274-8501 Japan*
[2] *Department of Applied Chemistry, Faculty of Science, Tokyo University of Science, 1-3 Kagurazaka, Shinjyuku-ku, Tokyo 162-0826, Japan*

Single-Walled carbon nanotubes (SWNTs) have been regarded as one of the best candidates for future applications in nanoelectronic devices due to its high mobility, high current-carrying capacities, and so on. The drawback for nanoelectronics using SWNTs is that almost all of the current available technologies for the SWNTs growth can only produce a mixture of metallic and semiconducting one. We demonstrate the novel technique to synthesize as-grow semiconducting SWNTs with approximately 1.1 nm in diameter including (14,0), (13,2), (10,6), (9,7) chiralities using free electron laser (FEL) irradiation with the wavelength of 800 nm during growth[1]. However, the mechanism to control the chirality and the diameter by the FEL has not been clear yet. The aim of this study is to elucidate the role of the FEL irradiation for the selective SWNTs growth.

Figure1 shows the Raman spectra of the SWNTs grown with the 765 nm FEL irradiation for RBM. The appearance of a lot of peaks indicates that the selective growth is not achieved by the 765nm-FEL. From the Kataura plot and the RBM peaks of the SWNTs grown with the 765nm-FEL, grown SWNTs had both of semiconducting and metallic properties. Same results were obtained using 835nm-FEL. Considering the CVD condition is suitable to grow SWNTs with 1.1 nm, the 800nm-FEL is effective for selective growth with specific chirality. The origin is expected to be the catalyst diameter just before CVD. We will clarify the relationship between the catalyst diameter and suitable FEL wavelength for selective growth, which must be connected to the role of the FEL irradiation for the selective growth.

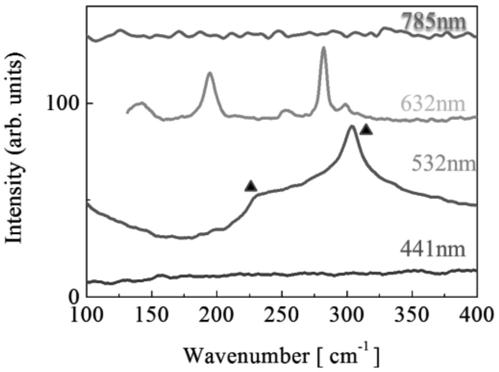

Fig.1 Raman spectra of the SWNTs grown with the 765 nm FEL. Used excitation laser was 441 nm, 532 nm, 632 nm and 785 nm.

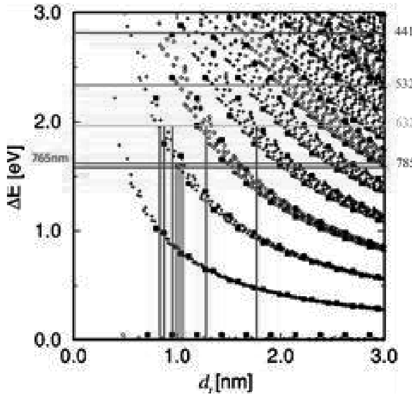

Fig.2 Diameter of the SWNTs grown with the 765 nm FEL on Kataura plot[2].

[1] K.Sakai, *et al.*, IEICE TRANS. Electron, **E94-C** (2011) 1861.
[2] R. Saito, PHYSICAL REVIEW B, VOLUME 61, 2981 (2000)

3P-31

Tuning the Seebeck coefficient of single-wall carbon nanotubes by encapsulation of guest materials

○Tomohiro Ueda[1], Yusuke Nakai[1], Yasumitsu Miyata[1,2] and Yutaka Maniwa[1]
[1] *Department of Physics, Faculy of Science, Tokyo Metropolitan University, 1-1 Minami-Osawa Hachioji, Tokyo 192-0397, Japan*
[2] *JST, PRESTO, Kawaguchi, 332-0012, Japan*

Modification of the electronic state of single-wall carbon nanotubes (SWCNTs) is a method of generating novel physical properties. One simple method of modifying the electronic structure of SWCNTs is encapsulating molecules or atoms into channels of SWCNTs. Our recent study has shown that highly-enriched semiconducting SWCNTs films exhibit a large Seebeck coefficient [1]. Since the Seebeck coefficient is sensitive to the electronic state, it is expected that the Seebeck coefficient varies with introducing guest materials into the channels of SWCNTs. In order to achieve a better thermoelectric performance in SWCNT films, we investigate the effects of various materials encapsulated inside SWCNTs on the Seebeck coefficient.

In order to examine encapsulation of guest materials in the inner channels, we performed powder X-ray diffraction (XRD) measurements of SWCNT films which we conducted encapsulation treatment through a vapor phase method. We found that the intensity of (1 0) peak from SWCNT bundles is weaker than that of empty SWCNTs, and that new characteristic XRD peaks appear after the encapsulation treatment. These results suggest that guest materials are encapsulated in the channels of SWCNTs. We then measured Seebeck coefficient of the SWCNTs samples encapsulating various materials, and found that their Seebeck coefficient is significantly different from empty SWCNTs. These results suggest that introducing guest materials into the channels of SWCNTs is an effective way to tune the thermoelectric performance.

[1] Y. Nakai *et al*., to appear in Appl. Phys. Express.

Corresponding Author: Y. Nakai
Tel: +81-42-677-2498-, Fax: +81-42-677-2483,
E-mail: nakai@tmu.ac.jp

3P-32

Molecular structure of the thiophene oligomers encapsulated in single-walled carbon nanotubes by molecular dynamics simulations

○Hiromu Tabata[1], Akinori Sekine [1], Kazumi Inoue[2], Yousuke Kataoka [2]
and Hironori Ogata[1,2,3]

[1] *Graduate School of Engineering, Hosei University, Koganei, 184-8584, Japan*
[2] *Department of Faculty of Bioscience and Applied Chemistry, Hosei University, Koganei, 184-8584, Japan*
[3] *Research Center for Micro-Nano Technology, Hosei University, Koganei, 184-0003, Japan*

Single-walled carbon nanotubes (SWNTs) have a hollow space in the nanometer size that can be encapsulated various functional molecules. Recently, thiophene oligomer encapsulated SWNTs are synthesized and their optical properties were reported[1,2]. Their optical properties depend on the orientation of thiophene oligomers encapsulated. π -stacking type or herringbone type has been reported to the molecular arrangement of thiophene oligomers. However the systematic studies of thiophene oligomers encapsulated in SWNTs with various diameters and chirality's have not been reported. In this study, we report the effects of chirality and tube diameter of SWNTs on the molecular orientations of the thiophene oligomers by using molecular dynamics(MD) simulations.

In our MD simulations, we used the Dreiding intramolecular potential and the OPLS intermolecular potential. By placing the SWNT and quaterthiophene in a rectangular cell, to obtain a stable structure at 298K after the relaxation in the 1 K with the NVT ensemble.

Figure 1 shows the structure of the molecular orientation of quaterthiophenes(4T) encapsulated in (10,10) tube. 4T molecules are oriented in units of three molecules in parallel along the longitudinal axis of the tube. The detailed systematic results that effects of chirality and tube diameter has on the thiophene oligomers in SWNTs will be presented.

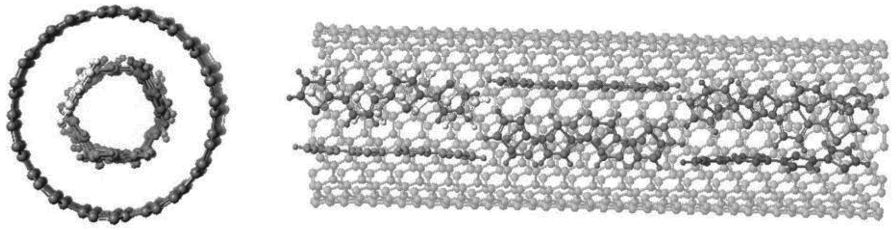

Figure 1. The structure of 4T@SWNT

[1] Loi, M. A. *et al. Adv. Mater*. **2010**, 22, 1635.
[2] Gao,J *et al. Small* **2011**, 7, 1807.
[3] Yamashita, H.; Yumura, T. *et al.*, *J. Phys. Chem. C* **2012**, *116,* 9681

Corresponding Author: Hironori Ogata,
Tel: +81-42-387-6229, Fax: +81-42-387-6229, E-mail: hogata@hosei.ac.jp

3P-33

Influence of growth substrates on chemical reactivity of CVD graphene

○Ryosuke Inoue[1], Yasumitsu Miyata[1,2], and Yutaka Maniwa[1]
[1]Department of Physics, Tokyo Metropolitan University, Hachioji, 192-0397, Japan
[2]JST, PRESTO, Kawaguchi, 332-0012, Japan

The control of chemical reactivity of graphene is one of the important issues for its chemical functionalization and etching. In many cases, graphene is grown on metal substrates such as copper foil by chemical vapor deposition (CVD). It remains an unsettled question how the growth substrates affect the chemical reactivity of graphene. Especially, it is reported that generally-used cupper foil is polycrystalline and its surface shape strongly depends on crystal faces [1]. Such surface shape could relate to the reactivity through the change in crystallinity and internal stress of graphene. To test this hypothesis, we have investigated that the effect of crystal faces on chemical reactivity of CVD graphene.

Graphene was grown on commercially-available copper foil (Nilaco) by methane CVD. The graphene grown was then etched by annealing under hydrogen or oxygen atmospheres. The surface of the used copper foil mainly consists of (111) face with large roughness and of relatively-flat (100) face. After the hydrogen etching, we found that there is a large difference in etching rates between the (111) and (100) faces (Fig.1a). This difference means that the (100) face can produces more stable graphene than on the (111) face. Raman imaging reveals that there is non crystal-face dependence in the intensity of D-band and 2D-band of graphene (Fig.1b-d). This result suggests that the reactivity of CVD grapene on cupper foil is infuluenced by not its crystallinity but the roughness of substrates. The present finding gives a useful guide for the control of graphene etching and functionalization .

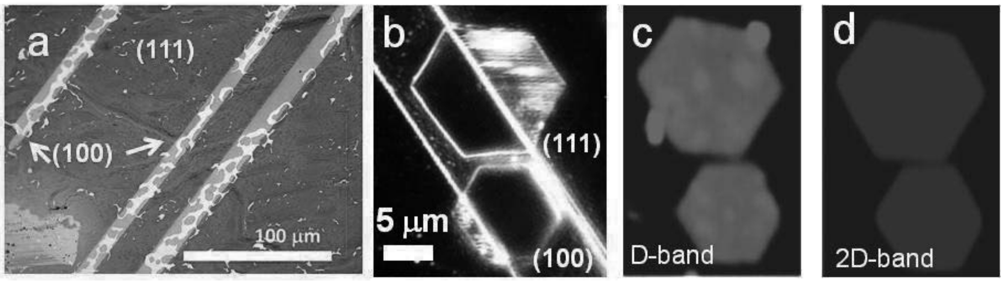

Fig.1 (a) Optical microscope image of graphene on Cu foil after hydrogen etching. (b) Dark-field image, (c) D-band intensity, and (d) 2D-band intensity maps of the same graphene grains.

[1] X. H. Kong, et al., Appl. Phys. Lett. 103, 043119 (2013)

Corresponding Author: Yasumitsu Miyata
TEL:+81-42- 677-2508, FAX:+81- 42-677-2483, E-mail: ymiyata@tmu.ac.jp

3P-34

Synthesis and Characterization of Metal Intercalated bilayers Graphene

○Imai Kentaro, Shogo Sato, Kuniharu Matsuki, Nobuyuki Iwata, Hiroshi Yamamoto

College of Science &Technology, Nihon University, 7-24-1 Narashinodai, Funabashi-shi, Chiba 2748501

Graphite intercalation compounds (GIC) is prepared on various substances. Superconducting transition temperature *Tc* of GIC with Ca are reported at 11.5K[1]. In this study we aim at realizing a room temperature superconductivity (RTS) in a metal intercalated bilayer graphene due to an electron-exciton coupling rather than electron-phonon coupling. The *Tc* is expected to be higher than room temperature as long as a disorder and a roughness of the graphene layers are much reduced.

Graphene was prepared by chemical vapor deposition (CVD) method. We grew graphene on copper foil with a 20 μm thickness at temperatures up to 1000°C for 30 min by CVD of carbon using a mixture of methane and hydrogen. After the graphene growth on copper foil, the specimen was coated by a poly methyl methacrylate (PMMA) layer[2]. The copper foil was etched completely as soaking the specimen in an iron(III) nitrate aqueous solution. The PMMA/graphene layer was transferred on the SiO_2/Si substrate, and evaluated by a micro Raman spectroscopy and a four probes electric measurement system.

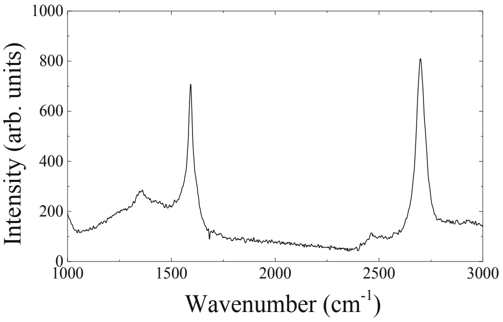

Figure1:Raman spectra of graphene between 1500 and 3000 cm^{-1}.

Figure1 shows the Raman spectrum of graphene. The peaks of G, D, and G', respectively, were observed at 1593, 1347 and 2699.4 cm^{-1}, indicating the presence of a graphene sheet. Figure2 shows the temperature dependence of the sheet resistance of the graphene. The sheet resistivity increased as decreasing temperature. It is expected that the defect and/or roughness are present.

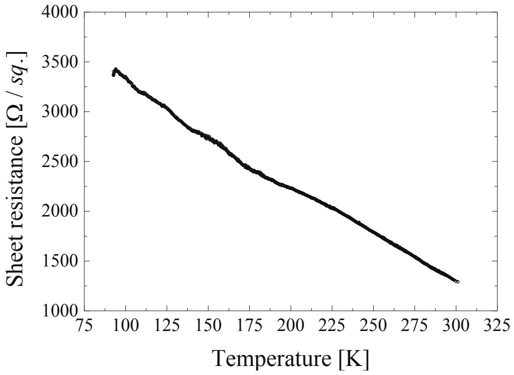

Figure2: Tenperature Resistivity characterization at 300~90k

The result of synthesis and characterization intercalated bilayers graphen will be discussed.

[1] N. Emery *et al.*: Phys. Rev. Lett. **95** (2005) 087003

[2] A Reina *et al.*: Nano letters. **9** (2009) 30.

3P-35

CVD Growth of Graphene Nanoribbons on Cu (100) Film

○ Rozan Mohamad Yunus[1], Masahiro Miyashita[1], Masaharu Tsuji[1,2], Hiroki Hibino[3], and Hiroki Ago[*,1,2]

[1] Graduate School of Engineering Sciences, Kyushu University, Fukuoka 816-8580, Japan
[2] Institute for Materials Chemistry and Engineering, Kyushu University, Fukuoka 816-8580, Japan
[3] NTT Basic Research Laboratories, NTT Corporation, Kanagawa 243-0198, Japan

Graphene is a one-atom thick lattice of honeycomb arranged carbon atoms, which exhibits excellent electronic, optical, thermal, and mechanical properties [1]. Unlike the semiconductor silicon, graphene has no band gap which is crucial for electronics applications such as field-effect transistors with a high on/off ratio. Theoretical and experimental works have demonstrated that quantum confinement into a one dimensional structure, so called graphene nanoribbons (GNRs), can potentially open the band gap [2]. Recently, several approaches have been developed to produce GNRs such as lithographic methods and unzipping of carbon nanotubes. The reliable production of narrow GNRs by a bottom up approach has still not been well established and is a significant challenge.

Previously, we studied the domain structures of single-layer graphene grown on heteroepitaxial metal films in terms of crystalline plane dependence [3-5]. Based on these results, we have developed a novel method to synthesize GNRs using CVD. Ambient pressure CVD growth on a flat epitaxial Cu (100) metal film was performed at 900-1000 ºC under a flow of $CH_4/H_2/Ar$ mixed gas. We observed the growth of nanoribbons on the entire metal surface where the nanoribbons alignment reflects the crystallographic orientation of the underlying Cu film. From SEM measurements, narrow GNRs with the width about 40-50 nm were obtained as shown in Figure 1. The Raman spectrum of transferred GNRs on SiO_2/Si revealed that these nanoribbons are single-layer graphene with low defects. Moreover, the dark-field low energy electron microscope (LEEM) measurements suggested that these GNRs have zigzag edges regardless of the nanoribbons width. Our bottom-up approach offers a new method to grow single-layer GNRs which are oriented in a specific direction of the metal film for future carbon-based electronics and spintronics applications.

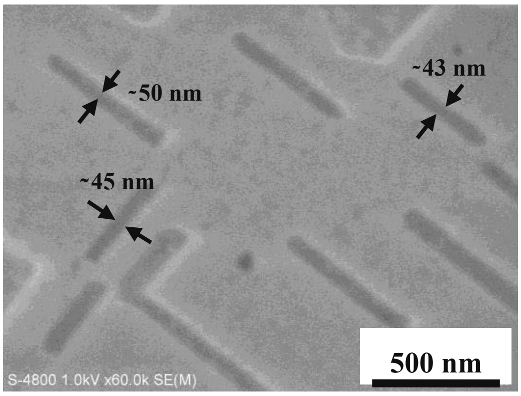

Figure 1: SEM image of GNRs on SiO_2/Si

[1] A. K. Geim, Science, **324**, 1530 (2009)., [2] X. Li. et al., Science, **319**, 1229 (2008)., [3] H. Ago et al., ACS Nano, **4** (2010) 7407., [4] Y. Ogawa et al., J. Phys. Chem. Lett., **3** (2012) 219., [5] H. Ago et al., J. Phys. Chem. Lett., **3** (2012) 2228.

Corresponding Author: Hiroki Ago (Tel & Fax: +892-583-7817, E-mail: ago@cm.kyushu-u.ac.jp)

3P-36

Liquid-phase exfoliation of graphene from graphite with triphenylene derivatives

○Ryusuke Funahashi[1,2], Gang Liu [1], Shuji Aonuma[2], Takahide Kimura[1],
Naoki Komatsu[1]

[1] *Department of Chemistry, Shiga University of Medical Science, Otsu 520-2192, Japan*
[2] *Department of applied chemistry, Osaka Electro-Communication University,*
Osaka 572-8530, Japan

Liquid phase exfoliation has been frequently used for production of graphene from graphite in the presence or absence of an exfoliant. A flat π-conjugated molecule such as pyrene or porphyrin derivatives is reported to be efficient exfoliant [1-2], because π-π and hydrophobic interactions between the flat molecule and graphene can accelerate the exfoliation of graphite and stabilize the resulting graphene in solution. In this paper, we applied triphenylene derivatives (Fig. 1) as novel exfoliants for liquid phase exfoliation of graphene from graphite.

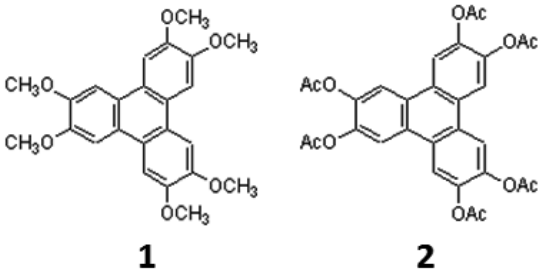

Fig. 1 Structures of triphenylene derivatives **1** and **2**

After a mixture of graphite and the triphenylene **1** or **2** was bath-sonicated in THF, the resulting suspension was centrifuged at 114 g or 1028 g to give black supernatant. The supernatants were analyzed with absorption and Raman spectroscopies, and STEM.

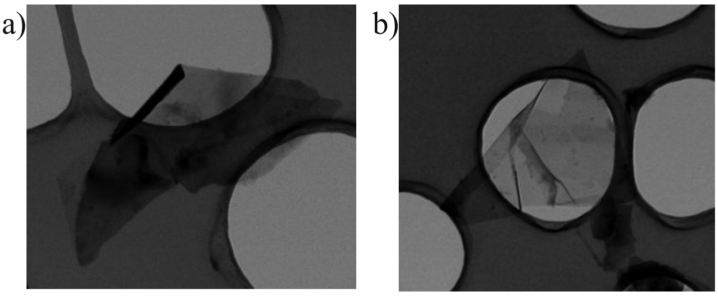

Fig. 2 STEM images of exfoliated graphene with **1** (a) and **2** (b)

The existence of graphene was confirmed by the STEM shown in Fig. 2. The Raman spectra shown in Fig. 3 indicate that a few-layer graphene is considered to exist judging from the ratio of G' / G and the symmetrical shape of G' band. It is concluded that triphenylene derivatives have the ability to exfoliate graphite to produce graphene in solution phase.

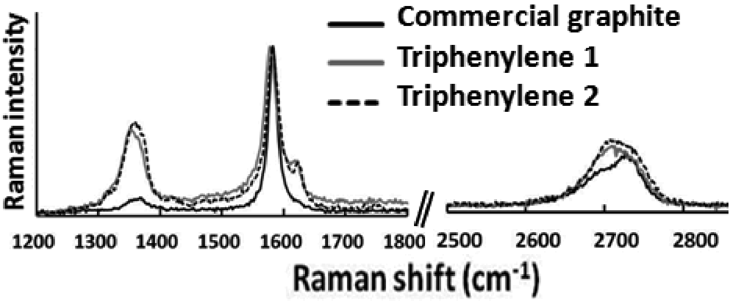

Fig. 3 Raman spectra of commercial graphite, and exfoliated graphene with triphenylenes **1** and **2**

[1] C. Casiraghi *et al. Carbon*, 53, 357 (2013). [2] Hee-Tae Jung *et al. Chem. Commun.*, 46, 5091 (2010).

Corresponding Author: Naoki Komatsu Tel: +81-77-548-2102, Fax: +81-77-548-2405,
E-mail: nkomatsu@shiga-med.ac.jp

3P-37

Plasma effects on growth of graphene nanoribbon from nickel nanobar under rapid heating plasma CVD

○Hiroo Suzuki, Toshiaki Kato, Toshiro Kaneko

Department of Electronic Engineering, Tohoku University, Sendai 980-8579, Japan

Graphene nanoribbons combine the unique electronic and spin properties of graphene with a transport gap that arises from quantum confinement and edge effects. This makes them an attractive candidate material for the channels of next-generation transistors. Although nanoribbons can be made in a variety of ways, the reliable site and alignment control of nanoribbons with high on/off current ratios remains a challenge. Plasma chemical vapor deposition (CVD) is known as fruitful method for the structural-controlled growth and damage-free functionalization of nano carbon materials such as carbon nanotubes [1-3] and graphene [4,5].

We have developed a new, simple, scalable method based on the advanced plasma CVD method for directly fabricating narrow (~23 nm) graphene nanoribbon devices with a clear transport gap (58.5 meV) and a high on/off ratio (>10^4) [6]. Since the establishment of our novel graphene nanoribbon fabrication method, direct conversion of a Ni nanobar to a graphene nanoribbon is now possible. The growth mechanism of graphene nanoribbon, however, is not well understood, which is important for the stable fabrication of graphene nanoribbon devices. We investigate the growth mechanism of graphene nanoribbon by comparing evaporation rate of nickel between plasma and thermal CVD (Fig. 1). It is found that the evaporation rate of nickel is low in plasma CVD compared with that of thermal CVD. This should relate with the difference of carbon concentration in nickel. In plasma CVD, large amount of hydrocarbons can be supplied to nickel due to high rate dissociation of carbon source gas. The balance of evaporation rate of nickel and amount of supplying carbon closely relates with growth of graphene nanoribbon.

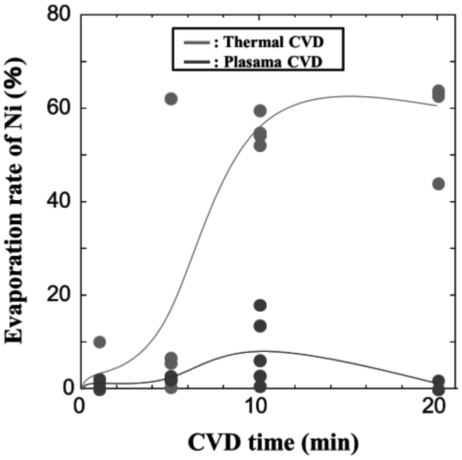

Fig.1: Nickel evaporation rate as a function of CVD time.

[1] T. Kato and R. Hatakeyama, J. Am. Chem. Soc. **130**, 8101 (2008).
[2] T. Kato and R. Hatakeyama, ACS Nano **4**, 7395 (2010).
[3] Z. Ghorannevis, T. Kato, T. Kaneko, and R. Hatakeyama, J. Am. Chem. Soc. **132**, 9570 (2010).
[4] T. Kato, L. Jiao, X. Wang, H. Wang, X. Li, L. Zhang, R. Hatakeyama, and H. Dai, Small **7**, 574 (2011).
[5] T. Kato and R. Hatakeyama, ACS Nano **6**, 8508 (2012).
[6] T. Kato and R. Hatakeyama, Nature Nanotechnology **7**, 651 (2012)

Corresponding Author: H. Suzuki
Tel: +81-22-795-7046, Fax: +81-22-263-9225,
E-mail: suzuki12@ecei.tohoku.ac.jp

3P-38

Influence of electrolyte concentration for electrochemical exfoliation of graphene

○Haruya Okimoto, Hiroki Kuronuma, and Masahito Sano
Department of Polymer Science and Engineering, Yamagata University, Yonezawa, 992-8510, Japan

Recent developments in liquid phase exfoliation of graphite to give graphene mean it is now possible to prepare dispersed grapehene cheaply and easily. For example, the electrochemical exfoliation using electrolyte is one of low-cost synthesis of graphene. However the mechanism of the electrochemical exfoliation are usually more complicated as compared to those of the chemical intercalation since the former relates to several components of the system(solvent, voltage etc.) which can interfere with the major process. Understanding the influence of several components leads to the control of the properties of exfoliated graphene. In this study, we demonstrate how electrolyte concentration for electrochemical exfoliation of graphite affects the shape and thickness of exfoliated graphene.

Electrochemical exfoliation was done in an electrolysis cell. This cell has graphite foil(Grafoil, Grafguard) as anode and Pt plate as cathode in electrolyte solution. Na_2SO_4 was used as electrolyte for exfoliation. The electrolyte concentration was 1 mmol/L to 1 mol/L.

Fig. 1 shows the AFM image of exfoliated graphene using 10 mmol/L and 100 mmol/L electrolyte solutions. The edge of the exfoliated graphene at 10 mmol/L was usually etched structure than that at high electrolyte concentration. At low electrolyte concentration, the exfoliation process become very slow compared with exfoliation at high electrolyte solution. In the electrochemical reaction between graphite and acid, graphite intercalation was accompanied with graphite oxidation at positive potential.[1] Therefore, the long-time applied voltage for exfoliation of thin graphene at low concentration leads to oxidize graphene surface. As a result, the exfoliated graphene at 10 mmol/L was damaged than that at 100 mmol/L.

Fig. 2 shows the thickness diagram of exfoliated graphene by 1 mmol/L and 1 mol/L concentration. The low concentration of electrolyte led to thicken the thickness of graphene. If grafoil was exfoliated by sonication, the thickness of exfoliated graphene was 10 to 100 nm. Therefore, we suggest that the changing of the electrochemical exfoliated graphene thickness depends on the electrolyte concentration.

As a result, we suggest that the electrolyte concentration affects the shape and thickness of exfoliated graphene by electrochemical exfoliation.

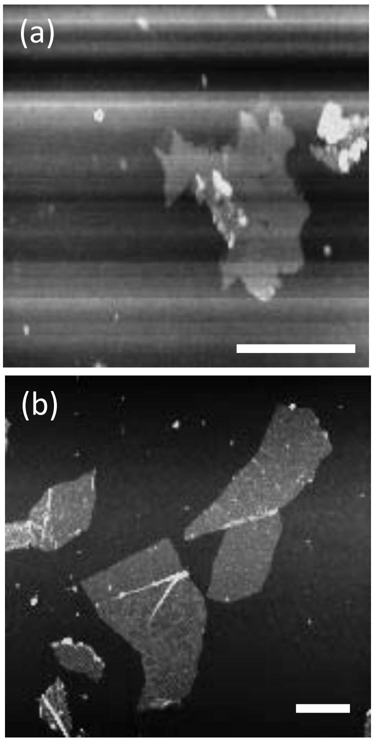

Fig. 1 AFM image of exfoliated graphene at (a) 10 mmol/L and (b) 100 mmol/L.

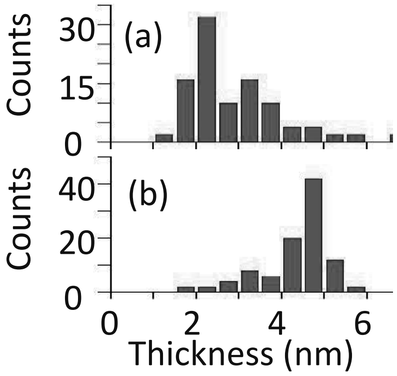

Fig 2 Histograms of graphene thickness at (a) 100 mmol/L and (b) 1 mmol/L.

Corresponding Author: H. Okimoto Tel/FAX: +81-238-26-3074
E-mail: haruya@yz.yamagata-u.ac.jp

[1]D.C. Alsmeyer and R.L. McCreery, *Anal. Chem.*, 64, 1528(1992).

3P-39

High gain CMOS inverters based on transition metal dichalcogenides

○Jiang Pu [1], Jing-Kai Huang [2], Yoshihiro Iwasa [3,4], Lain-Jong Li [2], Taishi Takenobu [1,5]

[1] Department of Applied Physics, Waseda University, Tokyo 169-8555, Japan
[2] Institute of Atomic and Molecular Sciences, Academia Sinica, Taipei 11529, Taiwan
[3] Department of Applied Physics, The University of Tokyo, Tokyo 113-8656, Japan
[4] RIKEN Center for Emergent Matter Science (CEMS), Wako 351-0198, Japan
[5] Kagami Memorial Laboratory, Waseda University, Tokyo 169-0051, Japan

Two dimensional (2D) materials such as monolayer transition metal dichalcogenides (TMDCs) are attracting potential electronic applications as a transistor fabricated for logic electronics because of its large bandgap and high mobility. Owing to their atomic scale thickness, 2D TMDCs offer a high degree of electrostatic control than those of bulk forms, which provide significant advantage for constructing low-power electronic devices. Recently, integrated circuits based on bilayer MoS_2, including inverters and ring oscillators, have demonstrated [1]. Although the MoS_2 transistors typically show n-type behavior, further advances require CMOS circuits composed of n-type and p-type transistors. Moreover, current researches have been performed on mechanically exfoliated TMDCs, which hamper the practical utility of TMDCs for application to large-area integration. In this paper, we demonstrate CMOS inverters fabricated with large-area MoS_2 and WSe_2 electric double layer transistors (EDLTs). The huge capacitance of ion gels enables the strong depletion of donor carriers and efficient carrier doping, resulting in realizing high gain CMOS inverters.

The large-area trilayer MoS_2 and monolayer WSe_2 films were synthesized on sapphire substrates through chemical vapor deposition [2-4]. The gold electrodes, ion gels and top-gate Pt foil were stacked on film surface to build EDLTs. The fabricated WSe_2 EDLTs exhibited high hole mobility of 55cm^2/Vs and excellent current on/off ratio of 10^7, whereas the MoS_2 EDLTs showed high electron mobility of 60 cm^2/Vs. Because of large specific capacitance of ion gels, the CMOS inverters constructed from p-type WSe_2 and n-type MoS_2 operated at significantly low voltage of 0.5V, which consequently yielded extremely high gain of 110 that is the highest value in atomically thin 2D materials (Fig. 1). Our results provide the substantial possibility of 2D materials for large-area low-power CMOS logic devices.

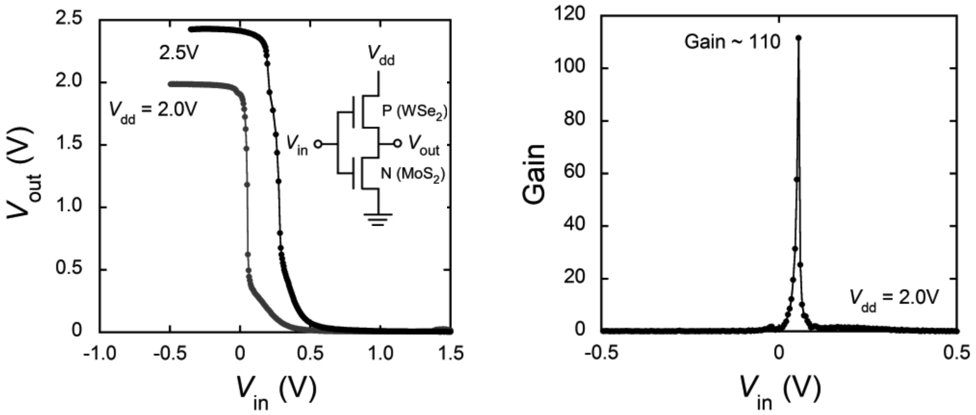

Fig. 1 Output (left) and gain (right) characteristics of a WSe_2 and MoS_2 based CMOS inverter

[1] H. Wang *et al*. Nano. Lett. **12**, 4674 (2012).
[2] J. Pu, T. Takenobu *et al*. Nano. Lett. **12**, 4013 (2012).
[3] J. Pu, T. Takenobu *et al*. Appl. Phys. Lett. **103**, 023505 (2013).
[4] J. K. Huang, J. Pu, T. Takenobu *et al*. ACS. Nano. DOI: 10.1021/nn405719x (2013).

Corresponding Author: T. Takenobu
Tel/Fax: +81-3-5286-2981
E-mail: takenobu@waseda.jp

3P-40

High efficiency graphene doping

Kai-Wen Cheng[1], Po-shin Lin[1] ,Ya-Ping Hsieh[1]
[1] *Graduate of Institute of Opto-Mechatronics, National Chung Cheng University, ROC*

Graphene, a monoatomic layer of carbon, has inspired work in many fields from fundamental science to application oriented research. Due to its unique combination of metallic character and its limited absorption due to its atomic thickness, graphene is well suited as a transparent optical conductor (TOC). To compete with mature TOC technologies, such as Indium tin oxide, graphene's performance as an electrical conductor has to be improved.

Increase of carrier concentration has been identified as the most feasible route to improving graphene film conductance. As an alternative, chemical doping has been widely used .While impressive results have been shown, the produced samples are still falling short of the requirements on conductance and transmittance to replace ITO.

We here present a novel approach to increasing the conductance of graphene. For these experiments we utilize single layer polycrystalline graphene synthesized by chemical vapor deposition on Cu substrate to produce high quality samples of centimeter scale. Our approach relies on considering the effect of doping on carrier mobility instead of focusing on maximizing the doping density, as has been the most common route for chemical doping. By carefully tuning the concentration of dopant we are able to identify a transport region in which the positive effect of charge addition is outweighing the detrimental consequences of charged impurity scattering. We accomplish this fine doping control by in-situ measurement of carrier concentration and mobility throughout the doping process and find that we can increase the film conductivity by up to 300%.

We furthermore demonstrate that a second doping step can further increase the charge carrier density without significantly deteriorating the carrier mobility as identified by electrical and Raman measurements. Consequently an additional increase of conductivity by up to 300% can be seen. The reason of this additional increase was found to be interactions of the first and second dopant.

The presented results not only improve our understanding of the doping process and its relation to the graphene morphology but have significant impact on the commercial potential of graphene. The doping process increases graphene conductivity by almost one order of magnitude and thus produced samples exhibit some of the highest conductivity reported in the literature and can rival ITO. Our findings therefore open the field of graphene-based transparent circuits and electrodes for novel applications

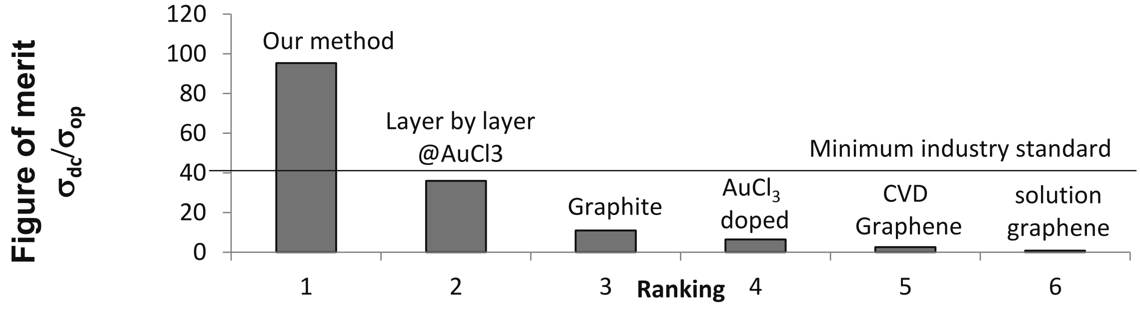

Figure 1 Comparison of Figure of Merit for different graphene samples

Corresponding Author: Ya-Ping Hsieh
E-mail: yphsieh@ccu.edu.tw

3P-41

Drastic Change in Photoluminescence Properties of Size-separated Graphene Quantum Dots

○Naoto Fuyuno[1], Daichi Kozawa[1], Yuhei Miyauchi[1, 2], Shinichiro Mouri[1], Ryo Kitaura[3], Hisanori Shinohara[3], Toku Yasuda[4], Naoki Komatsu[4], and Kazunari Matsuda[1]

[1]*Institute of Advanced Energy, Kyoto University, Uji, Kyoto 611-0011, Japan*
[2]*Japan Science and Technology Agency, PRESTO, 4-1-8 Honcho Kawaguchi, Saitama 332-0012, Japan*
[3]*Department of Chemistry and Institute for Advanced Research, Nagoya University, Nagoya 464-8602, Japan*
[4]*Department of Chemistry, Shiga University of Medical Science, Otsu 520-2192, Japan*

Graphene quantum dots (GQDs), which are nanometer-size graphene flakes, have attracted a great deal of interest from the viewpoints of fundamental physics and optoelectronics. It has been reported that GQDs show photoluminescence (PL) in visible light region, however, the mechanism of PL in GQDs has not been well understood. Considering quantum size effect, the optical properties of GQDs should be affected by their overall size, although the size-dependent PL in GQDs is controversial.

In the present study, we conducted size separation of GQDs by high performance liquid chromatography (HPLC) and observed drastic change in PL depending on the overall size of GQDs. The GQDs were fabricated by acid treatment of pitch-based carbon fibers [1] and size of GQDs was confirmed by transmission electron microscope (TEM) images. Figure 1a shows size distribution histograms of large and small GQDs sample separated by HPLC. Average sizes of large and small GQDs are 10.8 and 6.8 nm, respectively. Figure 1b shows PL spectra of large and small GQDs obtained from excitation wavelength of 280 nm. The large and small GQDs show emission peak at 530 nm and 330 nm, respectively. By detail measurements, PL of GQDs is found to be composed of four discrete features and drastic PL change by size separation is understood by the change in relative intensity of those PL features. These results indicate that PL originates from small sp^2 fragments embedded in GQDs and drastic PL shift is explained by the change in the population of sp^2 fragments in the GQDs with different overall sizes.

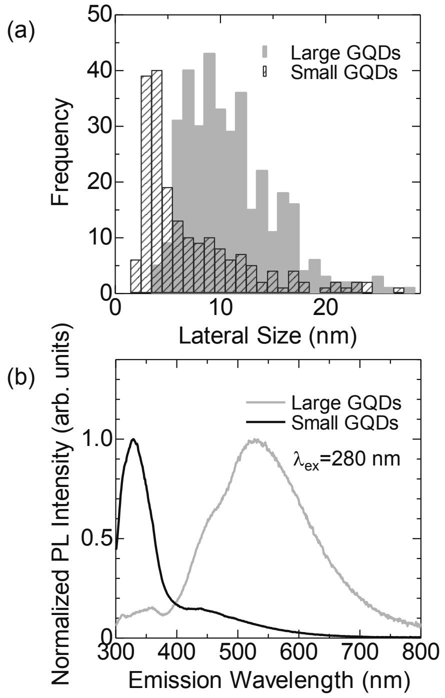

Fig. 1 (a) Size distribution histograms and (b) normalized PL spectra of GQDs separated by HPLC.

[1] J. Peng *et al.*, *Nano lett.* **12**, 844 (2012).

Corresponding Author: N. Fuyuno
Tel: +81-774-38-3465, Fax: +81-774-38-3467
E-mail: fuyuno.naoto.67n@st.kyoto-u.ac.jp

3P-42

Energetics and Electronic Structure of Graphene Edges

○Ayaka Yamanaka, Susumu Okada

Graduate School of Pure and Applied Sciences, University of Tsukuba, Tennodai, Tsukuba 305-8577, Japan

Graphene is attracting much attention due to its possible application for semiconductor electronic devices. In particular, graphene is regarded as the one of promising emerging materials in the next generation. Therefore, it is urging us to unravel fundamental properties of graphene for designing and fabricating graphene-based electronic devices. In this work, we study the energetics and electronic structure of graphene with various edge structures to provide a theoretical insight for fabricating the graphene devices with nano-scale.

All calculations are performed by using the density functional theory. To express the exchange correlation potential among interacting electrons, we apply the local density approximation. We use an ultrasoft pseudopotential to describe the interaction between valence electrons and ions. The effective screening medium (ESM) method is applied to investigate behaviors of graphene nanoribbon under the electric field in the framework of the first-principles calculations.

In this study, we consider graphene nanoribbons with various edge shape of which edge angles are θ = 0° (armchair), 8°, 16°, 23°, and 30° (zigzag) shown in Figs. 1 (a), 1 (b), 1 (c), 1 (d), and 1 (e), respectively. As shown in Fig. 1 (f), the edge formation energy depends on the edge angle: edge formation energy keep constant value of 0.35 eV up to the angle θ = 15°, while the energy monotonically increase with increasing the edge angle. Therefore, the edge with near armchair shapes are energetically favorable for the H-terminated graphene ribbon. Small edge formation energy is ascribed to the semiconducting electronic properties of graphene nanoribbons with near armchair edges. On the other hand, increase of density of state at E_F arising from edge states leads to the monotonical increase of edge formation energy for large θ. We also study the electronic structures of these graphene nanoribbons under a parallel electric field. We find that the π and π^* states repulse each other under the electric field leading to the decrease of edge formation energy.

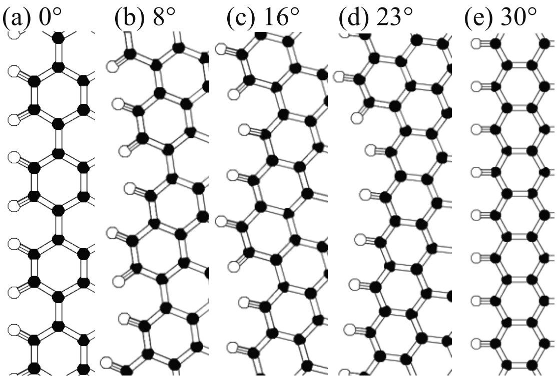
(a) 0° (b) 8° (c) 16° (d) 23° (e) 30°

(f) Edge Formation Energy

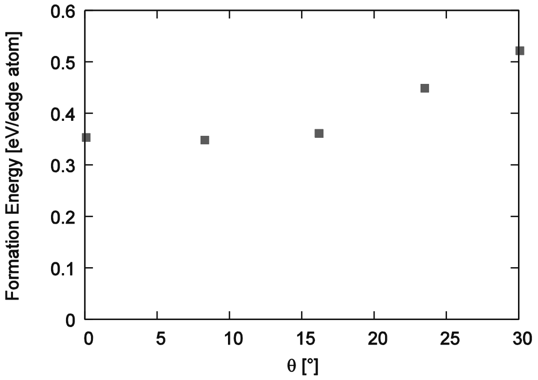

Fig.1 (a)-(e) Geometric structures and (f) edge formation energy of hydrogenated graphene nanoribbons.

Corresponding Author: A. Yamanaka
Tel: +81-29-853-5600 (ext. 8233),
Fax: +81-29-853-5924,
E-mail: ayamanaka@comas.frsc.tsukuba.ac.jp

3P-43

Fine Control of Oxidation of Graphitic Carbons by Oxidation of Graphite or Reduction of Highly Oxidized Graphene Oxide

○Yuta Nishina[1,2], Naoki Morimoto[1]

[1] Research Core for Interdisciplinary Sciences, Okayama University,
Okayama 700-8530, Japan
[2] Precursory Research for Embryonic Science and Technology, Japan Science and
Technology Agency, 4-1-8 Honcho, Kawaguchi, Saitama 332-0012, Japan

Control of oxidation level in the graphite- and graphene-like materials is important to tailor the functionality to suit the relevant areas of applications that include optoelectronics, physical-, biological-, and energy-related materials. For example, carboxyl group-free graphene oxide (GO) would be desirable for the production of defect free graphene by reduction. In contrast, oxygen functional groups are necessary for the synthesis of GO composites with nanoparticles, organic molecules, and heteroatoms. Application for conductive films, electrodes for lithium ion battery, super capacitor, and catalyst for fuel cell would often require the functionalization processes to improve GO's performance.

We have achieved the fine tuning of the oxygen content by oxidation and reduction processes. The oxidation content was analyzed by elemental analysis, and properties of each GOs were measured by XPS, XRD, electron conductivity, oxidation ability, and cyclic voltammetry.

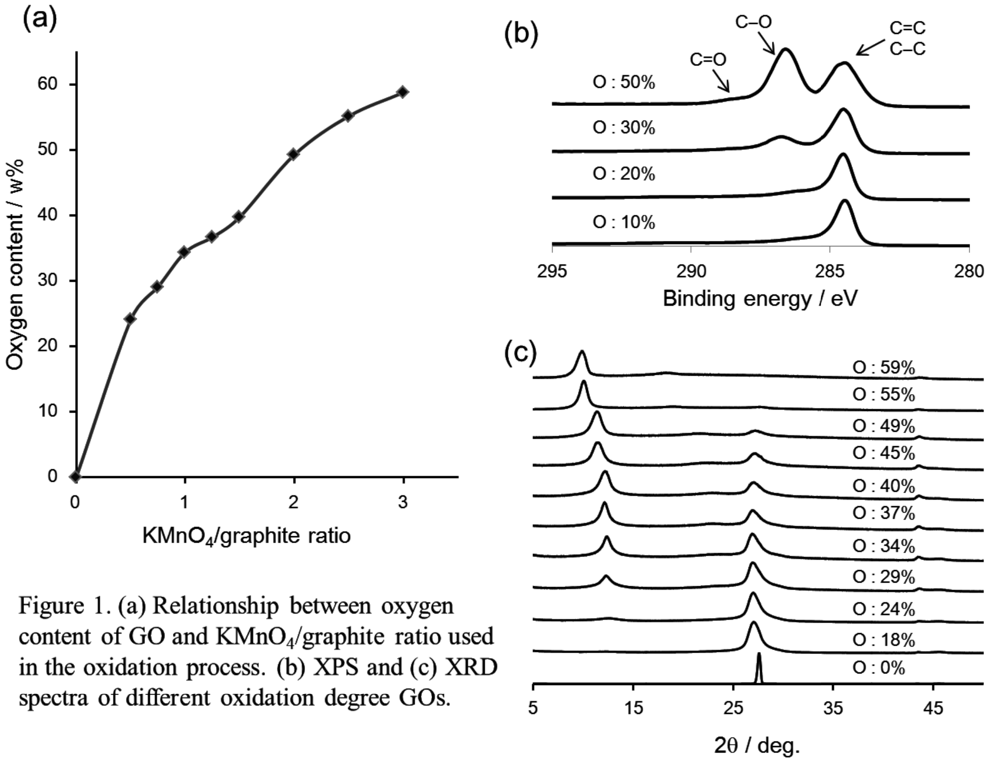

Figure 1. (a) Relationship between oxygen content of GO and $KMnO_4$/graphite ratio used in the oxidation process. (b) XPS and (c) XRD spectra of different oxidation degree GOs.

Corresponding Author: Y. Nishina
Tel: +81-86-251-8483
E-mail: nisina-y@cc.okayama-u.ac.jp

Structural and magnetic changes of nanodiamond-copper composites during HPHT Sintering Process

Fedor Shakhov [1], Vladimir Osipov [1], Sergei Kidalov [1], Kazuyuki Takai [2], Toshiaki Enoki [3], Alexander Vul' [1]
[1] Ioffe Physical-Technical Institute, St. Petersburg 194021, Russia
[2] Department of Chemical Science and Technology, Hosei University, Tokyo 184-8584, Japan
[3] Department of Chemistry, Tokyo Institute of Technology, Tokyo 152-8551, Japan

The surface modification of nanodiamond is important in view of the investigation of the origin of the spin magnetism of nanodiamond. Especially, building a nano-composite is interesting method which enables to introduce the interface between nanodiamond surface and transition metal chemically inert for carbon. In this study, a series of copper composites with detonation nanodiamonds (DND) [1] was prepared at high pressure-high temperature (HPHT) conditions, and evaluated in terms of the spin magnetism.

The composite synthesis was performed by sintering a mixture of DND and Cu-particles under the temperature varied from 1100 °C to 1900 °C and the pressure of ~7 GPa for ~ 60 sec. The weight contents of DND phase were about 20 wt.% in all synthesized Cu / DND composites. The magnetic susceptibilities of prepared composites were studied by using SQUID magnetometer in the temperature range 2 - 300 K.

The magnetic susceptibilities of all the samples well follow the Curie-Weiss law in the temperature range below 100 K. The Curie-Weiss term in the magnetic susceptibility is related with the presence of paramagnetic spins ($S = 1/2$) of unpaired free radicals locating in the DND particles and not in the host copper matrix which is well conductive. Recently, we found that these paramagnetic spins ($S = 1/2$) are originated from the own vacancy-based defects of diamond lattice located within thin (~ 1.5 nm) undersurface layer of DND particles with mean size ~5 nm [2]. The concentrations of localized spins in a DND phase of synthesized composites is about $5.4 - 6.0\times10^{19}$ g^{-1}, which are a little bit lower than those in pristine DND in the powder form (~ 6.3×10^{19} g^{-1}). The increasing in the temperature of HPHT synthesis from 1100 °C to 1900 °C does not practically affect on the concentration of unpaired radicals in DND phase, although the subtle reducing with raising the synthesis temperature is observed. These results mean that vacancy-based defects of DND are not so movable at short time of HPHT synthesis. Moreover, during rapid HPHT synthesis of Cu / DND composites, DND particles inside the matrix do not subjected to the intensive graphitization process causing additional spin magnetism and their crystalline cores are well conserved and stable in melted copper even at temperatures up to 1900 °C. The observed structural stability is understood taking the fact into account that copper does not create covalent bonds and interfacial compounds with external carbon atoms of DND. Further development and optimization the synthesis technique of DND / Cu composites will be also discussed in this paper. This work was supported by the Japan-Russia Research Cooperative Program within the grants: RFBR 12-02-92107 ЯФ_a and JSPS.

[1] A. Aleksenskiy, M. Baidakova, V. Osipov, A. Vul. The Fundamental Properties and Characteristics of Nanodiamonds. In: "Nanodiamonds: Applications in Biology and Nanoscale Medicine" Ed. Dean Ho. Spinger New York, Dordrecht, Heidelberg. London. 2009. p.55-78.
[2] A.I. Shames, V.Yu. Osipov, A.E. Aleksenskiy, E. Ōsawa, A.Ya. Vul'. Diamond Relat Mater., **20**, 318 (2011).

Corresponding Author: Fedor Shakhov (fedor.shakhov@mail.ioffe.ru).

3P-45

Synthesis and characterization of Pt , Pt-Ru nanoparticles on carbon nanomaterials by one-step electrodeposition

○[1]Shohei Hayase, [1]Haruhiko Yoshitake, [2]Wang Zhipeng [1,3]Hironori Ogata

[1] Department of Chemical Science and Technology,Hosei University Koganei 184-8584 Japan
[2] Institution for Sustainability Research and Education, Shinshu University Nagano 380-8553 ,Japan
[3]Research Center for Micro-Nano Technology,Hosei University,Koganei 184-0003,Japan

Direct methanol fuel cells (DMFCs) are one of the most promising transportable power sources which can be used in mobiles, laptops, and small power generation. The basic operation principle of DMFCs involves methanol oxidation and oxygen reduction on the precious metal catalysts, which are loaded on the support surfaces. As is well-known, the dispersion of Pt-based alloys on carbon supports as well as catalyst particle size and shape plays a dominant role in the electrochemical performance for fuel cells. In this study, we explore the carbon materials as a catalyst support for Pt-based nanoparticles by one-step electrodeposition. The morphology, microstructure, chemical compositon, and electrochemical properties of the carbon nanosheets (CNS) -, Single walled Carbon Nanotubes(SWNTs) or highly ordered pyrolytic graphite(HOPG) supported Pt-based nanoparticles were systematically investigated.

Figure.1 shows the one example of the CV responses of Pt-Ru/HOPG and table.1 shows the electrochemical characteristic of methanol oxidation. The detailed results on the relationship between the condition of electrodeposition, the chemical compositon of nanoparticles and their electrocatalytic performance for methanol oxidation will be presented.

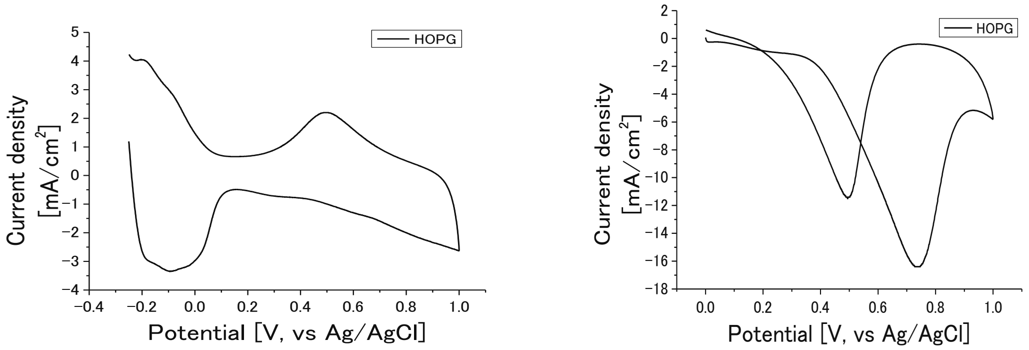

Figure 1. CV responses of Pt-Ru/HOPG

Table.1 Electrochemical characteristic of methanol oxidation

Active area	forward current density	If/Ib ratio	Forward voltage of oxidation of Methanol [V]
6.66×10^2	16.4	1.16	0.727

1) Zhipeng Wang, Mao Shoji and Hironori Ogata, *Appl. Surf. Sci.*__259__(2012)219-224.

Corresponding Author: Hironori Ogata,
Tel: +81-42-387-6229, Fax: +81-42-387-6229, E-mail: hogata@hosei.ac.jp

3P-46

Hydration of Nanodiamond Surface Revisited: Intercalation Hypothesis

○Ryoko Yamanoi[1], Amanda Barnard[2], Shuichi Sasaki[1], and Eiji Ōsawa[1*]

[1] *NanoCarbon Research Institute, AREC, Shinshu University, Ueda, 386-8567, Japan*
[2] *CSIRO, Material Science and Engineering, Clayton, Victoria 3052, Australia*

Self-polarization across diamond core and graphitic shell in the detonation nanodiamond (DND) led to novel facet-dependent multi-pole charge-distribution for particles with diameters smaller than 3nm [1,2]. Early observation by Korobov *et al.* on water layers freezing at -8°C on the surface of DND hydrogel by means of DSC[§] was interpreted as strong H-bonding of water molecules to the highly negative-charged {111} facets [3]. However, it was recently realized that the DND particles they used contained substantial fractions of the smallest oligomers of primary particles. Our recent success in isolating true primary particles of detonation nanodiamond (PPDND) with a record low average diameter of 2.8±0.5 nm [4] prompted us to repeat the DSC experiments on the hydrogel. In addition to the H-bond peak, now appearing at -11°C, a broader peak centered at -16°C was detected during melting (**Fig. 1**). The purpose of this presentation is to assign the origin of the latter peak.

SCC-DFTB[#] calculations of 3nm diamond models revealed substantial space below the surface shell (**Fig. 2**). Furthermore, the central region of every {111} facet has negative curvature which must be accompanied with large strain. If these regions were etched off the surface during drastic oxidation process to remove soot in the purification of crude DND, the holes thus formed will serve as passages for solvent molecules, which will eventually be intercalated tight in the narrow space surrounded by deformed graphene patches. We suggest these trapped water molecules constitute the peak at -16°C in **Fig. 1.**

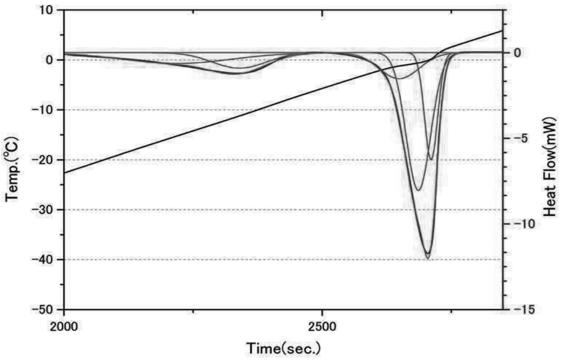

Fig. 1. DSC[§] trace of melting PPDND

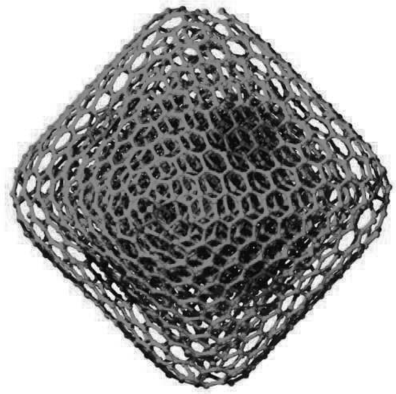

Fig. 2. Optimized geometry of a PPDND model

The possibility of intercalation pockets accessible from the open surface, although still hypothetical, explains superb suppression of side effects in our DDS that uses DND as drug carrier and being developed for cancer thermotherapy [5]. When an anti-cancer drug molecules (doxorubicin ammonium salt) are loaded on DND by salting-in technique, they will go deep into the pockets below the particle surface inactivated, and won't come out until pulled out by changing pH of blood or salting-out.

---

[1] Barnard, A. S.; Sternberg, M. J. Mater. Chem., **17**, 4811 (2007). [2] Barnard, A. S.; Osawa, E. *Nanoscale* **6,** 1188 (2014). [3] M. V. Korobov *et al.*, J. Phys. Chem. C. **111**, 7330 (2007). [4] S. Sasaki *et al.*, Presented in this General Symposium. [5] Moore, L. K. *et al.*, Disruptive Sci. Technol. **1**, 54 (2012). [§]Differential scanning calorimetry. [#]Self-consistent charge density function tight binding theory. *Corresponding Author: osawa@nano-carbon.jp, Tel: +81-268-75-8381, Fax: +81-268-75-8551.

3P-47

Doping of zinc to the iron oxide nanotubes by using a poly-condensation of metal nitrate hydrates on the surface of surfactant

○ Yuta Kosugi[1], Shunji Bandow[2]

Department of Materials Science & Engineering[1] and of Applied Chemistry[2],
Meijo University, Nagoya 468-8502, Japan

The iron oxide nanotubes (Fe-ox-NTs) are formed by the sol-gel technic using a poly-condensation of iron nitrate hydrate on the surface of self-assembled block-copolymer of a Pluronic F-127 [1-3], and the structural properties of the product were studied [4]. From these studies, we found that the structure of crude Fe-ox-NTs was classified into amorphous like disordered γ-Fe_2O_3 or Fe_3O_4. By annealing the sample in open air at 320°C, such disordered phase was relaxed and the structure was changed to α-Fe_2O_3 without destructing the tube structure. An annealing temperature dependence of the band gap estimated by using the Kubelka-Munk analysis [5,6] of the optical absorption indicated a minimum of ca. 2.3 eV when annealing at ~300°C as shown in Fig. 1. Although the magnitude of this minimum is just located in the green light region where the radiant flux of the sun light shows maximum, a LUMO level of the iron oxide is slightly deeper than the reduction potential of hydrogen. In the present study, we tried to dope Zn element to Fe-ox-NTs in order to approach a LUMO level to the reduction potential of hydrogen. A doping of Zn to Fe-ox-NT was carried out by mixing a zinc nitrate hydrate to an iron nitrate hydrate up to a few tens wt %. As a result, we found from TEM observation that the tubule structure was dominantly formed in the low concentration of zinc nitrate hydrate by ~10 wt %, but increasing the particle contents (Fig. 2). Although XRD profiles of all the products are also assignable to amorphous like disordered γ-Fe_2O_3 or Fe_3O_4 even adding Zn, XPS clearly indicated the existence of Zn element. These features, including the band gap determined from the optical absorption, will be presented in the poster.

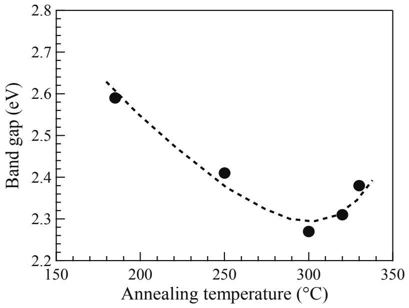

Fig. 1. Annealing temperature dependence of the band gap of Fe-ox-NTs determined by the Kubelka-Munk analysis.

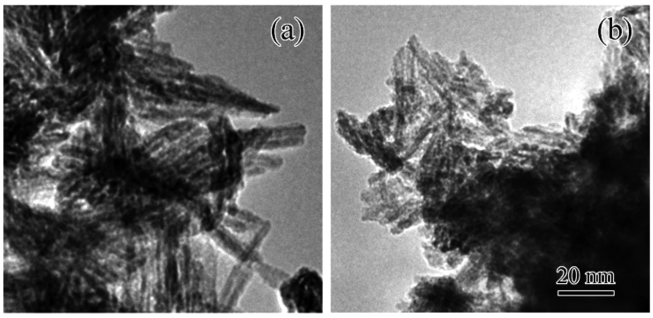

Fig. 2. TEM of Zn-Fe-ox-NTs prepared from (a) 2 wt % of Zn nitrate hydrate mixture and (b) 10 wt %. Black-contrasted materials in (b) are the particles agglomerated.

[1-3] Y. Shiraki *et al.*, 42nd FNT, March 6-8 (2012), Tokyo, **3P-49**, 43rd FNT, Sep. 5-7 (2012), Sendai, **3P-38**, 44th FNTG (March, 2013), **2P-45**. [4] S. Bandow *et al.*, 45th FNTG, Aug.5-7 (2013), Osaka, **3P-14**. [5] V. Džimbeg-Malčić *et al.*, Technical Gazette **18**, 117 (2011). [6] S.S. Kumar *et al.*, Inter. Nano Lett. **3**, 30 (2013).

Corresponding Author: S. Bandow, Tel: +81-52-838-2404, E-mail: bandow@meijo-u.ac.jp

3P-48

Synthesis of high purity carbon nanocoils on the sheet-like carbon deposits and reduction of byproducts using Fe fine particles

○Yoshiaki Shimizu[1], Koji Maruyama[1], Tetsuo Iida[1], Yoshiyuki Suda[1], Hideto Tanoue[1],
Hirofumi Takikawa[1], Hitoshi Ue [2], Kazuki Shimizu [3], Yoshito Umeda[4]

[1] *Department of Electrical and Electronic Information Engineering, Toyohashi University of Technology, Toyohashi, Aichi 441-8580, Japan*
[2]*Fuji Research Laboratory, Tokai Carbon Co., Ltd., Oyama, Shizuoka 410-1431, Japan*
[3]*Development Department, Shonan Plastic Mfg. Co., Ltd., Hiratsuka, Kanagawa 254-0807, Japan*
[4] *Toho Gas Co., Ltd., Nagoya, Aichi 456-8511, Japan*

1. Introduction

Carbon nanocoil (CNC) is a nano-carbon material with “coiled” structure composed of fibers with diameters of 100－500 nm. It is very important to take into account the purity of CNCs during application, such as in electromagnetic wave absorbers. Generally, CNCs are synthesized from composite catalysts including Fe-Sn. In our laboratory, we have synthesized high purity CNCs grown from the surfaces of the sheet-like carbon deposits using Fe particles of 3－5 μm diameters. The sheet-like carbon deposits consist of fibrous carbon materials containing CNCs and other carbon materials (byproducts). The CNCs mainly exist on the surfaces of the sheet-like carbon deposits. In our previous study, we have improved the purity of CNCs more than 90 % (1). In this study, we used Fe fine particles with 0.02 μm diameters and focused on reducing of byproducts.

2. Experimental

Fe catalyst particles of 0.02 μm (The Nilaco Corporation, 224050) or 3－5 μm (Kojundo Chemical Laboratory Co., Ltd, 085523) diameters and SnO_2 solutions (Kojundo Chemical Laboratory Co., Ltd, 235061) were dissolved in ethanol. The surfaces of Si substrates were spin-coated or drop-coated with the solution and sintered at 350°C in air for 5 min. The substrates supporting catalytic particle layer were placed into an automatic CVD apparatus (1). Nitrogen (N_2) and acetylene (C_2H_2) gases were supplied to the apparatus for 10 min to grow CNCs while temperature at 780°C. The N_2 and C_2H_2 flow rates were 1400 and 350 ml/min, respectively. Products were observed using a scanning electron microscope (SEM).

3. Results

Cross sectional SEM images of synthesized sheet-like carbon deposits with Fe catalyst particles of 0.02 μm and 3－5 μm diameters are shown in Fig. 1. We can see that numerous CNCs grew. However, a byproduct layer also formed at the base of the CNCs (2). Fig. 1(a) shows that the byproduct layer thickness is 20 μm. It is less than that with Fe catalyst particles 3－5 μm (120 μm). The purity of CNCs is more than 90 % and became the highest in this study when the mole ratio of Fe:Sn=1:2.6.

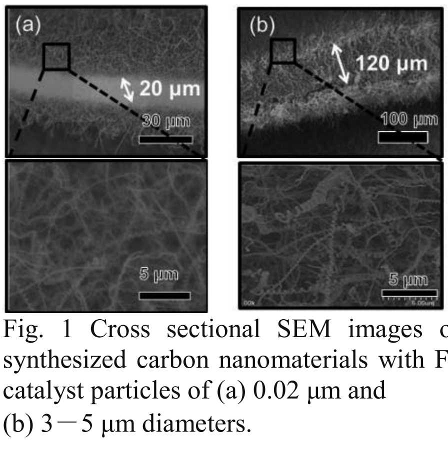

Fig. 1 Cross sectional SEM images of synthesized carbon nanomaterials with Fe catalyst particles of (a) 0.02 μm and (b) 3－5 μm diameters.

[1] M. Yokota, *et al*: J. Nanosci. Nanotechnol, 10 (2011) 3910
[2] K. Hirahara, *et al*: Carbon, 56 (2013) 264

Corresponding Author: Y. Shimizu
E-mail: shimizu.yoshiaki@pes.ee.tut.ac.jp

3P-49

Synthesis and characterization of two-dimensional semiconductor heterojunction based on transition metal dichalcogenides

○Shohei Mori[1], Yasumitsu Miyata[1,2], Yutaka Maniwa[1]

[1]*Department of Physics, Tokyo Metropolitan University, Hachioji, 192-0397, Japan*
[2] *JST, PRESTO, Kawaguchi, 332-0012, Japan*

The heterojunctions in two-dimensional materials have attracted much attention because of their interface-related properties and electronics applications. To date, several groups have reported the synthesis of metal-insulator junction consisted of graphene and hexagonal boron nitride [1-3]. In contrast, realizing the two dimensional semiconductor heterojunctions is still highly desired as components of various electronic devices. To solve this issue, we focus our attention on the heterostructure of two different kinds of transition metal dichalcogenides (TMDs) as shown in Fig.1a.

In this presentation, we report the formation of the heterojunction consisting of single-layer WS_2 and MoS_2. As precursors of these TMDs, thin films of WO_3 and MoO_3 were prepared on Si wafers by vacuum deposition. These oxide thin films were sulfurized by annealing under sulfur/argon atmosphere. The heterostructure of WS_2/MoS_2 was prepared by two-step growth processes of WS_2 and MoS_2 on the same substrate. Optical microscope observations reveal that two-dimensional crystals grown consist of two kinds of films with different contrast and sharp interface (Fig.1b). Furthermore, the existence both of single-layer MoS_2 and WS_2 is confirmed from their photoluminescence spectra (Fig.1c). These results show that the TMD-based semiconductor heterojunction can be formed by the two-step sulfurization process. The present semiconductor heterostructure would provide a promising system for the realization of one-dimensional electron gas and electronic devices such as p-n junctions.

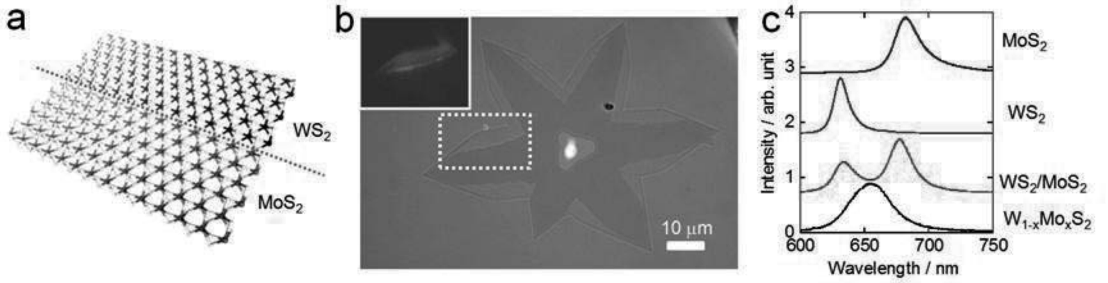

Fig.1 (a) Schematic illustration of WS_2/MoS_2 heterojunction. (b) Optical microscope image and fluorescent image in the box (inset) of typical WS_2/MoS_2 heterostructure. (c) Photoluminescence spectra of WS_2/MoS_2 sample at different points (MoS_2, WS_2, and WS_2/MoS_2) and single-layer $W_{1-x}Mo_xS_2$. The spectrum of $W_{1-x}Mo_xS_2$ is shown for comparison.

[1] Y. Miyata, et al. Appl. Phys. Express 5 (2012) 085102.,

[2] M. Levendorf et al. Nature, 488 (2012) 627., [3] P. Sutter et al. Nano Lett., 12 (2012) 4869.

Corresponding Author: Yasumitsu Miyata
TEL:+81-42- 677-2508, FAX:+81- 42-677-2483,
E-mail: ymiyata@tmu.ac.jp

3P-50

Electro-Chemical Doping Properties of MoS_2-Single Wall Carbon Nanotube Hybrid Film

Hideaki Endo, ○Hideki Kawai, Kai Hasegawa, Seiya Kaji, Kazuhiro Yanagi

Department of Physics, Tokyo Metropolitan University, Tokyo 192-0397, Japan

The transition-metal dichalcogenide MoS_2 has attracted great interest due to its distinctive electronic and optical properties. The layered materials can be shaped into mono-layer which shows distinct physical properties from their bulk counterpart. The materials are typically prepared by mechanical exfoliation techniques or chemical synthesis. Extraction of mono-layers by dispersion of bulk materials (liquid exfoliation) is also possible,[1] but formation of uniform film of monolayer is technically difficult by just aggregating the dispersed MoS_2. In this study, we tried to control the aggregation processes of the dispersed MoS_2 by inserting single-wall carbon nanotubes (SWCNT) in order to demonstrate the properties of monolayer MoS_2 in the film. Here we produced the MoS_2- SWCNT hybrid films, and we investigated their optical and electronic properties by the carrier injection using electro-chemical doping techniques. First we dispersed MoS_2 to sodium cholate 2% solutions by tip-type ultra-sonicators, and the solutions were purified by several centrifugation processes, and mixed with electronic type selected SWCNT solutions. Then the thin films were formed. Figure 1 shows the change of optical absorption spectra of the MoS_2-metallic SWCNT hybrid films by the electro-chemical doping techniques. The A and B optical absorption peaks of MoS_2 were clearly disappeared as the shift of the potential to - 2.0 V (vs Ag/Ag+), suggesting the success of the electron injection to MoS_2. Figure 2 shows the Raman spectra of MoS_2-metallic SWCNT hybrid films. The two peaks around 385 cm^{-1} and 400 cm^{-1} were attributed to E_{2g} and A_{1g} modes of MoS_2, respectively. As the shift of potential to -2.8 V, the A_{1g} mode was clearly disappeared. This is consistent to the results of electrochemical doping upon the monolayer of MoS_2 reported by Chakraborty et al.[2] In the transport properties of MoS_2-metallic SWCNTs hybrid films and metallic SWCNT films, we observed the distinct enhancement of current in the hybrid films around the positive gate voltage, 3.5V, reflecting the carrier injection to MoS_2. The results indicate that the optical and electrical characteristics of MoS_2-SWCNT hybrid films were controlled by electro-chemical doping techniques.

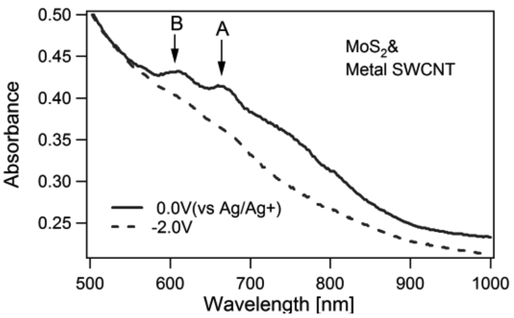

Figure 1 optical absorption spectra of MoS_2-metallic SWCNT hybrid films as a function of potential voltages

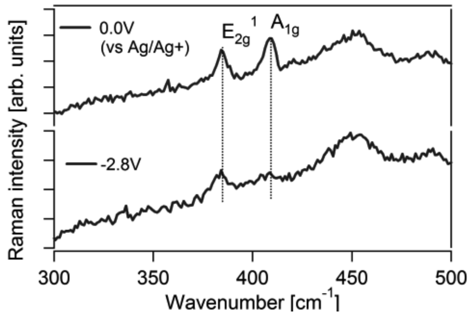

Figure 2 Raman spectra of MoS_2-metallc SWCNT hybrid film as a function of potential voltages

Ref: [1] J. Coleman et al., Science 331, 568 (2011) [2] Chakraborty et al., PRB 85, 161403(R) (2012)

Corresponding Author: Kazuhiro Yanagi
Tel: +81-42-677-2494
E-mail: yanagi-kazuhiro@tmu.ac.jp

発表索引
Author Index

Author Index

< A >
Abe, Shigeaki 3P-19
Abe, Yurika 2P-49
Abiko, Yoshihiro 2P-24
Achiba, Yohji 1P-6, 2-4, 2P-49, 3P-15
Ago, Hiroki 1P-44, 2P-45, 3P-35
Akama, Toshiki 2P-24
Akasaka, Takeshi 1P-12, 3P-1
Akiyama, Wataru 1P-4, 2P-5
Akizuki, Naoto 1P-13, 3P-7
Akutagawa, Tomoyuki 2-11
Alberti, Mariza N. 1P-2
Ando, Yoshinori 1P-33, 2P-28
Aoki, Nobuyuki 1P-4, 2P-5
Aonuma, Shuji 3P-36,
Aoyagi, Shinobu 2P-7, 2-11
Arai, Shigeo 2P-33
Araki, Takuma 1P-9
Asaka, Kinji 3-1
Asaka, Koji 2P-40
Asano, Satoshi 1P-26
Ata, Seisuke 3-3

< B >
Baba, Keisuke 2P-1
Bandow, Shunji 3P-47
Barnard, Amanda 3P-46
Bayer, Thomas 3-6
Berber, Mohamed 1P-24
Bird, Jonathan P 1P-4, 2P-5
Bishop, Sean 3-6
Bissett, Mark 2P-45

< C >
Carvalho, Alexandra 1-8
Castro Neto, Antonio H. 1-8
Cha, JinHyeok 2P-18
Chen, Zhongming 1P-10
Cheng, Kai-Wen 3P-40
Chenxing, Wang 2P-40
Chiang, Bo-Suei 3-11
Chiashi, Shohei 1P-34, 2-1, 2S-5, 2-8, 2P-15, 2P-18, 2P-32, 2P-41, 3P-9, 3P-28

< D >
Diederich, François 1P-2
Ding, Wuxiao 2P-36

< E >
Eda, Goki 1-8, 1P-48, 1P-49
Endo, Hideaki 3P-50
Endo, Hitomi 2P-49
Endo, Tomoaki 2P-7
Endoh, Hiroyuki 1P-20
Enoki, Toshiaki 3P-44

< F >
Fujigaya, Tsuyohiko 1P-22, 1P-24, 1P-29, 2P-25, 3P-16, 3P-27
Fujii, Hiromu 1P-47
Fujii, Keisuke 2P-28
Fujii, Shunjiro 1P-26, 1P-28, 2P-31
Fujimoto, Taiyo 3P-18, 3P-20
Fujimoto, Yoshitaka 1-7
Fujita, Hayato 1P-35
Fujita, Wataru 1P-6
Fukumaru, Takahiro 3P-27
Fukumori, Minoru 2P-43
Fukuzawa, Masashi 2P-29
Fukuzumi, Shunichi 1P-5, 1P-18, 3P-3, 2-12
Funahashi, Kazuma 2P-44
Funahashi, Ryusuke 3P-36
Futaba, Don 2-2, 3-3
Fuyuno, Naoto 3P-41

< G >
Goto, Takumi 1P-21
Guldi, Dirk M. 1P-2

< H >
Hamahata, Hiroki 3P-18
Harima, Hiroshi 2P-10
Hasdeo, Eddwi H. 1P-11, 3P-6
Hasegawa, Kai 2P-30, 3P-50
Hasegawa, Kei 1P-10, 1P-41, 2P-18, 3-2, 3P-22, 3P-29
Hasegawa, Tadashi 1P-12, 3P-1
Hasegawa, Yuri 2P-7
Hashikawa, Yoshifumi 2P-2

Hashimoto, Kenro 2-4
Hashimoto, Yu 3P-23
Hasobe, Taku 2-12
Hasuike, Noriyuki 2P-10
Hasuike, Yuhei 1P-12
Hata, Katsuhiko 1P-19
Hata, Kenji 2-2, 3-3
Hata, Tomoyuki 2P-13
Hatakeyama, Rikizo 2P-24
Hayase, Shohei 3P-45
Hayashi, Kenjiro 3-5
Hayashi, Tatsuya 1-3
Hibino, Hiroki 3P-35
Higuchi, Kentaro 1P-19
Hino, Shojun 1-2
Hirabayashi, Tatsuya 3-3
Hiraiwa, Atsushi 2P-19, 2P-21
Hirakawa, Takuya 1P-28
Hirana, Yasuhiko 1P-15
Hirano, Atsushi 1P-28, 2-7, 2P-31
Hiroshiba, Yasuhiro 1-5
Hisama, Kaoru 2-1
Hiura, Hidefumi 3-10
Hofmann, Mario 1P-43, 3-11, 3-12
Homma, Naoki 2P-15
Homma, Yoshikazu 1P-30, 2S-5, 2-6, 2P-15, 2P-16, 2P-41, 3P-9
Hong, Liu 1P-16
Hongmei, Qin 3P-21
Honma, Itaru 2P-39
Hoshino, Norihisa 2-11
Hsieh, Ya-Ping 1P-43, 3-7, 3-11, 3-12, 3P-40
Huang, Jing-Kai 3P-39
Huang, Wenxin 2P-25

< **I** >
I, Akiko 3-5
Ichida, Masao 2P-47
Ichihashi, Toshinari 1P-39
Iida, Ryosuke 3P-1
Iida, Tetsuo 3P-48
Iijima, Sumio 1P-38, 1P-39, 2P-36
Ikenaga, Eiji 2-3
Ikuma, Naohiko 2-9, 2-10, 3P-3
Im, Inseob 1-3
Imai, Kentaro 3P-34
Inaba, Daiki 3P-1
Inaba, Masafumi 2P-19, 2P-21
Inoue, Chozo 1P-40
Inoue, Kazumi 1P-1, 3P-32
Inoue, Ryosuke 3P-33
Inoue, Sakae 1P-33
Inoue, Taiki 2-8, 3P-28
Inoue, Yoshihisa 1-6
Inukai, Ryota 3P-18
Irie, Michiko 1P-39
Ishii, Akihiro 2P-17, 3P-5, 3P-13
Ishii, Koji 1P-17, 3P-30
Ishiyama, U 3P-8
Ito, Masahiro 2-6, 2P-16
Ito, Yasuhiro 1P-28
Ito, Yoshiaki 1P-4
Ito, Yosuke 3P-15
Ito, Yusuke 2-6, 2P-16
Itoh, Chihiro 1P-9, 2P-10, 3-1
Iwaizako, T 1P-44
Iwasa, Yoshihiro 2P-44, 3P-39
Iwata, Nobuyuki 1P-17, 3P-30, 3P-34
Izumi, Yudai 2-3

< **J** >
Jang, Jin 1-3
Jeon, IL 2P-3, 3P-23
Jinnouchi, Ryota 1-5
Jippo, Hideyuki 3-4
Juhasz, Gergely 1P-15

< **K** >
Kaji, Seiya 2P-22, 3P-50
Kako, Masahiro 3P-1
Kanazawa, Naoki 1P-27
Kaneko, Toshiro 2P-24, 3P-26, 3P-37
Kasama, Yasuhiko 2P-7
Kaskela, Antti 2P-23
Kataoka, Yosuke 1P-1
Kataoka, Yousuke 3P-32
Kataura, Hiromichi 1P-26, 1P-28, 2-7, 2P-31
Kato, Hiroki 1P-30, 2-6, 2P-16
Kato, Toshiaki 2P-24, 3P-26, 3P-37
Kato, Yuichi 2P-29,
Kato, Yuichiro K. 2P-17, 3P-5, 3P-13
Kauppinen, Esko I. 2P-23, 3S-7
Kawabata, Akio 2-3

Kawachi, Kazuhiko 2P-7
Kawahara, Kenji 1P-44
Kawai, Hideki 2P-22, 2P-30, 3P-50
Kawai, Hiroki 2P-13
Kawai, Tsuyoshi 1P-25, 2P-20
Kawarada, Hiroshi 2P-19, 2P-21
Kawasaki, Shinji 2P-14
Kawashima, Yuki 1P-5, 2-12
Kawasuzuki, Tomoya 2-1
Kidalov, Sergei 3P-44
Kigure, Shota 2P-35
Kihara, Hideyuki 2P-27
Kikuchi, Hayato 1P-32
Kikuchi, Koichi 1P-6
Kim, Dong Young 1P-10, 3-2, 3P-22
Kim, Junpil 3-9
Kimura, Takahide 3P-21, 3P-36
Kishikawa, Keiki 3P-24
Kishimoto, Shigeru 1P-19, 1P-23, 2P-23
Kisoda, Kenji 1P-9, 2P-10
Kitakawa, Haruki 2P-43
Kitaura, Ryo 1P-31, 1P-42, 2P-6, 2P-33, 2P-38, 3P-4, 3P-41
Kiyomiya, Masaharu 1P-26, 1P-37
Kobashi, Kazufumi 3-3
Kobayashi, Keita 1P-37
Kobayashi, Tatsuki 1P-6
Kobayashi, Toshiyuki 3S-8
Kobayashi, Yoshihiro 2P-43
Kodama, Takeshi 1P-6, 2-4
Kohmoto, Shigeo 3P-24
Kohno, Naoki 1P-18
Koinuma, Michio 2P-46
Kokubo, Ken 2-9, 2-10, 3P-3
Komatsu, Ken-ichirou 2P-7
Komatsu, Naoki 3P-21, 3P-36, 3P-41
Konabe, Satoru 1P-46, 1P-49
Kondo, Daiyu 3-5
Konno, Toshio 1P-3
Koretsune, Takashi 1-7, 3P-12
Kosaka, Masaki 1P-41
Kosugi, Yuta 3P-47
Kotsugi, Masato 2-3
Kozawa, Daichi 1-8, 1P-50, 2P-26, 2P-47, 3P-41
Kudo, Hikaru 2P-22
Kumamoto, Yusuke 3P-5, 3P-13
Kumar, Amara Kiran 1-8
Kumar, Rajeev Sharma 1-8
Kunioka, Masao 1P-38
Kuronuma, Hiroki 3P-38
Kurumi, Satoshi 1P-36
Kusunoki, Michiko 1P-35, 2P-19, 2P-21, 2P-42
Kutsuzawa, Dai 3P-23
Kuwahara, Yuki 3P-25
Kwon, Eunsang 2P-7

< L >
Laiho, Patrik 2P-23
Lee, Chih-Yu 2P-19, 2P-21
Lee, Heaseong 1-3
Lee, Jeonyoon 2P-18
Lee, Seungjoo 1-3
Li, Lain-Jong 2P-44, 3P-39
Li, Yan 2S-4
Lin, Po-shin 3P-40
Liu, Gang 3P-36
Liu, Jianfeng 3-6
Lyth, Stephen 3-6

< M >
Ma, Shao-Wei 3-7
Machida, Tomoki 1-6, 1P-45
Maeda, Michihiko 1P-19
Maeda, Yutaka 1P-12, 3P-1
Manako, Takashi 1P-20, 2P-37
Maniwa, Yutaka 3P-10, 3P-31, 3P-33, 3P-49
Maruyama, Koji 3P-48
Maruyama, Mina 2P-9
Maruyama, Shigeo 1P-34, 2-1, 2-8, 2P-18, 2P-32, 2P-41, 3P-28
Masubuchi, Satoru 1-6, 1P-45
Masuda, Hideki 1P-8
Masuda, Hiroyuki 2-9, 2-10
Masuda, Yoshiho 2P-19, 2P-21, 2P-42
Matsuda, Kazunari 1-8, 1P-13, 1P-16, 1P-28, 1P-31, 1P-48, 1P-49, 1P-50, 2P-26, 2P-47, 3P-7, 3P-41
Matsuda, Ken-ichi 1P-36
Matsuda, Mitsuaki 2P-10
Matsuki, Kuniharu 3P-34

Matsumoto, Morihiro 1-9
Matsumoto, Yasumichi 2P-46
Matsuo, Shintaro 3-9
Matsuo, Yutaka 1P-5, 2P-3, 2P-4, 3P-23
Matsushita, Tomohiro 2-3
Matsuura, Tomohiro 2P-14
Matsuzaki, Satoki 3P-18
Matsuzawa, Yoko 2P-27
Mieno, Tetsu 3P-14
Mikami, Ninako 1-5
Mikie, Tsubasa 2-10
Minami, Kazuya 3P-1
Mitoma, Nobuhiko 1-9
Miura, Asuka 2P-18
Miyabe, Kyosuke 3P-1
Miyamoto, Katsuhiko 2P-5
Miyashita, Masahiro 3P-35
Miyata, Yasumitsu 1P-31, 3P-10, 3P-31, 3P-33, 3P-49
Miyauchi, Yuhei 1P-13, 1P-16, 1P-28, 1P-31, 1P-48, 1P-49, 1P-50, 2P-26, 2P-47, 3P-7, 3P-41
Miyazaki, Daiki 1P-27
Miyazaki, Takafumi 1-2
Miyazawa, Kun'ichi 1-1, 1P-3
Mizuno, Masashi 2P-11, 2P-48
Mohamed, Berber 1P-22
Momiyama, Daiki 1P-4, 2P-5
Mori, Shohei 3P-49
Morikawa, Sei 1-6, 1P-45
Morimoto, Naoki 3P-43
Morimoto, Takahiro 1P-14
Moriya, Rai 1-6, 1P-45
Moriyama, Hiroshi 1-3, 3P-3
Mouri, Shinichiro 1P-16, 1P-48, 1P-49, 1P-50, 2P-26, 2P-47, 3P-7, 3P-41
Mukai, Ken 3-1
Munkh-od, Batbuyan 3P-19
Murakami, Tomo 2-3
Murakami, Toshiya 1P-9, 2P-10, 3-1
Murakoshi, Koshi 3P-26
Muraoka, Yoshimi 3P-17
Murata, Michihisa 2P-2
Murata, Yasujiro 2P-2
Muro, Takayuki 2-3
Myodo, Miho 2P-21

< **N** >
Na, Nuri 3P-29
Nagahama, Taro 3P-23
Nagao, Kyohei 3P-15
Nagasawa, Hiroshi 3P-15
Naitoh, Yasuhisa 2P-30
Nakagawa, Takafumi 2P-4
Nakahara, Hitoshi 2P-40
Nakahara, Kentaro 2P-37
Nakai, Yusuke 3P-10, 3P-31
Nakajima, Yuta 1P-19
Nakamura, Hiroko 2-2
Nakamura, Keisuke 3P-21
Nakamura, Maki 1P-39
Nakamura, Naoto 1P-4, 2P-5
Nakanishi, Yusuke 2P-6, 3P-4
Nakano, Haruhisa 3-5
Nakano, Kaichiro 2P-37
Nakano, Motohiro 1P-25
Nakashima, Naotoshi 1P-13, 1P-15, 1P-16, 1P-22, 1P-24, 1P-29, 2-5, 2P-12, 2P-25, 2P-29, 3P-16, 3P-27
Nakashima, Takuya 1P-25
Nakazaki, Tafu 2P-3
Narita, Kouhei 2P-8
Naruse, Shihono 2P-38
Nasibulin, Albert 2P-23
Natsume, Yuhei 3P-11
Negishi, Ryota 2P-43
Negishi, Yuichi 2P-3
Nihei, Mizuhisa 2-3
Nihey, Fumiyuki 1P-20, 3P-25
Nii, Daisuke 2-6, 2P-16
Nishigaki, Hiroshi 2P-10
Nishina, Yuta 3P-43
Niwa, Hiroyuki 2P-6, 3P-4
Noda, Shoko 1-2, 2P-6
Noda, Suguru 1P-10, 1P-41, 2P-18, 2P-38, 3-2, 3P-22, 3P-29
Noguchi, Takuya 2-1
Noji, Naoki 1P-1
Nomura, Kazuya 1P-7
Nonoguchi, Yoshiyuki 1P-25, 2P-20

Norimatsu, Wataru 1P-35, 2P-19, 2P-21, 2P-42
Nouchi, Ryo 1-9
Nugraha, Ahmad R. T. 1P-11, 3P-6
Numata, Hideaki 1P-20

< **O** >
Ochiai, Yuichi 1P-4, 2P-5
Ogami, Shinji 3P-15
Ogasawara, Kazuki 1P-34, 2P-32
Ogata, Hironori 1P-1, 2P-1, 3P-32, 3P-45
Ogawa, Takuji 2P-43
Ogawa, Tomoyuki 2P-7
Ogumi, Keisuke 2P-4
Ohashi, Kenji 2P-20
Ohfuchi, Mari 3-4
Ohkochi, Takuo 2-3
Ohkohchi, Masato 2P-28
Ohkubo, Kei 1P-5, 1P-18, 2-12, 3P-3
Ohmori, Shigekazu 3P-25
Ohno, Yutaka 1P-19, 1P-23, 2P-23, 2P-26
Ohto, Tatsuhiko 2P-13
Oka, Nobuto 2P-39
Okada, Hiroshi 1P-5, 2-11
Okada, Susumu 1P-7, 1P-46, 1P-49, 2P-8, 2P-9, 2P-35, 3P-8, 3P-42
Okazaki, Toshiya 1P-14
Okimoto, Haruya 3P-38
Omachi, Haruka 1P-31, 1P-42, 3P-4
Omatsu, Takashige 2P-5
Ono, Akira 1P-27
Ono, Shoichi 2P-7
Onoe, Jun 1P-8
Osawa, Eiji 1-4, 3P-46
Osawa, Toshio 1P-10
Osipov, Vladimir 3P-44
Otsuka, Keigo 2-8
Ozaki, Taisuke 3-4
Ozao, Akihiko 3P-9

< **P** >
Pac, Chyongjin 1-3
Peng, Fei 2S-4
Pu, Jiang 2P-44, 3P-39

< **Q** >
Qin, Xiaojun 2S-4
Quintero, Ricardo 3-2

< **R** >
Rahman, Mohammad Jellur 3P-14
Ribeiro, Ricardo Mendes 1-8
Ryan, James 2P-3

< **S** >
Sada, Takao 1P-29
Saeki, Akinori 2-10
Sagara, Takumi 1P-17, 3P-30
Sagara, Takuya 1P-36
Sagawa, Wataru 3P-24
Saito, Riichiro 1P-11, 2P-11, 2P-48, 3P-6, 3-8
Saito, Susumu 1-7, 3P-12
Saito, Takeshi 1P-26, 1P-37, 3-1, 3P-10, 3P-25
Saito, Yahachi 2P-40
Sakai, Hayato 2-12
Sakai, Keijiro 1P-14
Sakai, Seiji 2P-7
Sakurai, Shunsuke 2-2
Sano, Masahito 3P-38
Sano, Yoshiaki 2P-1
Sano, Yosiaki 1P-1
Sanzen, Toshitada 2P-23
Sasaki, Kazunari 3-6
Sasaki, Mikio 1S-1
Sasaki, Shuichi 1-4, 3P-46
Sastre-Santos, Angela 2-12
Sato, Hiroki 3P-17
Sato, Kentaro 3-8
Sato, Satoshi 3-9
Sato, Shintaro 3-5
Sato, Sho 2P-7
Sato, Shogo 3P-34
Schweizer, W. Bernd 1P-2
Seino, Yuuma 1-2
Seki, Shu 2-10
Sekido, Masaru 1P-21, 3P-2, 3P-17
Sekine, Akinori 3P-32
Sekita, Michael 1P-2
Sekitani, Tsuyoshi 1P-20
Serita, Noboru 3P-10

Shakhov, Fedor 3P-44
Shibuya, Megumi 2P-19, 2P-21
Shimada, Takashi 3P-5
Shimada, Toshihiro 3P-23
Shimizu, Kazuki 3P-48
Shimizu, Ryo 3P-20
Shimizu, Yoshiaki 3P-48
Shimomura, Shuichi 1-1
Shinohara, Hisanori 1-2, 1P-31, 1P-42, 2P-6, 2P-33, 2P-38, 3P-4, 3P-41
Shiomi, Junichiro 2P-18
Shirae, Hiroyuki 3P-22
Shiraishi, Tomonari 1P-13
Shiromaru, Haruo 2-4, 2P-49
Solís-Fernández, Pablo 2P-45
Someya, Takao 1P-20
Song, Hayong 2P-14
Suda, Yoshiyuki 3P-48
Sugai, Toshiki 1-5, 1P-32, 1P-34, 2P-32
Sugimoto, Kunihisa 2-11
Sugisaki, Yuma 1P-42
Sugita, Tomoko 1P-26
Sun, Bo 1P-33
Suzuki, Hiroo 3P-37
Suzuki, Kaoru 1P-36
Suzuki, Kazuma 2P-19, 2P-21
Suzuki, Shinzo 1P-27, 3P-15
Suzuki, Tomoko 1P-33

< **T** >
Tabata, Hiromu 3P-32
Tachibana, Masaru 1-1
Tada, Tomofumi 2-1
Tajima, Yusuke 2S-6
Takada, Tomoya 3P-19
Takada, Yuko 2P-27
Takagi, Yuki 2P-30, 3P-20
Takahashi, Makoto 3-5
Takahashi, Masahiro 3P-24
Takahashi, Migaku 2P-7
Takai, Kazuyuki 3P-44
Takashima, Akito 2-3
Takashima, Kengo 1P-47
Takenobu, Taishi 1P-4, 2P-22, 2P-30, 2P-44, 3P-18, 3P-20, 3P-39
Takesue, Masafumi 1P-19
Takikawa, Hirofumi 3P-48
Tamura, Noriyuki 2P-37
Tanaka, Hirofumi 2P-43
Tanaka, Takeshi 1P-26, 1P-28, 2-7, 2P-31
Tanaka, Yu 1P-27
Tancini, Francesca 1P-2
Taniguchi, Takaaki 2P-46
Taniguchi, Takashi 1-6, 1P-45
Tanoue, Hideto 3P-48
Tashiro, Kosuke 2P-14
Terada, Katsuhide 1P-32
Terashima, Yoshiki 1P-21
Thendie, Boanerges 1P-31
Tobari, Yuta 1P-34, 2P-32
Toh, Minglin 1-8, 1P-48, 1P-49
Tokutomi, Hisashi 3P-2
Tomai, Takaaki 2P-39
Tomura, Takuya 1P-19
Tonouchi, Noriyuki 1P-20
Toriumi, Naoto 1P-4, 2P-5
Toshimitsu, Fumiyuki 2-5, 2P-29, 3P-27
Toyokuni, Shinya 1S-2
Tsai, Shang-Lin 1P-43
Tsuboi, Yuka 1P-49, 1P-50
Tsuda, Yusaku 1P-17, 3P-30
Tsuji, Masaharu 1P-44, 2P-45, 3P-35
Tsuzuki, Akiko 2P-12
Tsuzuki, Mayumi 2P-31

< **U** >
Uchida, Yuya 3P-12
Uda, Takushi 2P-17, 3P-13
Ue, Hitoshi 3P-48
Ueda, Tomohiro 3P-31
Ueda, Yuto 2P-17
Ueno, Hiroshi 3P-3
Ueno, Keiji 1S-3
Umeda, Yoshito 3P-48
Umemura, Kazuo 2-6, 2P-16
Umino, Takanori 3P-28

< **V** >
Vul', Alexander 3P-44

< **W** >
Wada, Yoshifumi 2P-30, 3P-18, 3P-20

Wakabayashi, Tomonari 2P-50
Wakahara, Takatsugu 1-1, 1P-3
Wakamiya, Atsushi 2P-2
Wang, Feijiu 2P-26
Wang, Huafeng 1P-30, 2P-41
Wang, Qing 2P-33
Wang, Yi-Wen 3-12
Wang, Zhiyong 2P-6, 3P-4
Wardle, Brian L 2P-18
Watanabe, Kenji 1-6, 1P-45
Wei, Xiaojun 1P-28

< X >
Xu, Bin 3P-26

< Y >
Yagi, Hajime 1-2
Yajima, Hirofumi 1P-17, 3P-30
Yamada, Atsuo 3-2
Yamada, Chisato 1P-30
Yamada, Maho 2-2
Yamada, Michio 1P-2, 1P-12, 3P-1
Yamada, Takeo 3-3
Yamada, Tatsuya 1P-23
Yamada, Yasuhiro 3-9
Yamada, Yoichi 2P-7
Yamada, Yuki 3-2
Yamaguchi, Genta 3P-9
Yamaguchi, Junichi 3-5
Yamaguchi, Takehiro 1-6
Yamakawa, Kenichi 1P-17, 3P-30
Yamamoto, Hiroshi 1P-17, 3P-30, 3P-34
Yamamoto, Takahiro 1P-47, 2P-15, 2S-5
Yamamoto, Takayuki 1P-33
Yamamoto, Yuki 2P-10
Yamamoto, Yuta 2P-33
Yamanaka, Ayaka 3P-42
Yamanoi, Ryoko 1-4, 3P-46
Yamasaki, Akira 1P-27
Yamashita, Hiroki 2P-34
Yamashita, Koichi 2P-13
Yamazaki, Yu 2-9
Yanagi, Chihiro 1P-33
Yanagi, Kazuhiro 2P-22, 2P-30, 3P-18, 3P-20, 3P-50
Yanase, Takashi 3P-23
Yang, Feng 2S-4
Yang, Juan 2S-4
Yang, Mei 1P-38, 2P-36
Yang, Zehui 1P-22
Yasuda, Hidehiro 1P-8, 1P-37
Yasuda, Toku 3P-41
Yeo, Kee Sheng 2P-3
Yokoi, Hiroyuki 2P-46
Yokoo, Kuniyoshi 2P-7
Yokota, Tomoyuki 1P-20
Yokoyama, Akio 3P-5
Yokoyama, Naoki 2-3, 3-5
Yomogida, Yohei 2P-31
Yoo, JongTae 3P-16
Yoshida, Keisuke 1P-17, 3P-30
Yoshida, Masahiro 2P-17, 3P-5, 3P-13
Yoshida, Masaru 2P-27
Yoshitake, Haruhiko 3P-45
Yudasaka, Masako 1P-38, 1P-39, 2P-36
Yuge, Ryota 1P-39, 2P-37
Yumura, Motoo 3-1
Yumura, Takashi 2P-34
Yunus, Rozan Mohamad 3P-35

< Z >
Zhang, Jinying 2P-6
Zhang, Minfang 1P-38, 2P-36
Zhao, Li 3P-21
Zhao, Pei 2P-41
Zhao, Weijie 1-8
Zhipeng, Wang 3P-45
Zhou, Bo 3-5
Zhou, Lizhong 1P-48, 1P-49

複写をご希望の方へ

フラーレン・ナノチューブ・グラフェン学会は、本誌掲載著作物の複写に関する権利を一般社団法人学術著作権協会に委託しております。

本誌に掲載された著作物の複写をご希望の方は、（社）学術著作権協会より許諾を受けて下さい。但し、企業等法人による社内利用目的の複写については、当該企業等法人が社団法人日本複写権センター（（社）学術著作権協会が社内利用目的複写に関する権利を再委託している団体）と包括複写許諾契約を締結している場合にあっては、その必要はございません（社外頒布目的の複写については、許諾が必要です）。

権利委託先：一般社団法人学術著作権協会
〒107-0052　東京都港区赤坂 9-6-41　乃木坂ビル 3 階
電話：03-3475-5618　FAX：03-3475-5619　E-Mail：info@jaacc.jp

注意：複写以外の許諾（著作物の引用、転載・翻訳等）に関しては、（社）学術著作権協会に委託致しておりません。直接、フラーレン・ナノチューブ・グラフェン学会へお問い合わせください。

Reprographic　Reproduction outside Japan

- Making a copy of this publication

Please obtain permission from the following Reproduction Rights Organizations (RROs) to which the copyright holder has consigned the management of the copyright regarding reprographic reproduction.

- Obtaining permission to quote, reproduce; translate, etc.

Please contact the copyright holder directly.

Users in countries and regions where there is a local RRO under bilateral contract with Japan Academic Association for Copyright Clearance(JAACC) are requested to contact the respective PROs directly to obtain permission.

Users in countries or regions in which JAACC has no bilateral agreement are requested to apply for the license to JAACC.

Japan Academic Association for Copyright Clearance (JAACC)
Address：9-6-41 Akasaka, Minato-ku, Tokyo 107-0052 Japan
Website：http://www.jaacc.jp/
E-mail：info@jaacc.jp
TEL：81-3-3475-5618　FAX：81-3-3475-5619

2014 年 3 月 3 日発行

第 46 回フラーレン・ナノチューブ・グラフェン総合シンポジウム
講演要旨集

＜フラーレン・ナノチューブ・グラフェン学会＞
〒113-8656 東京都文京区本郷 7-3-1
東京大学大学院工学系研究科　機械工学専攻
丸山研究室内
Tel：03-3830-4848
Fax：03-3830-4848
E-mail：fntg@photon.t.u-tokyo.ac.jp
URL：http://fullerene-jp.org
印刷　/　製本　（株）創志企画

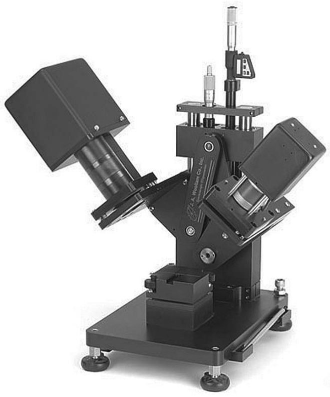

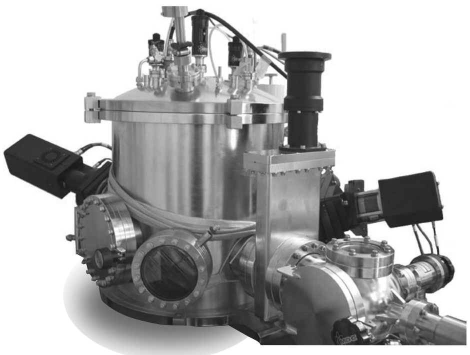

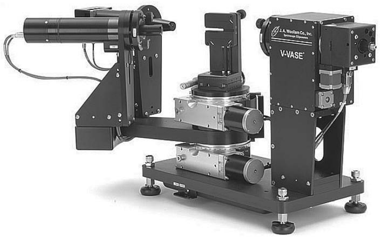

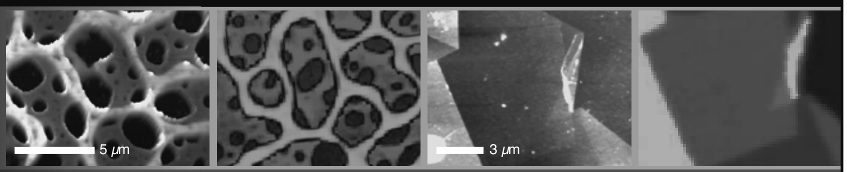
5 μm
3 μm

JEOLの最新表面分析装置

JEOL
Solutions for Innovation

マイクロからナノスケール領域の観察・分析に!

Surface Analysis

JEM-ARM200F

原子分解能分析電子顕微鏡

Cold

新たな扉を開く鍵……

材料・情報通信・ライフサイエンス・環境などあらゆる分野の研究にとって根幹の技術になっているナノテクノロジーは、21世紀の基幹産業といわれ主要各国が国家戦略として取り組んでいます。JEOLの電子光学機器は物質のナノオーダー領域や極表面層の解析装置として基礎研究、最先端材料開発に貢献しています。

お問い合わせは、電子光学営業本部（EO販促室） TEL:042（528）3353

日本電子株式会社 **本社・昭島製作所** 東京都昭島市武蔵野3-1-2 TEL（042）543-1111 http://www.jeol.co.jp/
営業企画室 東京都立川市曙町2-8-3 TEL（042）528-3381 | **西日本ソリューションセンター** 大阪市淀川区西中島5-14-5 TEL（06）6305-0121

■**東京** **電子光学機器営業グループ** TEL（042）528-3261 | **分析機器営業グループ** TEL（042）528-3281 | **産業機器営業グループ** TEL（042）528-3481
半導体機器営業部 TEL（042）528-3491 | **医用機器営業グループ** TEL（042）528-3341

■**札幌** TEL（011）726-9680 | ■**仙台** TEL（022）222-3324 | ■**筑波** TEL（029）856-3220 | ■**大手町事務所** TEL（03）6225-2256 | ■**横浜** TEL（045）474-2181
■**名古屋** TEL（052）581-1406 | ■**大阪** TEL（06）6304-3941 | ■**広島** TEL（082）221-2500 | ■**高松** TEL（087）821-0053 | ■**福岡** TEL（092）411-2381

誘導体化フラーレン用HPLCカラム

COSMOSIL® Buckyprep-D

● 誘導体化フラーレン用HPLCカラム

● トルエン移動相中で誘導体化フラーレンが分離可能

■C60インデン付加体の分析例

C60インデンは誘導体化フラーレンの一種であり、有機薄膜太陽電池のn型半導体材料として注目されている化合物です。コスモシール Buckyprep-Dを用いることにより高い分離性能が得られます。

COSMOSIL Application Data

Column:
Column size: 4.6mmI.D.-250mm
Mobile phase: Toluene
Flow rate: 1.0 ml/min
Temperature: 30°C
Detection: UV 325nm

Sample: C_{60} [Indene]$_2$ (1.0mg/ml)
Inj.Vol.: 1.0μl

Buckyprep

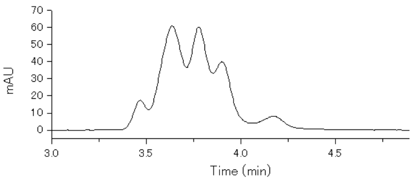

Buckyprep-D

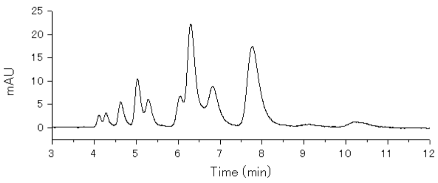

Data courtesy of Yusuke Tajima, Dr. Sci.
Organic Optoelectronics Laboratory, RIKEN (Institute of Physics and Chemistry)

NACALAI TESQUE, INC

■Buckyprepシリーズの用途

フラーレン分離のスタンダードカラム → COSMOSIL Buckyprep
誘導体化フラーレンの分離 → COSMOSIL Buckyprep-D
金属内包フラーレンの分離 → COSMOSIL Buckyprep-M

・誘導体化フラーレン (Buckyprep-D)

COSMOSIL Application Data

Column: Buckyprep-D
Column size: 4.6mmI.D.-50mm
Mobile phase: Toluene
Flow rate: 1.0 ml/min
Temperature: 30°C
Detection: UV325nm

Sample: 1; C_{60} (0.125mg/ml)
2; C_{70} (0.250mg/ml)
3; [*6,6*]-Phenyl-C_{61} Butyric Acid Methyl Ester [PCBM] (0.125mg/ml)
4; [*6,6*]-Phenyl-C_{71} Butyric Acid Methyl Ester [[70]PCBM] (0.375mg/ml)
Inj.Vol. 1.0μl

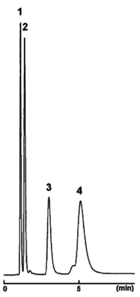

NACALAI TESQUE, INC

・金属内包フラーレン (Buckyprep-M)

COSMOSIL Application Data

Column: Buckyprep-M
Column size: 4.6mmI.D.-250mm
Mobile phase: Toluene
Flow rate: 1.0 ml/min
Temperature: 30°C
Detection: UV312nm

Sample: $Sc_2@C_{76}$(I)
$Sc_2@C_{78}$
$Sc_2@C_{80}$(I)
C_{86}

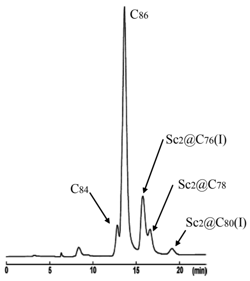

Sample courtesy of Prof. H.Shinohara,
Department of chemistry, Nagoya University

NACALAI TESQUE, INC

詳しい情報はWeb siteをご覧ください。

ナカライテスク株式会社

〒604-0855　京都市中京区二条通烏丸西入東玉屋町498

価格・納期のご照会　フリーダイヤル　0120-489-552
製品に関するご照会　TEL : 075-211-2746　FAX : 075-211-2710
Web site :http://www.nacalai.co.jp

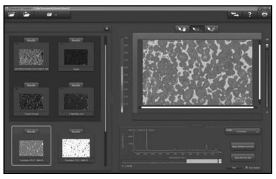

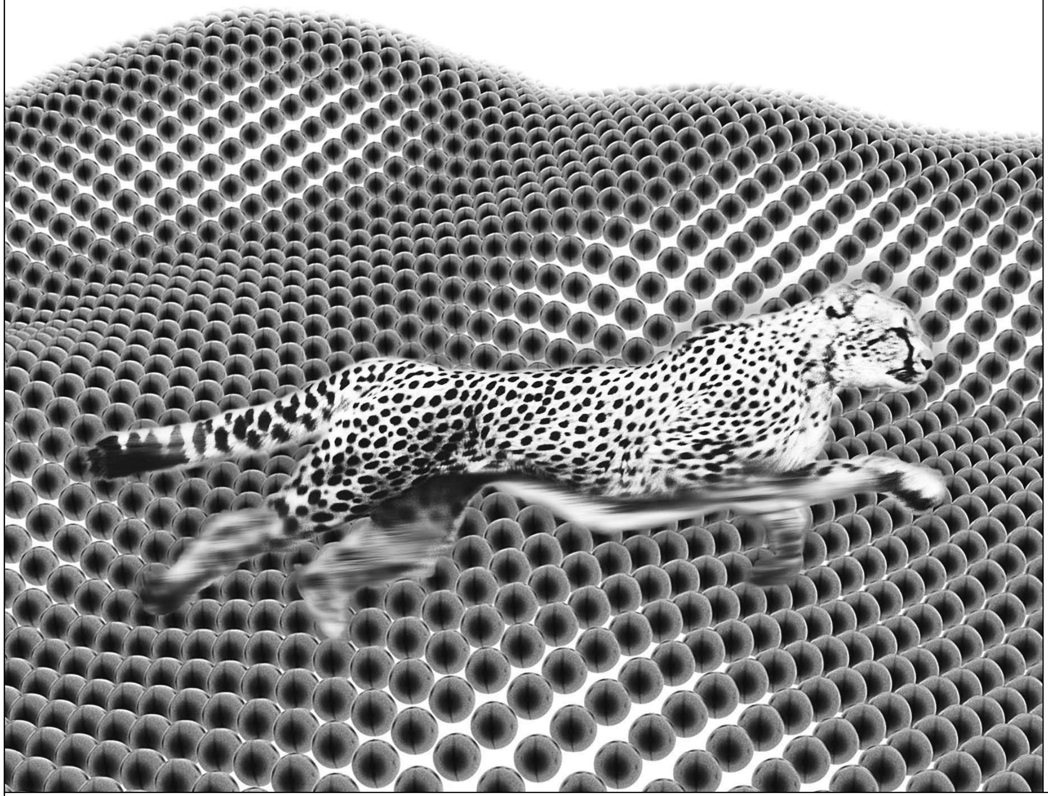

溶液中の粒子のナノレベル微細化・分散に

BRANSON 超音波ホモジナイザー

ホーン先端部の振幅の安定性を、より高めた Advance タイプ になりました。

近年のナノテクノロジーの発展及び粉体関連技術の向上により、より微細な粒子に対する乳化分散処理の要望が増えてまいりました。
超音波ホモジナイザーを使用し、均質な乳化分散処理を行い、安定させることにより製品の機能は向上します。
ブランソン社では 20kHz 機と、40kHz 機の 2 タイプを用意しております。
1 次粒子の凝集力にも拠りますが、20kHz 機では 100nm 程度までの分散力があります。40kHz 機は、さらに細かいレベルで分散ができる可能性があります。

20KHz 超音波ホモジナイザー
BRANSON　SONIFIER シリーズ

高周波 40KHz 超音波ホモジナイザー
BRANSON SLPe シリーズ

ブランソン社の製品は、ホーン先端部の振幅の安定性が高く、強力なキャビテーションが得られ、効率良く、再現性の高い分散処理が行えます。

主なアプリケーション

分散

カーボンナノチューブ　有機顔料　無機顔料　セラミック　セメント　感光体　記録材料
磁性粉　粉末冶金　酸化鉄　金属酸化物　シリカ　アルミナ　カーボンブラック
ポリマー　ラテックス　製紙　ファンデーション
研磨剤　電池　フィラー　光触媒　触媒　ワクチン　体外診断薬　歯磨き粉　シャンプー
半導体　電子基盤　液晶　貴金属　金属　宝石　タイヤ　発酵菌類　その他

乳化

エマルジョン製剤　農薬　トナー　ラテックス　界面活性剤　クリーム　乳液　クリーム　等

株式会社 セントラル科学貿易
本社：111-0052 東京都台東区柳橋 1-8-1
Tel 03-5820-1500 Fax 03-5820-1515
URL http://www.cscjp.co.jp/

大阪支店：　Tel 06-6325-3171 Fax 06-6325-5180
福岡営業所：Tel 092-482-4000 Fax 092-482-3797
札幌出張所：Tel 011-764-3611 Fax 011-764-3612

http://www.oceanphotonics.com

CNTの
特性評価に
最適

M SQUARED

Mスクエアレーザー社製

全自動・超コンパクト・波長可変

CW単一周波数Ti:Sapphireレーザ SolsTiS

テラ・スキャン（連続掃引域：700-1000nm）の充実した機能

- **point ①** 驚愕の操作性：全制御はレーザ付属のパソコンで設定
- **point ②** 全自動掃引：全波長域を任意掃引波長幅で対応
- **point ③** 掃引スピード：標準(20GHz/s)、高速(100GHz/s)

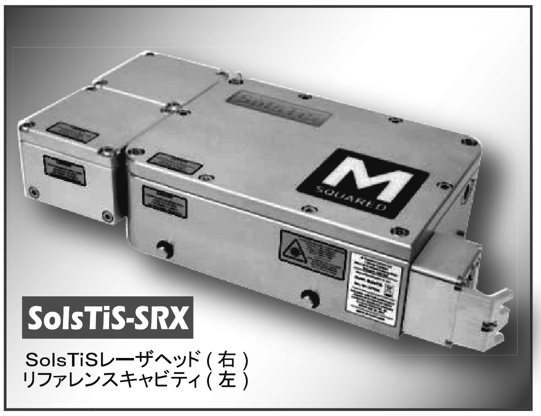

SolsTiSレーザヘッド（右）
リファレンスキャビティ（左）

仕 様

- 低ノイズ：＜0.1%RMS
- 高出力：＞ 4.0 W @18W励起/ピーク波長
- 線幅：＜50 kHz~20GHz
- 掃引周波数：＞25 GH z
- コンパクト (289×168 mm レーザヘッド)
- 広帯域自動波長可変：700〜1000nm
  （単一ミラーセット）
- 短、長波長用高出力ミラー：670-710nm、950-1050nm

※上記は標準仕様です。その他カスタマイズは別途承ります。

特長

- ✓ チタンサファイアレーザの煩わしいメンテナンスから解放
- ✓ ユーザフレンドリな外部プログラムで波長の自動制御も可能
- ✓ 測定装置組込みで完全自動制御

SolsTiSを使用したカイラル指数測定サンプル

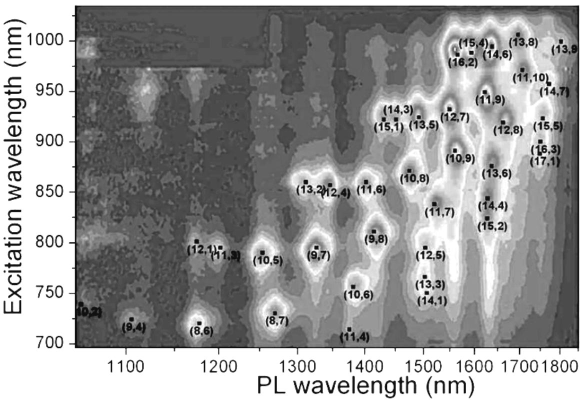

※ 製品の仕様は予告無く変更することがあります。

Ocean Photonics

日本総代理店
オーシャン フォトニクス 株式会社 M2レーザー課
〒169-0051 東京都新宿区西早稲田 3-30-16 ホリゾン１ビル　TEL 03-6278-9470　FAX 03-6278-9480
E-mail: sales@oceanphotonics.com　URL: http://www.oceanphotonics.com

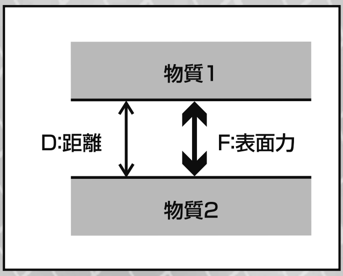
物質1
D:距離
F:表面力
物質2

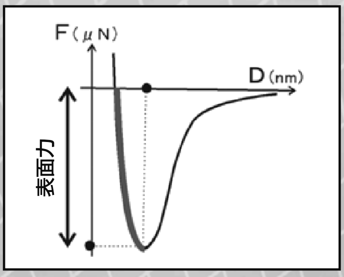
F（μN）
D（nm）
表面力

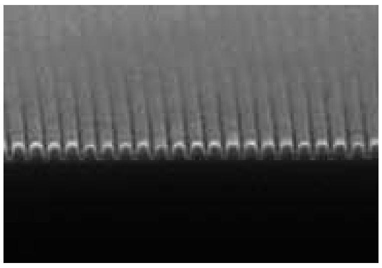

nanom フロンティアカーボンのフラーレン製品

銘　柄		分子構造	純度（HPLC面積%、代表値） 内容他	最低数量 （g）
nanom purple **フラーレンC60**	**ST**	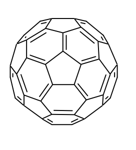	99	10
	TL		99.5	2
	SU		99.5/昇華精製品	2
	SUH		99.9/昇華精製品	1
	SC		99.9/昇華精製/単結晶品	1
nanom orange **フラーレンC70**	**ST**	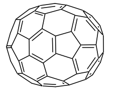	97	1
	SU		98/昇華精製品	0.5
nanom mix **混合フラーレン**	**ST**	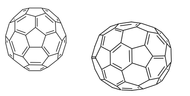	C60,C70,その他高次 フラーレンの混合物 ※微粒化品（ST-F）もあります	50
nanom spectra **[60]PCBM** (phenyl C61-butyric acid methyl ester)	**E100**	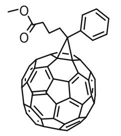	99	1
	E100H		99.5	1
	E102		99.9	0.5
nanom spectra　E400 **bis[60]PCBM** (bis-phenyl C61-butyric acid methyl ester)		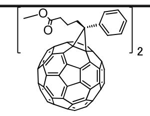	98/異性体トータル ※位置異性体の混合物	1
nanom spectra　E124 **[60,70]PCBM**		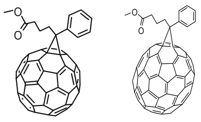	[60]PCBM、[70]PCBMの混合物	1
nanom spectra **[70]PCBM** (phenyl C71-butyric acid methyl ester)	**E110**	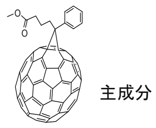	99/異性体トータル ※位置異性体の混合物	0.5
	E112		99.5/異性体トータル ※位置異性体の混合物	0.5
nanom spectra　Q100 **[60]インデン付加体**		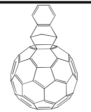	99	0.5
nanom spectra　Q400 **[60]インデン２付加体**		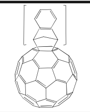	99/異性体トータル ※位置異性体の混合物	1
nanom spectra　D100 **水酸化フラーレン**		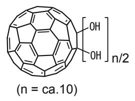	$C_{60}OH_n$　n=10を主成分とする混合物	1
nanom spectra　A100 **水素化フラーレン**		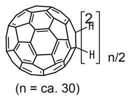	$C_{60}H_n$　n=30を主成分とする混合物	1

銘柄、取扱数量等は予告無く変更する場合がございます。予めご了承下さい。

当社製品は、下記から購入いただけます。直接お問い合わせください。

・関東化学株式会社　試薬事業本部
〒103-0022 東京都中央区日本橋室町2-2-1　TEL:03-6214-1090　FAX:03-3241-1047
http://www.kanto.co.jp　E-mail:reag-info@gms.kanto.co.jp

＜本資料に関するお問い合わせ先＞
フロンティアカーボン株式会社【担当：梶原】
〒100-8086　東京都千代田区丸の内2-6-1丸の内パークビルディング24階
TEL:03-3210-2620　FAX:03-3210-4606　http://www.f-carbon.com
※弊社へのお問い合わせはHPよりお願いいたします。

Frontier Carbon Corporation